Novel Bioactive Cements to Promote Bone Regeneration

By:

Altair Teresa Contreras Jaimes MEng MSc

A thesis submitted in partial fulfilment of the requirements for the degree of Doctor of Philosophy

The University of Sheffield

Faculty of Medicine, Dentistry, and Health

November 2017

Abstract

Currently available cements and granules for bone repair include devices based on glass ionomer cement (GICs) technology. These cements are based on the setting reaction between an aluminium containing fluorosilicate glass, poly (acrylic acid) (PAA) and a setting modifier. The glass powder is acid degradable, which crosslinks with the ionised acid, resulting in a matrix of polyacrylates salts with reacted glass particles. However, bone demineralisation, as well as neurotoxicity in craniofacial applications are drawbacks associated with aluminium. These disadvantages have created a scientific interest on developing aluminium free compositions with the potential to be used as cements and bone grafts. Therefore, new glass compositions have been researched to substitute the alumina (Al_2O_3) with oxides such as ZnO, GeO, MgO, and TiO. However, no previous detailed study has investigated variations of the classic Hench Bioglass® composition ($45SiO_2$-$24.5Na_2O$-$24.5CaO$-$6P_2O_5$ wt. %) for preparation of cements, with Mirvakily studying this system, but focusing solely on one cement composition (Mirvakily, 2009).

In the present work, eight glasses were prepared and characterised by X-ray diffraction (XRD), differential thermal analysis (DTA), scanning electron microscopy (SEM), and Fourier transformed infrared spectroscopy (FTIR-ATR). These glasses were mixed with varying quantities of poly (acrylic acid), and a phosphoric acid solution ($H_3PO_{4\ (sol)}$), to evaluate their cement forming properties and setting times. The most suitable glasses were chosen along with the optimised cement combination, this being a powder/liquid (P/L) ratio of two, 10.7 % PAA powder and 25% $H_3PO_{4\ (sol)}$, to further investigate their mass change, ion release and conductivity when immersed in distilled water, along with their setting chemistry.

Results showed that glasses based on a SiO_2-Na_2O-CaO-SrO-P_2O_5 system could be used to produce setting pastes that were stable in distilled water, with net setting times varying between 34 min and 115 min. The setting mechanism was found to have similarities to GICs, by release of Ca^{2+}, Sr^{2+}, and Na^{+} after PAA ionisation and formation of the respective polyacrylate salts. The use of phosphoric acid was found to be essential to prevent the gelation in water of aged cements (set for one day, 37 °C), suggesting that this addition aided glass dissolution and precipitation of phosphate containing salts. Their mass loss in distilled water, reached its maximum after one day for the cements prepared with the 45S5 and 45S5Sr10 glasses (with lower SiO_2 content),

while this peak was observed after one week for the cements prepared with the 49P9 and 53P4 glasses (with higher SiO_2 content). The cement dissolution was further confirmed by the release of Si, Ca, Na, and P; with the direct *in vitro* short-term test showing that the cement based on the 45S5 glass was not cytotoxic. The study carried out with the commercial cement Serenocem™, showed that its dissolution and ion release was very low, which suggested the limited solubility of the Al containing glass. Therefore, the findings of this research provide an alternative system for the preparation of aluminium free cements for craniofacial applications, showing that no additional ionic substitution was required to produce a setting cement with ion release comparable to that of bioactive glasses.

Acknowledgments

I would like to thank my Supervisors Dr Cheryl Miller, Professor Paul Hatton, and Professor Ian Brook, for allowing me to do this PhD as a Staff Candidate and later as a full time PhD, and for all their support from an academic and personal point of view. I would like to thank Dr Robert Moorehead, who joined as a supervisor during my writing up period, for his detailed corrections, continuous support, and for his assistance in glass melting and calculations during my work as Staff Candidate for PhD. For funding I would like to thank The School of Clinical Dentistry, the IKC funding and Regener8 through the EPSRC, BBSRC and the Technology Strategy Board under grant number EP/G032483/1.

This PhD project would not be complete without all the staff that gave their technical support at various stages: at the School of Clinical Dentistry, to Dr. Felora Mirvakily for initial training on cement preparation, Dr Abigail Pinnock for her training in cell culture, Dr David Thompson for SEM preparation assistance, and Dr. Yulia Ryabenkova for FTIR-ATR training. At the Department of Chemistry, to Neil Bramall for performing the ICP analysis, Dr Michael Hippler and Thomas Smith for FTIR-ATR training, and Mr David Towers for technical support in the lab. At the Faculty of Engineering: to Dr Nick Reeves-McLaren for XRD training, Ian Watts for preliminary assistance on glass making, Professor Russel Hand and Professor John Provis for allowing me to attend their lectures in Glasses and Cements. At the Materials Department of Sheffield Hallam University to Robert Burton and Dr Anthony Bell for XRF analysis; to Corinthian Surgical Ltd. for providing the commercial cement capsules and Dr Barry Woodfine from Advanced Healthcare Ltd. for supplying the poly (acrylic acid) for the preliminary tests.

To The University of Sheffield and their student support team involved in the Springboard for Women, Think Ahead, and 301 Skills for workshops and 1:1 assistance in statistics with MASH, which overall improved my research and transferable skills. To my mentor as staff, Dr Janine Kirby, for her time and advice, my thesis mentor Dr Hilary Jones, for her valuable advice and motivation during writing, and to my tutor at the School of Dentistry, Dr Daniel Lambert for his approachable nature and advice.

To my previous thesis supervisors at the University of Nottingham and at the Universidad Central de Venezuela for their continuous career guidance. To all my friends and colleagues at the University of Sheffield for making my time at Uni a very special time to always remember. To all my family and a very special mention to my mom and aunt, for their endless support and love.

Table of Contents

Acknowledgments V
Table of Contents VII
List of Figures X
List of Tables XIX
Abbreviations XXI
1 Introduction 1
2 Literature Review 3
2.1 Bone tissue 3
2.1.1 Bone repair 5
2.2 Biomaterials 8
2.2.1 Glasses as biomaterials 10
2.3 Glass 15
2.3.1 Glass melting 18
2.3.2 Glass theory 21
2.3.3 Glass structure: network formers and modifiers 24
2.3.4 Theoretical glass structure 27
2.4 Glass characterisation 30
2.4.1 X-ray diffraction 30
2.4.2 Scanning electron microscopy 30
2.4.3 Differential thermal analysis 31
2.4.4 Fourier transformed infrared spectroscopy with attenuated total reflectance 32
2.5 Cements used as biomaterials 34
2.5.1 Poly (methyl methacrylate) 34
2.5.2 Calcium phosphates cements 34
2.6 Cements in dentistry 35
2.6.1 Zinc phosphate cements 36
2.6.2 Zinc polycarboxylate cements 37
2.6.3 Dental silicate cements 37
2.7 Glass ionomer cements 39
2.7.2 *In vitro* testing and biocompatibility of GICs 47
2.8 Drawbacks of aluminium (Al) containing GICs for clinical applications 49
2.9 Aluminium free glass ionomer cements 52
2.10 Cement characterisation 57
2.10.1 Setting times 57
2.10.2 Behaviour in water: mass variation, pH and ion release 58
3 Aim and objectives 61
4 Materials and Methods 63

4.1 Glass preparation 63
4.2 Cement preparation 65
4.3 Materials characterisation 67
4.3.1 X-ray powder diffraction 67
4.3.2 Wavelength dispersive X-ray fluorescence 68
4.3.3 Differential thermal analysis 69
4.3.4 Scanning electron microscopy 70
4.3.5 Fourier transformed infrared spectroscopy with attenuated total reflectance 71
4.3.6 Handling characterisation for cement pastes 72
4.3.7 Degradation in water of cements: mass change 74
4.3.8 Inductively coupled plasma spectrometry 75
4.3.9 Dissolution testing: pH and conductivity 76
4.4 Short term direct contact *in vitro* test 77
4.4.1 Pre-treatment of cement samples 77
4.4.2 Cell culture protocol 77
4.4.3 Cell viability measurement with PrestoBlue® assay 78
4.4.4 Light microscopy and SEM 78
4.5 Statistical Analysis 79
5 Results Glasses and Cements 80
5.1 Glass preparation 80
5.1.1 X-Ray powder diffraction 80
5.1.2 Wavelength dispersive X-ray fluorescence 81
5.1.3 Differential thermal analysis 82
5.1.4 Fourier transformed infrared spectroscopy with attenuated total reflectance 88
5.2 Cement preparation 89
5.3 Preliminary study on cement preparation 89
5.3.1 Other variables related to paste preparation 93
5.3.2 Second stage of cement assessment 94
5.4 Handling characterisation of cement pastes 95
5.4.1 Mixing time 95
5.4.2 Initial setting time 96
5.4.3 Net setting time 98
5.4.4 Degradation in water of cements: mass change 100
5.4.5 Inductively coupled plasma spectrometry 104
5.5 Dissolution testing: pH and conductivity 111
5.6 Cement setting by Fourier transformed infrared spectroscopy with attenuated total reflectance 114
5.7 Short term *in vitro* direct contact test 123
5.7.1 Washing protocol study: measurement of pH and conductivity 123
5.7.2 *In vitro* short term direct contact test: 45S5C4 cement and Serenocem™ 129
6 Discussion 133

6.1 Glass preparation 133
6.2 X-ray powder diffraction 134
6.3 Wavelength dispersive X-ray fluorescence 134
6.4 Differential thermal analysis 136
6.5 Scanning electron microscopy 139
6.6 Fourier transformed infrared spectroscopy with attenuated total reflectance 139
6.7 Preliminary study on cement preparation 141
6.8 Handling characterisation of cement pastes 143
6.9 Degradation in water of the cements: mass change 146
6.10 Inductively coupled plasma spectrometry 147
6.11 Dissolution testing: pH and conductivity 151
6.12 Cement setting by Fourier transformed infrared spectroscopy with attenuated total reflectance 153
6.13 Short term *in vitro* direct contact test 155
7 Conclusions 158
8 Future work 162
9 Appendix 179

List of Figures

Figure 2-1 Structural organization in bone showing from left to right the porous and compact bone, with the osteon as the basic unit, and on the right side, the organisation of bone structure at a micro level, with the bundles of collagen fibrils a calcium phosphate nanocrystals. Reprinted with permission from Hench (2005). Copyright 2005 Elsevier Books 4

Figure 2-2 A schematic drawing of bone remodelling *in vitro* a) osteoclasts resorb bone b) organic and inorganic matrix are dissolved with some collagen fibres remaining in the lacuna c) osteoblast-like cells degrade the remaining organic matrix, followed by new organic matrix synthesis d) final mineralisation by osteoblast like cells e) the cement line formation, which is the boundary of the osteon, is initiated after the osteoclastic bone resorption and continues after osteoblastic collagen removal. Reprinted with permission from Mulari *et al* (2004). Copyright 2004 Calcified Tissue International 7

Figure 2-3 Glasses system based on SiO_2-CaO-Na_2O and 6% P_2O_5 for bioactive glasses. The diagram delimits the compositional boundaries for bone bonding (A); non-bonding for glasses with low reactivity (B) and glasses with high reactivity (C); soft tissue bonding (S); and E for the Bioglass® composition. Reprinted with permission from Hench (2006). Copyright 2006 Journal of Materials Science Materials in Medicine. ... 12

Figure 2-4 Representation of the ionic exchange and reactions occurring at various levels on the glass surface, with the formation of Si rich layer and Ca-P rich layer in simulated body fluid (SBF). Reprinted with permission from Peitl *et al.*(2001). Copyright 2001 Journal of Non-Crystalline Solids..... 14

Figure 2-5 Relationship between the volume/enthalpy of a liquid and temperature, at a constant pressure and melting temperature. The slow cooling of the liquid produces a glass transition at Tga, while the faster cooling rate produces a glass at Tgb. Reprinted with permission from Debenedetti and Stillinger (2001). Copyright 2001 Nature..... 17

Figure 2-6 2D lattice representation of atomic structure for a) A_2O_3 crystal lattice b) A_2O_3 equivalent glass structure. Black circles correspond to the cation and white circles to the anion. Reprinted with permission from Zachariasen (1932). Copyright 1932 American Chemical Society..... 22

Figure 2-7 Structural distribution of SiO_4 tetrahedra showing a) three tetrahedra units and the bond angle (ß) between two neighbouring tetrahedra (Si_1-O_4-Si_2 angle) and b) the torsion angle α, formed between the Si_1-O_1 and the Si_1-Si_2 axes . Reprinted with permission from Wright *et al* (1980). Copyright 1980 Journal of Non-Crystalline Solids. 23

Figure 2-8. Bioactive glass structure showing the SiO_2 tetrahedra (Si: grey spheres, O: red spheres) and Q_2 units formed through depolymerisation of the glass with oxides such as Na_2O and CaO. The sodium (Na) is represented by the purple spheres; calcium (Ca) and strontium (Sr) are represented by the green spheres. The Na, Ca and Sr, occupy network modifier positions and depolymerise the glass network (some shown in black circles). Reprinted with permission from O'Donnell (2011). Copyright 2011 Acta Biomaterialia. Note: the black background in the original image was removed. 26

Figure 2-9 Configuration of phosphorus in the glass network as a network former entering the silicate network and forming Si-O-P bonds (a) and as isolated orthophosphates, showing one bond with a terminal oxygen, and the bond with either Ca or Na, the latter being the structure shown (b). Reprinted with permission from Elgayar (2005) Copyright 2005 Journal of Non-Crystalline Solids.....27

Figure 2-10 a) XRD pattern of crystalline silica known as cristobalite b) XRD pattern of vitreous silica. Reprinted with permission from Warren and Biscce (1938). Copyright 1938 Journal of the American Ceramic Society 30

Figure 2-11 Scanning electron microscopy images showing coarse and fine powders of a melt derived 45S5 glass. Reprinted with permission from Sepulveda (2011). Copyright 2001 Journal of Biomedical Materials Research Part A.....31

Figure 2-12 Schematic description of cements used in dentistry, according to the nature of the liquid component: with phosphoric acid, poly (alkenoic) acids and with eugenol. Adapted from Wilson (1978). 36

Figure 2-13. Phosphate based complexes formed due to ionisation of phosphoric acid in cements containing an aluminosilicate glass (Adapted from Wilson, 1978).....38

Figure 2-14 Schematic of glass particles surrounded by silica gel in the salt reacted matrix Griffin and Hill (1998). Reprinted with permission from Springer. Copyright 1998. Journal of Materials Science. 42

Figure 2-15. Setting reaction of a GIC showing the release of ions such as Ca^{2+}, Al^{3+}, F^{-} and PO_4^{3-} after acid attack from the poly (acrylic acid), with the formation of a siliceous gel coating around the reacted glass particles and the cement matrix formed by the polyacrylate salts Griffin and Hill (1998). Reprinted with permission of Elsevier. Copyright 1999. Journal of Biomaterials 42

Figure 2-16. Acrylic acid unit Adapted from Smith (1998) with permission from Elsevier 45

Figure 2-17 Attachment of stapes prosthesis to the long process of the incus using a glass ionomer cement Tysome and Harcourt (2005). Reprinted with permission of John Wiley & Sons. Copyright 2005. Journal of Clinical Otolaryngology 49

Figure 4-1 Glass melting stages showing a) high temperature melting of raw materials, (b) melt quenching in demineralised water (c) glass frit after quenching (d) glass powder preparation (e) sieving of the powder. Pictures are courtesy of Dr Hasan Merie 65

Figure 4-2 Cement disc preparation for preliminary assessment of cement stability (a) glass slab used for traditional mixing of dental cements, showing the powder mix (glass and PAA) and the liquid component (phosphoric acid solution and distilled water) (b) 4 x 1 mm cement samples let to set in a silicon mould (at 37ºC for one day) (c) sample immersed in distilled water for visual assessment of stability 66

Figure 4-3 Schematic of the content of poly (acrylic acid), % $H_3PO_{4\ sol}$ and powder/liquid (P/L) ratios tested for the second stage of the cement study. 66

Figure 4-4 Differential thermal analysis (DTA) general showing the direction of the exothermic and endothermic reactions Reprinted with permission from West (2014). Copyright 2014 John Wiley & Sons Ltd. 69

Figure 4-5. Differential thermal analysis curve showing the glass transition temperature (T_g.), and the positioning of the tangent lines used definition of the glass transition temperature, and the glass crystallisation temperature (T_p). Reprinted with permission of Clupper and Hench (2003). Copyright 2003 Journal of Non-Crystalline Solids. Headings were modified from the original picture to improve its reading. 70

Figure 4-6. SEM working principle. Reprinted with permission from West (2014).Copyright 2014 John Wiley and Sons Ltd. 70

Figure 4-7 Attenuated Total Reflectance infrared spectroscopy (ATR-IR) schematic Adapted from Ratner (1992) with permission from Elsevier. 71

Figure 4-8 Experimental setting for use of FTIR-ATR a) materials preparation for paste mixing b) detail of set up of the machine after pressure was applied onto the sample c) detail of the diamond tip in complete contact with the cement paste 72

Figure 4-9 Gillmore needle setting for measurement of initial and net setting time 73

Figure 4-10 Detail of Gillmore needle indenters a) 2 mm diameter indenter used to measure the initial setting time b) 1 mm diameter indenter used to measure the net setting time 74

Figure 4-11 Preparation of cement samples for investigation of mass change following immersion in water (n=4). Samples were set for one day at 37 °C before testing. 74

Figure 4-12 Storage container used for investigation of mass change in distilled water, with an example of a cement disc stable in water 75

Figure 4-13 Ion release measurement by ICP a) Spectro Ciros Vision machine b) Capillary in which the leachate is transferred to the internal chamber c) Detail of plasma flame 76

Figure 5-1 XRD diffraction patterns of melt derived glasses based on the SiO_2-Na_2O-CaO-SrO-P_2O_5 system. These patterns showed a characteristic amorphous halo with no apparent crystallisation peaks. The curves are positioned to show glasses with increasing SiO_2 content 81

Figure 5-2 Differential thermal analysis (DTA) curves showing the thermal degradation behaviour of the glasses based on the SiO_2-Na_2O-CaO-SrO-P_2O_5 system. The glass transition temperature, crystallisation peak (s) and melting temperature(s) are identified with T_g, T_{p1}/T_{p2} and T_{m1}/T_{m2} respectively. The curves are positioned to show glasses with increasing silica content 83

Figure 5-3 Scanning electron microscopy images of the melt-derived glasses. Powders were obtained by milling and sieving the glass frit; scale bar is 200 µm 86

Figure 5-4 Scanning electron microscopy images of the melt-derived glasses. Powders were obtained by milling and sieving the glass frit; scale bar is 20 μm 87

Figure 5-5 FTIR-ATR spectra of the melt-derived glasses based on the SiO_2-Na_2O-CaO-SrO-P_2O_5 system, showing the peaks corresponding to the C-O, Si-O-Si, Si-O-NBO, Si-O-2NBO and P-O vibrations.....89

Figure 5-6 Mixing time of cements (C4 formulation), measured from the start of mixing the power and liquid components until obtaining a visually homogenous paste. Pairs of cements with statistically significant differences ($p < 0.05$) are identified with brackets. Error bars= ± SD; n=4.....96

Figure 5-7 Initial setting time of cements (C4 formulation) and commercial product Serenocem™ measured using the Gillmore needle. The initial setting time was measured from the start of mixing until the time in which the lighter needle failed to make an indention on the surface of the cement. Error bars= ± SD; n=4.. 97

Figure 5-8 Net setting time for the cements (C4 formulation) and commercial product Serenocem™ measured using the Gillmore needle. The net setting time was measured from the start of mixing until the heavier needle failed to make an indentation the surface of the cement. The brackets show the compositions with statistically significant differences ($p < 0.05$) with a Games-Howell post hoc test. Error bars= ± SD; n=4. 99

Figure 5-9 Mass change of cement discs (9 x 2 mm) set for one day at 37ºC. The formulations corresponding to 45S5C4, 45S5Sr10C4, 49P9C4, 53P4C4 and Serenocem™ are shown after one hour, one day, one week, one month, two months and three months after immersion in distilled water. Error bars= ± SD; n=4.....101

Figure 5-10 Si ion release (mg/L) for cement discs (9 x 2 mm) set for one day at 37ºC, at one hour, one day, one week, one month and two months after immersion in distilled water. Values reported as negligible or not detected were assumed to be 0.0005. Error bars= ± SD; n=3 105

Figure 5-11. Ca ion release (mg/L) for cement discs (9 x 2 mm) set for one day at 37ºC, at one hour, one day, one week, one month and two months after immersion in distilled water. Values reported as negligible or not detected were assumed to be 0.0005. Error bars= ± SD; n=3. 106

Figure 5-12 Sr ion release (mg/L) for cement discs (9 x 2 mm) set for one day at 37ºC, at one hour, one day, one week, one month and two months after immersion in distilled water. Values reported as negligible or not detected were assumed to be 0.0005. Error bars= ± SD; n=3. 107

Figure 5-13 Na ion release (mg/L) for cement discs (9 x 2 mm) set for one day at 37ºC, at one hour, one day, one week, one month and two months after immersion in distilled water. Values reported as negligible or not detected were assumed to be 0.0005. Error bars= ± SD; n=3. 108

Figure 5-14 P ion release (mg/L) for cement discs (9 x 2 mm) set for one day at 37ºC, at one hour, one day, one week, one month and two months after immersion in distilled water. Values reported as negligible or not detected were assumed to be 0.0005. Error bars= ± SD; n=3. 109

Figure 5-15 Al ion release (mg/L) for cement discs (9 x 2 mm) set for one day at 37ºC, at one hour, one day, one week, and one month after immersion in distilled water. Values reported as negligible or not detected were assumed to be 0.0005. Error bars= ± SD; n=3. 110

Figure 5-16 pH variation for cement discs (9 x 2 mm) set for one day at 37ºC for the 45S5C4, 45S5Sr10C4, 49P9C4, 53P4C4 and Serenocem™ cements, at one hour, one day, one week, one month and two months after immersion in distilled water. Error bars= ± SD; n=4. 112

Figure 5-17 Conductivity (µs/cm) variation for cement discs (9 x 2 mm) set for one day at 37ºC for the 45S5C4, 45S5Sr10C4, 49P9C4, 53P4C4 and Serenocem™ cements, at one hour, one day, one week, one month and two months after immersion in distilled water. Error bars= ± SD; n=4. 113

Figure 5-18 FTIR-ATR spectra of 45S5C4 cement, showing the setting from the start of mixing to 60 min. The spectra of the parent glass, PAA and $H_3PO_{4\,(sol)}$ are included for reference 115

Figure 5-19 FTIR-ATR spectra of 45S5C4 cement corresponding to region A shown in Figure 5-18, with the main peaks observed for this area. Graphs are stacked for comparison purposes 116

Figure 5-20 FTIR-ATR spectra of 45S5C4 cement corresponding region B shown in Figure 5-18, with the main peaks observed for this area. Graphs are stacked for comparison purposes 117

Figure 5-21 FTIR-ATR spectra of 45S5Sr10C4 cement, showing the setting from the start of mixing to 60 min. The spectra of the parent glass, PAA and $H_3PO_{4(sol)}$ are included for reference 118

Figure 5-22 FTIR-ATR spectra of 45S5Sr10C4 cement corresponding region A shown in Figure 5-21, with the main peaks observed for this area. Graphs are stacked for comparison purposes 118

Figure 5-23 FTIR-ATR spectra of 45S5Sr10C4 cement corresponding region B shown in Figure 5-21, with the main peaks observed for this area. Graphs are stacked for comparison purposes 119

Figure 5-24 FTIR-ATR graph showing the setting of the 49P9C4 cement the start of mixing to 60 min. The spectra of the parent glass, PAA and $H_3PO_{4(sol)}$ are included for reference 120

Figure 5-25 FTIR-ATR spectra of 49P9C4 cement corresponding region A shown in Figure 5-24, with the main peaks observed for this area. Graphs are stacked for comparison purposes 120

Figure 5-26 FTIR-ATR spectra of 49P9C4 cement corresponding region B shown in Figure 5-24, with the main peaks observed for this area. Graphs are stacked for comparison purposes 121

Figure 5-27 FTIR-ATR spectra of 53P4C4 cement, showing the setting from the start of mixing to 60 min. The spectra of the parent glass, PAA and $H_3PO_{4(sol)}$ are included for reference 122

Figure 5-28 FTIR-ATR spectra of 53P4C4 cement corresponding to region A shown in Figure 5-27, with the main peaks observed for this area. Graphs are stacked for comparison purposes 122

Figure 5-29 FTIR-ATR spectra of 53P4C4 cement corresponding to region B shown in Figure 5-27, with the main peaks observed for this area. Graphs are stacked for comparison purposes 123

Figure 5-30 Variation of pH values for 45S5C4 discs (9 x 2 mm) pre-treated in 20 ml and 50 ml of distilled water. Error bars= ± SD; n=3. 124

Figure 5-31 Variation of conductivity values (µs/cm) for 45S5C4 cement discs (9 x 2 mm) pre-treated in 20 ml and 50 ml of distilled water. Error bars= ± SD; n=3. 125

Figure 5-32 Variation of conductivity values for 45S5C4 discs (4 x 1 mm) for the preliminary washing protocol carried out for the *in vitro* testing. The maximum conductivity registered for the distilled water was 20 µs/cm. Error bars= ± SD; n=4.. 126

Figure 5-33 Light microscopy images showing the wells with the 45S5C4 pre-treated and non-treated cement discs, and comparison with the tissue culture plastic (TCP) used as control. L929 mouse fibroblasts cells were seeded at 50,000 cells/well. Scale bar is 100 µm 127

Figure 5-34. Preliminary Presto Blue® results showing the % Fluorescence for the 45S5C4 pre-treated cements and the tissue culture plastic (TCP) used as control ($p < 0.05$). L929 mouse fibroblasts cells were seeded at 50,000 cells/well. Error bars= ± SD; n=4. 127

Figure 5-35 SEM images showing 45S5C4 pre-treated cements (from Figure 5-33) after nine days from cell seeding. The SEM images show one area of the disc surface with good cell coverage and attachment. L929 mouse fibroblasts cells were seeded at 50,000 cells/well 128

Figure 5-36 Fluorescence % results for the Presto Blue® cell viability test between 45S5C4 and Serenocem™ after one and two days . Discs (4 x 1 mm) were pre-set in dry conditions for one day at 37 °C and washed according to protocol described in section 4.4.1. Error bars= ± SD; n=9. 130

Figure 5-37 Light microscopy images after one day from cell seeding, showing the L929 cell distribution on the well plate (left row) and near the cement disc (right row); scale bar = 100 µm. 131

Figure 5-38 Light microscopy images after two days from cell seeding showing the L929 cell distribution on the well plate (left row) and near the cement disc (right row). Scale bar = 100 µm 132

List of Tables

Table 2-1 Types of tissue attachment with various materials used in research for medical applications. Reprinted with permission from Cao and Hench (1996). Copyright 1996 Ceramics International 9

Table 2-2 Characteristics of glasses and crystals. Adapted from Paul (1990) and Varshneya (2006) 15

Table 2-3 Decomposition reactions and temperatures during batch melting for raw materials used for fabrication of bioactive glasses 19

Table 2-4 Raw materials and glass preparation for bioactive glasses used in bone grafting and compositions used to prepare aluminium-free cements 20

Table 2-5 Reference values reported in the the literature for differential thermal analysis (DTA) of various bioactive glasses, indicating the particle size range, heating rate; and the glass transition temperature , crystallisation temperature T_{p1} (°C) and melting range T_{m1}, T_{m2} (°C) 32

Table 2-6 Bands positioning for silicate based glasses, corresponding to C-O, Si-O-Si, Si-O-Non-Bridging Oxygen (NBO) and P-O functional groups. 33

Table 2-7 Description of commercially available products based on the glass ionomer cement technology 41

Table 2-8. G-200 glass original composition (Wilson and Mclean, 1988) 44

Table 2-9. Summary of preparation parameters of aluminium free GICs, describing the use of additives, powder/liquid (P/L) ratios and characterisation regarding handling characteristics and in vitro testing 53

Table 4-1 Melt derived glass compositions (wt. %) with melting temperatures (°C) 63

Table 4-2 Melt derived glass compositions (mol %) with network connectivity (NC'). 64

Table 4-3 Cement matrix formulations with variation of P/L ratio, % H_3PO_4 in liquid component with constant percentage of PAA powder content in mixture (10.7% of total powder) 67

Table 4-4 Description of media and supplements added for L929 and MG63 cell line maintenance protocols.....78

Table 5-1 XRF data showing the composition values (wt. %) of the melt-derived glasses based on the SiO_2-Na_2O-CaO-SrO-P_2O_5 system. The data shown corresponds to one glass sample 82

Table 5-2 XRF data showing the difference (in wt. %) between the theoretical glass compositions and the XRF values (from Table 5-1). Wt. % differences were obtained by subtracting the theoretical compositions from the individual oxides from the XRF results. The data shown corresponds to one glass sample 82

Table 5-3 DTA results showing the glass transition temperatures, crystallisation temperatures (T_{p1} and $T_{p2)}$, and melting temperatures (T_{m1} and $T_{m2)}$ of the glasses based on the SiO_2-Na_2O-CaO-SrO-P_2O_5 system 83

Table 5-4 Cements combinations corresponding to samples stable in water (Type I). The mass of glass used to prepare the samples was 125 mg. 91

Table 5-5 Cement combinations corresponding to samples with reduced stability in water (Type II) All samples were prepared with a base glass of 125 mg 91

Table 5-6 Cement combinations corresponding to samples that dissolved in water (Type III). All samples were prepared with a base glass of 125 mg 92

Table 5-7. Games-Howell post hoc test p values for the initial setting times. Pairs with significant differences are marked with an asterisk 98

Table 5-8 Games-Howell post hoc test p values for net setting time. Pairs with significant differences are marked with an asterisk 99

Table 5-9 Post hoc test p values for mass change of the cements. Pairs with significant differences are marked with an asterisk. Levene's P value is shown under each time point. For $p<0.05$, a Games-Howell post hoc test is used; otherwise a Tukey's test was used. 103

Abbreviations

BO	Bridging oxygen
DTA	Differential thermal analysis
ENT	Ear Nose and Throat
ECM	Extra cellular matrix
FTIR-ATR	Fourier transformed infrared spectroscopy
GIC	Glass ionomer cements
ICP	Inductively coupled plasma
NBO	Non-bridging oxygen
NC	Network connectivity
P/L	Powder/Liquid
PAA	Poly (acrylic acid)
pHA	Precipitated hydroxyapatite
SBF	Simulated body fluid
SEM	Scanning electron microscopy
TCP	Tissue culture plastic
T_g	Glass transition temperature
T_m	Melting temperature
T_p	Crystallisation temperature
XRD	X-ray diffraction

1 Introduction

The replacement and repair of damaged and diseased tissue, signifies a continuous need for the development of materials with potential for clinical use. In the case of bone repair, the use of artificial or synthetic grafts is preferred due to their ease of availability and decreased risk of contamination. On this regard, research has been focused on materials that can mimic the basic structure of the tissue that is being replaced, or induce a biologically compatible cellular response when implanted.

Within this group of materials, bioactive glasses and specifically the 45S5 Bioglass® composition, designed by Larry Hench, was the first material to be catalogued as bioactive, due to its ability to bond to bone and soft tissues, by inducing the formation of an apatite layer chemically equivalent to natural bone. The fast degradation of this glass, associated with its high content of network modifier oxides (CaO and Na_2O) with respect to the network former (SiO_2), could represent an issue if the glass degrades faster than the rate in which the bone is formed. However, this is a property that was overlooked for cement applications where a rapid release of ions could be beneficial for the setting process.

Regarding the area of cements for medical applications, glass ionomer cements (GICs) have been used in dentistry as luting and restorative materials. Their beneficial properties include low exothermic reaction during setting, reduced shrinkage, ease of application and shaping after setting. These properties widened their scientific interest in orthopaedics and ENT (Ear Nose and Throat), with applications including reconstructions of bone defects (Engelbrecht *et al.*, 2000), fixation of the long process of the incus (Tysome and Harcourt, 2005), cochlear implants and mastoid surgery (Righini-Grunder *et al.*, 2015). The setting reaction of these cements is based on the acid base reaction between an aluminium containing fluorosilicate glass and a polyalkenoate acid, with the initial reaction involving the degradation of the glass, and release of aluminium (Al), calcium (Ca) and fluoride (F) ions, that crosslink with the ionised acid to form a cement matrix with embedded unreacted glass particles.

The use of GICs gained interest on the orthopaedic field as injectable pastes and as bone grafts. Nonetheless, long term limitations have been reported and attributed to the Al release, especially for ENT applications, where it was associated with Alzheimer's disease, and catalogued as a neurotoxin. Furthermore, an aluminium containing cement called SerenoCem granules (Corinthian Surgical Ltd., UK), was recently withdrawn from the market, due to its relation with bone reabsorption. The analogue cement capsules are still commercialised. However, GICs are currently contraindicated for applications requiring direct contact with nerves (Brook and Hatton, 1998) and cerebrospinal fluid due to concerns associated with their biocompatibility (Hurrell-Gillingham *et al.*, 2003). Therefore, all GICs formulations based on the traditional fluoro-aluminosilicate systems (SiO_2-Al_2O_3-CaF_2, SiO_2-Al_2O_3-CaF_2-$AlPO_4$ and SiO_2-Al_2O_3-CaF_2-$AlPO_4$-Na_3AlF_6) (Wilson and Mclean, 1988) present similar limitations. Previous research was aimed at substituting Al for ions that maintained the glass degradability and biocompatibility, such as iron (Fe), zinc (Zn), and magnesium (Mg). Nonetheless, these variations showed drawbacks such as restricted fabrication feasibility (Hurrell-Gillingham *et al.*, 2006), reduced metabolic activity and poor cell spreading for a range of $ZnCl_2$ content (Brauer *et al.*, 2011a), while Mg was reported to decrease the glass solubility and apatite formation (Diba *et al.*, 2012).

The applications of the 45S5 glass in the field of setting cements was previously studied by Mirvakily (2009). The resulting cement had a slow cement setting profile, however, it was found to be promising as a growth factor delivery medium and proven to be osteoconductive when implanted in rat femurs with no fibrous tissue formation four weeks after implantation. Nonetheless, this study was based on the 45S5 glass only and research was carried out with one cement formulation, with a focus on its biological response. Consequently, this research aims to prepare and characterise a series of glasses based on a SiO_2-Na_2O-CaO-SrO-P_2O_5 system, to evaluate their cement forming properties, and define the optimum parameters for further characterisation in terms of mass change, ion release, pH, conductivity, and in vitro response, as aluminium free cements for bone related applications.

2 Literature Review

2.1 Bone tissue

Tissues are an organised array of cells of embryonic origin, which function together to carry out specialised activities (Tortora and Derrickson, 2010) and these are classified according to their function in: epithelial, muscular, nervous and connective tissues.

Bone is a type of connective tissue, responsible for various basic functions comprising: deposition of additional matrix on free surfaces (Alberts, 2008), support of soft tissue (muscle, tendons, skin and ligaments among others), assistance for movement, mineral homeostasis, blood cell production and storage of adipose cells (Tortora and Derrickson, 2010).The two main constituents of bone within the connective tissue are specialised bone cells and the extracellular matrix (ECM). The specialised bone cells are osteogenic cells, osteoblasts, osteocytes and osteoclasts; and the ECM is formed by a viscous watery fluid that surrounds cells, containing a network of proteins and polysaccharides (Alberts, 2008;Martin and Hine, 2008).

The osteogenic cells are unspecialised stem cells, which develop into osteoblasts after cell division. The osteoblasts are fibroblastic cell types that deposit the bone matrix, by synthesizing and secreting collagen fibres and organic components that are required to build the ECM. By secreting newly formed matrix, the osteoblasts form a collagen based soft structure called osteoid, that are later converted into hard bone matrix by deposition of calcium phosphate. These osteoblasts, after being embedded in the hard matrix, do not undergo further division and are referred as osteocytes. The osteocytes are mature bone cells that occupy a small cavity called lacuna, from which cell processes radiate to form gap junctions with adjacent osteocytes. The function of these cells is related with the exchange of nutrients and waste with the blood. Finally, osteoclasts are large multinucleated cells that originate in the bone marrow. These cells release enzymes and acids at resorption sites, where they digest proteins and mineral components of the bone ECM (Alberts, 2008;Tortora and Derrickson, 2010). Additionally, the osteoblasts are responsible for signalling specialised proteins to recruit and activate other osteoclasts and regulate their activity, resulting in a balance between matrix deposition and erosion (Alberts, 2008).

The second component is the ECM, formed by a viscous watery fluid that surrounds cells, containing a network of proteins and polysaccharides. In bone tissue, the ECM is secreted by osteoblasts and assembled into an organised meshwork. It constitutes a scaffold to stabilise physical structures in the tissue, and has a role in the migration, proliferation, shape, and function of cells. There are two types of extracellular macromolecules in the ECM: the first ones are the glycosaminoglycans (GAGs) and proteoglycans, and the second ones are proteins of a structural (e.g. collagen) and adhesive nature (e.g. fibronectin and laminin) (Alberts, 2008;Martin and Hine, 2008).

Collagen is a structural fibrous protein, formed by 300 nm collagen molecules that appear as a banded fibril. As shown in Figure 2-1, collagen is organised in triple helix coils, which confers high tensile strength and flexibility to bone (Hench, 2005). There are almost thirty genetically unique types of collagen, with Type I being found in bone, tendons, and ligaments to maintain the integrity of the tissue (Salih and Thomas, 2013).

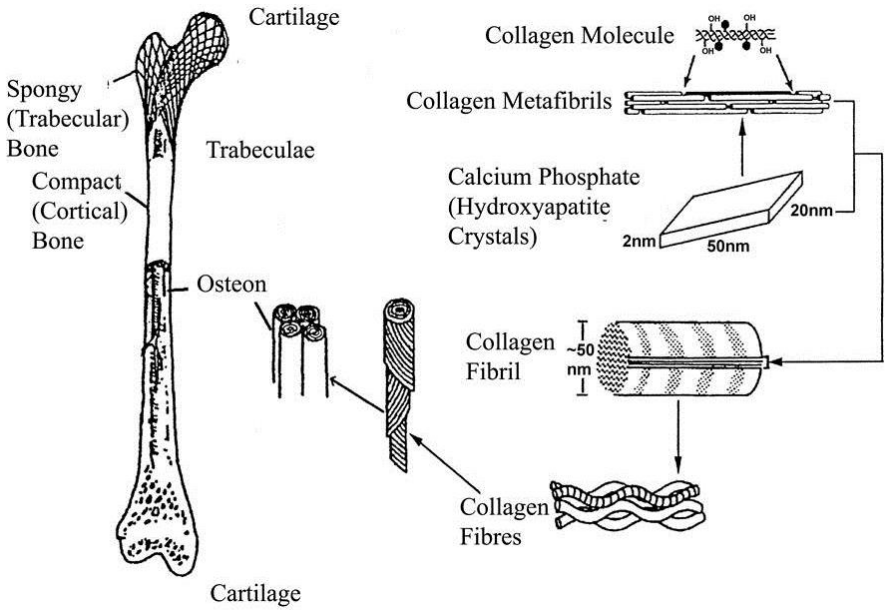

Figure 2-1 Structural organization in bone showing from left to right the porous and compact bone, with the osteon as the basic unit, and on the right side, the organisation of bone structure at a micro level, with the bundles of collagen fibrils a calcium phosphate nanocrystals. Reprinted with permission from Hench (2005). Copyright 2005 Elsevier Books

The crystallised inorganic salts deposited in the early bone matrix, are hydroxycarbonate apatite or HCA (Figure 2-1). These are formed during bone mineralization within and between the Type I collagen. Their composition is based on CaO, P_2O_5, and OH^- molecules, which results in the formation of hydroxyapatite, represented by the chemical formula $Ca_5(PO4)_3OH$. These crystals are aligned along the

axis of the collagen helix, where they reinforce the final composite. The different orientations of the HAp crystals, creates structural units called osteons, which confer the anisotropic properties to the bone (Hench, 2005b). In addition to bone, dentine and enamel are mineralised tissues, with enamel being the hardest substance found in the body, containing almost 97% of calcium phosphate salts in the form of large apatite crystals (Park and Lakes, 2007).

Figure 2-1, shows the two types of structures found in mature bone, differentiated by their porosity and mechanical properties. The first one is called cancellous bone (trabecular or spongy bone), which has a porous morphology and a low compressive strength that ranges between 2 and 12 MPa, and the second one is called cortical or compact bone. The compact bone is able to withstand higher compressive strengths varying between 100 and 230 MPa, due to its dense structure and the reinforcing effect of calcium phosphate crystals (Hench, 2005b).Bone tissue has the ability to remodel itself (Hench and Jones, 2005;Joon Bu and Park, 2007); though there are situations in which tissue replacement is required due to congenital defects, trauma, tumour removal or fractures. Therefore, the next section introduces the mechanism of bone repair and the use of biomaterials for bone tissue applications.

2.1.1 Bone repair

Bone repair is a continuous process where tissue is replaced due to a controlled resorption and deposition process. The remodelling occurs at different rates depending on the region, and it is caused either by a natural remodelling or due to repair of injured bone. This process starts by diverse factors such as: a fracture, unequal mechanical loading, physical exercise, and changes in diet (Tortora and Derrickson 2010). Any deviation in these mechanisms results on the formation of an excessively thick and dense bone or the loss of bone tissue, causing osteopetrosis or osteoporosis respectively (Alberts, 2008).

One of the causes for bone repair are fractures, which occur when the bone is broken down, either as a crack or as a complete breakage (Tortora and Derrickson, 2010). When this occurs, small diversions from the original position of the bone alter stress patterns that regulate bone remodelling through activation of homeostatic mechanisms. In areas where there is an increase of compressive forces, the rate of bone deposition increases. Conversely, in the areas where these forces decrease, the rate of bone deposition decreases relative to the rate of erosion (Alberts, 2008). The effect of

physical immobilisation in humans (decrease of applied force) causes bone loss and excretion of calcium and phosphorus. However, loading requirements of different bones might differ according to their function (Park and Lakes, 2007).

The remodelling process involves four stages: firstly, phagocytes that are cells that are able to engulf and break down debris (Martin and Hine, 2008), remove dead bone tissue, for chondroblasts to bridge the boundaries of the broken bone. The third stage involves the conversion of fibrocartilage to spongy bone by osteoblasts, while the damaged bone is absorbed by the osteoclasts. During remodelling, there are two key ions that are involved in the healing process: calcium (Ca) and phosphorus (P), although other factors such as magnesium (Mg), vitamins A, C, D and hormones are also involved (Tortora and Derrickson 2010). Calcium is mainly stored in bone, and as previously described, bone is involved in mineral homeostasis, by releasing Ca^{2+} in the blood through the action of osteoclasts or depositing it, by the action of osteoblasts (Tortora and Derrickson, 2010). Figure 2-2 shows the schematic drawing of the bone remodelling *in vitro.*

This natural bone remodelling process would be insufficient for its regeneration in cases where there is a need for repair, replacement, or augmentation. A replacement structure then becomes necessary when bone loses its function and structure due to age, trauma, disease, cancer or congenital defect (Bonassar and Vacanti, 1998;Hench and Jones, 2005).

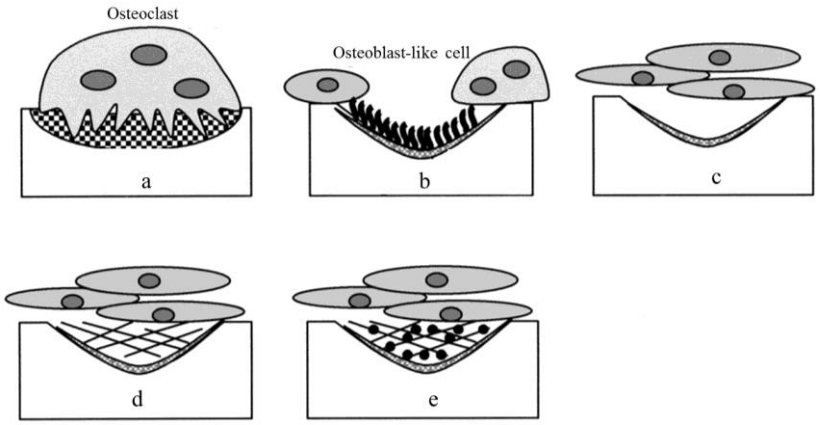

Figure 2-2 A schematic drawing of bone remodelling *in vitro* a) osteoclasts resorb bone b) organic and inorganic matrix are dissolved with some collagen fibres remaining in the lacuna c) osteoblast-like cells degrade the remaining organic matrix, followed by new organic matrix synthesis d) final mineralisation by osteoblast like cells e) the cement line formation, which is the boundary of the osteon, is initiated after the osteoclastic bone resorption and continues after osteoblastic collagen removal. Reprinted with permission from Mulari *et al* (2004). Copyright 2004 Calcified Tissue International

One of the alternatives for repair and replacement of tissues are transplants from a natural source. There are three types of transplants: autografts, homografts and heterograft or xenografts. Firstly, autografts correspond to those tissues harvested from the same patient to substitute another tissue or organ. Secondly, homografts, correspond to tissues transplanted from one patient to another, and lastly heterograft or xenografts, correspond to a transplant or tissue sourced from another species (e.g. porcine valves, demineralised bovine bone), to replace a tissue in a human patient. However, there are disadvantages associated with these transplants: amount of autologous tissue used without compromising the function at the donor site (Bonassar and Vacanti, 1998), potential rejection due to immunological response, limited supply (Hench, 2005), secondary effects due to immunosuppressive drugs and ethical considerations (Joon Bu and Park, 2007). Consequently, the use of synthetic materials to repair and replace damaged tissues, and specifically bone, is a key aspect in the medical field, due to their decreased risk of contamination (Hench, 2005), availability, reproducibility and reliability (Jones and Hench, 2001). Therefore, the next section provides a summary of synthetic materials to repair body tissues, known as biomaterials, and their classification according to the nature of the bone-implant attachment.

2.2 Biomaterials

The use of manufactured materials to repair body tissues was already in use since early civilizations: with Mayans using nacre teeth derived from sea shells, metallic dental implants dating 200 AD, and Egyptians using linen as sutures. Nonetheless, most implants developed before the 1950s had low success due to a limited understanding on biocompatibility and sterilisation techniques (Ratner *et al.*, 2004).

The post war era emphasised the necessity for replacement of diseased or damaged body parts, with the use of materials such as silicon, titanium, stainless steel, and polyurethane. Furthermore, some of the devices developed during this time included: intraocular lenses fabricated from Perspex poly (methyl methacrylate), hip prostheses, made from chrome-based alloys and stainless steel, dental implants fabricated from titanium, and vascular grafts made from nylon (Ratner *et al.*, 2004).

Later in the 1960's the first generation of materials designed for specific medical purposes were developed. Some examples include hydrogels for soft contact lenses and cell encapsulation, lactic-glycolic acid based polymers for sutures and for controlled release of proteins. Moreover, biomimetic materials were developed as a novel approach to simulate the natural tissues in the body. Within this group, hydroxyapatite (HAp)and Bioglass® are the most representative examples (Ratner *et al.*, 2004).

The term biomaterial has been associated with various fields, such as naturally derived fuels and substances that are produced by living organisms. However, Williams limited the definition of biomaterials as a health care related term as "a substance that has been engineered to take a form which, alone or as part of a complex system, is used to direct, by control of interactions with components of living systems, the course of any therapeutic or diagnostic procedure, in human or veterinary medicine" (Williams, 2009).

Biomaterials interact with the surrounding tissue by different mechanisms that are related mainly to their chemical composition and microstructure. As a result, biomaterials are divided in four types according to their implant-tissue attachment nearly inert, porous, resorbable and bioactive (Cao and Hench, 1996), as shown in Table 2-1

Table 2-1 Types of tissue attachment with various materials used in research for medical applications. Reprinted with permission from Cao and Hench (1996). Copyright 1996 Ceramics International

Type of implant	Type of attachment	Example
Nearly inert	Mechanical interlock (morphological fixation)	Metals, Al_2O_3, Polyethylene (PE)
Porous	Ingrowth of tissues into pores (biological fixation)	Hydroxyapatite (HAp), HAp coated porous metals
Resorbable	Replacement with tissues	Tricalcium phosphate (TCP) Polylactic acid (PLA)
Bioactive	Interfacial bonding with tissues (bioactive fixation)	Bioactive glasses, HAp Apatite-Wollastonite (A-W)

The nearly inert materials induce the formation of a fibrous layer that differentiates in an abnormal manner. These are not rejected by the body but exhibit a "micro-rejection" response at the implant-tissue interface (Hench *et al.*, 1971), due to the non-chemical/biological bond type (Cao and Hench, 1996). Materials within this group such as stainless steel, titanium alloys and cobalt alloys, are usually chosen due to their high mechanical properties, however, these are prone to corrosion from body fluids (Hench and Jones, 2005). Secondly, the group defined as porous, provide a biological fixation by ingrowth of tissue into the materials' pores, providing an interfacial fixation. However, these materials require the presence of pores with sizes over 100 μm, to allow blood supply into the ingrown tissue (Hench, 1991;Cao and Hench, 1996).

The third group corresponds to the resorbable materials, usually applied as bone graft substitutes, and typically manufactured as granules, porous blocks or hardening pastes. These materials are designed to disappear over time, through various mechanisms such as dissolution, conversion to an apatite or cell mediated resorption mechanisms. Examples of this group are ceramic or polymer based materials such as dicalcium phosphate (DCP), octacalcium phosphate (OCP), precipitated HAp crystals, chitosan and polycaprolactone (Bohner, 2010).

The fourth group corresponds to bioactive materials: the term bioactivity was formally introduced in the 1970s, with the development of the bioactive glasses and bioactive glass-ceramics that achieved direct bone bonding. Thus a material is considered bioactive when it "elicits a specific biological response at the interface of the material which results in the formation of a bond between the tissues and the material" (Cao and

Hench, 1996;Jones and Hench, 2001). The bioactivity is expressed by the formation of a hydroxyl carbonate apatite layer, with the stages for HAp layer formation in bioactive glasses further discussed in section 2.2.1

Hench and Wilson described two types of bioactive materials according with the rate of bone deposition that they elicit: Class A and Class B. Those materials catalogued as Class A, such as bioactive glasses, are osteoproductive, and can bond to both bone and soft tissue. This effect is due to the release of soluble Si, Ca, P and Na; that promote intracellular (due to ion release) and extracellular responses (e.g. by chemisorption of bone growth proteins) at the implant-physiological environment interface. Secondly, Class B materials such as Apatite-Wollastonite (A-W) ceramics and synthetic HAp refer to osteoconductive implants that have the ability to generate tissue growth along the implant surface, and promote bone migration along the interface through extracellular responses only (Cao and Hench, 1996;Oonishi *et al.*, 2000;Hench, 2006).

Thus far, this section has reviewed aspects associated with bone structure and function, bone tissue remodelling and synthetic materials used to replace and repair tissues. As previously described, bioactive glasses are catalogued as Class A materials through their ability to release ions involved in the formation of a Ca deficient HAp layer. Due to their relevance in the biomaterials field, bioactive glasses, specifically based on the 45S5 Bioglass® composition, have been used in a variety of medical applications as: filling of bone after tumour removal, spine fusion, facial reconstruction, alveolar ridge augmentation and sinus elevation (Hench, 2013). Therefore, the next two sections, review their use as biomaterials, and the principles associated with glasses regarding structure, composition, and characterisation techniques.

2.2.1 Glasses as biomaterials

The use of glass as a biomaterial was pioneered by Larry Hench with the discovery in 1969 of Bioglass® also called 45S5 glass, and it was the first material to be catalogued as bioactive. The composition of Bioglass® is based on a melt derived soda-lime silicate system composed of $45SiO_2$-$24.5Na_2O$-$24.5CaO$-$6P_2O_5$ wt. %. The nomenclature of the glass 45S5 refers to its composition by having 45 wt. % of SiO_2, and a Ca/P ratio of five (Hench *et al.*, 1971).

This glass was successfully translated to a clinical setting with the approval in 1985 of the Bioglass® Ossicular Reconstruction Prosthesis, aimed at replacing the bones of the

middle ear to treat conductive hearing loss (Hench, 2006). Current applications include fillers for periodontal defects, cysts, sinus elevation (PerioGlas®), dental putty, and the orthopaedic bone filler NovaBone® (NovaBone®, Alachua, USA). Additionally, Novamin® glass particles (Glaxo Smithkline, UK), are used in Sensodyne® Repair & Protect toothpaste, to treat tooth sensitivity by occluding the dentine tubules (Jones *et al.*, 2016). A variation of the 45S5 composition with a 10 mol % substitution over Ca is currently commercialised as StronBone™ (RepRegen Ltd., UK). This product is based on irregular shaped glass particles (100-700 μm) and its applications are related to its use in toothpaste, porous sintered scaffolds (Hill and Stevens, 2009), and grafting of alveolar sockets after tooth extraction (Hill *et al.*, 2014). Strontium substitutions in 45S5 based glasses, were reported to have little change in the chemical structure of the glass (Fredholm *et al.*, 2010), and to have a beneficial effect on bone remodelling, especially when substituted in a 10% mol basis, due to a balancing effect between the Sr influence and the negative effect attributed to pH increase for *in vitro* cell cultures (O'Donnell *et al.*, 2010).

In addition to the commercial products based on 45S5 glass, BonAlive® (BonAlive Biomaterials Ltd., Finland) is used as granules for hand and maxillofacial surgery, bone cavity filling, chronic osteomyelitis, and ENT surgery (Bonalive®, 2017). This product is based on the S53P4 glass composition ($53SiO_2$-$23Na_2O$-$20CaO$-$4P_2O_5$ wt. %), with initial research on this glass aimed at studying bone bonding when Al_2O_3 was not included to control the solubility of the glass (Andersson and Karlsson, 1991).

The clinical importance of bioactive glasses relies on their capacity to release ions that can be beneficial for medical applications: calcium and phosphorus due to their proven association with the formation of apatite (Pantano *et al.*, 1974;Andersson and Karlsson, 1991), fluoride in dental applications due to formation of fluorapatite (Brauer *et al.*, 2010), strontium for improvement of bone turnover (O'Donnell *et al.*, 2010;Hill *et al.*, 2014;Santocildes-Romero *et al.*, 2015), and zinc due to its role in bone formation and mineralisation (Brauer *et al.*, 2011a;Lakhkar *et al.*, 2013).Figure 2-3 shows the Bioglass® soda-lime silicate system (with 6 wt. % P_2O_5). In this diagram, Hench denoted six areas delimited by kinetic boundaries that correlated the glass compositions with the type of bone bonding. The “E area” corresponds to Bioglass®, having the compositional range with the highest level of bioactivity and rapid bone healing (Hench, 2006). This bonding ability is associated with the formation of a bioactive calcium deficient hydroxyapatite layer (HCA) *in vitro* and *in vivo*, on the glass surface in contact

with body fluid (Hench, 1991), and it is chemically similar to the mineral part of the bone (Arcos *et al.*, 2003). The "C area", with silica content between 52 % and 60 % exhibits slower bonding rates, while compositions in the B area, with more than 60 % silica, do not bond to bone and therefore are considered bionert (Hench, 2006). However, it is important to mention that these compositional ranges and bone-bonding mechanisms, are based on glasses prepared by a melt-quench route, since in 1991, it was shown that it was possible to prepare bioactive glasses with silica content over 60 wt. % via the sol-gel route (Hench, 2006).

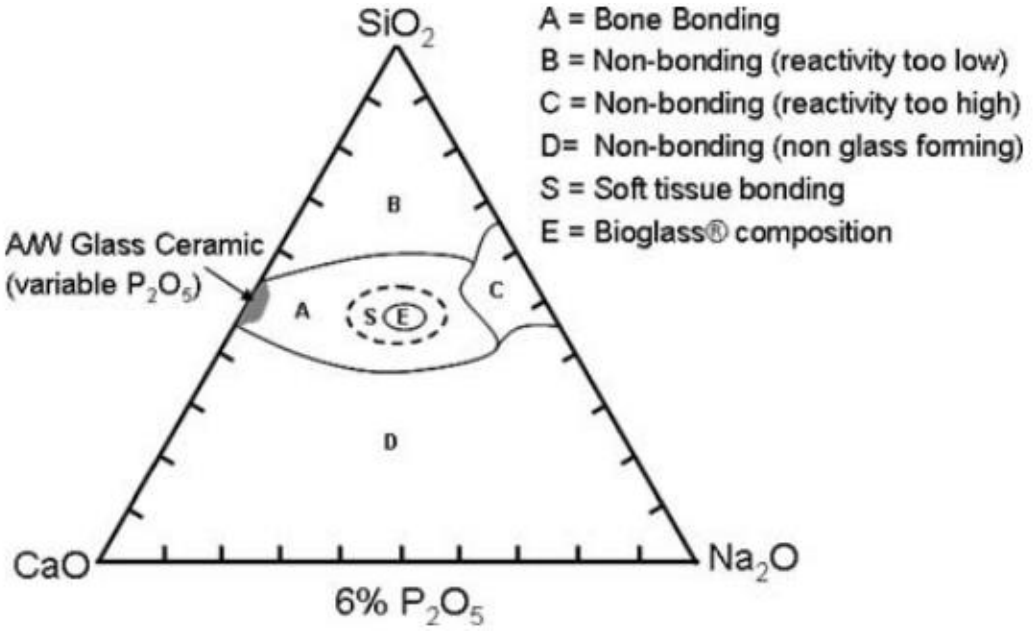

Figure 2-3 Glasses system based on SiO_2-CaO-Na_2O and 6% P_2O_5 for bioactive glasses. The diagram delimits the compositional boundaries for bone bonding (A); non-bonding for glasses with low reactivity (B) and glasses with high reactivity (C); soft tissue bonding (S); and E for the Bioglass® composition. Reprinted with permission from Hench (2006). Copyright 2006 Journal of Materials Science Materials in Medicine.

The development of a bond between a bioactive glass and bone was explained by a series of surface reactions that occur in the Bioglass® implant surface when it is exposed to an aqueous medium. These surface reactions are associated with the formation of an amorphous SiO_2 rich layer and the crystallisation of a CaO-P_2O_5 rich phase (Pantano *et al.*, 1974). This sequence of reactions is described in five stages (Hench, 2006)

Stage 1: this stage is diffusion controlled, and starts when alkali metal ions such as Ca^{2+} and Na^{+} are leached from the glass, allowing a rapid exchange with H^{+} available in the aqueous medium, producing the hydrolysis of silica groups from the glass and formation of Si-OH groups. The pH of the solution increases due to the replacement of hydrogen ions in the solution by the cations.

Stage 2: the hydrolysis of the silica groups, produce soluble $Si(OH)_4$ which migrate into solution. This stage is an interface controlled reaction dependant on time. The nucleation of a $CaO\text{-}P_2O_5$ layer occurs on the glass surface but growth proceeds by incorporation of Ca and P ions from body fluids and the glass network.

Stage 3 to 5: condensation and re-polymerisation of the Si-OH groups is expected to occur, generating a silica rich layer on the surface of the glass. Ca^{2+} and PO_4^{3-} ions migrate through the silica rich layer forming a $CaO\text{-}P_2O_5$ compound. This film crystallises by incorporating OH^- and CO_3^{2-} anions from the solution to form an HCA layer.

Finally, Hench proposed a stage associated with the biological response, which involves the adsorption and desorption of growth factors, leading to the proliferation and differentiation of osteoblasts and matrix mineralisation, with the presence of mature osteocytes in the collagen-HCA matrix (Hench, 2006).

Figure 2-4 shows a schematic of the CaP layer formation in simulated body fluid (SBF), which is a solution that contains inorganic ions in concentrations similar to blood plasma. The bulk glass dissolves by leaching soluble ions (Stage 1), causing the formation of a Si rich layer (Stage 2 and 3), migration of Ca^{2+} and PO_4^{3-} to the surface through the Si rich layer, which precipitate to form an amorphous $CaO\text{-}P_2O_5$ (Stage 4), and finally crystallises by incorporation of OH and CO_3^{2-} to form a mixed HCA layer (Stage 5) (Peitl *et al.*, 2001).

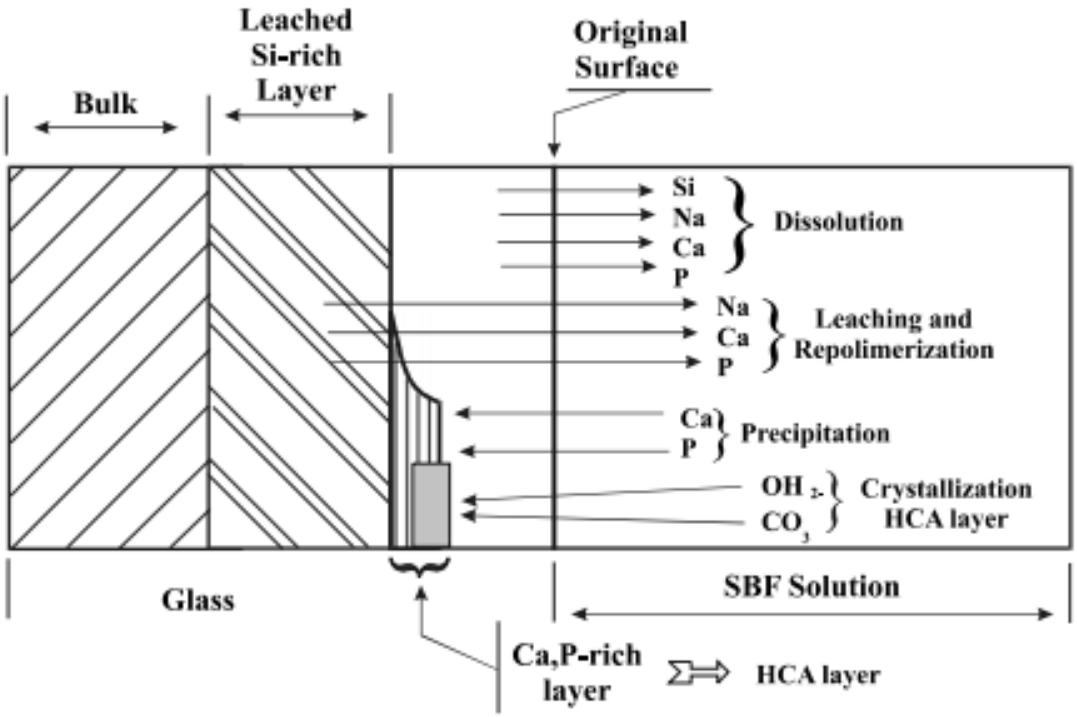

Figure 2-4 Representation of the ionic exchange and reactions occurring at various levels on the glass surface, with the formation of Si rich layer and Ca-P rich layer in simulated body fluid (SBF). Reprinted with permission from Peitl *et al.* (2001). Copyright 2001 Journal of Non-Crystalline Solids

The occurrence of these steps and the formation of a calcium phosphate layer were described as a requirement for a glass to bond to bone. Even though the presence of phosphate ions and dissolution of silica were suggested to have an important role in the formation of the apatite layer, Andersson and Karlsson, reported that a glass with 46 SiO_2 wt. % and no phosphate bonded to bone. In addition, the calcium phosphate formation was observed within the silica gel rather than occurring on top of it. In this work, it was suggested that Si has an active role in the formation of the calcium phosphate layer (Andersson and Karlsson, 1991).

The previous section described the importance of bioactive glasses for biomedical applications and their potential in applications requiring specific ion release. The adaptability of their chemical composition and its direct impact on their dissolution is closely related with their structure. Therefore, the following section describes how a glass is defined by its structure, properties and methods used in their fabrication.

2.3 Glass

Glass has been around human kind for thousands of years: in prehistoric times, volcanic derived obsidian natural glass was used to make knives and arrow tips (Zarzycki, 1991), in Egyptian civilization glazed stone beads and jewels for decorative purposes were made, and in the Middle Ages used for stained windows mainly for religious buildings (Varshneya, 2006). This long term interest in glasses that extends to present times is related to a variety of properties such as transparency, durability, formability and light transmittance (Shelby, 1997;Varshneya, 2006) that gives this material a clear advantage for applications in storage, lighting, insulation and fibres, among others (Varshneya, 2006).

The definition of glasses has evolved according to advances in its manufacture process. From a traditional point of view the Terminology for Glass and Glass Products ASTM standard defines a glass as "an inorganic product of fusion that has cooled to a rigid condition without crystallizing" (ASTM, 2015). However, nowadays, there are exceptions that do not comply with this definition: two well-known examples are the glassy metals and those produced by sol-gel, with the latter not requiring fusion of its components. For this reason the following definition by Varshneya was thought to address the limitations of previous descriptions, defining a glass as "A solid having a non-crystalline structure which continuously converts into a liquid upon heating" (Varshneya, 2016).

With respect to their structure, glasses have marked differences from crystals, due to their atomic distribution and isotropic properties (Paul, 1990), and as a result considered as "an extrapolation of the liquid state to lower temperatures" (Varshneya, 2006). On the other hand, glasses are similar to their corresponding crystal in terms of density, mechanical and thermal properties (Varshneya, 2006). In relation to this, Table 2-2 shows various characteristics that reference this dual nature of glasses.

Table 2-2 Characteristics of glasses and crystals. Adapted from Paul (1990) and Varshneya (2006)

Glass	Crystals
Glass transition range temperature (do not have a sharp melting point)	Defined melting point of the corresponding liquid
Do not have cleavage planes during fracture	Defined cleavage planes during fracture
Short range order	Short and long range crystallographic order
Fixed shape and volume after solidification, not adapting to the shape of the container	Fixed shape and volume after solidification, not adapting to the shape of the container

A fundamental property of glasses is the glass transition temperature or glass transition range. The glass transition range can be associated with the atomic arrangement in a glass: Zachariasen described very early on, that a glass is structurally inequivalent, for which the energy required to detach each atom in the network varies for each position. This heterogeneity would suggest that the breakdown of the network would not occur at a definite point, as it happens in a crystalline lattice, which rather results in a continuous phenomenon (Zachariasen, 1932) that defines the corresponding glass transition range.

Figure 2-5 represents the relationship between the Volume-Enthalpy and Temperature (V-T) between glassy, liquid, and solid states and therefore the energetic pathways in which crystalline and glassy materials form. From this diagram, Tg is the temperature at which the liquid and glass lines intersect, which occurs at approximately 2Tm/3, being Tm the melting temperature of the corresponding liquid (Debenedetti and Stillinger, 2001). Additionally, Tg is defined as the temperature at which the shear viscosity of the materials is very high at about 10^{12} Pa.s (Paul, 1990;Debenedetti and Stillinger, 2001). As a result, Tg is not a static property, meaning that for two glasses with the same composition and prepared by the same method, Tg can vary due to factors such as the cooling rate (Paul, 1990).

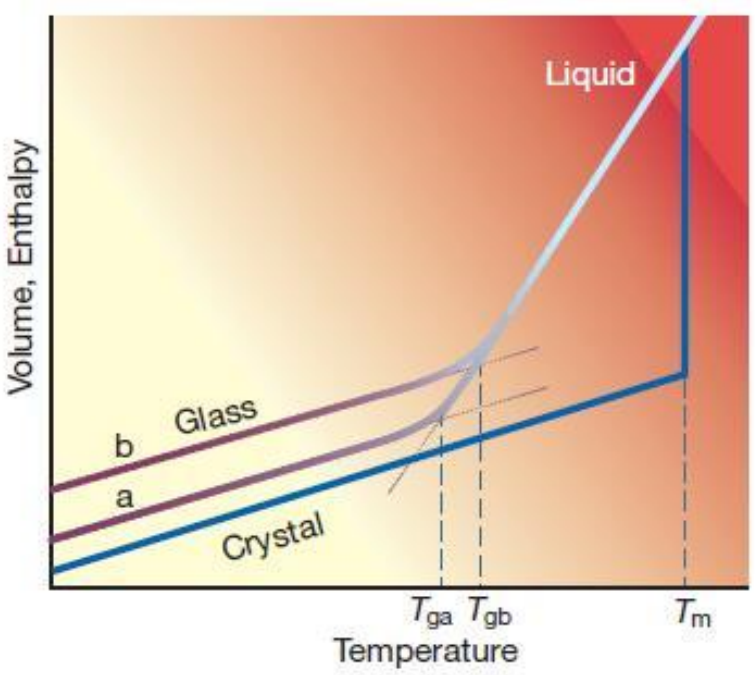

Figure 2-5 Relationship between the volume/enthalpy of a liquid and temperature, at a constant pressure and melting temperature. The slow cooling of the liquid produces a glass transition at Tga, while the faster cooling rate produces a glass at Tgb. Reprinted with permission from Debenedetti and Stillinger (2001). Copyright 2001 Nature

For crystalline materials, when the liquid is cooled down slowly enough, there is more time available for the system to have a periodic configuration, allowing nuclei formation and further crystallization at the melting temperature (T_m). At T_m, the volume decreases abruptly, allowing the material to contract at a constant cooling rate (Paul, 1990). At this point the equilibrium enthalpy is reached, generating a material with a characteristic cell unit that repeats throughout (Shelby, 1997). On the other hand, when a liquid is cooled rapidly enough, crystallization would not occur at T_m and the volume contraction would not take place along the dark blue line, but along the light blue line until T_g is reached. Below this point the liquid is transformed into a glass following a parallel cooling trajectory with respect to its corresponding crystalline structure. Slightly below T_g the volume will slowly decrease until the glass reaches a more steady condition known as stabilisation" (Paul, 1990). The cooling process occurs at a rate in which the enthalpy of the system decreases is faster than the rate in which the atoms are able to rearrange (Rawson, 1991;Shelby, 1997) forming a non-equilibrium system.

Another significant aspect to consider when describing glasses is their processing route. Glasses can be produced using various techniques such as: melting, sol-gel, vapour deposition, and bombardment of a crystal by high energy particles, among others. Nevertheless, some of these techniques are costly and specific for specialised glasses. As a result, the melting route for inorganic glasses is the most used method, especially for glasses of commercial interest, due to being highly effective in terms of cost and time (Varshneya, 2006). Hence, the section below, describes the glass melting process, commonly used raw materials and parameters for silicate based glasses, and specifically bioactive glass based compositions.

2.3.1 Glass melting

The melting technique consists of a batch preparation of raw materials, which usually decompose at high temperatures (>1200 °C) to obtain the required chemistry. The duration depends on the time required to obtain a homogeneous and crystal free melt. The final step corresponds to a rapid quenching of the melt (e.g. in water) to obtain a granular frit, or onto a mould to produce specific geometries (e.g. rods, blocks) (Shelby, 1997). The majority of the glass forming compounds are oxides, with examples of glass families being: vitreous silica (SiO_2), soda-lime silicates (Na_2O-CaO-SiO_2), borosilicates (alkalis-B_2O_3-SiO_2), lead silicate glasses (PbO-SiO_2) and aluminosilicates (MgO-CaO-Al_2O_3-SiO_2) (Varshneya, 2006).

For glass melting, the raw materials are classified depending on their purpose in the melt into glass former, flux and property modifier. A flux is the component added to lower the melting point of the glass former when this temperature is too high from a practical point. For silicate based glasses, SiO_2 melts at a temperature higher than 2000 ^{0}C, but with the addition of an alkali oxide such as Na_2O, the melting temperature can reach temperatures under 1600 ^{0}C. Property modifiers, usually alkaline earth and transition metal oxides such as aluminium are used to improve chemical stability of the glasses that contain a flux component (Shelby, 1997). In silicate glasses, CaO is added to improve chemical durability, since Ca-O bonds are stronger in the glass structure when compared with the Na-O bonds. Table 2-3, shows the raw materials commonly used to prepare bioactive glasses by the melt-quench route: SiO_2 was not included since it is directly added as silica (laboratory grade reagent powder or sand). Table 2-4 shows the reported parameters for glass melting of five compositions used for biomedical

applications, including the 45S5 and 53P4 glasses, and aluminium free compositions used for preparation of glass ionomer cements (GICs).

Table 2-3 Decomposition reactions and temperatures during batch melting for raw materials used for fabrication of bioactive glasses

Batch raw material	Decomposition reaction	Melting point (^{0}C)
Na_2CO_3	$Na_2CO_3 \longrightarrow Na_2O + CO_2$	850 (Paul, 1990)
$CaCO_3$	$CaCO_3 \longrightarrow CaO + CO_2$	775 (Shelby, 2005)
$CaHPO_4$	$2CaHPO_4 \longrightarrow P_2O_5 + 2CaO + H_2O$	>450 (Aldrich, 2015)
$SrCO_3$	$SrCO_3 \longrightarrow SrO + CO_2$	1494 (NIH, 2014)

Table 2-4 Raw materials and glass preparation for bioactive glasses used in bone grafting and compositions used to prepare aluminium-free cements

Application	Glass	Raw Materials	Glass preparation	Reference
Bioactive glasses	45S5	Not disclosed*	Batch melted in a platinum crucible at 1350-1450 °C and cast into a graphite mould (annealed at 450 - 475°C)	(Hench *et al.*, 1971) (Pantano *et al.*, 1974)
	45S5	Loch Aline sand $CaHPO_4$ $CaCO_3$ Na_2CO_3	Batch melted in a platinum crucible at 1350°C for 3 h using a rotatory platinum paddle (60 rpm). Glass was quenched in water and milled until particles sizes were <45µm	(Mirvakily, 2009)
	53P4	SiO_2 Na_2CO_3 $CaCO_3$ $CaHPO_4.2H_2O$	Batch melted in a platinum crucible at 1340 °C to 1410 °C for 2-3 h and casted into a preheated graphite mould, annealed and powdered into particle sizes ranging between 297-500 µm	(Andersson *et al.*, 1990)
	53P4	Belgium sand Na_2CO_3 $CaHPO_4$ $CaCO_3$	Powders were melted at 1360 °C for 3 h, casted into a mould and allowed to cool down to room temperature and used as dry ground powder (< 45µm)	(Salonen *et al.*, 2009)
Glasses for aluminium free GICs	Zinc containing glass	SiO_2 ZnO $CaCO_3$	Powders were mixed in a ball miller for an hour, dried in a vacuum oven (100 °C, 1 h). Pre-fired glass was transferred to a mullite crucible for firing at 1480 °C. Glass melt was quenched into demineralised water. The resulting frit was dried, ground and sieved (< 45 µm)	(Brauer *et al.*, 2011a)
	Iron containing glass	Loch Aline sand $CaHPO_4$ $CaCO_3$ Fe_2O_3 CaF_2	Glasses were melted in platinum crucibles at 1450 °C for 2 h using an electric heated box furnace. Glasses were powdered using a porcelain ball mill for 3 h. to obtain particles < 45µm	(Hurrell-Gillingham *et al.*, 2006)
	Borate containing glass	Na_2CO_3 $CaCO_3$ TiO_2 $AgNO_3$ H_3BO_3	Batch was melted in a platinum crucible at temperatures ranging 1000 and 1200 ^{0}C for 90 min in an electrical furnace. Melt was quenched onto a steel plate frit was crushed and powdered.	(Shen *et al.*, 2014)

*The paper corresponds to early work by Pantano, Clark, and Hench, and similarly to other literature by these authors within this time period, it was not possible to obtain the raw materials. Later work by Hench, was developed with commercially available 45S5 glass provided by U.S Biomaterials, and therefore processing is not disclosed

The next two sections describe the principles of structural theories of glass formation (Goldschmidt, Zachariasen, Smekal, and Sun), the kinetic theory, and role of network formers and modifiers on glass structure. These principles, associated with glass composition are relevant due to their influence of glass structure, bonding nature and variations in network modifiers, in the glass dissolution and therefore on cement setting.

2.3.2 Glass theory

Goldschmidt: the earliest theory about glass formation was developed by Goldschmidt, who proposed that the R_a/R_o (cation to anion) ratio in a glass forming substance of the A_mO_n form ranged between 0.2 and 0.4. Even though all ionic glass formers satisfy the rule, other compounds that comply with it, such as BeO, are not glass formers. (Zachariasen, 1932;Avramov *et al.*, 2003). For this reason, experts in the field such as Varshneya have described this theory as of historical interest only (Varshneya, 2006).

Zachariasen: the random network theory defines that the most important condition to produce a glass is that the "substance can form extended three dimensional network lacking periodicity with an energy content comparable with that of the corresponding crystal network" and also defines the following rules for glass formation (Zachariasen, 1932):

- "An oxygen atom is linked to not more than two atoms A", where A corresponds to the glass forming cation.

- "The number of atoms surrounding atom A must be small", determining trigonal or tetrahedral configurations

- "The oxygen polyhedron share corners with each other, not edges or faces," and for three dimensional networks, "at least three corners in each oxygen polyhedron should be shared." Figure 2-6 shows the difference between crystalline and glassy structures: crystalline geometries of a compound of the A_2O_3 form illustrates the maintenance of the bonding angles between the oxygen atoms and the adjacent silicon atoms. However, for the equivalent glassy structure, the bonding angles vary throughout the lattice.

This 2D lattice representation by Zachariasen (Figure 2-6) describes the structure of the silica glass. For this structure, the silicon is coordinated in a tetrahedral unit to four oxygens which function as connectors between each tetrahedral unit, and ultimately forms the polymerised glass network (Shelby, 1997). In the vitreous silica structure (Figure 2-7) the distortion is introduced in the network by the bond angle ß and torsion angle α_1. The bond angle (ß) is defined between the two neighbouring tetrahedra, and the torsion angle (α) is formed between the Si_1-O_1 and the Si_1-Si_2 axes (Wright *et al.*, 1980;Varshneya, 2006).

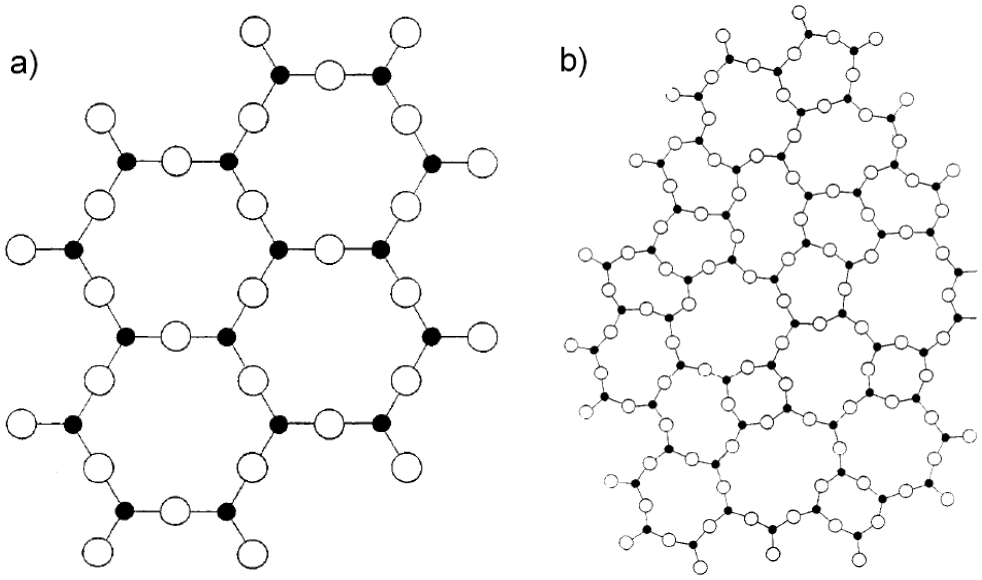

Figure 2-6 2D lattice representation of atomic structure for a) A_2O_3 crystal lattice b) A_2O_3 equivalent glass structure. Black circles correspond to the cation and white circles to the anion. Reprinted with permission from Zachariasen (1932). Copyright 1932 American Chemical Society

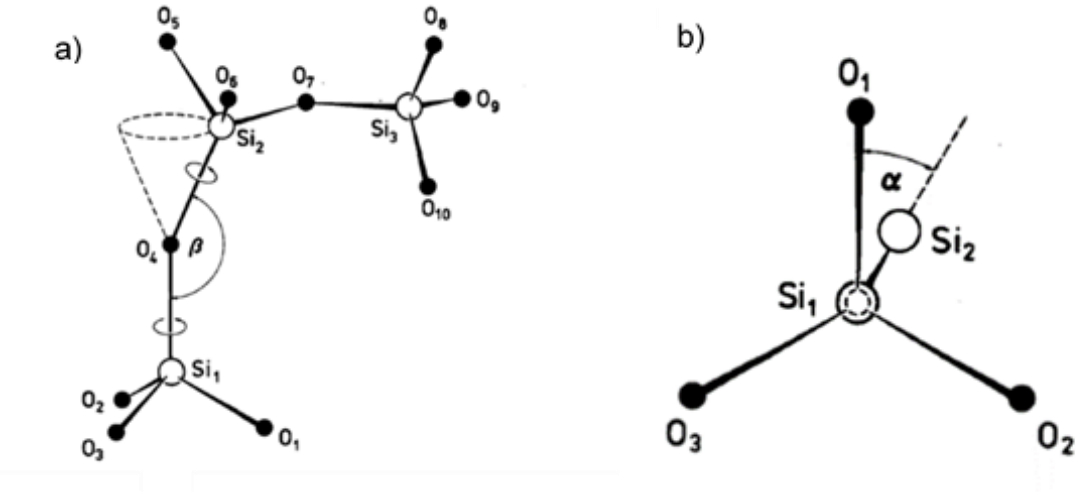

Figure 2-7 Structural distribution of SiO_4 tetrahedra showing a) three tetrahedra units and the bond angle (ß) between two neighbouring tetrahedra (Si_1-O_4-Si_2 angle) and b) the torsion angle *α*, formed between the Si_1-O_1 and the Si_1-Si_2 axes . Reprinted with permission from Wright *et al* (1980). Copyright 1980 Journal of Non-Crystalline Solids.

As mentioned above, various hypotheses exist to understand the parameters affecting the role of an oxide on glass formation. In this review, the mixed bond hypothesis (Smekal's theory) and single bond strength (Sun Theory) are briefly described, as several of its principles are used to classify the nature of the oxide's bonds and their classification into network formers, intermediates and modifiers, which will be discussed further in section 2.3.3.

Smekal's mixed bond hypothesis: described that compounds with purely covalent bonds were not able to form a disordered glass structure due to their defined bond lengths and angles, while purely ionic bonds lacked any directional characteristic. Thus, this hypothesis sustained that there were three required conditions for glass forming substances (Paul, 1990):

a) Inorganic compounds where bonds are covalent and ionic.

b) Elements that have "…chain structures with covalent bonds within the chain and Van der Waals' between the chains."

c) "Organic compounds containing large molecules with covalent bonds within the molecule and Van der Waals' forces between them."

Sun's single bond strength: this theory discusses the relation between the bond strength of the M-O single bond in an oxide of the M_mO_n form and its ability to form a glass.

This theory is based on the feasibility of atomic rearrangement before crystallisation in which oxides with higher bonding strength, and therefore higher heat of dissociation would have more probabilities of forming disordered networks. In this case, the rearrangement process during cooling is less dynamic due to the high energies required for bond breakage thus increasing the possibility of glass formation (Paul, 1990).

Sun's theory classified oxides as network formers or modifiers according to their bond strength energy: when this value exceeds 80 kcal/mol, the oxide is classified as a glass network former, and if this value is less than 60 kcal/mol, the oxide is classified as a glass network modifier. A new category was introduced by Sun for oxides with bond strength values between 60 and 80 kcal/mol, which was denoted as intermediate oxides (Varshneya, 2006).

Kinetics and thermodynamics barriers to glass formation: studies by Turnbull described that glass formers can be found in every group of the periodic table independently of their bonding type, whether it is covalent, ionic, metallic or governed by Van der Waals' forces. This led to a different approach on glass formation, in which not only factors such as coordination number, electronegativity and bonding energy were involved in glass formation. In this theory, additional factors such as cooling rate and nuclei density were considered, for which a more important condition for glass formation was to define the required cooling rate to avoid crystallisation. Subsequently, this formulation led Uhlmann to develop a time-temperature-% transformation diagram (T-T-T) that showed the boundaries in which it was possible to obtain a glass with the minimum volume of detectable crystallinity (Uhlmann, 1972).

2.3.3 Glass structure: network formers and modifiers

The ability of a material to form a glass depends on how fast it can be cooled down without undergoing crystallization, and glass former liquids are usually those which have very high viscosities at the melting temperature with exceptions found in systems such as the TeO_2-PbO (Paul, 1990). There is not a unique rule to classify the network formers, intermediates and modifiers, although various principles have been described in the literature:

-Network formers: also called glass formers, these are oxides that can form a glass by themselves. These also constitute the base for other glasses formed by a mixture of oxides. Examples of network formers are: SiO_2, P_2O_5, and B_2O_3

-Intermediates: these oxides correspond to cations with lower electronegativity, and have an ionic bond with oxygen. Consequently, these do not form glasses by themselves but can partially replace cations from the networks former group. These cations can reinforce the network when having a coordination number of four or loosen it when their coordination numbers are between six and eight. For example, alumina behaves as a glass former in aluminosilicate glasses and as an intermediate oxide in silicate glasses (Shelby, 1997).

-Network modifiers: these cations have very low electro negativities usually from Group I and II (alkaline and alkaline earth), and form highly ionic bonds with oxygen. Some examples include Na, Ca, Sr, and Ba. Due to their characteristic weak ionic bonding, they are very mobile and influence dissolution and reactions involving ion exchange (Rawson, 1991) by disrupting the Si-O-Si bonds and generating non-bridging oxygens (NBOs), specially Na, that has high diffusivity and is known to reduce the durability of the glasses (Murphy *et al.*, 2009).

Addition of network modifiers increase the availability of NBOs which decreases the connectivity number, creating a less polymerised structure that would potentially be more susceptible to dissolution when in contact with aqueous solutions. From a practical point of view, addition of these oxides, decrease the melting temperature of silica, and allows the preparation of glasses in a cost-effective manner. For example, replacing SiO_2 for Na_2O by 10 mol % reduced the T_g from ~1480 K in pure SiO_2 to ~800 K (Kerner and Phillips, 2000).

As previously mentioned in section 2.2.1, the Bioglass® composition is based on Si as the network former, Ca and Na as network modifiers and P is mostly found as an isolated orthophosphate. Figure 2-8 shows an example of a bioactive glass structure, in which the phosphate is not part of the silicate network and Sr is present as a network modifier; where the oxygens connecting the silica tetrahedra units, are called bridging oxygens (BOs).

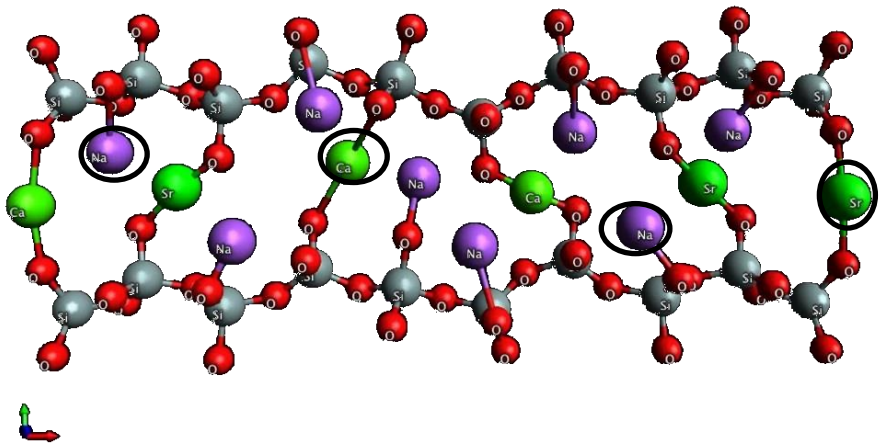

Figure 2-8. Bioactive glass structure showing the SiO_2 tetrahedra (Si: grey spheres, O: red spheres) and Q_2 units formed through depolymerisation of the glass with oxides such as Na_2O and CaO. The sodium (Na) is represented by the purple spheres; calcium (Ca) and strontium (Sr) are represented by the green spheres. The Na, Ca and Sr, occupy network modifier positions and depolymerise the glass network (some shown in black circles). Reprinted with permission from O'Donnell (2011). Copyright 2011 Acta Biomaterialia. Note: the black background in the original image was removed.

To describe the polymerisation degree of the glass network and therefore the average number of bridging oxygens per silica tetrahedron, a Q_n notation is used, where n=0…4; being Q_4 the structure corresponding to a glass network where the building blocks are silicon tetrahedra linked by four BOs (vitreous silica), and Q_0 consisting of isolated silica tetrahedra charge balanced by non-bridging oxygens. The Q_n model assumes that two types of units coexist in a glass, where the oxygens atoms are considered to be distributed between them (Shelby, 1997).

While the role of Si, Na, and Ca in a bioactive glass applies to the description of network formers and modifiers mentioned above, regarding the P_2O_5, there are two theories concerning its role in the glass. The first theory describes that phosphate enters the silicate network forming Si-O-P bonds, while the second describes that it forms isolated orthophosphate units, however, the distribution between the two was reported to be dependent on the glass composition (Figure 2-9). The orthophosphate theory in bioactive glasses (45S5) was described by Tilocca and Cormack (2007) through a Molecular Dynamics (MD) simulation model and by O'Donnell (2009) through a Nuclear Magnetic Resonance (NMR) study. The MD simulation showed that a combination of isolated orthophosphates (P-O-P) with Si-O-P bonds were present. It was suggested that P_2O_5 additions had two effects: removing Ca and Na ions that have a higher affinity to phosphate which re-polymerises the silicate network, and generates a less soluble glass. The second effect was described as an increase in the amount of free

orthophosphate groups that would improve the glass dissolution ability. However, the combined effect of the two mechanisms was reported to vary with composition (Tilocca and Cormack, 2007). Even though most phosphates are isolated in the 45S5 glass, for less bioactive compositions, these were found to be linked to one or even two silicon atoms (Tilocca, 2010). Additionally, NMR studies by O'Donnell (2009) on a glass series that maintained the Na_2O/CaO ratio constant showed an increase of Q_3 units and a decrease of Q_2 units when the phosphate content was raised, which also indicated an increase in the polymerisation of the glass, as described by Tilocca and Cormack (2007).

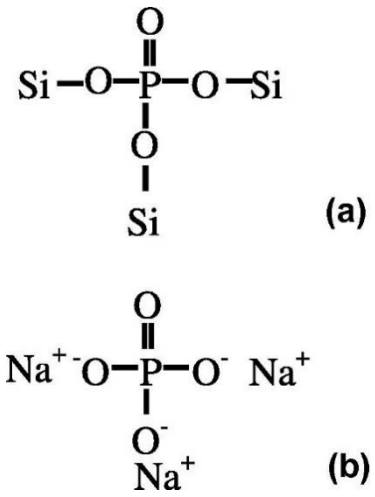

Figure 2-9 Configuration of phosphorus in the glass network as a network former entering the silicate network and forming Si-O-P bonds (a) and as isolated orthophosphates, showing one bond with a terminal oxygen, and the bond with either Ca or Na, the latter being the structure shown (b). Reprinted with permission from Elgayar (2005) Copyright 2005 Journal of Non-Crystalline Solids.

2.3.4 Theoretical glass structure

The connectivity number, which represents the polymerisation degree of a glass, was described by Shelby (1997), as the average number of bridging bonds per network unit (Shelby, 1997). In bioactive glasses, a comparable number defined as network connectivity (NC), was used by Hill to describe a supplementary explanation for the Bioglass® degradation mechanism (section 2.2.1), by associating this parameter to the glass ability to degrade *in vitro* (Hill, 1996), and it has been reported as an indication of the glass network structure in aluminium free cement studies (Wren *et al* 2012;Wren *et al* 2013; D'Onofrio *et al* 2016).

In a similar manner to the Q_n structure and the network connectivity (NC) previously described in section 2.3.3, this criterion applies for bioactive glasses, where a value of two corresponds to a linear polymer chain, and a value of four corresponds to a pure silica glass. For calculation of the NC, Hill described the following structural assumptions:

-Si^{4+} is coordinated by four oxygens in tetrahedral configuration.

-Structure homogeneity is assumed and consequently, the connectivity number is an average value of the bulk glass.

-P^{5+} is in the glass network in a tetrahedral configuration, in which one of the oxygens has a terminal bond with phosphorus.

After consideration of these structural assumptions, the NC reported for the 45S5 glass was 1.90 with other bioactive compositions having NC values between 1.87 and 2.60 (Hill, 1996), with a value close to two being optimum for the glass surface to induce apatite formation (Hill and Brauer, 2011). As described in the previous section, when phosphorus is considered to form isolated orthophosphates (O'Donnell and Hill, 2010), the glass polymerisation increases due to a preference of Na and Ca to charge balance the P units, with the network connectivity referred as NC'. Thus, 45S5 glass NC' value, described in the equations below, increases to 2.12 (Sriranganathan *et al.*, 2015).

Hill suggested that the dissolution of a glass with this NC would not require the hydrolysis of the silica (Si-O-Si) groups (stage 2) as proposed by Hench's model, and that the presence of phosphate groups would react more readily due to their higher solubility in water. Nevertheless, two glasses reported as AlP1S10 and S52P3, both with a NC of 2.47, were described as bioactive and non-bioactive respectively. The author then suggested that this criterion could be used as a guidance to formulate bioactive glass compositions instead of a definite theory, since small compositional and ionic species variations would influence differently the rate of apatite deposition *in vitro*, and *in vivo* (Hill, 1996).

Other authors also considered the linkage between the bioactivity of the glass and its ability to degrade in the body (Serra *et al.*, 2003;O'Donnell *et al.*, 2010;Jones and Clare, 2012). Indeed, Hench highlighted in his early work the importance of SiO_2 as a network former that decreased the solubility of other ions and provided the required stability to the system (Hench *et al.*, 1971). Therefore, an important consideration would

be to produce glasses with a NC' value that is low enough for the glass to be able to dissolve and release therapeutic ions, but that is high enough to remain structurally stable to allow bone tissue regeneration.

The equations below are used to calculate the NC': the BO term represents the total fraction of bridging oxygens per network forming oxide (SiO_2); the NBO corresponds to the total fraction of non-bridging oxygens per network modifier ion (Ca, Na, Sr), and the G term is the total fractional number of glass forming units (SiO_2) (Hill, 2011).

$$\mathrm{NC}' = 2 + \frac{\mathrm{BO} - \mathrm{NBO}}{\mathrm{G}}$$

Where BO is

$$\mathrm{BO} = 4\mathrm{SiO}_2$$

NBO is

$$\mathrm{NBO} = 2\mathrm{CaO} + 2\mathrm{Na}_2\mathrm{O} + 2\mathrm{SrO} + 2\mathrm{P}_2\mathrm{O}_5 3$$

And G is

$$\mathrm{G} = \mathrm{SiO}_2$$

With all the quantities referred in mol percent.

Thus far, this section has reviewed the glass structure and the role of oxides in the 45S5 Bioglass® composition. The next section contains a summary of the techniques used for glass characterisation: definition of the theoretical glass structure, X-ray diffraction (XRD), differential thermal analysis (DTA) and Fourier transformed Infrared spectroscopy with attenuated total reflectance (FTIR-ATR). These techniques were used to characterise the melt-derived glasses, for comparison with results in the literature, and as a starting point for the study of the bioactive glass based cements.

2.4 Glass characterisation

2.4.1 X-ray diffraction

X-ray diffraction (XRD) is a characterisation technique used to distinguish the presence of peaks, representing crystalline phases, which could delay ion release and therefore cement setting.

The absence of peaks in the XRD patterns for glassy materials is well known and associated to their short range atomic order. As an example, Figure 2-10 (a) shows the XRD pattern of crystalline silica, known as cristobalite. In contrast, Figure 2-10 (b) illustrates vitreous silica, in which the main peak occurs as a "broad hump", since glasses do not generate a coherent Bragg's interference (Varshneya, 2006).

Early works in silicate glasses by Warren and Biscce, defined the vitreous silica as a continuous random network, in which the "crystal" size was in order of a few Ångströms. In addition, the authors noted that the main peak in the cristobalite pattern was located in a similar position to the main peak of vitreous silica, due to both structures being based on silica tetrahedra geometries (Warren and Biscce, 1938). In an aluminium free glass based on the SiO_2-P_2O_5–CaO-CaF_2-Na_2O system, this peak was similarly described as a broad hump located between 29 and 35º2Θ (Brauer *et al.*, 2011b).

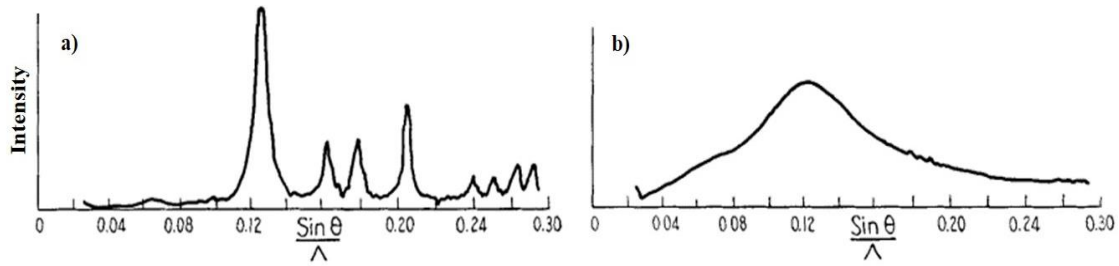

Figure 2-10 a) XRD pattern of crystalline silica known as cristobalite b) XRD pattern of vitreous silica. Reprinted with permission from Warren and Biscce (1938). Copyright 1938 Journal of the American Ceramic Society

2.4.2 Scanning electron microscopy

Scanning electron microscopy (SEM) is a technique frequently used to characterise glass particle size and morphology. For melt derived glass powders, it is standard to obtain particles with angled and irregular shapes, and a combination of coarse, medium,

and fine sizes. For example, Sepulveda *et al*. (2001) described the morphology of melt derived commercial powders by SEM (Figure 2-11). This study, showed a size distribution with these size ranges and with fine particles forming agglomerates. Additionally, the surface of the particles was described to be smooth and non-porous with small defects. The presence of agglomerates was attributed to Van der Waals forces, and a characteristic feature of the milling method used to reduce the particle size of the frit.

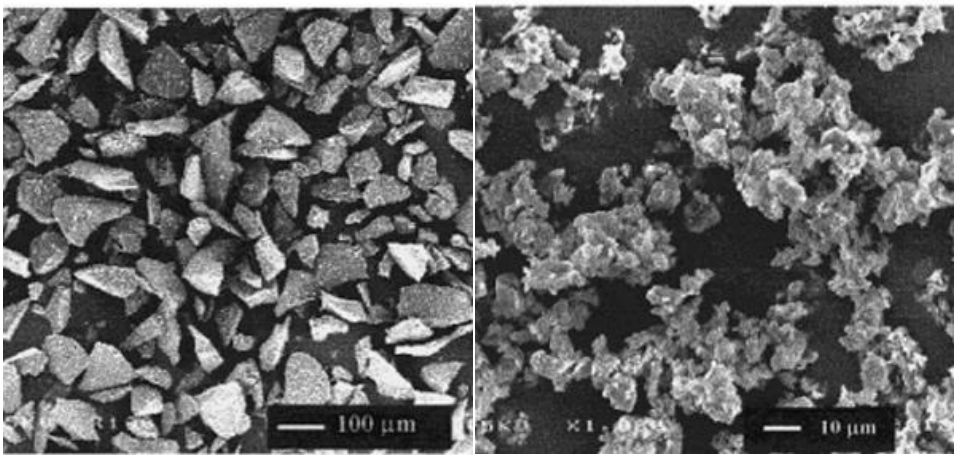

Figure 2-11 Scanning electron microscopy images showing coarse and fine powders of a melt derived 45S5 glass. Reprinted with permission from Sepulveda (2011). Copyright 2001 Journal of Biomedical Materials Research Part A

2.4.3 Differential thermal analysis

Differential thermal analysis (DTA) is a useful technique to define thermal features of glasses: glass transition temperature, crystallisation, and melting temperatures, and these are used to determine sintering and annealing temperatures for glasses requiring further thermal treatment, and/or to confirm that the thermal behaviour of the experimental glasses is comparable to those reported in the literature.

This technique is used to evaluate thermal changes with a continuous increase in the temperature, in which an endothermic peak corresponds to a bond breaking event such as the glass transition range (T_g) and melting (T_m). In contrast, an upward or exothermic peak corresponds to a bond forming event such as the crystallisation of a phase (T_p) (O'Donnell, 2012). These values vary depending on parameters such as: heating rate, particle size and rate of cooling. For example: as heating rate increases, T_g and T_p shift towards higher temperatures (Bretcanu *et al.*, 2009), T_p varies for fine powder (<45 µm)

compared to coarse powder (300-500 µm), while the peak intensity and broadness are related to the crystallisation mechanism (Massera *et al.*, 2012a).

For soda lime silicate glasses, devitrification starts around 580-650 °C, which is approximately 100 °C below the glass transition temperature. Vedel *et al*. described that bioactive glasses that devitrify at low temperature, mainly formed sodium calcium silicate crystals, and glasses with higher T_g, typically crystallised as Wollastonite ($CaSiO_3$). The high tendency for devitrification of soda lime silicate glasses such as the 45S5 and 53P4 compositions, prevents their use as fibres and other applications that require sintering, thus alternative compositions such as the 13-93 ($54SiO_2$-$6Na_2O$-$22.1CaO$-$7.9K_2O$-$7.7MgO$-$1.7P_2O_5$ mol. %) were developed for drawing continuous fibres (Vedel, 2007). Table 2-5 shows the reported values in the literature (glass transition, crystallisation and melting range) for various bioactive silicate glasses

Table 2-5 Reference values reported in the the literature for differential thermal analysis (DTA) of various bioactive glasses, indicating the particle size range, heating rate; and the glass transition temperature , crystallisation temperature T_{p1} (°C) and melting range T_{m1}, T_{m2} (°C)

Glass composition	Particle size (µm)	Heating rate (°C/min)	Tg (°C)	T_p (°C)	T_{m1},T_{m2} (°C)	Reference
45S5	20-63	10 °C/min	560	720	1100 1250	(Chatzistavrou *et al.*, 2004)
	≤ 38	10 °C/min	538	736	1190 1275	(O'Donnell *et al.*, 2010)
	≤ 45	10 °C/min	525	682	Not specified	(Santocildes-Romero *et al.*, 2015)
	≤ 45	15 °C/min	552	715	1180 1248	(Massera *et al.*, 2012a)
45S5Sr10	≤ 38	10 °C/min	525	729	1145 1259	(O'Donnell *et al.*, 2010)
53P4	≤ 45	15 °C/min	561	748	Not specified	(Massera *et al.*, 2012a)
	300-500	Not specified	547	796	Not specified	(Massera *et al.*, 2012b)
ICIE1	≤ 45	10 °C/min	513	629 676	> 1200	(O'Donnell *et al.*, 2008)

2.4.4 Fourier transformed infrared spectroscopy with attenuated total reflectance

Fourier transformed infrared spectroscopy with attenuated total reflectance (FTIR-ATR) is a technique used to evaluate the bonding environments of the constituent atoms. Understanding the atomic bonding environment of the parent glass is of importance because it indicates the degree of polymerisation of the glasses and its association with

the network connectivity number. Additionally, it allows identifying changes in the Si-O-Si and Si-O-NBO functional groups with compositional changes in the glass (Serra *et al.*, 2002).

Table 2-6 presents the values corresponding to the assigned peaks for the characteristic vibrations reported for bioactive glasses. The dominant bands correspond to the silica tetrahedra (Si-O-Si), and the Si-O-non bridging oxygen (Si-O-NBO), due to the presence of network modifiers (Na, Ca, and Sr) that disrupt the glass network.

Table 2-6 Bands positioning for silicate based glasses, corresponding to C-O, Si-O-Si, Si-O-Non-Bridging Oxygen (NBO) and P-O functional groups.

Peak region	Description	References
~1500	C-O	(Cerruti *et al.*, 2005) (Massera *et al.*, 2012b) (Massera and Hupa, 2013)
~1040	Si-O-Si	(Sepulveda *et al.*, 2002) (Serra *et al.*, 2003) (Young *et al.*, 2004) (Massera *et al.*, 2012b)
~940	Si-O-NBO	(Serra *et al.*, 2003) (Cerruti *et al.*, 2005) (Massera *et al.*, 2012b)
~700-800	Si-O-Si	(Cerruti *et al.*, 2005)
~500	Si-O-Si	(Jones *et al.*, 2001) (Sepulveda *et al.*, 2002) (Cerruti *et al.*, 2005) (Massera and Hupa, 2013)
~500-400	P-O	(Jones *et al.*, 2001) (Sepulveda *et al.*, 2002)

The present section reviewed the use of artificial grafts as biomaterials and their role in bone repair of damaged and diseased tissues; and the applications of bioactive glasses based on Hench's 45S5 composition for bone grafting. Furthermore, glass structure and fabrication was presented to have an overview on how structure and composition are closely related to the glass dissolution and bioactivity, in addition to the potential that this material has, with variation of network modifiers, to aid dissolution and release of biologically beneficial ions. In the following section, a review on cements used as biomaterials is presented, with emphasis on glass ionomer cements, and previous research on aluminium free glass ionomer cements.

2.5 Cements used as biomaterials

2.5.1 Poly (methyl methacrylate)

Poly (methyl methacrylate) (PMMA) bone cements are a two component system composed of a polymer and a liquid monomer. It was originally developed for dental applications, but widely used in joint replacement surgery. John Charnley successfully developed a technique to use PMMA in total hip replacement surgery, defining PMMA as an acrylic based bone cement (Wang and Dunne, 2008). Charnley initially described PMMA as a cold curing cement that is mixed by adding the liquid to the powder, until a dough is formed, with the cold curing being a exothermic reaction, with no danger to living tissue (Charnley, 1960). However, a few drawbacks were associated in the long term: a histological study associated the presence of macrophages with PMMA, either as a solid or as debris, with a link between the fibrous tissue and the proportion of macrophages present at the interface (Freeman *et al.*, 1982). Similarly, bone death was correlated with the generation of wear particles that cause aseptic loosening (Kenny and Buggy, 2003;Wang and Dunne, 2008), while high heat evolution during polymerisation was associated also with bone necrosis (Revell *et al.*, 1998).

2.5.2 Calcium phosphates cements

Calcium phosphate cements (CPCs) were firstly researched by Brown and Chow in the mid 1980's (Bohner, 2000) with the development of a calcium phosphate and phosphoric acid based composition used as a dental cement with remineralisation properties (Brown and Chow, 1986). CPCs consist on mouldable self-setting paste, which have been used in treatment of osteoporotic fractures, maxillofacial bone substitutions and vertebroplasty (Ginebra *et al.*, 2010).

These cements have an acid and a basic component, which after mixing result in one or more by-products (Khashaba *et al.*, 2010), and can be prepared by precipitation from an aqueous solution at room temperature, or by thermal reactions at high temperatures (Bohner, 2000). Precursors for calcium phosphate cements include dibasic calcium phosphate dehydrate (DCPD), tetracalcium phosphate (TTCP), alpha tri-calcium phosphate (α-TCP) and hydrated calcium phosphate ($CaHPO_4$) (Ginebra *et al.*, 2010). These components can be mixed with water and additives such as citric acid, which depending on the pH of the reaction, form brushite (DCDP) or precipitated hydroxyapatite (pHA) (Ginebra *et al.*, 2010): brushite is formed at pH values lower than 4 (Hofmann *et al.*, 2006) and pHA at pH values higher than 4.2 (Ginebra *et al.*, 2010);

resulting in structures that differ in crystallinity and resorption rates (Van der Stok *et al.*, 2013).

The setting reaction consists of a repeated dissolution and precipitation process, allowing the material to harden and gain mechanical strength through successive crystal entanglement. CPCs are highly biocompatible due to their calcium carbonate based composition and structure which imitates the bone mineralised tissue (Ginebra *et al.*, 2010). However, resorption rates are difficult to control due to the complex pH dependant chemistry and handling and preparation for clinical applications is also complex.

Various examples of commercially available calcium phosphate cements are: Bonesource® (Stryker), Calcibon® (Biomet), and ChronOS Inject™ (Depuy Synthes). The compressive strength of these cements is characteristic of ceramics and values are within the range of the trabecular or porous bone, varying between 1 MPa and 34 MPa (Van der Stok *et al.*, 2013)

Having briefly described the PMMA based cements and CPCs, the next section covers cements traditionally used in dentistry as bonding and filling agents such as: zinc phosphate cements, zinc polycarboxylate cements, dental silicate cements, and finally glass ionomer cements (GICs).

2.6 Cements in dentistry

Dental cements are used to attach crowns to teeth, line cavities for protection of dental pulp and for direct filling of cavities. The cement hardening is based on the reaction between a powder and a viscous hydrogen bonded liquid, forming a plastic paste that sets to hard salt like gels. The powder component, such as zinc oxide and aluminosilicates is a slightly basic substance which acts as a proton receptor; whereas the liquids are water based or organic compounds acting as acids or proton donors. The use of cements for dental applications requires four preferred properties: good handling properties in surgery, ability to harden after application, adherence to the tooth surface, and chemical resistance to the acids derived from sugar associated bacteria (Wilson, 1978). According to the main oxide component in the powder and the acid, dental cements were developed and classified: Figure 2-12 shows a general scheme of dental cements based on the aqueous component and the main oxides in the glass: with

phosphoric acid, with poly (alkenoic) acids and with eugenol. The next subsections further explain the first two groups due to their relevance for the present research.

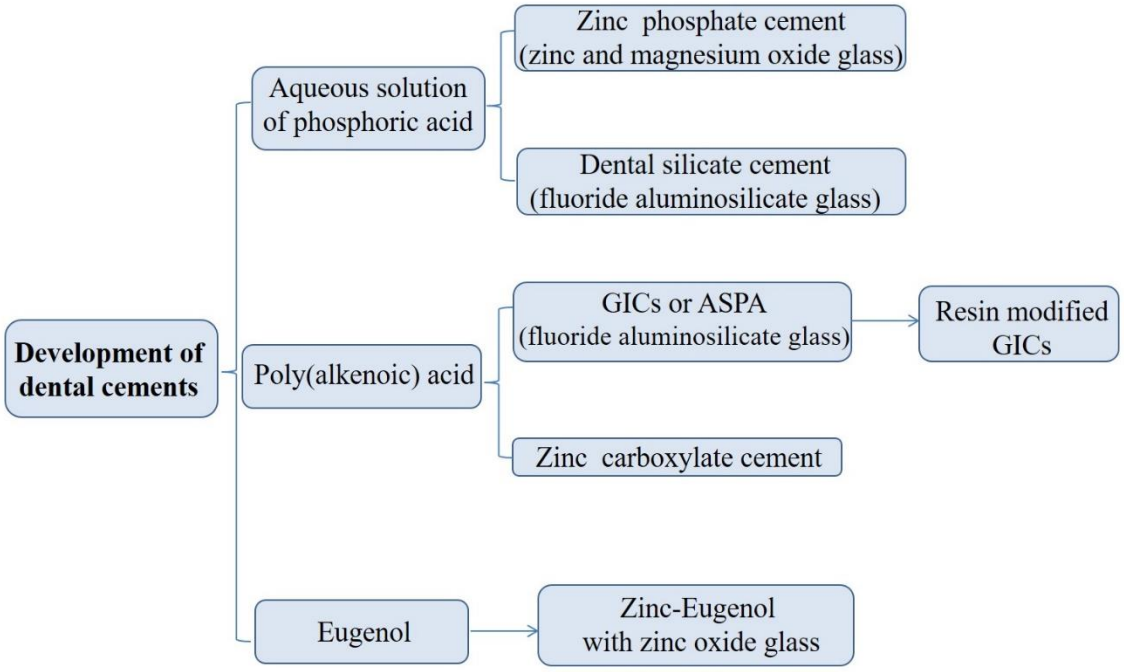

Figure 2-12 Schematic description of cements used in dentistry, according to the nature of the liquid component: with phosphoric acid, poly (alkenoic) acids and with eugenol. Adapted from Wilson (1978).

2.6.1 Zinc phosphate cements

Zinc phosphate cements are formed between a zinc oxide containing powder (SiO_2-Al_2O_3-MgO-ZnO), and a liquid component based on a phosphoric acid solution. This liquid component is composed of a 45-60% phosphoric acid solution, that contains additives such as aluminium and/or zinc salts, forming aluminium and zinc phosphates. The setting reaction occurs with the interaction of the positively charged zinc ions and the negatively charged phosphate groups (Kenny and Buggy, 2003) and it was suggested to set with the formation of glassy matrix of amorphous zinc orthophosphate (Wilson, 1978).

These cements are used for luting crowns and inlays due to their handling characteristics and strength (Wilson, 1978), and they adhere to the surface of the tooth by a mechanical interlocking mechanism (Kenny and Buggy, 2003). However various drawbacks included brittleness, highly exothermic setting reaction, solubility in acids

and irritant to tissues, which reduced their use when composite resins and glass ionomer cements (GICs) were developed (Wilson, 1978).

2.6.2 Zinc polycarboxylate cements

Zinc polycarboxylate cements were developed by Smith in 1968 (Hill and Labok, 1991). These are a modification of the zinc phosphate cements, and were used as cavity liners, adhesives for crowns and for orthodontic applications. Their hardening mechanism is comparable to the glass ionomer cements (GICs), which set by an acid base reaction. The components are a zinc oxide powder prepared by fusion with magnesium oxide, and the liquid component is a polycarboxylic acid, which is usually poly (acrylic acid). The resultant material is composed by unreacted metal oxide particles in a zinc polyacrylate matrix, where the zinc ions released from the ZnO particles crosslink the PAA chains (Kenny and Buggy, 2003).

2.6.3 Dental silicate cements

The dental silicate cements are the only dental major cement in which the glass component is not based on a zinc oxide powder, since it is based on a calcium aluminosilicate glass, with high aluminium content (Al:Si ratio approaches one). For these glasses, Al^{3+} can isomorphically replace Si^{4+} in the glass network, leading to a structure of silica and aluminium individual tetrahedra linked by Al-O-Si bridges. The replacement of Al in the silica structure increases the negative charge of the network, though balanced with network modifier ions such as Ca^{2+} and Na^{2+}. This structure is susceptible to acid attack, when H^{+} ions disrupt Al^{3+} sites and therefore the Al-O-Si links. These H^{+} ions are provided by the liquid component of the cement, based on phosphoric acid, which ionises to $H_2PO_4^{-}$ and leads to the formation of an ion depleted silica gel. The sharp setting of the cement occurs when approximately 50% of the phosphate precipitate (Wilson, 1978), in the form of insoluble phosphate salts (Crisp and Wilson, 1974).

The final structure is composed by well-defined fluorite crystallites (CaF_2) (Wilson *et al.*, 1972), silica gel (Wilson, 1978) and augite ($Al_2PO_4(OH)_3$) (Wilson *et al.*, 1972;Kuhn and Wilson, 1985). The setting reaction in this cement was described by Kuhn and Wilson, to occur over time, varying from months to years (Kuhn and Wilson, 1985).

Role of phosphoric acid in the setting of dental cements

In dentistry, phosphoric acid (H_3PO_4) is used for enamel acid etching and as an additive in dental cements. As an etchant, its makes the enamel surface more responsive to the bonding of restorative materials, by increasing at micro levels its surface roughness, and the subsequent formation of a mechanical interlocking between the enamel and the material. This process is due to an acid-base reaction between the phosphoric acid and the hydroxyapatite that goes into solution (Van Noort, 2013). As an additive, Crisp and Wilson, discussed the effect of phosphoric acid on the pH of the ASPA cement (PAA based). The higher pH obtained when the cements contained H_3PO_4, was associated with its lower acid dissociation constant (pKa) (2.12) in comparison with the PAA, which varies between 5 and 6 (Crisp and Wilson, 1974).

As previously described, in zinc phosphates cements, the liquid component contained phosphoric acid, as an important additive for cement setting. However, Wilson explained that increasing its concentration slowed the setting reaction. This was associated to a possible deficiency of water in the system to aid ionic transport and hydrate reaction products. Conversely, the compressive strength and resistance to acid attack is improved with phosphoric acid concentration (Wilson, 1978). In dental silicate cements, phosphoric acid concentration slightly increases the setting time in concentrations between 50-60% w/w and very sharply above 68% w/w. This was linked with a reduction in the viscosity of the paste, and similarly to the effect in zinc phosphate cements, to a deficiency of water, required to transport ions and hydrate reactions products, such as aluminium complexes and silica gel. Figure 2-13 shows the insoluble aluminium complexes and soluble salts that form upon complexing of the H^+ ions with the ions released from the glass (Wilson, 1978).

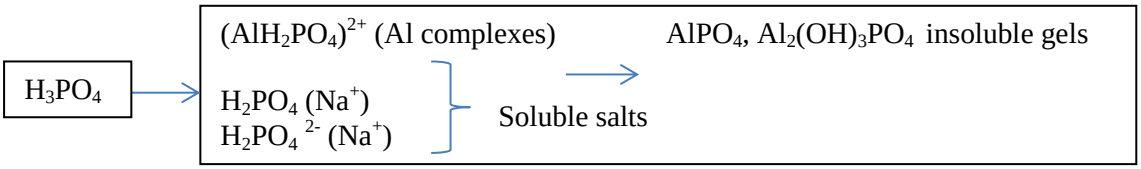

Figure 2-13. Phosphate based complexes formed due to ionisation of phosphoric acid in cements containing an aluminosilicate glass (Adapted from Wilson, 1978)

In GICs Milne *et al*., used phosphoric acid as a setting accelerator with PAA, reporting that it was necessary to promote the rigidity of the cement, and the recrystallization of the aluminosilicate matrix. Furthermore, the use of phosphoric acid was thought to prevent the formation of calcium carbonate when PAA was mixed an aluminium containing glass, which was reported to induce dissolution of the cement when in contact with acid solutions. When mixed with PAA and H_3PO_4, calcium carbonate was not formed and this was explained by the stabilisation of calcium by phosphoric acid and the formation of an insoluble calcium phosphate according to the following reaction (Milne *et al.*, 1997).

$$3Ca^{2+} + 2(PO_4^{3-}) > Ca_3(PO_4)_2$$

More recently, Bakry *et al*. studied the effect of a 45S5 glass-phosphoric acid solution mixture as a paste for the treatment of dentine hypersensitivity, and described that the phosphate ions released from the glass, along with those derived from the phosphoric acid, could react with the Ca ions also leached from the glass and dentine to form a calcium phosphate salts such as brushite (Bakry *et al.*, 2013).

This section has described the composition and applications of zinc phosphate cements, zinc polycarboxylate cements, and dental silicate cements. However, due to a few drawbacks such as poor adherence to tooth, mouth erosion (Wilson, 1996) and irregular disintegration patterns (Wilson *et al.*, 1972), an alternative cement was developed, namely as glass ionomer cements (GICs) (Wilson, 1996).

2.7 Glass ionomer cements

Glass ionomer cements (GICs) have been traditionally used in dentistry as restorative materials, as amalgam bases and luting materials for fixation of crowns and bridges (Deb and Nicholson, 1999). The first glass ionomer cement developed by Alan Wilson and Bryan Kent in 1969 (Nicholson, 1998b;Davidson, 2006) was a product of an acid-base reaction between a basic fluoro-aluminosilicate glass powder and a polycarboxylic acid in the presence of water (Alan and Wilson, 1993;Davidson, 2006).

The main focus for the development of the GICs was to obtain a material with similar characteristics to dental silicate cements with improved biocompatibility (Wilson, 1996;Guida *et al.*, 2002). The first nomenclature used for these cements was ASPA for aluminosilicate polyacrylic acid, and it was later that Kent described this material as a glass-ionomer cement, while The International Standard Association (ISO, 2007)

definition is glass polyalkenoate cements (Wilson, 1996). GICs were traditionally mixed manually, and involved mixing the powder and liquid on a glass surface at ambient conditions (23 ºC and 50% relative humidity) (Crisp *et al.*, 1980). Nowadays, GICs are produced as capsules where the powder and liquid component are in two compartments, activated manually and mixed in a shaker.

GICs appeared when composite resins were available and performing well in terms of ease of use, aesthetics and setting, however, these cements also have additional features such as permanent adherence to untreated dentine and fluoride release (Wilson, 1996). Furthermore, fluoride is slowly released after implantation and contributes to the prevention of secondary caries (Deb and Nicholson, 1999;Wren *et al.*, 2013). This release was reported to possibly result in mineralisation with fluorapatite during bone formation (Brook and Hatton, 1998). Moreover, an additional benefit of GICs was its buffering capacity when exposed to acid lactic solutions, by increasing the pH of the storage solution. This was described to be beneficial also for caries prevention since the critical pH for caries formation is 4.5 (Czarnecka *et al.*, 2002).

The final breakthrough for GICs was achieved by Mclean in the 1970s due to his ability to transform the material into a clinical success by utilising its benchmarking advantages: adhesion to enamel and dentine, fluoride release, biocompatibility and anti-staining properties. Moreover, the implementation of new procedures in dentistry diversified further the use of GICs. Some of the new techniques developed by Mclean were the minimal cavity and tunnel preparation of micro cavities, and for bonding of composite resins to the tooth which are still in use (Wilson, 1996).

An important advantage of GICs is their lower exothermic reaction during setting when compared with traditional PMMA based cements, due to their setting mechanism based on the formation of salts and a silicate matrix, instead of a polymerization reaction, which results in reduced tissue damage after implantation. GICs also adhere to metallic surfaces and bone as well as having a reduced shrinkage rate (Brook and Hatton, 1998). Other benefits are related to a relative ease of production and low costs of raw materials, processing and setting profiles, which could be in theory, tailored to match the required clinical need. Table 2-7 presents examples of commercially used GICs, with applications and working and setting times.

Table 2-7 Description of commercially available products based on the glass ionomer cement technology

Commercial name	Application	Working time	Setting time
Aquacem ® Denstply	Cementation of crowns, inlays, bridges, orthodontic bands	1 min 30 s	2.5 to 5 min
Ketac Cem™ 3M Espe	Cementation of inlays, crowns, bridges, endodontic and post orthodontic appliances, cavity lining	3 min	7 min
Riva Luting SDI	Pit and fissure sealing, roots and tooth surface protection, hypersensitivity protection, temporary fillings, linings	2-3 min	2 to 5 min

2.7.1.1 Glass ionomer cements (GICs) setting mechanism

As previously mentioned, the setting of GICs is based on a neutralization reaction between the calcium and aluminium ions that are released from the glass surface and the hydrogen ions from the COO^- groups are released from the poly (acrylic acid) (Nicholson, 1998b;Smith, 1998;Kenny and Buggy, 2003;Wren *et al.*, 2013).

This initial reaction is called gelation and corresponds to the formation of a weak crosslinking, and it is governed by the particle size of the glass, mixing (Smith, 1998) and glass composition (Nicholson, 1998b). This stage also corresponds to the formation of the initial cement matrix, an important factor in the early stabilization of GICs, and it is composed by calcium and aluminium polyacrylate salts (Deb and Nicholson, 1999). Figure 2-14 shows an illustration of the resulting material, consisting of a composite of cross-linked poly(acrylic acid) reinforced with unreacted glass particles (Griffin and Hill, 1998). Initially, it was believed that setting started with a sequential release of calcium and aluminium (Figure 2-15) but other species are also released at different rates (Wasson and Nicholson, 1993). In early studies, it was noted that calcium polyacrylate salts formed earlier than aluminium polyacrylates salts, which appeared one hour later for a cement formulation with a P/L of 1.5 (Wilson, 1978). Aluminium plays an important role in the glass degradation (hydrolysis of Si-O-Al bonds), and in the stability of cements by cross-linking of poly (acrylic) chains by Al^{3+}. After maturation for 24 hours, the crosslinking of aluminium continues and the susceptibility of the cement to moisture decreases due to an increase in the content of bound water (Wasson and Nicholson, 1993).

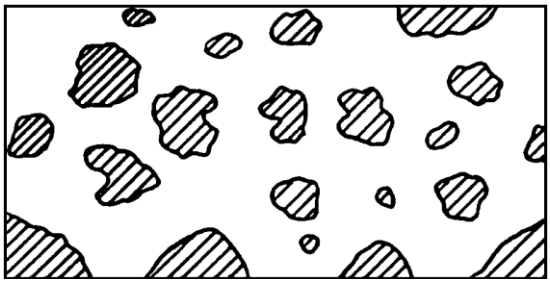

Figure 2-14 Schematic of glass particles surrounded by silica gel in the salt reacted matrix Griffin and Hill (1998). Reprinted with permission from Springer. Copyright 1998. Journal of Materials Science.

Wasson and Nicholson suggested that a silicate matrix is formed in the post hardening phase (Wasson and Nicholson, 1991), with Hatton and Brook confirming this secondary setting reaction by Transmission Electron Microscopy (Temenoff and Mikos), and the presence of ions from the glass particles throughout the matrix of the set cement (Hatton and Brook, 1992). This suggested the reconstruction of the silicate network, which contributes to the latter stages of maturation (Deb and Nicholson, 1999). The large proportion of silicon in storage solutions, suggested that the release of calcium and aluminium is not the result of an ion exchange process but the result of the complete dissolution of a fraction of the glass (Nicholson, 1998b;Deb and Nicholson, 1999).

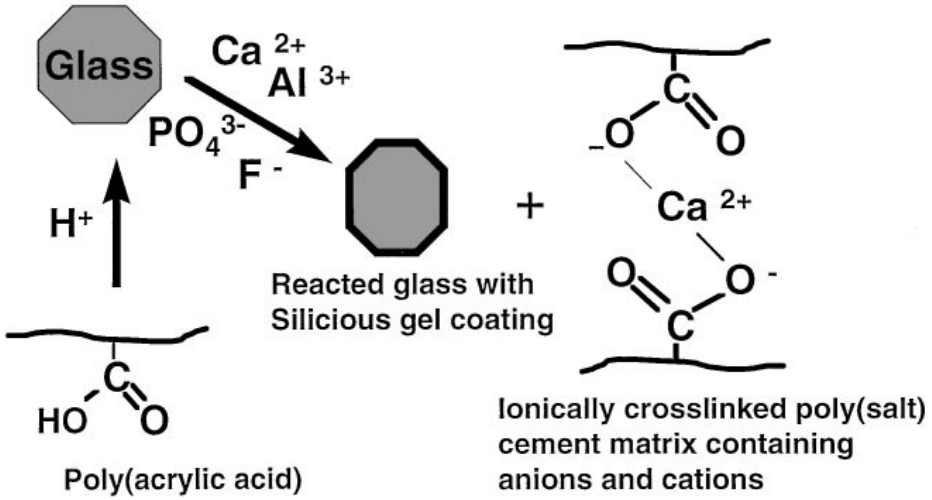

Figure 2-15. Setting reaction of a GIC showing the release of ions such as Ca^{2+}, Al^{3+}, F^- and PO_4^{3-} after acid attack from the poly (acrylic acid), with the formation of a siliceous gel coating around the reacted glass particles and the cement matrix formed by the polyacrylate salts Griffin and Hill (1998). Reprinted with permission of Elsevier. Copyright 1999. Journal of Biomaterials

Glass powder

The glasses used in GICs are fluoro-aluminosilicate powders, prepared from a mixture of silica, alumina, calcium fluoride, sodium hexafluoroaluminate and aluminium phosphate (Wilson, 1996), with examples of these glass systems being: SiO_2-Al_2O_3-CaO, SiO_2-Al_2O_3-CaF_2-$AlPO_4$ and SiO_2-Al_2O_3-CaF_2-$AlPO_4$-Na_3AlF_6 (Wilson and Mclean, 1988). These are degradable glasses, comparable to those used for dental silicates cements, however due to the PAA being weaker than the H_3PO_4 liquid used for silicate cements, the Al_2O_3/SiO_2 ratio is higher (Wilson, 1978). This ratio required to be at least 1:2, making the glass more susceptible to acid degradation due to the replacement of silica by aluminium in the glass structure (Wilson and Mclean, 1988).

The microstructure of these glasses is described as a calcium aluminosilicate phase with randomly distributed spherical droplets that could be partially or completely crystallised corresponding to a fluorite phase (Crisp and Wilson, 1973). These glasses are based on the G-200 composition (Table 2-8), and was researched by Wilson and colleagues, who examined 199 glass compositions, resulting in the final G-200 formulation (Wilson, 1996). It consisted of a melt derived aluminosilicate glass with high content in calcium and fluoride, and low in sodium and phosphate (Crisp and Wilson, 1974). Similar cements, prepared with the G338 glass (SiO_2-Al_2O_3-AlF_3-CaF_2-NaF-$AlPO_4$), had poor translucency and aesthetics; however, the formulation was promising due to an optimum working time, strength, and aqueous stability. This glass overcame previous issues, in which hydrolytically stable cements had long working and setting times, while those with appropriate working and setting times were not hydrolytically stable. This improvement was attributed to the high fluoride content: even though aluminium played an important role in crosslinking the PAA, the fluoride allowed the formation of alumino-fluoride compounds which momentarily withdrew the aluminium ions and retarded crosslinking (Wilson, 1996). Later, tartaric acid was introduced as an additive, which extended the application of these cements (Wilson, 1996).

Table 2-8. G-200 glass original composition (Wilson and Mclean, 1988)

Oxide	Composition (wt. %)
SiO_2	30.1
Al_2O_3	19.9
AlF_3	2.6
CaF_2	34.5
NaF	3.7
$AlPO_4$	10.0

The melting temperature of the glass and particle size, were reported as variables influencing the cement setting properties: a G-200 glass melted at 1300 ºC produced a cement that was too reactive for clinical applications when compared with the same glass melted at a lower temperature (1150 ºC) (Crisp and Wilson, 1974). Regarding particle size, Prentice *et al.,* studied the influence of fine (3.4 µm) and large (10 µm) particle mixtures on the cement handling properties, showing that on average, fine particles produced cements that were too viscous and set too fast for clinical use, due to an increased particle-particle contact and surface area. In contrast, large particles, produced a non-cohesive paste (Prentice *et al.*, 2005). Early research on GICs, implemented particle size ranges used in traditional materials such as Portland cements, with variations between 5 and 30 µm (Bentz *et al.*, 1999) and 42 µm (Crisp and Wilson, 1974).

Poly (acrylic acid)

Figure 2-16 shows the structure of the acrylic acid unit. This acid is a water soluble polyelectrolyte from the carboxylic acid family (Kuhn and Wilson, 1985) that dissociates according to the equation below:

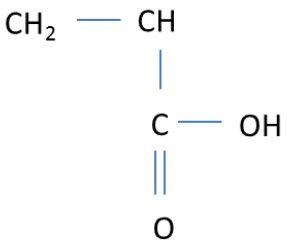

Figure 2-16. Acrylic acid unit. Adapted from Smith (1998) with permission from Elsevier

The effect of PAA is complex: when the PAA chain length increases, the working and setting time decrease due to fewer cations being required to form a cross linked network, and when the molecular weight is increased, the setting time increases due to a longer time for the PAA particles to dissolve and cations to migrate (Wilson, 1989).

In GICs, PAA is present as a low molecular weight acid, allowing its use in high concentrations without gelation, however PAA acid solutions tend to gel when their concentration in water approaches 50% by mass (Alan and Wilson, 1993). This drawback was later addressed with the use of dicarboxylic and tricarboxylic acids such as itaconic or maleic acid copolymer due to a higher number of carboxylic groups per chain unit and the higher acidity (Smith, 1998;Kenny and Buggy, 2003), that increased the reactivity of the liquid, decreased viscosity and the gelation tendency (Alan and Wilson, 1993). However the addition of these copolymers bonded less strongly to enamel and dentine than PAA, although adhesion differed depending on the mixing ratio (Smith, 1998). An additional drawback with changes in the molecular weight and distribution of the polyacid was associated with the viscosity of the liquid: higher molecular weight copolymers improve mechanical properties by influencing the viscosity; however, this can produce a paste that is not fluid enough to allow complete mixing. This issue was subsequently addressed by adding the PAA as a powder that could be mixed with water or a tartaric acid solution (Guggenberger *et al.*, 1998;Smith, 1998).

The molecular weight of the PAA depends on the glass system and cement applications. A diverse range of PAA Mw were reported in the literature: as powders or aqueous solution: 23k in 0.5% w/w aqueous solution (Crisp and Wilson, 1974), 52k (Hurrell-Gillingham *et al.*, 2006), 25k–80k in 25% aqueous solution (Boyd *et al.*, 2008a) and 23k in 45%- 50% aqueous solutions (Bertolini *et al.*, 2009). In aluminium free GICs, the use of PAA with Mw lower than 26k produced hydrolytically unstable cements after

one day of setting, however further maturing time, produced stable cements after seven and thirty days, depending on the glass composition (Towler *et al.*, 2002). This outcome coincided with research by Brauer *et al.*, in an Al free GIC prepared with a Mg containing silicate glass: without the use of a copolymer, the cements were not hydrolytically stable in water. Conversely, a cement stable in water was later prepared with a comparable glass composition (SiO_2-CaO-CaF_2-MgO) and poly (vinyl phosphonic-co-acrylic) acid (PVPA-PAA) (Brauer *et al.*, 2011a;Fuchs *et al.*, 2015).

Water

Water is the medium where the ionic species interact, by allowing the dissociation of the acid and therefore the availability of protons for the reaction. It is also thought to have other functions as a plasticiser (Alan and Wilson, 1993) and a reaction product (Alan and Wilson, 1993;Nicholson, 1998b). As a medium, water is required to allow the acids to dissociate enabling the metal ions to enter the liquid phase; as component, water coordinates certain sites around the metal ions; and as a reaction product, it hydrates the silica hydrogel that forms after the initial ion release (Nicholson, 1998b).

In traditional GICs, water is known to be present in at least two states: bound or non-evaporable water and not bound or evaporable water. This hydration mechanism makes cements very susceptible to dehydration after the second setting stage starts. In this stage, an increase of the bound to not bound water ratio, decreases the cements dehydration susceptibility over time, which positively influences their compressive strength (Anstice and Nicholson, 1992). If dehydration initiates, the post hardening stage will be interrupted and the potential maximum strength of the material would not be achieved (Alan and Wilson, 1993;Nicholson, 1998b), while too much water would prevent the cement from setting (Milne *et al.*, 1997).

Tartaric acid

The addition of tartaric acid, allowed preparation of workable cements for glasses with lower concentration of fluoride, that was beneficial to increase the translucency of the cements. This effect was described to be associated with the initial reaction between the glass and the tartaric acid, that supressed the ionisation of the PAA, reducing the viscosity of the pastes, delaying gelation and accelerating the hardening after gelation. The final cement matrix was composed of a tartrate containing cement incorporated into

a structure with polyacrylate salts and metal ions, which probably involved the presence of fluoride ions (Wilson and Mclean, 1988).

2.7.2 *In vitro* testing and biocompatibility of GICs

In vitro testing is an essential part for the evaluation of new medical devices and biomaterials by assessing the preliminary response of cells when they are exposed to their surface or by-products. Testing on cell lines has been implemented as an alternative for *in vivo* experiments, due to the ethical issues related to animal testing, costs and regulatory approval (Harmand, 1997). *In vitro* testing also provides a source of techniques which in general are simple and reproducible on cellular events (Freshney, 1994). Therefore, an important part of a biomaterials' assessment is to evaluate its toxicity in a cellular environment, considering cytotoxicity as "a factor being destructive to living cells" (Martin and Hine, 2008) which can vary depending on the material's application and cell type.

A general guidance was established on the ISO 90993 Part 5 Standard for testing cytotoxicity in vitro (Harmand, 1997). The chosen indicators would vary depending on the objective of the study, whether this would be to evaluate cell death, morphology changes, or metabolism. Examples of cell lines established in the standard as guidance are: L929 (mouse connective tissue) and MRC5 (human foetal fibroblasts) (Harmand, 1997). The standard describes tests by indirect (diffusion) and direct contact for evaluation of cytotoxicity *in vitro* (Harmand, 1997). The ISO 90993 Part 5 Standard direct contact method is based on a sample that is placed in the centre of a near confluent cell monolayer to cover one tenth of the cell layer and cytotoxicity evaluated in triplicate after different type points e.g. 24 h, 48 h and 72 h. This test provides semi-quantitative information of cytotoxicity by observation of morphological features such as percentage of cell death within an area. For direct contact tests, typical tissue culture methods are based on the use of pre-treated polystyrene well plates (TCP) for optimal cell attachment, where samples are placed in the well containing a cell specific medium.

A protocol based on resazurin reduction, has been extensively used for quantitative analysis of cell viability. Resazurin is a non-fluorescent blue coloured dye which is reduced to resorufin (pink and highly fluorescent) and further reduced to hydroresorufin which is uncoloured and non-fluorescent (O'Brien *et al.*, 2000). The change in colour, measured using a spectrometer in absorbance or fluorescence mode, occurs as a

response to the cellular metabolic activity (Serotec, 2014). This assay is non-destructive, meaning that with an appropriate washing protocol, cells can be kept in culture after performing the analysis. The commercial products using resazurin are PrestoBlue® cell viability assay and alamarBlue® assay.

With respect to the biocompatibility of GICs, it has been compared with dental silicates and zinc phosphates cements and studies confirmed they are at least as biocompatible. Studies showed that toxicity was mainly observed when GICs were in contact with pulpal tissue, although this effect decreased over time as the setting proceeds (Nicholson *et al.*, 1991), with previous studies showing that incomplete setting resulted in cell death. Furthermore, the exothermal reaction during setting is very low when compared with other acid based dental cements, reducing the possibility of inflammatory tissue reactions by means of a neutralization reaction that occurs relatively fast, and decreases the presence of free acidic ions that could produce tissue damage (Nicholson *et al.*, 1991).

As previously described in section 2.7, GICs are used mainly in dentistry for luting and restorative applications. However, their low exothermic reaction when setting and ability to release ions have expanded their research and development into orthopaedic applications. On this matter, GICs have been studied for fixation of acetabular cup in orthopaedic surgery, reconstruction of mastoid cavity, and for ossicular chain reconstruction (Kupperman and Tange, 2001), having found applications in middle ear surgery (Figure 2-17) due to the formation of a waterproof union between the cement and the adjacent bone, and their ability to be shaped after setting (Kupperman and Tange, 2001). Nonetheless, these Al containing cements have been associated with bone mineralisation issues and neurotoxicity. Hence, the next three sections account for a description of the negative features linked to Al, clinical studies describing the use of Al containing cements and granules, and techniques used for cement characterisation.

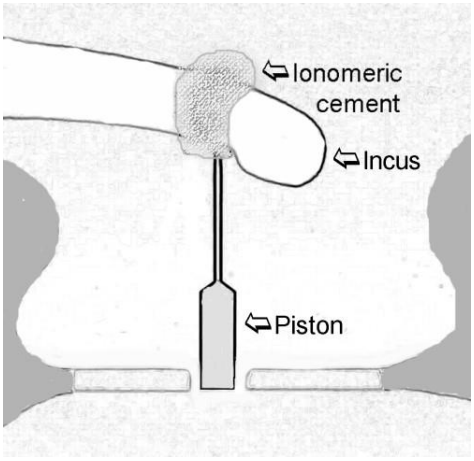

Figure 2-17 Attachment of stapes prosthesis to the long process of the incus using a glass ionomer cement (Tysome and Harcourt, 2005). Reprinted with permission of John Wiley & Sons. Copyright 2005. Journal of Clinical Otolaryngology

2.8 Drawbacks of aluminium (Al) containing GICs for clinical applications

From a biological point of view, aluminium (Al) has various drawbacks: Al is stored in the bones, where it interrupts bone turnover, and therefore is associated with inadequate mineralisation, inducing problems such as osteomalacia, and has been recognised as a major issue for patients with end stage renal disease. Furthermore, this interruption of bone turnover, was associated with inhibition of bone cell proliferation and decreased number of osteoblasts and osteoclast, by a mix effect of defective collagen production and matrix mineralisation (Malluche, 2002).

The presence of Al was associated with plaques outside cells in damaged nervous tissue in the brain (Williams, 2007), and linked to Parkinson's disease (Wren *et al.*, 2013). At pH values higher than 7, aluminium is in various forms: $Al(OH)_4^-$, $Al(OH)_3$ and Al^{3+}. It also has high affinity for phosphates, forming $AlPO_4$ and $AlPO_4$. H_2O at a pH value of 6.6 (Martin, 2007). This affinity, could be related to the pathological effect mentioned by Malluche, that linked aluminium with the inhibition of hydroxyapatite formation and growth (Malluche, 2002). Additionally, a study of biocompatibility of soda lime silicate glasses by Stanley *et al*., used porous Al_2O_3 implants as a negative control, since it was reported that there was no ion exchange occurring between pure alumina and the biological environment (Stanley *et al.*, 1976).

Regarding the use of GICs outside dentistry, a well-known adaptation was Ionocem or Ionos cement (Ionos, Germany). It was reported to contain a calcium fluoro-aluminosilicate glass powder molten from SiO_2, Al_2O_3, CaF_2, $NaAlF_6$, AlF_3 and $AlPO_4$

and a liquid consisting of a poly (acrylic)/maleic acid copolymer and tartaric acid (Erbe *et al*, 1996) The positive outcome in animal models promoted the use of this cement for fixation of hip and knee prosthesis, and for closure of large bone defects in orthopaedic surgery. Nonetheless, side effects with similar symptoms to Alzheimer's disease were later diagnosed for patients that had undergone surgeries in which GICs type cements were in contact with spinal fluid (Engelbrecht *et al.*, 2000). Furthermore, Kupperman *et al.* linked Ionocem with adverse tissue reaction and higher rates of extrusion of the cement, due to frequent infections and development of cysts (Kupperman and Tange, 2001).

Ionocem was also produced as granules (Ionogran), with sizes ranging between 0.5-1.0 mm and between 2.0-5.00 mm, with reported advantages including biocompatibility, ease of use and possibility to be re-sterilised. For instance, a clinical study by Engelbrecht *et al.*, reported their use for aseptic loosening in hip replacement. Their application was carried out as a mixture of granules with ground cancellous bone to allow better initial stability, and its use was reported as an advantage when compared with autologous bone without additives. This study revealed mixed results, since radiographic post-operative examinations showed that the granules allowed for improved early prosthesis stabilization, however, revision surgery increased by at least 17% in comparison with surgeries where homologous bone was used. Moreover, histological samples taken from the bone-acetabular component interface, showed presence of osteoclasts and absence of osteoblasts, and a high concentration of macrophages with aluminium particles in the osteoid of the cancellous bone and the serum extracted from the acetabular component (Engelbrecht *et al.*, 2000).

Similar results were reported by Buric *et al.* and Carter *et al.*: Buric *et al.* reported a high concentration of aluminium ions in a revision arthroplasty study, and as previously described, this outcome was associated with the inhibition of bone mineralization and osteoblastic activity (Buric *et al.*, 2003). Similarly, Carter *et al.* compared the Ionogran granules (referred in the paper as Vo-S) with an aluminium free filler, based on an experimental calcium-sodium fluorosilicate composition (ALFVo-S). This study, reported the formation of lamellar bone for the early stages, with more mature bone remaining poorly mineralised, and an increase in the Al release over time for the Vo-S granules. In contrast, the defects filled with ALFVo-S, healed with the presence of small amounts of bone that appeared to be fully mineralised (Carter *et al.*, 1997).

GICs have also been used for reconstruction of the incus long process following erosion: a cement currently known as Serenocem™ (Corinthian Surgical Ltd., UK) is based on a fluorosilicate glass composition with a reduced aluminium content. The exact composition of the glass is not directly reported by the manufacturer, however, it was referenced as a fluoro-aluminosilicate glass, known as LG26 (Clark and Bottrill, 2007) with a composition of $4.5SiO_2$-$3.0Al_2O_3$-3.0CaO-$2.0CaF_2$-$1.5P_2O_5$ (Hurrell-Gillingham *et al.*, 2003;Fredholm, 2011), and a reported network connectivity of 3.30 (Kusumoto *et al.*, 2016). This cement is supplied as a two-part capsule, that is activated by applying pressure to a plunger, mixed in a vibrating machine for 10 s, and dispensed with an application gun (Tysome and Harcourt, 2005). The reported hardening time of Serenocem™ is 10 min (Tysome and Harcourt, 2005;Righini-Grunder *et al.*, 2015), after which the cement can be moulded.

Early studies on Serenocem™ were carried out by Tysome and Harcourt in a clinical study for fixation of prosthesis in middle ear surgery as an alternative to the crimping technique that uses a wire loop for fixation. This alternative was used as the crimping procedure showed long term drawbacks, such as prosthesis loosening and incus erosion, possibly due to a loose wire attachment and blood supply deficit. Even though the study did not include long term results, both groups showed satisfactory outcomes, with similar hearing recovery, showing that Serenocem™ could be used in middle ear surgery (Tysome and Harcourt, 2005). Therefore, this cement has been used for various ENT applications such as fixation of cochlear implants, reconstruction of canal walls, and for repair of the eroded long process of the incus (Clark and Bottrill, 2007;Righini-Grunder *et al.*, 2015). However, for clinical use, it is not advised for applications that require the paste to be in direct contact with cerebrospinal fluid (CSF) or brain tissue (Tysome and Harcourt, 2005;Hurrell-Gillingham *et al.*, 2006).

The granular pre-set cement based on Serenocem™, called SerenoCem Granules™ was designed for otological and maxillofacial hard tissue replacement (Bayode and Grumbridge, 2016). Nonetheless, this product was recently reported to be subjected to revision due to its association with bony erosion, with histological studies revealing local inflammation and fibrous tissue encapsulation, with no evidence of bone regeneration in the area surrounding the granules (Harrison *et al.*, 2017). These clinical outcomes, led to the withdrawal of this product from the market in 2016, with the issue of a medical device alert due to the risk of bone reabsorption (Bayode and Grumbridge, 2016).

2.9 Aluminium free glass ionomer cements

Glass ionomer cements have been previously researched due to their potential as an alternative material for applications in spinal fusion, ocular prosthesis, periodontal fillings, and middle ear surgery, however, as previously described their limiting aspect relies on the aluminium content. Various glass composition alternatives, have been researched with mixed outcomes in relation to handling properties and biocompatibility, but these have not been successful enough to the point of being scaled up for their use at a clinical level. Previous research was found to be mainly oriented into substituting aluminium ions by divalent and trivalent cations that could be leached from the glass and act as a network modifier to maintain the degradability of the glass. Table 2-9 presents a summary of various aluminium free glass compositions tested as cements, describing the additives, powder/liquid (P/L) ratios and characterisation regarding handling characteristics and *in vitro* testing.

Table 2-9. Summary of preparation parameters of aluminium free GICs, describing the use of additives, powder/liquid (P/L) ratios and characterisation regarding handling characteristics and in vitro testing

Glass system	Additives	P/L ratios	Cement assessment	Working time (WT) and setting time (ST)	*In vitro* testing	Reference
$0.4SiO_2$ - 0.32-$CaCO_3$-0.28ZnO	PAA Mw: 9270, 25700, 80,800) and 10% tartaric acid	Glass:2.0 g-0.4g PAA-0.6g $H_2O_{(d)}$ (and 10% tartaric acid)	Samples immersed in distilled water (5ml)	ST described as suitable for restorative purposes	L929 cells tested for neutral red assay and total protein assay (48 h direct contact)	(Towler *et al.*, 2002)
SiO_2-Fe_2O_3-P_2O_5-CaO. CaF_2	PAA Mw 52,000	Glass:1.0 g-PAA:0.2g-tartaric acid solution: 0.3 g 10% m/v	Cement discs : 9 mm x 1.5 mm	Not reported	Rat osteosarcoma cells tested with MTT assay, Total Protein Assay and SEM	(Hurrell-Gillingham *et al.*, 2006)
SiO_2-CaO-ZnO	PAA Mw 25,700-80,800	Glass:1g-PAA:0.36-0.455 g-Water: 0.25-0.55 ml	Working and setting times (ISO9917E), SBF test	WT: 24 s-218 s ST: 2.58 min-14.72 min	Not reported	(Boyd and Towler, 2005)
SiO_2-ZnO-CaO-SrO	PAA Mw 26,100 (25% m/v)	Glass:2 g-PAA:0.6--Water: 0.9 ml	Working and setting times (ISO9917E)	WT: 3 s-48 s ST: 2.8 min-9.81 min	Not reported	(Boyd *et al.*, 2008b)
SiO_2-CaO. CaF_2-SrO-SrF_2-MgO-ZnO and SiO_2-CaO-CaF_2-MgO	PAA Mw 80,000	Glass:0.5 g-0.1-0.1g PAA-0.15g distilled water	6x4mm cylinders. Set For 1h, 37 ^{0}C) immersed in water (4ml)	Reported to set within an hour	MC3T3-E1 mouse fibroblasts tested with a MTT test (ISO10993) Samples: 10 x 1 mm	(Brauer *et al.*, 2011a)
SiO_2-GeO_2-ZrO_2-ZnO-Na_2O-CaO-SrO	PAA Mw 12,700 (50% solution)	2:1.5 ratio glass powder to liquid acid	Working and setting times (ISO9917E)	WT: 22 s-10.02 min ST: 1.03 min-104.19 min	Not reported	(Dickey *et al.*, 2013)
Be_2O_3-TiO_2-ZnO-SrO-CaO-Na_2O-Ag_2O	PAA Mw 80,800	2:1.5 ratio glass powder to liquid acid	Working and setting times (ISO9917E)	WT: 140 s-196 s ST: 8.03 min-8.13 min	Not reported	(Shen *et al.*, 2014)

The early studies of bioactive glass cements were focused on the use of glass ceramics based compositions (apatite-wollastonite SiO_2-CaO-P_2O_5-MgO): Yoshihara *et al.*, showed the possibility of obtaining cements from bioactive glass powders, by mixing a SiO_2-CaO-CaF_2-P_2O_5 glass, with an ammonium phosphate solution (Yoshihara *et al.*, 1994). Matsuya *et al.*, later studied the preparation of cement pastes based on a SiO_2-CaO-P_2O_5-MgO glass with varying content of P_2O_5 (10, 15 and 20 %), PAA Mw varying between 2k and 90k (concentrations of 25 % and 50 %*)* and poly(methyl vinyl ether maleic acid) (Matsuya *et al.*, 1999). Shi *et al*., studied a similar glass system to the one described by Matsuya *et al.*, where a SiO_2-CaO-P_2O_5 based powder was mixed with an ammonium phosphate buffer. The paste had a good injectability and stability in simulated body fluid (SBF), with a structure based on amorphous silica and calcium deficient hydroxyapatite (dHa) nanocrystals (Shi *et al.*, 2006).

In addition, bioactive glasses were used as additives to improve the biocompatibility of traditional GICs: Yli Urpo *et al.* carried a bioactivity study with cement discs containing 10 and 30 wt.% of 53P4 glass powder that were added to a conventional cure GC Fuji II, and resin-light modified GICs (Fuji II LC Improved). Results showed that all GICs induced the formation of a calcium phosphate layer (CaP) in SBF, with an improved deposition observed for the resin modified cements, that increased in proportion with the glass content (Yli-Urpo et al., 2005).

Having described the early approach on cement preparation using glass-ceramics and bioactive glass as an additive in GICs, the next part describes the research carried out on aluminium free GICs, by considering the replacement of Al in the fluoro-aluminosilicate GIC glass with oxides from the following elements: zinc (Zn), strontium (Sr) iron (Fe), boron (B) and magnesium (Mg), including Zn based glasses modified with titanium (Ti), gallium (Ga) and germanium (Ge).

Zinc oxide (ZnO) substitutions

Zn substitutions in Al free GICs have been carried out due to the potential role of this ion to act as a network modifier in the glass structure (Boyd *et al.*, 2006), and due to its role in bone formation and mineralisation (Brauer *et al.*, 2011a;Lakhkar *et al.*, 2013). Even though Zn containing pastes were described to set (Towler *et al.*, 2002) (Brauer *et al.*, 2011a), the excessive release of Zn was associated with selective neuronal loss and Alzheimer's disease (Towler *et al.*, 2002). Furthermore, *in vitro* studies on L929 cells, was not satisfactory when tested with samples prepared with a SiO_2-ZnO-CaO glass

powder and PAA (Towler *et al.*, 2002). Similarly, Brauer *et al.*, found that cements prepared with SiO_2-ZnO-CaO-CaF_2-SrO-SrF_2-MgO and SiO_2-CaO-CaF_2-MgO glasses and PAA, had a lower metabolic activity when compared with the control, with this effect being reported to be dependent on Zn concentration (Brauer *et al.*, 2011a).

Variations of Zn based glasses have been developed with the addition of elements such as Ti, Ge and Ga. Wren *et al.*, studied the substitution of TiO_2 for SiO_2 on a SiO_2-ZnO-CaO-SrO system. In this work, it was reported that titanium acted as a network modifier in a similar manner as aluminium when the Si/Al ratio is greater than one. For lower titanium content, the setting times were too short to be clinically useful (less than two minutes). For the highest TiO_2 content, the setting time improved to a clinically relevant value, and was reported to be approximately 7 min. However, release of Ca^{2+}, Sr^{2+}, and Zn^{2+} was low for all the cement formulations, with further reduction in Ca^{2+} and Sr^{2+} with increasing Ti content in the glass (Wren *et al.*, 2013).

Dickey *et al.* examined the substitution of Ge in a series of glasses based on the 0.48SiO_2-0.36ZnO-0.12CaO-0.04SrO glass system, where compositional boundaries were also designed to add Zr and Na. The cement was tested to evaluate its potential as an injectable paste for minimally invasive procedures for vertebral body's fractures. The authors reported that the relationship between the working and the setting times was complex, however, the cements had longer working times, and these were more consistent in comparison with silica based glasses. The effect of Ge additions was found to be effective to prolong the working time without making a negative impact on setting, however the authors reported a decline on the mechanical integrity of the samples over time (Dickey *et al.*, 2013).

Regarding the use of Ga, Wren *et al.*, studied the substitution of Ga_2O_3 in a SiO_2-ZnO-CaO series, reporting that this cement system had potential applications as a therapeutic ion in bone cancer treatment, and fillers after tumour removal. The setting time of the cements prepared with the lower Mw PAA, were between 9 and 13 min, which the authors reported to be too long for the intended applications. On the other hand, when using a higher Mw PAA, the setting times were very short (~ 4 min), although no significant variations were observed when changing the PAA concentration. The increase in the setting times associated with the Ga addition was attributed to a higher level of disruption in the formation of Ca salts (Wren *et al.*, 2012)

Strontium oxide (SrO) substitution

Early research on GICs by Deb and Nicholson, studied the addition of SrO powder to the glass component of commercial GICs, to evaluate its cement forming properties and ability to act as a reinforcement of the cement matrix. This study found that SrO did not impede cement formation, but it slowed down the setting reaction, which was associated to a slower kinetics of release of Sr^{2+} (Deb and Nicholson, 1999).

Later studies on SrO in GICs were carried out by substituting SrO for CaO in the glass structure, due to its similar function as network modifier. Boyd *et al.* studied a SiO_2-ZnO-CaO glass. For this system, the setting time of the cements decreased with SrO substitutions, with variations between 1.7 and 1.9 min, however this effect did not occur for the minimum substitution of 0.08 moles. The authors attributed this result with a more basic character of SrO in comparison with CaO, since the structural characterisation of the glasses, showed no significant differences between the compositions (Boyd *et al.*, 2008b).Brauer *et al.* evaluated the antibacterial properties of SrO in a SiO_2-CaO-CaF_2-SrO-SrF_2-MgO system. These cements were reported to set within 60 min; however, the samples developed a rubbery appearance when immersed in water. In addition, the SrO addition was linked to a more degradable glass, which the authors associated with an improvement of the hydrolytic stability and shorter working times of the cements. SrO additions were beneficial for glass dissolution and therefore improved cement setting, however, as described by Brauer *et al.*, the relationship between the substitution and variation of properties (e.g. compressive strength) is not linear (Brauer *et al.*, 2012).

Iron oxide (Fe_2O_3) substitution

Hurrell-Gillingham *et al.* studied the substitution of Al_2O_3 by Fe_2O_3 in a SiO_2-Al_2O_3-P_2O_5-CaO glass system. This study was based on the SerenoCem™ glass composition as a possible aluminium free glass alternative. Results showed it was possible to obtain a setting paste by mixing this Fe containing glass with PAA and tartaric acid, resulting in similar setting times to commercially available cements. (Hurrell-Gillingham *et al.*, 2006). Nevertheless, the glass partially crystallised, with the presence of dendritic magnetite and apatite (Hurrell-Gillingham *et al.*, 2005). Due to the vitrification tendency of these glasses, an *in vitro* biocompatibility study was carried out, showing that cell viability increased with increasing the crystallinity of the glass. This improvement was attributed to the lower capability of the unreacted remnant glass to

rapidly release ions, as well as the presence of apatite as a biocompatible phase (Hurrell-Gillingham *et al.*, 2003).

Boron (B_2O_3) and magnesium (MgO) substitution

Shen *et al*. also proposed boron (B) as a network former, and aluminium was substituted by ions such as Zn, Ti, and Ag. The study showed that using a borate glass allowed the preparation of a polyalkenoate cement that was stable in water for a range of formulations (Shen *et al.*, 2014).

In the case of MgO, its addition into an Al free GIC, was reported to act either as a network former or modifier, and to produce a degradable glass when mixed with PAA and $H_2O_{(d)}$ (Brauer *et al.*, 2012). Fuchs *et al.* reported the formation of a setting cement with a SiO_2-CaO-CaF_2-MgO glass, and a poly (vinylphosphonic-co-acrylic acid). In this study, MgO was considered an intermediate oxide that could partially enter the silicate network, with a role similar to Al in traditional GICs (Fuchs *et al.*, 2015). However, setting times were not reported, and even though the indirect *in vitro* test showed that the cements were not cytotoxic, the release of Mg ions was previously described to reduce glass dissolution and apatite formation (Diba *et al.*, 2012).

2.10 Cement characterisation

2.10.1 Setting times

The setting time of cements are related to various factors such as temperature, humidity, and mixing method. For example, in PMMA based cements, setting time can be influenced by additional factors such as paste thickness and mould material (Li *et al.*, 2004). An additional factor influencing setting time in aluminium free GICs, is the particle size. This occurs in a similar manner to that described for traditional GICs: Gomes *at al.*, reported that setting time of cements prepared with particles less than 63 µm, set faster when compared with 63-125 µm and 125-250 µm (Gomes *et al.*, 2013). To reduce this effect on setting, a particle size range of less than 45 µm has been generally used in this area (Towler *et al.*, 2002;Boyd and Towler, 2005;Hurrell-Gillingham *et al.*, 2005;Kim *et al.*, 2013). In GICs, and specifically in Al free cements, the setting was also related to the degradability of the glass. For instance, Boyd and Towler, studied the cement forming properties of a glass based on a SiO_2-CaO-ZnO system, and reported that the glass with lower CaO content and higher ZnO content was

more reactive, and therefore had a lower working and net setting times (Boyd and Towler, 2005).

A few of the techniques used to study the setting reaction during the early research of dental cements were: spectroscopy, electric conductivity, and measurement of pH (Wilson, 1978). For Al free GICs, measurement of the setting time has been carried out by an indentation test using a Gillmore needle (Hurrell-Gillingham *et al.*, 2006), and more recently following the ISO9917E, that is based on the same principle of indentation (Boyd *et al.*, 2008b;Wren *et al.*, 2012;Wren *et al* 2013;Valliant *et al* 2016), oscillating rheometer (Brauer *et al.*, 2012), and measurement of viscosity (Dickey *et al.*, 2016).

As previously mentioned, spectroscopic techniques such as Fourier transform infrared spectroscopy (FTIR), were used to evaluate the setting of traditional GICs (Crisp and Wilson, 1974;Deb and Nicholson, 1999;Matsuya *et al.*, 1999;Kim *et al.*, 2004). FTIR was also used as a tool to study the setting of aluminium free GICs, usually measured from the start of the mixing for up to 60 min (Wren *et al.*, 2010;Dickey *et al.*, 2016), and was proposed in the literature as an additional step to study the setting of these cements with reduced variability and increased precision (Valliant *et al.*, 2016).

2.10.2 Behaviour in water: mass variation, pH and ion release

Traditionally, GICs have a low dissolution rate due to the highly polymerised character of the fluoro-aluminosilicate glasses, for which negligible mass loss is recorded. In contrast, bioactive glasses have high dissolution rates that imply a higher mass loss of the cement samples. Consequently, quantification of this change should be an important factor to consider when characterising bioactive glass based cements, since degradation could occur without a visible account of dissolution in the storage solution (e.g. loose particles or complete dissolution). Most studies in the field, focussed on chemical and kinetics characterisation in aluminium free GIC cements, for which a limited amount of comparison studies were found.

The physical properties of GICs have been related to various factors such as maturation time, powder/liquid (P/L) ratio and the concentration and molecular weight of the polyacid (Crisp *et al.*, 1980). However, early studies by Crisp *et al.*, in ASPA cements, described a method in which discs were immersed in water and their weight recorded after surface water removal with paper tissues (Crisp *et al.*, 1980). Additionally,

research by Czarnecka *et al.*, analysed the weight loss and ion release of a cement based on an fluoro-aluminosilicate glass (G338), which was moulded into cylinders (6 x 12 mm), and stored in distilled water and lactic acid (Czarnecka *et al.*, 2002). Furthermore, comparable studies were performed to evaluate mass loss and chlorhexidine release profiles in polymerised dental composites (Leung *et al.*, 2005), injectable polymeric adhesives (Young and Ho, 2008), and dental adhesives (Mehdawi *et al.*, 2009). The latter studies were used as a starting point to stablish the wet mass loss protocol used in this research, where the change in percentage of wet mass is established by the following equation (Young *et al.*, 2008;Mehdawi *et al.*, 2009):

$$\Delta m\% = 100\left(\frac{mo - mt}{mo}\right)$$

Where m_o equals the initial sample wet mass at the initial time point and M_t the wet mass at the specific time point

The mechanisms of mass loss and water absorption in GICs were described by Crisp *et al*.: firstly, mass loss was explained by the formation of Na water soluble salts, and to the slow reaction of Al with the matrix forming anions. Even though Al forms insoluble salts, the early slow release implies that it can be leached in water during the setting early stages. Secondly, water absorption, that translates into mass gain, was attributed to the formation of a silica gel that absorbs water and the formation of aluminium hydrates (Crisp *et al.*, 1980). Later, Kuhn and Wilson, compared the dissolution of dental cements to the leaching of radioactive waste from glass or cement matrices and identified the following stages: removal of loose particles or debris from the surface after exposure to aqueous media, dissolution from cracks and fissures, and diffusion of species through pores, cracks and fissures (Kuhn and Wilson, 1985).

The dissolution in GICs was not solely attributed to the glass composition and cement components. Kuhn and Wilson, described that storage media, cement geometry and morphology are involved in this process. For example, in nearly neutral media, the dissolution of the cement increases as a function of the storage volume and the frequency in which it is replaced; while changes in surface area to volume ratio influence ion release (e.g. disc vs. cylinder), with concentrations varying thorough the cement layers and porosity features (Kuhn and Wilson, 1985).

The dissolution behaviour of Al free cements has not been widely described. It is usually reported from a qualitative point of view, mentioning the external characteristics of the samples and/or the solution used to evaluate their stability, with some of the descriptions used to describe samples stable in water as not crumbling when immersed in water (Shi *et al.*, 2006), and absence of sample softening or water cloudiness (Towler *et al.*, 2002). Nonetheless, previous research methodology, evaluated dissolution by ion release, with techniques such as inductively coupled plasma (ICP); with the analysis of the leachate solution either from the glass, in a pH similar to that of the acid-base reaction (Fuchs *et al.*, 2015; Dickey *et al.*, 2016), or from the cement samples in various media such as distilled water (Wren *et al.*, 2013), simulated body fluid (SBF) and Tris Buffer (D'Onofrio *et al.*, 2016).

In addition to the mass change and ion release studies in GICs, the change in pH was previously reported to evaluate fluctuations on cements exposed to solutions of deionised water and lactic acid (Czarnecka *et al.*, 2002), and conductivity was used as a measure of the electrical capability to pass electrical flow, that gives an indication of the number of ions and their mobility in the cement (Crisp and Wilson, 1973). As an acid base reaction, GIC initial setting induces an increase in the pH, in which the glass powder acts as a proton acceptor and the liquid as a proton donor, with hydrogen ions being replaced by the metallic ions coming from the glass (Crisp and Wilson, 1974). Furthermore, GICs are reported to have a buffering capacity when stored in various pH conditions, and occurs by a slight increase of the pH in nearly neutral (distilled water) and acidic solutions (lactic acid). In a similar manner, they had shown to decrease pH when stored in slightly alkaline conditions.

To conclude this chapter, it was considered that in spite of the reported ion modifications used for traditional ionomeric glasses, there is still a gap regarding Al free GICs. Furthermore, the previous work on 45S5 based cements by Mirvakily (Mirvakily, 2009) did not cover further aspects of the characterisation of this cement, which therefore, presented an opportunity for further research with the definition of aim and objectives outlined in the next section.

3 Aim and objectives

The previous chapter presented the literature review describing the need for bone repair and development of aluminium free cements as an alternative for GICs in ENT applications as injectable pastes and bone grafts. As previously described, modifications of the fluoro-aluminosilicate glass composition used on these cements is varied, with the substitution of Al with alternative elements such as iron (Fe), zinc (Zn), magnesium (Mg), gallium (Ga), boron (B) and titanium (Ti). Furthermore, previous to the present research, a solely study by Mirvakily (Mirvakily, 2009) investigated GIC type cements where the glass component was completely replaced by a 45S5 Bioglass® composition. Nonetheless, this study was focused on its development as a scaffold for periodontal repair and as a drug delivery system, without considering variations in glass composition, setting times, and chemical changes during setting. Therefore, the aim of this project was to fabricate and characterise a series of aluminium-free glass ionomer cements based on the SiO_2-Na_2O-CaO-SrO-P_2O_5 bioactive glass system, to evaluate their cement forming properties as a bone graft substitute. Consequently, specific objectives were identified as follows:

a) To define a series of glass compositions based on Hench's SiO_2-Na_2O-CaO-SrO-P_2O_5 system, with variations in SiO_2 (mol %), P_2O_5 (mol %) and network connectivity (NC).

b) To fabricate and characterise the glass powders defined in point (a), via a melt-quench route, using methods previously described in the literature for bioactive glasses. These glasses will be characterised by X-ray diffraction (XRD), X-ray fluorescence (XRF), differential thermal analysis (DTA), scanning electron microscopy (SEM) and Fourier transformed spectroscopy with attenuated total reflectance (FTIR-ATR). From these results, the successfully melted glasses, characterised as amorphous, and with particles sizes of < 45 µm, will be used for cement preparation.

c) To investigate the cement-forming properties of the melt-derived glasses defined in point (b), by mixing these powders with a low molecular weight polycarboxylic acid, specifically poly (acrylic acid) (PAA), and either water or a setting modifier, such as phosphoric acid solution ($H_3PO_{4\ (sol)}$), prepared with a fixed concentration of 50% w/w. Their cement forming properties will be

assessed according to their malleability and stability in water. From these results, parameters such as powder/liquid ratio, PAA, and $H_3PO_{4\ (sol)}$ volume, will be used to stablish a second cement mapping.

d) From the study described in (c), identify a range of cement formulations to study the combination (s) that produce stable cements for all the glass compositions, and evaluate their handling properties: mixing time, initial and net setting times, to compare with a commercially available aluminium containing cement (Serenocem™).

e) To define four glass/cement formulations from (d) for further characterisation: by mass change in distilled water, ion release by inductively coupled plasma spectrometry (ICP), pH, conductivity and setting chemistry by Fourier transformed spectroscopy with attenuated total reflectance (FTIR-ATR); and comparison with a commercial aluminium containing cement (Serenocem™).

f) To define one glass/cement formulation for an *in vitro* direct contact test. This will be carried out by measurement of cell metabolic activity using Presto Blue® and qualitative evaluation by light microscopy and scanning electron microscopy (SEM).

On completion of this research, a series of cements based on the SiO_2-Na_2O-CaO-SrO-P_2O_5 system will be produced. As previously described, this glass system has not been extensively investigated for preparation of aluminium-free cements, for which this research aims to give an overview of the glass compositions and cement preparation parameters, in which stable cements can be achieved. Furthermore, through characterisation of the cements, it is expected to gain an understanding of their degradation in aqueous media and setting. Therefore, the findings derived from this research, could represent an alternative application for bioactive glasses, and a solution to the drawbacks of aluminium containing cements currently used in ENT applications.

4 Materials and Methods

4.1 Glass preparation

Bioactive glasses (SiO_2-Na_2O-CaO-SrO-P_2O_5) were prepared using a melt-quench route: SiO_2 content ranged between 35.8 and 60 mol%. The P_2O_5 content was kept constant at 2.6 mol. %., with two variations corresponding to half (49P3 glass) and double of this amount (49P9 glass) to evaluate the effect of phosphate content on the cement properties. For these calculations, the Si/Ca, Si/Na, and Na/Ca ratios were kept constant. A Sr substitution was studied, as a modification of the 45S5 glass named as 45S5Sr10, with 10 mol. % substitution over CaO.

Table 4-1 shows the glass compositions in wt. % with the chosen melting temperatures, and Table 4-2 shows the glass compositions in mol %, with their corresponding network connectivity values (NC') calculated as previously defined in Section 2.3.4. These compositions were described in a patent exemplification identified as WO2014102538 (Miller *et al* 2014), where the main aim was to study the cement forming properties of aluminium-free glasses based on the 45S5 Bioglass®, 53P4 glass, and the bone bonding area described by Hench (2006) occurring within 40 and 60 wt. % SiO_2. The notation used to name the glasses refers to the SiO_2 content in wt. %, followed by P and the corresponding P_2O_5 content wt. %, in a similar manner to the notation for the 45S5 Bioglass® composition.

Table 4-1 Melt derived glass compositions (wt. %) with melting temperatures (°C)

Glass	SiO_2	Na_2O	CaO	P_2O_5	SrO	Melting Temperature (°C)
35P6	35.0	30.0	29.0	6.0	-	1280
42P6	42.0	27.0	25.0	6.0	-	1360
45S5[*1]	45.0	24.5	24.5	6.0	-	1400
45S5Sr10	44.0	24.1	21.6	5.9	4.4	1400
49P3	50.7	22.6	23.6	3.1	-	1400
49P6	49.0	22.0	23.0	6.0	-	1400
49P9	46.4	20.7	21.6	11.3	-	1400
53P4[*2]	53.0	23.0	20.0	4.0	-	1360
58P6	58.0	24.0	12.0	6.0	-	1400

[*1] Composition referenced from (Pantano *et al.*, 1974)

[*2] Composition referenced from (Andersson *et al.*, 1990)

Table 4-2 Melt derived glass compositions (mol %) with network connectivity (NC')

Glass	SiO_2	Na_2O	CaO	P_2O_5	SrO	NC'
35P6	35.8	29.8	31.8	2.6	-	1.0
42P6	43.1	26.8	27.5	2.6	-	1.8
45S5	46.1	24.4	26.9	2.6	-	2.1
45S5Sr10	46.1	24.4	24.2	2.6	2.7	2.1
49P3	51.0	22.2	25.5	1.3	-	2.3
49P6	50.3	21.9	25.3	2.6	-	2.4
49P9	49.1	21.3	24.6	5.1	-	2.8
53P4	53.9	22.7	21.8	1.7	-	2.5
58P6	60.0	24.1	13.3	2.6	-	3.0

For glass preparation (Figure 4-1), mixtures of the following analytical grade reagents were used: SiO_2 (99% Riedel-de Haën), Na_2CO_3 (99% Fisher Scientific), $CaCO_3$ (98% Acros Organics), $CaHPO_4$ (99% Sigma-Aldrich, UK) and $SrCO_3$ (>98% Sigma-Aldrich, UK), and mixed in a rotatory plastic recipient for 15 min, after which the batch was transferred to a 150 ml platinum crucible (type BC20 Birmingham Metal, UK). This method was chosen after a test was carried out with a 100 ml crucible, but this volume was insufficient to completely melt the theoretical batch which required between three and four stages. The procedure involved adding approximately 30 mg of the glass batch per stage and waiting between twenty and thirty minutes until the mixture was melted and visually homogeneous. Nonetheless, and as explained in section 5.1, this method was not used further as it was not possible to obtain a clear frit.

The batches were melted in a chamber furnace (Model VF2, Vecstar Ltd., UK) at temperatures ranging between 1280°C and 1400°C for 4 h. The melt was cast into a stainless steel recipient containing 9 L of deionised water, to produce a granular frit that was dried at 150 °C for 2 h. This frit was reduced in size (< 2 mm) with a mortar and pestle, and powdered in a rotatory ball miller (Retsch PM100, Germany) for 4 h at 450 rpm with a glass: milling charge ratio of 1:1 (wt.%). The powder was passed through sieves with aperture sizes of 106, 75 and 45 µm (Endecotts Ltd., UK), to obtain a final particle size of less than 45 µm. The glass powders were stored in a desiccator until use for cement preparation.

Figure 4-1 Glass melting stages showing a) high temperature melting of raw materials, (b) melt quenching in demineralised water (c) glass frit after quenching (d) glass powder preparation (e) sieving of the powder. Pictures are courtesy of Dr Hasan Merie

4.2 Cement preparation

A preliminary study was carried out to assess the range of cements that were feasible to mix from a qualitative point of view, and produced stable samples when immersed in distilled water. This stage of the experimental protocol was based on a previous study by Mirvakily (Mirvakily, 2009), and the glass weight was fixed to 125 mg, with powder/liquid ratios (P/L) modified accordingly. PAA is used in GICs as the acid component: in this study a PAA powder with molecular weight of 45.5 kDa was chosen (Advanced Healthcare Ltd., UK), and a phosphoric acid solution, was used as a setting modifier previously described for zinc phosphate cements. This solution was prepared with 99.99% H_3PO_4 crystals (Sigma Aldrich, UK) at a 50 % w/w concentration in distilled water.

The cement samples were prepared with a conventional paste mixing technique used in dentistry as shown in Figure 4-2. Each glass was pre-mixed with PAA with the flat end of a stainless steel spatula, while the liquids were pre-mixed with a pipette tip. The powder was incorporated to the liquid and spatulated between three and five times, until the paste was visually homogeneous. The paste was then transferred onto to a disc shaped silicon mould (4 x 1 mm), sealed with paraffin paper to reduce early desiccation, and compressed with two PTFE plates. The discs were left to set for one day at 37 ^{0}C in an oven (Eurotherm, UK). Preliminary water stability of these samples was evaluated by immersing the aged cement discs in 5 ml of distilled water and stored at 37 °C for one day. At this stage, sample stability in water was evaluated daily by visual examination.

Samples were periodically inspected using a Leica Wild M3Z light microscope (Heerbrugg, Switzerland).

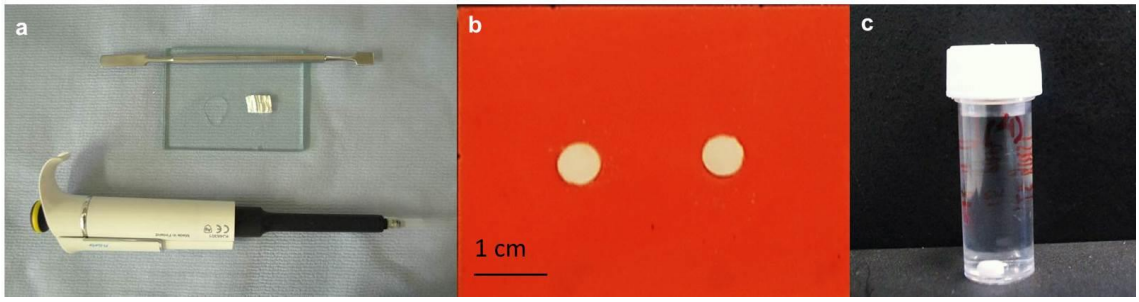

Figure 4-2 Cement disc preparation for preliminary assessment of cement stability (a) glass slab used for traditional mixing of dental cements, showing the powder mix (glass and PAA) and the liquid component (phosphoric acid solution and distilled water) (b) 4 x 1 mm cement samples let to set in a silicon mould (at 37ºC for one day) (c) sample immersed in distilled water for visual assessment of stability

The second stage of the study consisted on evaluating these results to define a systematic range of P/L ratios and $H_3PO_{4\ (sol)}$ concentration for further sample characterisation. The previously defined concentration of 50% $H_3PO_{4\ (sol)}$ was used by Mirvakily *et al.* (Mirvakily, 2010) for cement preparation. However, it was noted that small volume variations of this solution did not represent a significant difference in the final concentration, since water was also used as a plasticiser. Therefore, a comparative study (Figure 4-3 and Table 4-3.) was defined with P/L ratios of 2, 2.5, and 3. The $H_3PO_{4\ (sol)}$ with a 50 % w/w concentration was mixed accordingly with distilled water to achieve final concentrations of 20, 25, 30 and 35 %.

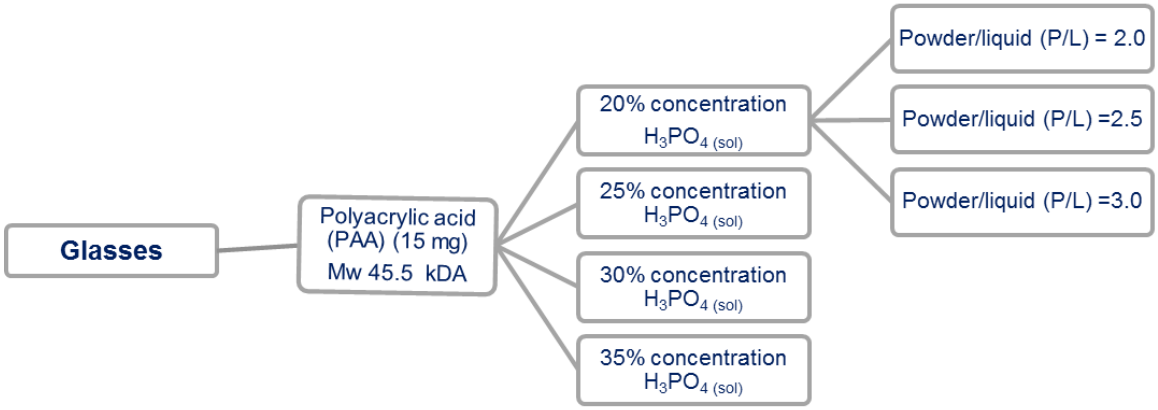

Figure 4-3 Schematic of the content of poly (acrylic acid), % $H_3PO_{4\ sol}$ and powder/liquid (P/L) ratios tested for the second stage of the cement study.

Table 4-3 Cement matrix formulations with variation of P/L ratio, % H_3PO_4 in liquid component with constant percentage of PAA powder content in mixture (10.7% of total powder)

Cement combination	Glass (mg)	PAA (mg)	H_2O (µl)	H_3PO_4 (µl) from 50% w/w	Ratio P/L theoretical	Final H_3PO_4 (sol)
C1	125	15	42.0	28.0	2.0	20.0
C2	125	15	33.6	22.4	2.5	20.0
C3	125	15	28.0	18.7	3.0	20.0
C4	125	15	35.0	35.0	2.0	25.0
C5	125	15	28.0	28.0	2.5	25.0
C6	125	15	23.3	23.3	3.0	25.0
C7	125	15	28.0	42.0	2.0	30.0
C8	125	15	22.4	33.6	2.5	30.0
C9	125	15	18.7	28.0	3.0	30.0
C10	125	15	21.0	49.0	2.0	35.0
C11	125	15	16.8	39.2	2.5	35.0
C12	125	15	14.0	32.7	3.0	35.0

4.3 Materials characterisation

Following preparation of the glasses and cements, characterisation was carried out through various techniques reported in the literature. The description of these techniques and corresponding sample preparation are explained in the section below.

4.3.1 X-ray powder diffraction

X-ray diffraction (XRD) is a technique used to characterise loose powders and aggregates and it is useful for qualitative and quantitative phase identification, determination of crystallinity, and lattice parameter evaluation. Analysis duration can vary: for qualitative studies, it could be approximately an hour and for quantitative analysis can vary between several minutes to several hours (Goehner and Nichols, 1986).

X-rays are electromagnetic radiation with a wavelength of approximately 1 Å, and occurs between the ɤ rays and the ultraviolet light. These are produced when highly energised particles, such as accelerated electrons with a specific voltage, e.g. 30kV, collide with matter, usually of metallic nature. The resulting X-ray spectra have two components: a broad wavelength spectra and a monochromatic one, with the latter used for powder characterisation (West, 1996). After X-rays are generated in a tube, they are

diffracted at the sample's atomic layers and are able to interfere according to Bragg's law:

$$n\lambda = 2dsin(\theta)$$

Where n is customary set to 1

ʎ is the wavelength of the rays, typically 1.54056 Å for a Copper target (Cukα)

d is the lattice spacing between layers of atoms

θ is the Bragg angle between the incident rays and the surface of the crystal

XRD was used to confirm the amorphous structure of the melt-derived glass powders (< 45 μm). The powders were powdered further with a mortar and pestle, uniformly spread between two acetate sheets, and secured onto an aluminium holder. This analysis was performed at the Department of Materials Science and Engineering (University of Sheffield, UK), using a Stoe Stadi P (CuPSD) X-ray Powder Diffractometer (Stoe & Cie, GmbH, Germany) with CuKα radiation, step of 0.03° 2θ, and a scan range between 10° to 60° 2θ. Phases were identified using WinXPOW (version 3.05) for files conversion and PDF- 4 + 2014 database search software, which record the patterns collection of the Joint Committee of Powder Diffraction Standards (JCPDS).

4.3.2 Wavelength dispersive X-ray fluorescence

Wavelength dispersive X-ray fluorescence (XRF) is an analytical technique used to determine the elemental composition of solid materials in bulk or thin film form. The sample is irradiated by an X-ray beam that discharges the inner shell electrons from the sample's atoms, causing the outer shell electrons to replace them. The difference in energy level results in the emission of X-rays (secondary radiation). The wavelength of these X-rays is characteristic for each element, and the intensity of the emission is dependent on their concentrations (Philips, 2011).

XRF was used to assess the post-melt compositions of the experimental glasses. This analysis was performed by the Materials and Engineering Research Institute (Hallam University, UK), using a Philips Analytical MagiX PRO model PW2440 with a sample changer model PW2540 at 20kV and 10mA. Sample preparation was carried out by mixing the glass powder and a $Li_2(BrO_2)_4$ flux (99% Fluore-X ATL 100) at a 1:10 ratio. This mix was melted in a platinum-gold crucible for approximately 12 min at 1200 ^{0}C,

and poured on a pre-heated mould to produce a glassy disc. Small quantities of potassium iodide were added to the melt in order to prevent cracking of the glass slab during cooling.

4.3.3 Differential thermal analysis

Differential thermal analysis (DTA) is a technique used to characterise the physical and chemical properties of a sample as a function of temperature, by measuring heat changes through a temperature gradient when a sample is heated at a certain rate. Figure 4-4, illustrates the general principle of this method, where thermal events such as melting, decomposition and phase transformations, are reflected as endothermic or exothermic peaks with respect to the base line (West, 1996).

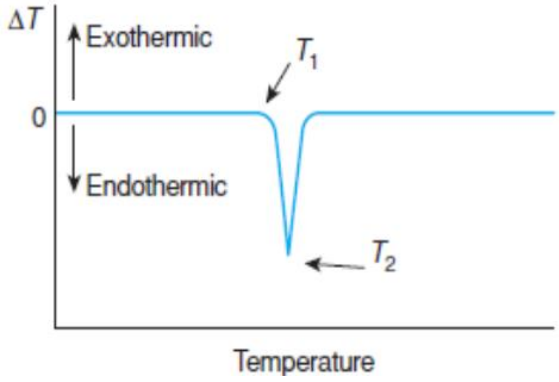

Figure 4-4 Differential thermal analysis (DTA) general showing the direction of the exothermic and endothermic reactions Reprinted with permission from West (2014). Copyright 2014 John Wiley & Sons Ltd.

This technique was used to determine the glass transition (T_g), crystallisation temperatures (T_p), and melting temperatures (T_m) of the melt-derived glasses (Table 4-2). This experiment was carried out using a Perkin Elmer Diamond TG/DTA, under a nitrogen atmosphere, where an aluminium pan was filled with the glass powder (< 45 µm) to 3/4 of its capacity (weight varying between 30 and 40 mg), with a two-step heating program: an isotherm at 50°C for 5 min, and from 50°C to 1300°C at 10°C/min. The T_g was estimated following a procedure by Clupper and Hench (Figure 4-5) and mjograph software version 4.6.1 (Makoto Tanahashi, Japan) (Clupper and Hench, 2003), while the crystallisation temperatures (T_p), and melting temperatures (T_m), were determined with the Pyris Software, incorporated in the TG/DTA instrument.

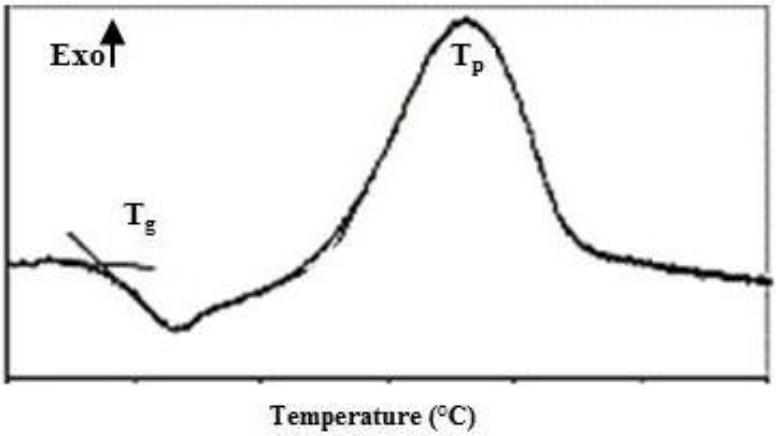

Figure 4-5. Differential thermal analysis curve showing the glass transition temperature (T_g), and the positioning of the tangent lines used definition of the glass transition temperature, and the glass crystallisation temperature (T_p). Reprinted with permission of Clupper and Hench (2003). Copyright 2003 Journal of Non-Crystalline Solids. Headings were modified from the original picture to improve its reading.

4.3.4 Scanning electron microscopy

Scanning electron microscopy (SEM) is an imaging technique used to visualise the topography of a sample with a 3D quality. Figure 4-6 shows the working principle of this technique, based on the emission of low energy secondary electrons from the sample when a high energy beam (5-100 keV) is directed at a specific spot (Ratner *et al.*, 2004). This spot can range between 50 and 500 Å with a penetration depth of up to 1 µm (West, 1996). The composition and geometry of the sample influences the intensity of the electrons' energy emission, which is captured and spatially reconstructed by a phosphor screen (Ratner *et al.*, 2004).

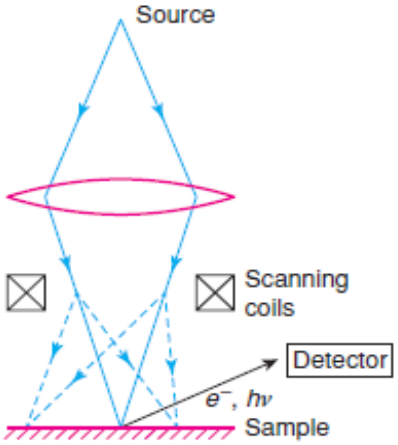

Figure 4-6. SEM working principle. Reprinted with permission from West (2014). Copyright 2014 John Wiley and Sons Ltd.

This technique was used to characterise the size range and morphology of the melt-derived glass powders, and for qualitative evaluation of cells cultured on the cement discs. This analysis was carried out at the Department of Biomedical Science (University of Sheffield, UK), using a Philips XL-20 SEM, at an accelerating voltage of 15 kV. Samples were mounted on an aluminium holder with adhesive carbon tape, and gold-coated for two min at a 15 kV current

4.3.5 Fourier transformed infrared spectroscopy with attenuated total reflectance

Fourier transformed infrared spectroscopy (FTIR) is a form of infrared spectroscopy, that provides information on the vibrations of atomic and molecular species. FTIR is a very sensitive technique with a penetration depth ranging between 1-5 μm (Figure 4-7) (Ratner *et al.*, 2004). The principle of FTIR, relies on the atomic vibration of solids at frequencies ranging between 10^{12} to 10^{13} Hz of infrared radiation; however, it is possible to elevate the atoms to a higher energy state by absorption of a specific frequency, where each peak in the spectra corresponds to a particular vibrational transition (West, 1996).

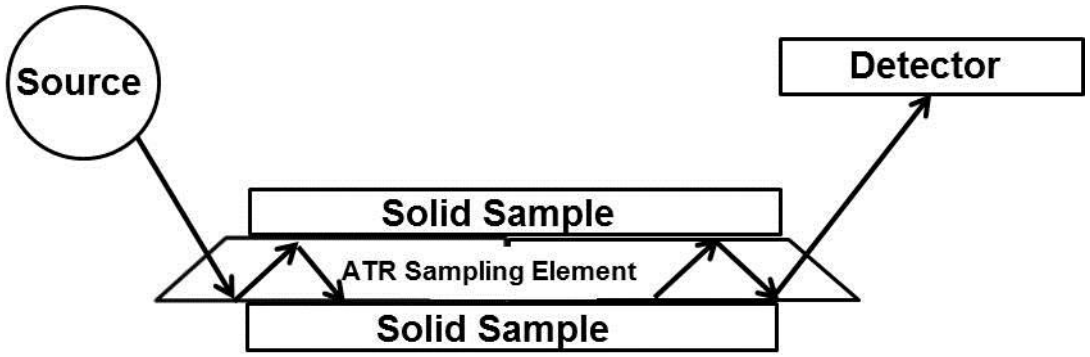

Figure 4-7 Attenuated Total Reflectance infrared spectroscopy (ATR-IR) schematic Adapted from Ratner (1992) with permission from Elsevier.

The ATR mode is useful to carry out the analysis directly on the surface of the sample, without preliminary preparation of a KBr disc. The ATR accessory consists of a high refractive index crystal, in which the reflected beam coming from the sample generates an attenuated evanescence wave that returns to the IR and exits the opposite of the crystal to the detector of the IR spectrometer (Elmer, 2005).

FTIR-ATR was used to characterise the functional groups of the experimental glasses, PAA, H_3PO_4, and to follow up the cement setting. This analysis was performed at the Department of Chemistry (University of Sheffield, UK), using a Bruker α Alpha-P with Opus 6.5 software (Bruker Optic, GmbH), and a diamond attachment in absorbance mode. The resolution was set at 4 cm^{-1}, and wavelength ranged between 358 cm^{-1} and 4000 cm^{-1}; with 32 scans per measurement. An initial background scan was carried out before each set of samples.

Figure 4-8 shows the setting used for this experiment. The preparation of the sample depended on the tested material: for glass powders, PAA, and H_3PO_4 no further preparation was carried out. For the cements, the pastes were mixed as previously described in section 4.2, and immediately placed on the FTIR plate, after which the ATR accessory was adjusted until complete contact with the sample was achieved. Measurements were taken directly after mixing, and then each 5 min up to 60 min.

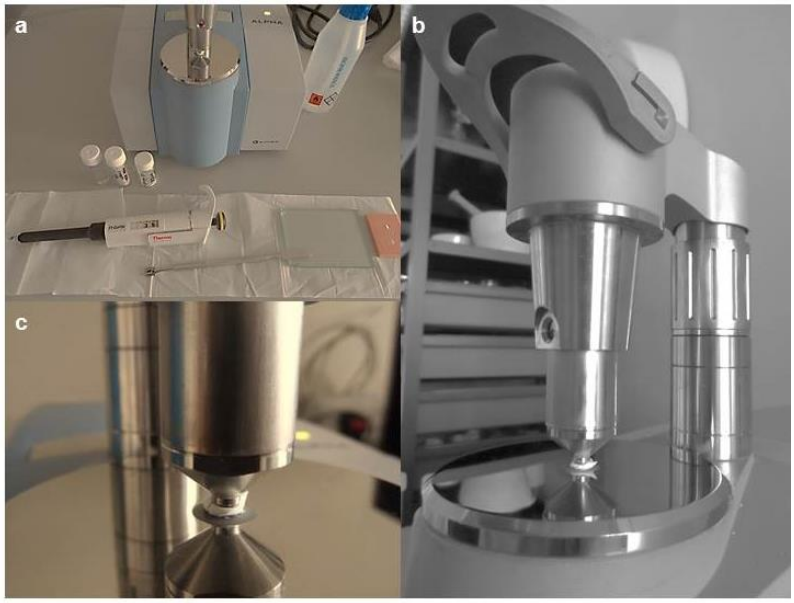

Figure 4-8 Experimental setting for use of FTIR-ATR a) materials preparation for paste mixing b) detail of set up of the machine after pressure was applied onto the sample c) detail of the diamond tip in complete contact with the cement paste

4.3.6 Handling characterisation for cement pastes

The used protocol was based on the guidelines stablished in the Standard for Water based cements Part 1. Powder liquid acid-based cements ISO 9917-1:2007 (ISO, 2007). On this standard, the mixing time is defined as "the part of the working time required to obtain a satisfactory mix of the components.". For this experiment, the satisfactory mix

was chosen at the point when it was possible to obtain a homogeneous paste in terms of colour and consistency.

The initial and net setting time was measured based on the ASTM standard for "Time of Setting of Hydraulic-Cement Paste by Gillmore Needles" number C266-15 (ASTM, 2015a). Figure 4-9 and Figure 4-10 show the experimental set-up and a detail of the Gillmore Needle indenters. The initial setting is defined by the time in which the lighter needle (Ø = 2 mm tip and 113 g of mass) does not make a mark on the surface of the cement. The net setting was defined as the period of time, measured from the end of the mixing, until the heavier needle (Ø = 1 mm tip and 453 g of mass) fails to make a complete circular indentation on the surface of the cement. The samples used for assessment of the setting time (n=4) were prepared as explained in section 4.2, using enough cement mix to completely fill an acrylate disc shaped (2.87 x 7.82 mm) mould while temperature and humidity were recorded for each set of samples.

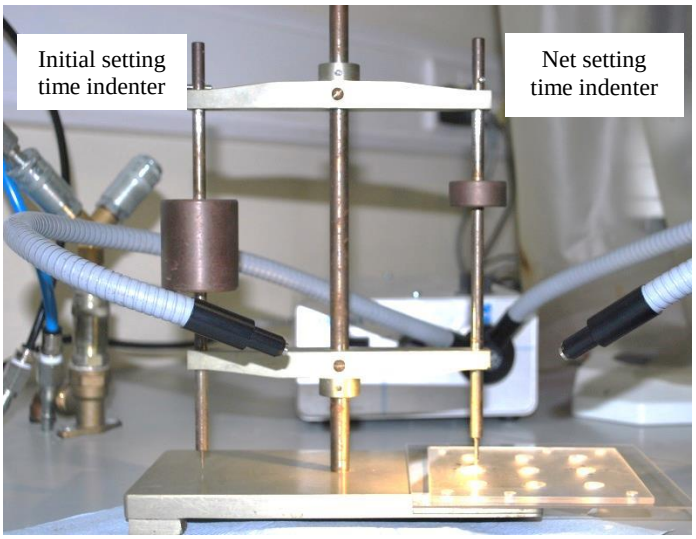

Figure 4-9 Gillmore needle setting for measurement of initial and net setting time

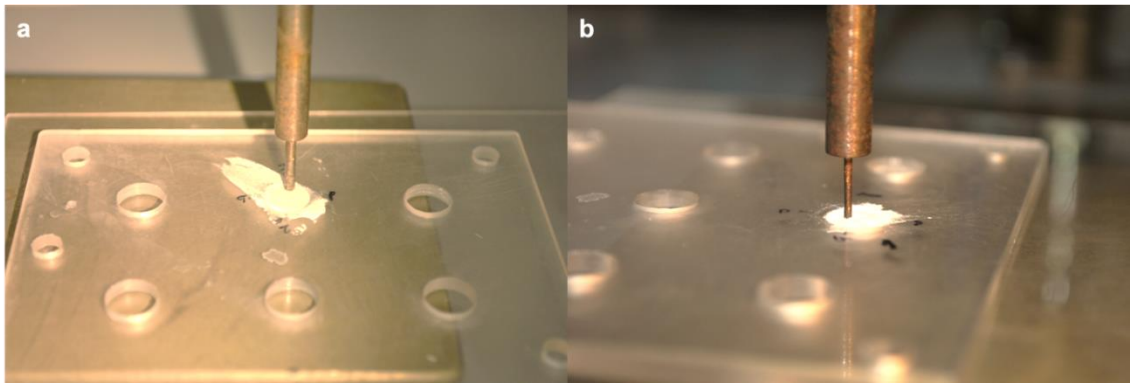

Figure 4-10 Detail of Gillmore needle indenters a) 2 mm diameter indenter used to measure the initial setting time b) 1 mm diameter indenter used to measure the net setting time

4.3.7 Degradation in water of cements: mass change

Cement samples were prepared by hand mixing on a glass slab using a stainless steel spatula at an average room temperature of 22 °C and humidity between 49 and 60%. The cement formulations used for this experiment were chosen after considering the combination that allowed the highest number of stable cements in water for all the experimental glasses, after the second stage for cement evaluation described in section 4.2. Cements were prepared by mixing the glass powder (< 45 μm), PAA and $H_3PO_{4\ (sol)}$ and transferred into disc shaped silicon moulds (9 x 2 mm, n=4) (Figure 4-11). The amount of glass was 250 mg, with PAA and liquid added accordingly, in order to prepare a paste that could fill the 9 x 2 mm mould. Additionally, Serenocem™ cement samples were prepared following manufacturer's instructions by activating the capsules (batch FG1401010) and mixing for 15 s in a dental machine mixer provided by Corinthian Ltd. (Nottingham, UK).

Figure 4-11 Preparation of cement samples for investigation of mass change following immersion in water (n=4). Samples were set for one day at 37 ºC before testing.

Cement stability in distilled water was evaluated by immersing set discs (one day, 37°C) in 20 ml of distilled water (Figure 4-12). For each measurement, the samples were carefully blotted dry with lab tissues, and the mass recorded at one hour, one day, one week, one month, two months, and three months. For the duration of the experiment, samples were stored at 37 °C in an oven, with the storage solution (distilled water) changed after each time point.

Figure 4-12 Storage container used for investigation of mass change in distilled water, with an example of a cement disc stable in water

4.3.8 Inductively coupled plasma spectrometry

Inductively coupled plasma spectrometry (ICP) is a technique used to evaluate ionic concentration in a solution or sample. The equipment is based on a spray chamber with a double tube with 98% discharged ions and 2% plasma at 9000^{0}C that excites atoms and ions to a higher energy level. It contains a digital camera that is able to capture wavelengths varying from 130 nm to 800 nm. The machine then compares the intensity counts obtained from the sample with the software, and makes the conversion by comparing with internal standards. The result is the equivalent of the number of photons emitted by the sample at different wavelengths, which corresponds to a particular element. This value is then comparable to the amount of ions in solution in ppm or mg/L (Bramall, 2015).

This analysis was performed by the Department of Chemistry (University of Sheffield, UK), using a Spectro Ciros Vision instrument with Smart Analyser Vision Multielement software (Figure 4-13). ICP was used for analysis of ion concentrations from the cements' storage solution, specifically Si, Na, Ca, P, Al and Sr. At each time point: one

hour, one day, one week, one month and two months, the 20 ml of distilled water was transferred to a universal and vortexed (Fisons Whirlimixer, UK) for approximately 20 s to allow homogenization prior analysis. From this volume, 10 ml were stored for ICP analysis and stabilised with four drops of high purity nitric acid. Samples corresponding to one week and one month were diluted in a 1 to 5 ratio, as suggested by the ICP specialist since the concentration of elements such as Na increased significantly between one hour and one day. The final concentration was adjusted according to this dilution factor.

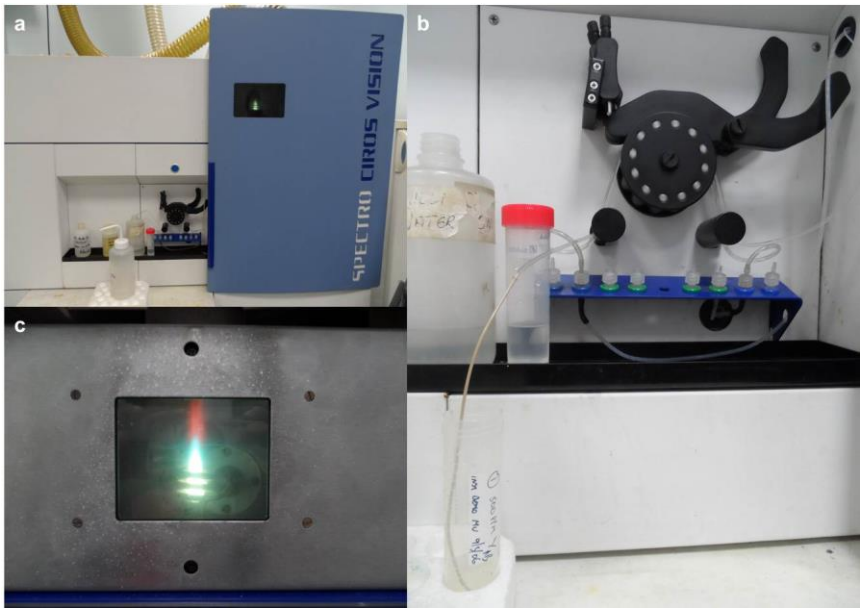

Figure 4-13 Ion release measurement by ICP a) Spectro Ciros Vision machine b) Capillary in which the leachate is transferred to the internal chamber c) Detail of plasma flame

4.3.9 Dissolution testing: pH and conductivity

The pH and conductivity of the storage distilled analysis was measured using a pH 211 pH meter (Hannah Instruments) and a FG3-Fivego™ conductivity meter (Mettler Toledo). At each time point: one hour, one day, one week, one month and two months, the 20 ml of distilled water was transferred to a universal and vortexed (Fisons Whirlimixer, UK) for approximately 20 s to allow homogenization prior analysis. All instruments were calibrated before use, and the pH meter electrodes were rinsed with distilled water and dried for each measurement.

4.4 Short term direct contact *in vitro* test

On this research, cell viability was evaluated by applying the principles of the direct contact method and analysed with a qualitative and quantitative technique: microscopy (light microscopy and SEM) and fluorescence (PrestoBlue® assay).

4.4.1 Pre-treatment of cement samples

A washing protocol was performed to reduce fast release of alkaline species (e.g. sodium) after sample immersion in the well A preliminary protocol was performed by testing 9 x 2 mm cements discs. Samples were divided in two sets (n=3) with 20 and 50 ml of distilled water following the protocol described on section 4.3.9, and solution changed until average conductivity values were below 100 µs/cm. This procedure was carried out with the objective of comparing if there was any significant difference on the washing time and cell survival with a variation on the water volume.

4.4.2 Cell culture protocol

Cements discs (4 x 1 mm) were prepared as described in section 4.2, set at 37 °C for one day, and autoclaved (Rodwell M25, UK) at 120 ºC for 15 min. L929 fibroblasts and MG63 human osteosarcoma cells (passage 28-31) were seeded at a density of 50,000 cells/well (growth area of 1.12 cm^2) directly onto a 24 well plate. Discs were placed in each well three hours after seeding, when cells appeared to be settled on the bottom of the well plate. Cells were incubated at 37 ºC and 5 % CO_2. For all the experiments, aseptic laboratory techniques were followed, by using sterile equipment, and sample manipulation was carried out in a Class 2 MSC safety cabinet. Basic procedures for *in vitro* cultures consisted of passaging and maintenance of cell lines: 2 ml of trypsin was used for cell passaging after washing the flasks with 10 ml of pre-warmed phosphate buffered saline (PBS, D8537, Sigma-Aldrich, UK). To allow cell detachment due to the trypsin, the flask was stored in the incubator (37ºC, 5% CO_2) until complete cell detachment was observed with a light microscope. In order to neutralise the trypsin, 4 ml of media (Table 4-4), was added to obtain a cell suspension that was transferred to a universal and centrifuged (5 min at 1000 rpm), after which the supernatant was pipetted out to re-suspend the cell pellet with new media. For cell counting before passaging and for seeding the cells onto the samples, 10 µl of cell suspension was added into the haemocytometer chambers for cell counting. If the cell number was sufficient for the *in*

vitro test, these were seeded onto a 24 well plate; otherwise the suspension was transferred to a new T75 flask until 80 to 90% of cell confluency.

Table 4-4 Description of media and supplements added for L929 and MG63 cell line maintenance protocols

Cell type	Media	Supplements
L929	Dulbecco's Modified Eagle Medium High glucose (D5671 Gibco)	10% fetal bovine serum (FBS), 2% antibiotic/antimycotic (Penicillin/Streptomycin), 2% HEPES buffer solution, 1% L-Glutamine and 1% of non-essential amino acids
MG63	Minimum Essential Medium Eagle- α modification (M4526 Sigma)	10% fetal bovine serum (FBS), 2% antibiotic/antimycotic (Penicillin/Streptomycin), 0.5% L-Glutamine

4.4.3 Cell viability measurement with PrestoBlue® assay

For the PrestoBlue® assay (Invitrogen, USA), the media was discarded and wells were washed three times with PBS. The dye solution was` prepared by mixing 10% of PrestoBlue® reagent with pre-warmed media. After this, one ml of the dye solution was added to each well. The plate was covered with aluminium foil and stored in the incubator (37 ºC, 5% CO_2), and placed 5 min on a Luckham 4RT (Luckham, UK) rocking table before each fluorescence reading, at 30, 60 and 180 min. At these time points, 100 µl were taken from each well in triplicate and transferred into a 96-well plate (CELLSTAR®, Germany) for fluorescence analysis. Nine additional wells were filled with dye solution as a background correction, to account for the cell/sample fluorescence interaction. The fluorescence was measured using a spectrophotometer (Infinite® 200 PRO, Tecan Co., Switzerland) at 535 nm excitation and 615 nm emission and the data was processed with a built in software (Magellan™, Tecan Co).

4.4.4 Light microscopy and SEM

Cells were checked daily with an Eclipse 100 light microscope (Nikon, Japan) if growth was occurring near the sample or towards the TCP surface. For SEM analysis, samples were washed twice with pre-warmed PBS (37 ^{0}C) and pre-fixed in a glutaraldehyde in 0.1 M cacodylate buffer and left overnight in the well plate at 4 ^{0}C. Samples were post fixed by washing three times with 0.1 M cacodylate buffer and replaced for 55 min by 1 ml of osmium (1% in distilled water) (Agar Scientific, UK). Samples were dehydrated with a series of ethanol dilutions in distilled water as follows: 70% (5 min), 95% (5 min), and 100 % (2 x 5 min). For final preparation, samples were washed in

hexamethyldisilazane (HMDS) (Sigma Aldrich, UK) (1 x 5 min and 1 x 10 min) and then excess was removed to allow samples to dry overnight.

4.5 Statistical Analysis

Mean values were calculated from at least three samples, with graphs prepared using GraphPad Prism 7 (GraphPad Software, USA). Statistical analysis was performed using SPSS Statistics version 23. One-way analysis of variance (ANOVA) was used, and the level of statistical significance was defined at $p < 0.05$. Homogeneity and Normality test were applied for each data set. For the homogeneity test, Levene's Test of Equality of Error Variances was applied: for $p > 0.05$ a Tukey HSD post-hoc test was chosen and for $p < 0.05$ a Games-Howell post-hoc test was chosen. The normal distribution of the data or normality test was carried out for Standardised Residuals. The p value used corresponded to the Shapiro-Wilk coefficient, which was recommended in the literature for a sample size of less than fifty (Ghasemi and Zahediasl, 2012).

5 Results Glasses and Cements

5.1 Glass preparation

The chosen time and temperature parameters were appropriate to melt all the glasses with exception of the 35P6 composition. For this glass, it was not possible to achieve melt homogeneity at the tested temperatures (1280°C and 1360°C), and consequently, it was not further characterised. For the rest of the compositions, transparent granules with no noticeable evidence of crystallisation were observed in the glass frit. Nonetheless, the final method, previously described in section 4.1, was standardised after preliminary trials using a smaller crucible (volume =100 ml). This volume was not sufficient to melt the glass batches in one stage, and consequently the powder was added in stages that varied between three and four depending on the glass composition. As a result, white opaque particles were observed in the frit of the 45S5 glass, suggesting that homogenisation of the melt was not fully achieved.

5.1.1 X-Ray powder diffraction

XRD was performed to confirm the amorphous nature of the melt-derived glasses. Figure 5-1 shows the XRD diffraction patterns with the typical broad peak or halo for glassy states. For all the patterns, this halo was observed between 26^0 and 37^0 2Θ with no evidence of defined peaks representing crystalline phases, which was in good accordance with the 2Θ range reported in the literature (Sepulveda *et al.*, 2002;Chen *et al.*, 2006;Mneimne *et al.*, 2011;Groh *et al.*, 2014).

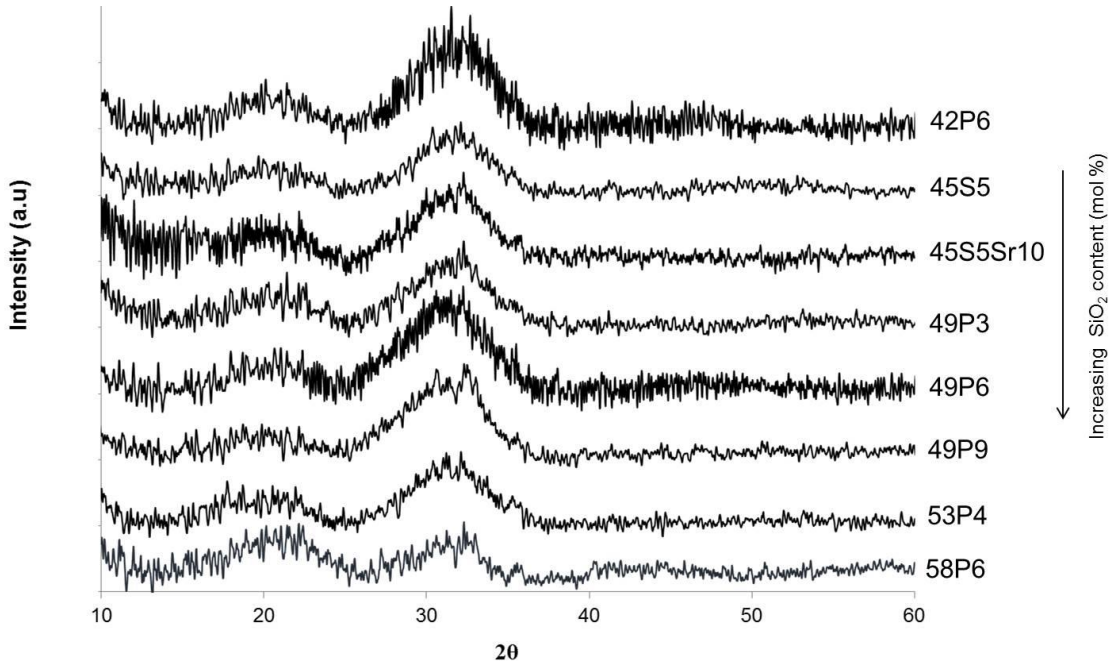

Figure 5-1 XRD diffraction patterns of melt derived glasses based on the SiO_2-Na_2O-CaO-SrO-P_2O_5 system. These patterns showed a characteristic amorphous halo with no apparent crystallisation peaks. The curves are positioned to show glasses with increasing SiO_2 content

5.1.2 Wavelength dispersive X-ray fluorescence

XRF was performed in order to verify the post-melt glass compositions and the presence of impurities. Table 5-1 shows the XRF raw data (wt. %) and Table 5-2 shows the difference between the theoretical values presented in Table 4-1 and the raw data presented in Table 5-1.

XRF data showed comparable results with the theoretical glass compositions, with the following specific variations: Firstly, all compositions had lower SiO_2 content when compared with the theoretical compositions. These variations ranged between 0.1 wt. % for the 45S5Sr10 and 49P6 glasses, and 1.0 wt. % for the 45S5 glass. Secondly, the Na_2O content was slightly higher when compared with the theoretical compositions, with values ranging between 0.1 wt. % and 0.9 wt. % for the 42P6 and 53P4 glasses respectively. Thirdly, the CaO content was below the theoretical compositions, with values ranging between 0.2 wt. % and 1.8 wt. % for the 49P9 and 45S5 glasses respectively. Finally, the P_2O_5 content was lower than the theoretical compositions, with a negligible variation for the 49P3 glass and 0.8 wt. % for the 45S5 glass respectively. The SrO in the 45S5Sr10 glass was slightly lower in the post-melt composition (0.2 wt. %). In addition, various impurities, all below 0.1 wt. %, were detected, corresponding

to: MgO, K_2O, TiO, MnO, FeO, ZrO BaO and Al_2O_3, with the Al_2O_3 varying between 0.04 wt. % and 0.09 wt. %.

Table 5-1 XRF data showing the composition values (wt. %) of the melt-derived glasses based on the SiO_2-Na_2O-CaO-SrO-P_2O_5 system. The data shown corresponds to one glass sample

Glass composition	SiO_2 (wt. %)	Na_2O (wt. %)	CaO (wt. %)	P_2O_5 (wt. %)	SrO (wt. %)
42P6	41.8	27.1	24.0	5.7	-
45S5	44.0	25.0	22.7	5.2	-
45S5Sr10	44.0	24.3	20.8	5.7	4.2
49P3	50.4	23.1	22.7	3.1	-
49P6	48.9	22.5	22.1	5.9	-
49P9	46.0	21.1	21.4	10.9	-
53P4	52.5	23.9	18.8	3.6	-
58P6	57.5	24.5	11.7	5.9	-

Table 5-2 XRF data showing the difference (in wt. %) between the theoretical glass compositions and the XRF values (from Table 5-1). Wt. % differences were obtained by subtracting the theoretical compositions from the individual oxides from the XRF results. The data shown corresponds to one glass sample

Glass composition	SiO_2 (wt. %)	Na_2O (wt. %)	CaO (wt. %)	P_2O_5 (wt. %)	SrO (wt. %)
42P6	0.3	-0.1	1.0	0.3	-
45S5	1.0	-0.5	1.8	0.8	-
45S5Sr10	0.1	-0.2	0.8	0.2	0.20
49P3	0.3	-0.5	1.0	0.0	-
49P6	0.1	-0.5	0.9	0.1	-
49P9	0.4	-0.4	0.2	0.4	-
53P4	0.5	-0.9	1.2	0.5	-
58P6	0.5	-0.5	0.3	0.1	-

5.1.3 Differential thermal analysis

DTA was used for thermal characterisation of the glass powders (45 µm). Figure 5-2 shows the curves recorded at a heating rate of 10 °C/min and Table 5-3 shows the glass transition temperature, crystallisation temperature (s) (T_{p1}, T_{p2}), and melting temperatures ($T_{m1,}$ T_{m2}) for all the glass compositions.

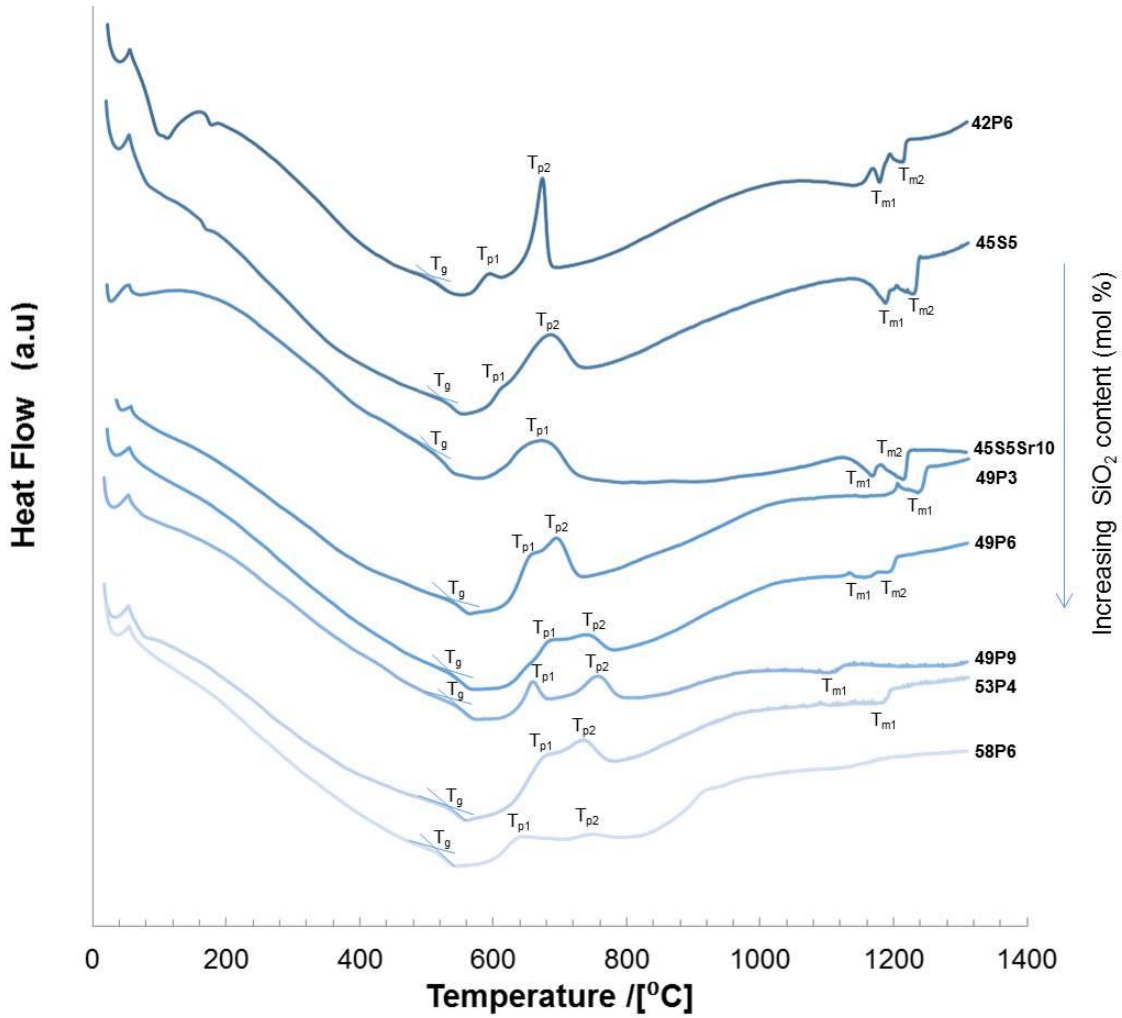

Figure 5-2 Differential thermal analysis (DTA) curves showing the thermal degradation behaviour of the glasses based on the SiO_2-Na_2O-CaO-SrO-P_2O_5 system. The glass transition temperature, crystallisation peak (s) and melting temperature(s) are identified with T_g, T_{p1}/T_{p2} and T_{m1}/T_{m2} respectively. The curves are positioned to show glasses with increasing silica content

Table 5-3 DTA results showing the glass transition temperatures, crystallisation temperatures (T_{p1} and $T_{p2)}$, and melting temperatures (T_{m1} and $T_{m2)}$ of the glasses based on the SiO_2-Na_2O-CaO-SrO-P_2O_5 system

Glass composition	$T_g(^0C)$	$T_{p1}(^0C)$	$T_{p2}(^0C)$	$T_{m1}(^0C)$	$T_{m2}(^0C)$
42P6	502	594	674	1179	1214
45S5	529	687	—	1187	1232
45S5Sr10	521	672	—	1169	1216
49P3	539	654	695	1240	—
49P6	535	681	741	1157	1195
49P9	545	658	761	1108	—
53P4	527	679	736	1194	—
58P6	516	638	749	> 1300	> 1300

Further study of parameters linked with thermal glass behaviour such as the working window (T_{p1}-T_g) are not included in this chapter since further glass processing (e.g. crystallisation and annealing) is not within the scope of the current research; therefore, this technique was used to compare these values with those reported in the literature

The T_g was calculated as described in section 4.3.3 and corresponds to the inflection point of the endothermic peaks in Figure 5-2. These values did not show significant differences between glass compositions. The lowest T_g recorded corresponded to the 58P6 glass at approximately 516 °C and the highest T_g for the 49P9 glass at approximately 545 °C.

The first and second crystallisation temperatures, denoted by T_{p1} and T_{p2} respectively, correspond to the exothermic peaks shown in Figure 5-2. T_{p1} ranged between 594 °C and 687 °C for the 42P6 and 45S5 glasses respectively and T_{p2} ranged between 674 °C and 761 °C for the 42P6 and 49P9 glasses respectively.

The melting of the crystals was indicated by the endothermic peaks at high temperatures, representing the first and second melting points ($T_{m1,}$ T_{m2}). All the DTA curves showed well defined melting points, with the exception of the 58P6 glass, which will be further described below. For the rest of the glasses, T_{m1} ranged between 1108 °C and 1240 °C for the 49P9 and 49P3 glasses respectively. The T_{m2} ranged between 1195 °C and 1232 °C for the 49P6 and 45S5 glasses respectively. In this temperature range the 49P3 and 49P6 glasses are not included since these compositions exhibited one melting point at (T_{m1}) as shown in Figure 5-2. For the curve corresponding to the 58P6 glass, it was not possible to identify the endothermic peak (s), for which the melting event was assumed to occur in a temperature range outside the maximum established for the chosen heating program (50 °C -1300 °C).

Scanning Electron Microscopy (SEM) was used to characterise the size and morphology of the glass powders. Figure 5-3 and Figure 5-4 show representative images of the sieved glass powders. The quantity of particles in the micrographs was not statistically representative to perform a rigorous study, since this technique was used solely to have a qualitative understanding of the glass powder size and morphology.

From the qualitative analysis of the SEM images, two groups were predominantly found: small particles (about 2-10 µm) and larger particles (about 37-64 µm). Similarly, the morphology was divided into two types: agglomerates with irregular rounded shapes

and particles with angular edges. It was observed that the agglomerates were represented by the lower size range, while the angular particles were represented by the larger size range. In terms of appearance, it could be noted that for the angular particles, their surface seemed to have a combination of smooth and patterned texture, which was similar to fracture or cleavage lines.

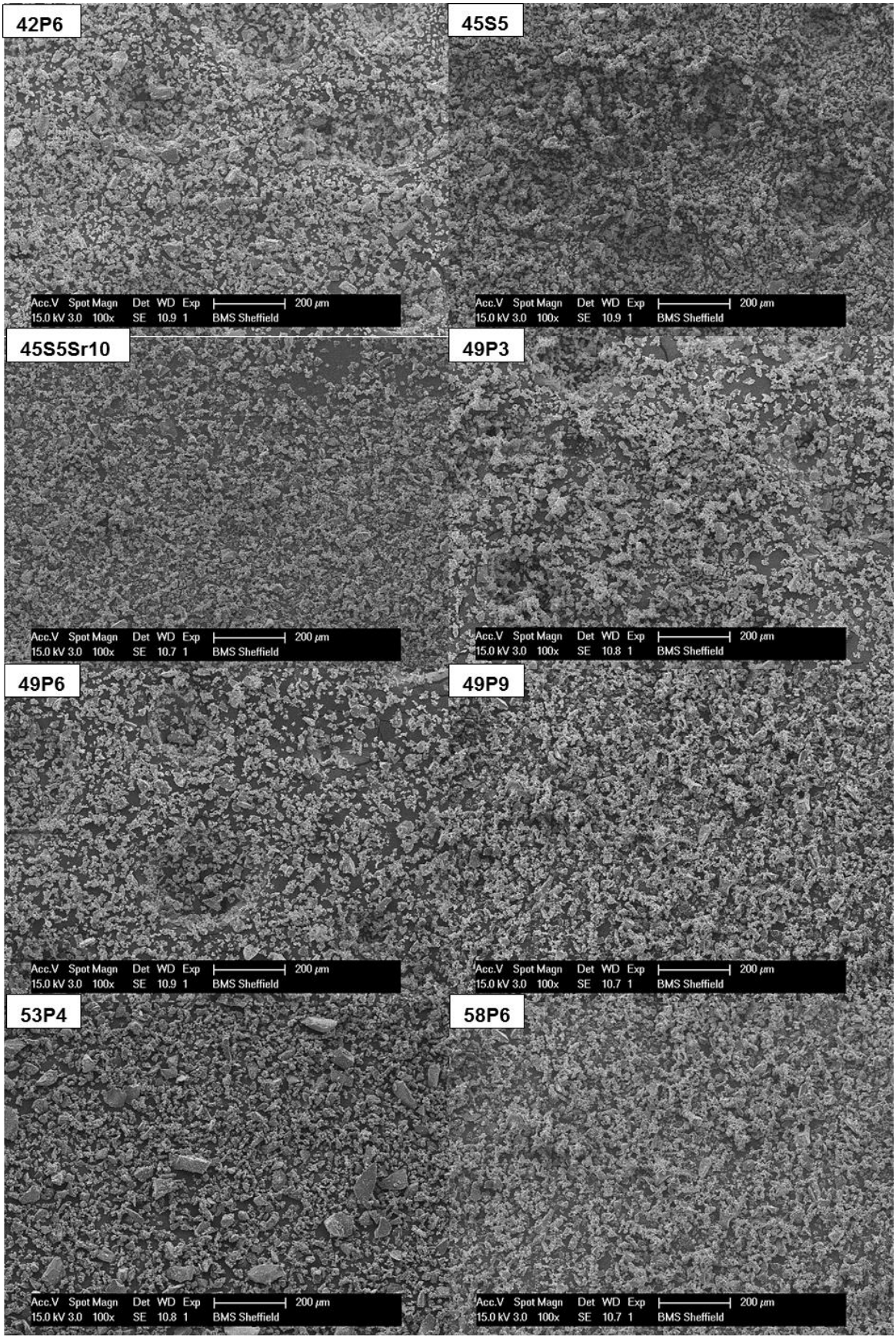

Figure 5-3 Scanning electron microscopy images of the melt-derived glasses. Powders were obtained by milling and sieving the glass frit; scale bar is 200 µm

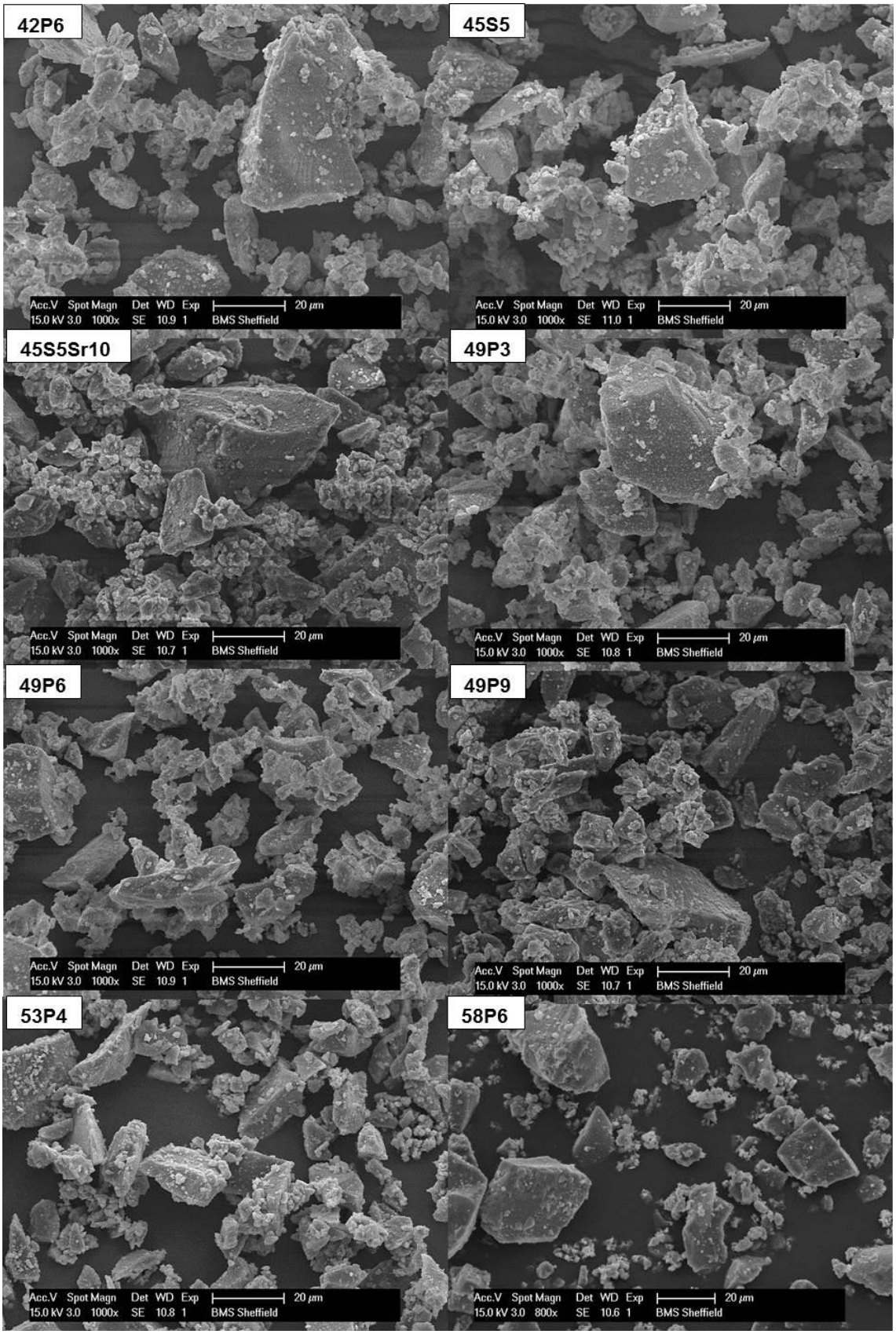

Figure 5-4 Scanning electron microscopy images of the melt-derived glasses. Powders were obtained by milling and sieving the glass frit; scale bar is 20 µm

5.1.4 Fourier transformed infrared spectroscopy with attenuated total reflectance

Figure 5-5 shows the spectra of the melt-derived glasses, with the peaks coinciding to those reported in the literature, as previously defined in section 2.4.4. Firstly, a peak at approximately 1500 cm^{-1} was identified for all the glass compositions, with slight intensity variations, and previously assigned in the literature to a carbonate reported within the 1400-1515 cm^{-1} region (Cerruti *et al.*, 2005;Massera *et al.*, 2012b; Massera and Hupa, 2013).

Secondly, in the region between 1200 cm^{-1} and 800 cm^{-1}, there were two broad peaks centred at approximately 1000 cm^{-1} and 910 cm^{-1}. The peak centred at approximately 1000 cm^{-1} appeared to slightly shift to higher wavenumbers with SiO_2 content increase, and was referred as a Si-O-Si group. The peak centred at approximately 910 cm^{-1}, was reported in the literature as a Si-O-NBO group (Serra *et al.*, 2003;Young *et al.*, 2004;Massera *et al.*, 2012b). In addition, a small peak was observed at approximately 840 cm^{-1} with no significant position shifts between compositions, however, the intensity decreased and appeared to be less defined when increasing SiO_2 content. This peak was reported as a Si-O-2NBO group (Serra *et al.*, 2003), and was less defined for the 49P9, 53P4 and 58P6 glasses, as it appeared to become a weak shoulder to become part of the 910 cm^{-1} peak for these compositions.

Thirdly, at approximately 750 cm^{-1}, a broad peak was observed for all the glasses, but became more defined for the 49P9, 53P4, and 58P6 compositions, and was previously assigned to a Si-O-Si group in bioactive glasses (Jones *et al.*, 2001;Sepulveda *et al.*, 2002;Cerruti *et al.*, 2005).

Finally, within the region between 600 cm^{-1} and 400 cm^{-1}, two broad bands were identified: the first one, corresponded to a low intensity peak, present at approximately 585 cm^{-1}, which did not appear to have marked differences between compositions, nonetheless, it was more defined for the higher phosphate content glass (49P9); and was associated in the literature to an amorphous P-O group. The second one corresponded to a broad band centred at approximately 450 cm^{-1}, which did not show significant variations between compositions either, and was assigned to a Si-O-Si group (Jones *et al.*, 2001;Sepulveda *et al.*, 2002).

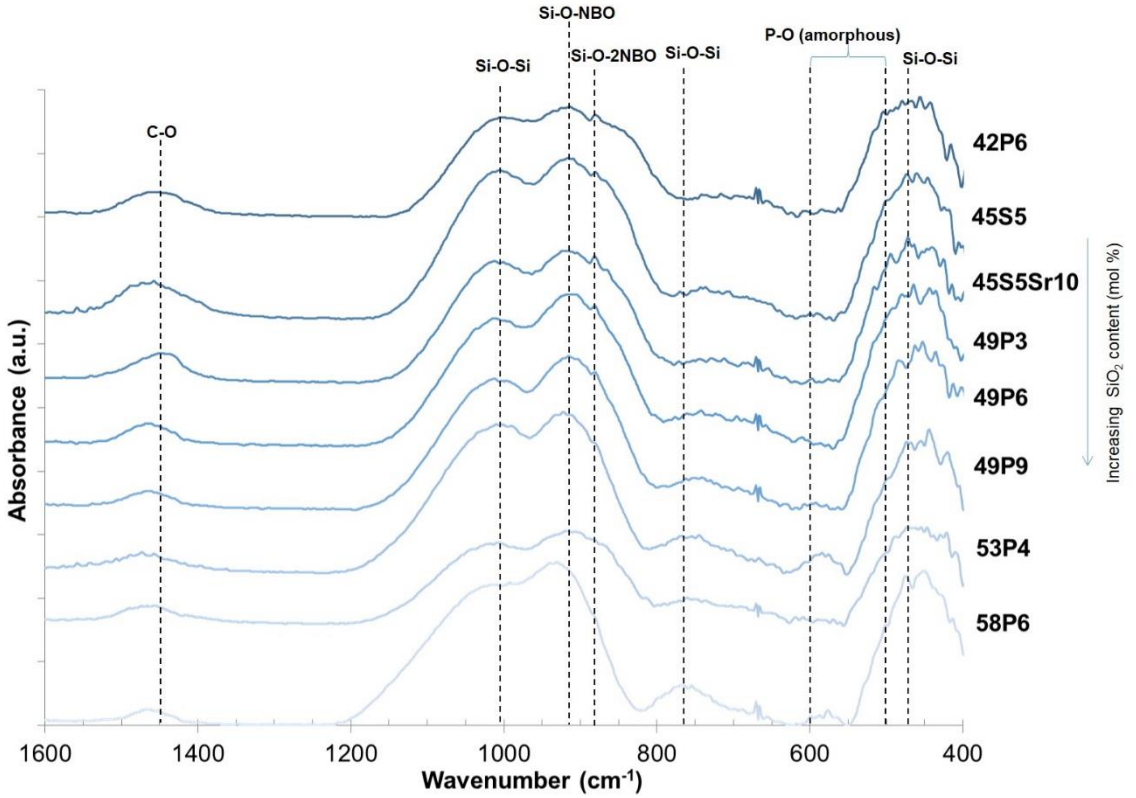

Figure 5-5 FTIR-ATR spectra of the melt-derived glasses based on the SiO_2-Na_2O-CaO-SrO-P_2O_5 system, showing the peaks corresponding to the C-O, Si-O-Si, Si-O-NBO, Si-O-2NBO and P-O vibrations.

5.2 Cement preparation

As previously described, preparation of the cements involved: a preliminary study to assess the malleability of the pastes and their stability in water for a range of formulations; a comparative study of the cements within a specific range of powder/liquid (P/L) ratios and $H_3PO_{4\ (sol)}$ concentrations; and definition of four cement combinations for further characterisation by: mass change in water, ion release by ICP, pH, conductivity, XRD, FTIR-ATR, and *in vitro* testing of the most promising composition.

5.3 Preliminary study on cement preparation

To assess the stability of the cements, a preliminary study was carried out by immersing pre-set cement discs (4 x 1 mm discs) in water. The parameters of powder/liquid (P/L) ratio and setting modifier ($H_3PO_{4\ (sol)}$), corresponded to variations from the initial study on aluminium free bioactive cements by Mirvakily (2009).

Table 5-4, Table 5-5 and Table 5-6; show the preliminary experimental data for the assessed cements. To study their stability, a comprehensive range of powder/liquid (P/L) ratios varying between 1.69 and 3.38 were prepared. These categories were defined based on the qualitative features of the discs, such as definition of the edges, structural integrity (presence of flakes or broken disc) and particles in the water, with descriptions for each type described below. From this preliminary study, three types of cements were found: samples visually stable in water (Type I), samples with reduced stability in water (Type II), and samples that gelled or dissolved in water (Type III).

-Type I: samples visually stable in water (Table 5-4). These discs had no apparent dissolution signs on the surface of the sample (softening), or in the storage water as visible particle loosening. The P/L ratio for Type I samples varied between 1.93 and 3.00.

-Type II: samples with reduced stability in water (Table 5-5). These discs had cracks or loose particles/flakes in the storage water. The P/L ratio for Type II samples varied between 2.07 and 3.38.

-Type III: samples that gelled or dissolved (Table 5-6). These samples had a gel-like/swollen appearance or dissolved completely. This change occurred at least two minutes after the sample was immersed in water. The P/L ratio for Type III samples varied between 1.69 and 2.5, and as can be seen from the table, this type of cements was mainly observed for those combinations without $H_3PO_{4\ (sol)}$.

Table 5-4 Cements combinations corresponding to samples stable in water (Type I). The mass of glass used to prepare the samples was 125 mg.

Glass composition	PAA (mg)	H_2O (µl)	$H_3PO_{4\ sol}$ (µl)	Ratio (P/L)
42P6A	15	35	35	2.00
42P6B	20	40	35	1.93
45S5A	15	35	35	2.00
45S5B	20	40	35	1.93
45S5Sr10A	15	35	35	2.00
49P3A	10	25	35	2.25
49P3B	15	35	35	2.00
49P6A	10	20	35	2.45
49P6B	15	35	35	2.00
49P6C	20	25	35	2.42
49P9A	10	20	25	3.00
49P9B	10	20	35	2.45
49P9C	15	35	35	2.00
53P4A	15	30	35	2.15
53P4B	15	30	40	2.00

Table 5-5 Cement combinations corresponding to samples with reduced stability in water (Type II) All samples were prepared with a base glass of 125 mg

Glass composition	PAA (mg)	H_2O (µl)	$H_3PO_{4\ sol}$ (µl)	Ratio (P/L)
42P6A	10	30	35	2.08
42P6B	15	25	35	2.33
42P6C	15	35	30	2.15
45S5Sr10A	10	30	35	2.08
45S5Sr10B	10	35	35	2.07
45S5Sr10C	20	35	35	2.07
49P3A	10	35	20	2.45
49P3B	10	35	30	2.08
49P3C	15	30	30	2.33
49P3D	15	20	35	2.55
49P3E	20	30	40	2.07
49P6A	10	25	35	2.25
49P6B	15	20	35	2.55
49P6C	15	25	35	2.33
49P6D	20	20	35	2.64
49P9A	10	20	20	3.38
49P9B	25	25	20	2.31

Table 5-6 Cement combinations corresponding to samples that dissolved in water (Type III). All samples were prepared with a base glass of 125 mg

Glass composition	PAA (mg)	H_2O (µl)	$H_3PO_{4\ sol}$ (µl)	Ratio (P/L)
45S5A	10	70	0	1.93
45S5B	10	80	0	1.69
45S5C	15	70	0	2.00
45S5D	20	70	0	2.07
45S5E	20	80	0	1.81
45S5Sr10A	15	80	0	1.75
45S5Sr10B	20	60	0	2.42
49P3A	10	20	35	2.45
49P3B	25	60	0	2.50
53P4A	15	60	0	2.33
53P4B	15	80	0	1.75
58P6A	15	30	40	2.00
58P6B	15	35	35	2.00

The main aspect to consider regarding the preparation of the cement paste was its malleability, which was influenced by the P/L ratio, volume of setting modifier $H_3PO_{4\ (sol)}$ and PAA: increasing the P/L ratio generally reduced the mixing time since the pastes hardened before it was possible to fully mix the components. This influenced the ability for the components to be completely mixed depending on the rest of the variables (glass composition and $H_3PO_{4\ (sol)}$), with shorter mixing times resulting in samples with irregular surfaces due to the non-homogeneous mixing. For P/L values below two, the pastes were liquid-like and started to harden after an hour, which is too long for a cement to be clinically relevant, while pastes with P/L ratios above three, produced pastes that were often too dry to complete mixing. The issue of a dry mix was solved by adding increments of 5 µl of water; however, this slowed the paste hardening.

The use of phosphoric acid ($H_3PO_{4\ sol}$) as a setting modifier was considered essential for cement stability in water, and to accelerate its hardening. Except for a few combinations, $H_3PO_{4\ sol}$ absence caused the cements to start dissolving or gelling (Type III) after two minutes from immersion in water. The addition of $H_3PO_{4\ (sol)}$ influenced mixing, by accelerating the hardening of the paste, thus, mixing needed to be faster to mould the paste before it hardened.

The effect of the PAA depended on the addition of $H_3PO_{4\ (sol)}$. If the setting modifier was not added, increasing the PAA improved the paste malleability. When 10 mg was used, the consistency of the paste was liquid-like, which in practical terms translated to a longer time to harden and sample dissolution. Additionally, 10 mg was not practical due to the small quantity of powder represented by this weight. Increasing PAA to 15

mg, improved paste consistency, similarly to the results when PAA weight ranged between 20 and 30 mg, however, this PAA range appeared to increase the gelation effect when the samples were immersed in water.

From these results, it was observed that the cement system based on the bioactive glasses, PAA and the setting modifier ($H_3PO_{4\ (sol)}$) was complex, with small variations of PAA and H_3PO_4 having an impact on the mixing and stability of the samples in water. This can be seen in the case of example 49P6A Table 5-4, which corresponded to a Type I cement; conversely, an increase of 5 ml in the water volume, Example 49P6A Table 5-5, corresponded to a Type II cement, showing that minor variations had a significant impact on the stability of the cements. Additionally, there was no direct relationship that could be identified between the malleability of the paste and the cement stability in water or the P/L ratio and the stability of the cements, for which their properties were attributed to the interaction of the aforementioned variables. Nonetheless, the P/L ratio had a large impact on the paste hardening and its malleability, both of which are important for practical applications.

5.3.1 Other variables related to paste preparation

In terms of the influence of glass composition with the malleability of the paste, there were marked differences between compositions. In general, for similar mixing conditions (P/L ratio and $H_3PO_{4\ sol}$), the fluidity of the paste appeared to decrease with increasing SiO_2 and P_2O_5 content, hence the pastes prepared with the 42P6 and 45S5Sr10 glasses were easy to mix, while the pastes prepared with the 49P6 and 49P9 glasses the most difficult to mix due to their rapid hardening. However, an exception was noted for the 53P4 and 58P6 glasses, with both producing pastes that were easy to mix, despite being the two compositions with the highest silica content.

Regarding the influence of P_2O_5, it was noted that increasing its content made the mixing more difficult due to a decrease in the paste fluidity; therefore, the paste had to be spatulated faster to be able to mould it into the discs. Regarding the 58P6 composition, the glass appeared to have a “moist” characteristic to it, which resulted in a liquid-like paste and the samples dissolved immediately after immersion in water. Due to this unexpected result, this glass batch was prepared again, to discount a mistake during glass making. In addition, the water volume to prepare the cement was reduced; however, these changes did not have any impact on the cement paste or its stability in water.

Other variables associated to the cement preparation were: sample surface quality, mixing technique, and ambient temperature. Firstly, it was observed that the stability of the cements in water appeared to be dependent on the surface quality of the samples, since non-uniform edges started dissolving first by particle loosening. The surface quality also appeared to be related to the homogeneity of the paste, since the pastes that hardened before achieving this had irregular surfaces than afterwards led to particle loosening. Secondly, the mixing order appeared to affect the paste quality. For instance, mixing first the PAA powder with water, instead of the glass powder; resulted in a very viscous solution, this made it difficult to obtain a homogenous paste. Due to this result, the standard procedure for all the cements was to mix the glass powder and the PAA powder thoroughly, and then proceed to incorporate into the liquid component. Finally, a room temperature higher than 22 °C appeared to accelerate the paste hardening. However, this was a qualitative observation due to these experiments being carried under non-controlled ambient conditions.

As previously mentioned, from these preliminary results, it was not possible to define a clear trend indicating a relation between the glass composition, PAA and $H_3PO_{4\ (sol),}$ due to small variations changing the cement stability in water. However, it was possible to outline four aspects to consider for the second stage of the cement assessment, as described in the next section. These aspects were the concentration boundaries used of $H_3PO_{4\ (sol)}$ to obtain stable cements in water, range of P/L ratio, PAA and $H_3PO_{4\ (sol)}$ boundaries in which malleable and stable cements could be obtained.

5.3.2 Second stage of cement assessment

Considering the previous results, a second cement assessment was designed to identify the cement formulations resulting in stable samples, and to establish a systematic evaluation for all the glasses. Therefore, boundaries were defined considering the formulations in which Type I cements were obtained. The glass mass was set to 125 mg and PAA weight to 15 mg, for a total powder content of 140 mg. The powder/liquid ratio (P/L) was evaluated at 2, 2.5 and 3, and % $H_3PO_{4\ sol}$ at 20, 25, 30, and 35%, as shown in Table 4-3

For all the glasses, the combinations that produced visually stable cements (Type I), were those corresponding to the C4 and C10 formulations described in Table 4-3, both with a P/L of and a $H_3PO_{4\ (sol)}$ content of 25% and 35% respectively. The cements prepared with C1 and C2 combinations ($H_3PO_{4\ (sol)}$ concentration at 20% and a P/L of 2

and 2.5 respectively), resulted in Type I and Type II sample. Furthermore, the cements prepared with the C5, C8, and C11 formulations ($H_3PO_{4\,(sol)}$ concentration at 25, 30 and 35% respectively and P/L of 2.5), hardened too fast to be moulded into disc shaped samples while the C3, C6, C9, C12 formulations ($H_3PO_{4\,(sol)}$ concentration at 20, 25, 30 and 35% respectively and P/L of 3) were too dry for mixing. The latter occurred due to the reduced amount of liquid to completely damp the powder component. These aspects affected similarly all the cement combinations with a P/L ratio of three.

In summary, C4 and C10 cement formulations were chosen for further analysis regarding mass change in water, ion release, pH, and conductivity. The size of the discs for these experiments was 9 x 2 mm, which required increasing the glass mass to 250.00 mg and the rest of components adjusted accordingly. However, for this increment in mass, it was only possible to prepare the samples corresponding to the C4 cements (250.00 mg of glass – 30.00 mg PAA - 70 µl H_2O - 70 µl H_3PO_4); since the samples corresponding to the C10 formulation either set too fast or the mix was too dry to homogenise the paste, probably indicating that the mixing had an important role on the paste preparation.

5.4 Handling characterisation of cement pastes

Measurement of mixing time, initial setting time and net setting time, were recorded for the cements prepared with the C4 formulation. The glass weighed for all the pastes was 250.00 mg, and the rest of the components adjusted accordingly. This adjustment allowed filling the mould in one step to obtain the required sample size.

For all the measurements, the glass mass ranged between 250.00 and 250.40 mg and PAA ranged between 30.0 and 30.7 mg. Mixing was performed under temperatures ranging between 21 and 23 ºC and humidity varying between 50 and 57%.

5.4.1 Mixing time

Figure 5-6 presents the experimental data corresponding with the mixing times for the C4 cement combinations. This value ranged between 40 ± 6 s and 52 ± 6 s for the 49P9C4 and 42P6C4 cements respectively, excluding the commercial cement Serenocem™ with a mixing time of 15 s as suggested by the manufacturer.

A one-way ANOVA was conducted to compare the mixing times of the cements. Normality and Levene's tests were carried out, and the assumptions met. There was a

significant difference in the mean value for mixing time between cements (p=0.270) and post hoc comparisons using the Tukey test were carried out.

There was a significant difference between the 42P6C4 paste and those prepared with the 49 % wt. SiO_2 glass series: 49P3C4 (p=0.023), 49P6C4 (p=0.047) and 49P9C4 (p=0.007). As shown in Figure 5-6, the mixing time for the 42P6C4 paste, was at least 10 s in average (49P6C4, p=0.047) slower when compared with these three pastes.

From a qualitative perspective, the reported mixing times were considered appropriate to obtain a visually homogeneous paste. Similarly to the results described in section 5.3.1, it was noted that the room temperature influenced the mixing of the paste, especially for the 49P6C4 and 49P9C4 cements that required to be repeated at least one time before the paste could be moulded and flattened to proceed with the measurement of setting times.

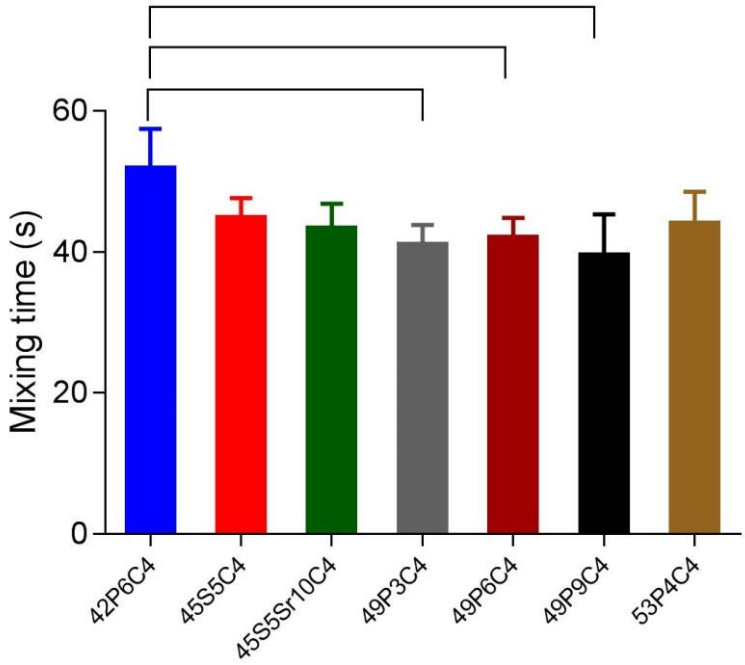

Figure 5-6 Mixing time of cements (C4 formulation), measured from the start of mixing the power and liquid components until obtaining a visually homogenous paste. Pairs of cements with statistically significant differences (p < 0.05) are identified with brackets. Error bars= ± SD; n=4.

5.4.2 Initial setting time

Figure 5-7 presents the experimental data corresponding with the initial setting time for the cements prepared with the C4 formulation, and the commercial product Serenocem™. The initial setting times ranged between 2.7 ± 0.5 and 13 ± 1.6 min for the

49P6C4 and 45S5Sr10C4 cements respectively, while Serenocem™ had an initial setting time of 10.4 ± 0.8 min.

From the graph below, it can be seen that the cements with the shortest initial setting time were those prepared with the 49P6 and 49P9 glasses, which set faster by at least 7.7 min (49P6C4, p <0.001) when compared with Serenocem™. In contrast, the cements with the longest initial setting times were the 42P6C4, 45S5Sr10C4, and Serenocem™.

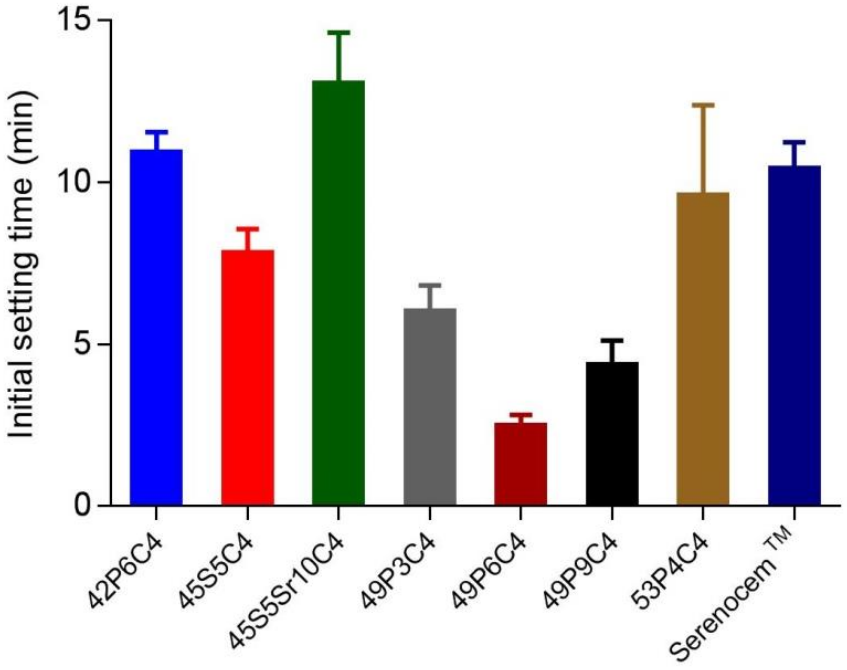

Figure 5-7 Initial setting time of cements (C4 formulation) and commercial product Serenocem™ measured using the Gillmore needle. The initial setting time was measured from the start of mixing until the time in which the lighter needle failed to make an indention on the surface of the cement. Error bars= ± SD; n=4.

Table 5-7 shows the p values between each sample pair, with statistically significant differences ($p < 0.05$) with a Games-Howell post hoc test. A one-way ANOVA was conducted to compare the initial setting times. Normality and Levene's tests were carried out. The normality test showed that standardised residuals were normally distributed ($p=0.281$), while Levene's homogeneity of variance could not be assumed ($p<0.001$).

There was a significant difference in the mean initial setting time between cements ($p<0.001$), and post hoc comparisons using the Games-Howell test were carried out. These comparisons revealed that the results could be divided into three groups: 42P6C4 - 45S5Sr10C4 - Serenocem™; 45S5C4 - 49P3C4, and 49P6C4 - 49P9C4. However, there was no statistically significant difference between the 49P3C4 and 49P9C4

cements. The 53P4C4 cement did not have significant differences with respect to any of the cements due to the high variability within this group. The Games-Howell test p values are shown in Table 5-7 to illustrate the specific interactions between groups.

Table 5-7. Games-Howell post hoc test p values for the initial setting times. Pairs with significant differences are marked with an asterisk

Cement	42P6C4	45S5C4	45S5Sr10C4	49P3C4	49P6C4	49P9C4	53P4C4	Serenocem™
42P6C4	X	0.010*	0.383	0.001*	<0.001*	<0.001*	0.965	0.972
45S5C4	0.010*	X	0.027*	0.154	0.001*	0.008*	0.889	0.036*
45S5Sr10C4	0.383	0.027*	X	0.008*	0.003*	0.004*	0.493	0.251
49P3C4	0.001*	0.154	0.008*	X	0.010*	0.215	0.415	0.003*
49P6C4	<0.001*	0.001*	0.003*	0.010*	X	0.134	0.092*	<0.001*
49P9C4	<0.001*	0.008*	0.004*	0.215	0.134	X	0.181	<0.001*
53P4C4	0.965	0.889	0.493	0.415	0.092	0.181	X	0.997
Serenocem™	0.972	0.036*	0.251	0.003*	<0.001*	<0.001*	0.997	X

5.4.3 Net setting time

Figure 5-8 presents the experimental data corresponding with the net setting time of the cements prepared with the C4 formulation, and the commercial product Serenocem™. This value ranged between 34.3 ± 3.9 and 115.5 ± 5.7 min for the 49P6C4 and 42P6C4 cements respectively, while Serenocem™ had the lowest net setting time of 21.9 ± 0.3 min.

A one-way ANOVA was conducted to compare the net setting times. Normality and Levene's tests were carried out. The normality test showed that standardised residuals were normally distributed (p=0.282), while Levene's homogeneity of variance could not be assumed (p=0.001).

There was a significant difference in the mean initial setting time between cements (p=0.001), and post hoc comparisons using the Games-Howell test were carried out. There was a significant difference between the 42P6C4, 45S5C4, 45S5Sr10C4, 49P3C4 and 53P4C4 cements respect to the 49P6C4, 49P9C4, and Serenocem™. However, within the first group there was a significant difference (p=0.031) between the 42P6C4 and 45S5C4 pastes, with the latter paste setting 24 min on average faster than the 42P6C4 cement. Within the second group, Serenocem™ set on average 12.3 min faster

than the 49P6C4, and 25.8 min faster than and 49P9C4 cement. The Games-Howell test p values are shown in Table 5-8 to illustrate the specific interactions between groups.

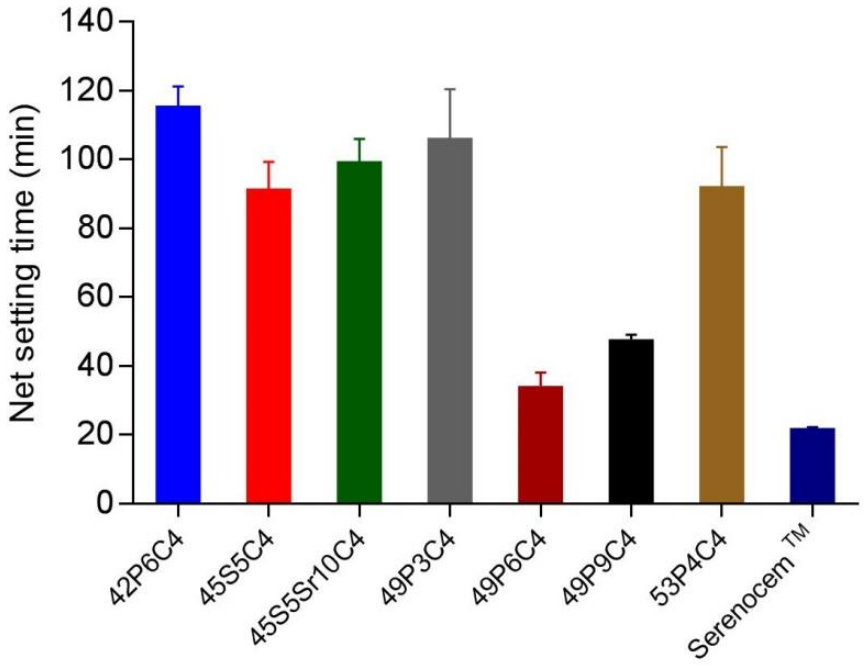

Figure 5-8 Net setting time for the cements (C4 formulation) and commercial product Serenocem™ measured using the Gillmore needle. The net setting time was measured from the start of mixing until the heavier needle failed to make an indentation the surface of the cement. The brackets show the compositions with statistically significant differences ($p < 0.05$) with a Games-Howell post hoc test. Error bars= ± SD; n=4.

Table 5-8 Games-Howell post hoc test p values for net setting time. Pairs with significant differences are marked with an asterisk

Cement	**42P6C4**	**45S5C4**	**45S5Sr10C4**	**49P3C4**	**49P6C4**	**49P9C4**	**53P4C4**	**Serenocem™**
42P6C4	X	0.031*	0.091	0.891	<0.001*	0.001*	0.131	<0.001*
45S5C4	0.031*	X	0.740	0.629	0.001*	0.008*	1.000	0.002*
45S5Sr10C4	0.091	0.740	X	0.974	<0.001*	0.002*	0.924	0.001*
49P3C4	0.891	0.629	0.974	X	0.009*	0.022*	0.761	0.008*
49P6C4	<0.001*	0.001*	<0.001*	0.009*	X	0.027*	0.007*	0.047*
49P9C4	0.001*	0.008*	0.002*	0.022*	0.027*	X	0.025*	<0.001*
53P4C4	0.131	1.000	0.924	0.761	0.007*	0.025*	X	0.007*
Serenocem™	<0.001*	0.002*	0.001*	0.008*	0.047*	<0.001*	0.007*	X

From a qualitative perspective, setting times seemed to be influenced by sample size, especially for the pastes that set faster (49P6C4 and 49P9C4). The mixture required to prepare the 9 x 2 mm discs appeared to harden faster than the smaller discs (4 x 1 mm). It was also noted that the hardening pattern changed depending on the side of the sample exposed to air or the PTFE plate: the surface in contact with the plastic (contrary to the measurement surface) appeared to harden slower and was more humid. At the end of each measurement, the samples were demoulded and all cements remained within their disc shaped geometry, except for the 53P4C4 formulation. For this cement, the surface remained "plastic" and broke, and the colour became translucent over time.

These handling properties were used to choose the glass compositions that were characterised further for mass change, ICP, pH, and conductivity analysis. Therefore, the 45S5 and 53P4 glasses were considered. The pastes prepared with the 45S5 glass had good workability, as these were easily mixed and with an appropriate initial setting time. Even though the setting time of the cement prepared with the 53P4 glass was not satisfactory, the glass is also commercially available (Bonalive®). Additionally, it was thought appropriate to study its stability in water and ion release, since it was one the glasses with higher network connectivity (NC'), and yet with a net setting time within the range of the lower NC' glasses. The 45S5Sr10 glass was chosen due to the reported properties of SrO in bone turnover, and finally the glass 49P9 due to the suitable setting times and paste quality results. When examining the handling properties for the 49P6 cement, it was evident that its properties were encouraging when compared to the commercial cement Serenocem™. Nevertheless, as previously pointed out, the paste mixing was closely dependant on ambient temperature, humidity and sample size, which was a drawback to obtain the required number of samples for further characterisation.

5.4.4 Degradation in water of cements: mass change

Figure 5-9 presents the experimental data corresponding with mass change (%) vs. Time, for all the C4 cement combinations and the commercial cement Serenocem™. As shown in Figure 5-9, the experimental cements reduced their mass, except for the 49P9C4 and 53P4C4 groups at one hour time point. At one hour, these two groups, showed an increase of 2.1 ± 1.1 and 0.6 ±1.2 %, respectively.

From this graph, it could also be noted that for the experimental cements, the mass variation was more pronounced at earlier time points (up to one week). The cements

prepared with the glasses with lower SiO_2 content (45S5C4 and 45S5Sr10C4) had a reduction in mass of at least 12 % after one day, which showed that the main dissolution stage for this group occurred within this time. On the other hand, the cements prepared with the glasses containing a higher SiO_2 content (49P9C4 and 53P4C4), showed a comparable reduction in mass after one week.

After three months immersed in water, the experimental cements had a mass loss that ranged between 20.0 ± 0.6 and 25.3 ± 0.3 % for 49P9C4 and 45S5Sr10C4 respectively. In contrast, the commercial cement Serenocem™, gained an average mass of up to 4.4 ± 0.9 % due to swelling. Therefore, the cement mass change in ascending order was: Serenocem™, 49P9C4, 45S5C4 and 45S5Sr10C4, with the 53P4C4 cement having the highest mass change, nonetheless, due to the variability in the samples, there were no significant differences with respect to the other cements.

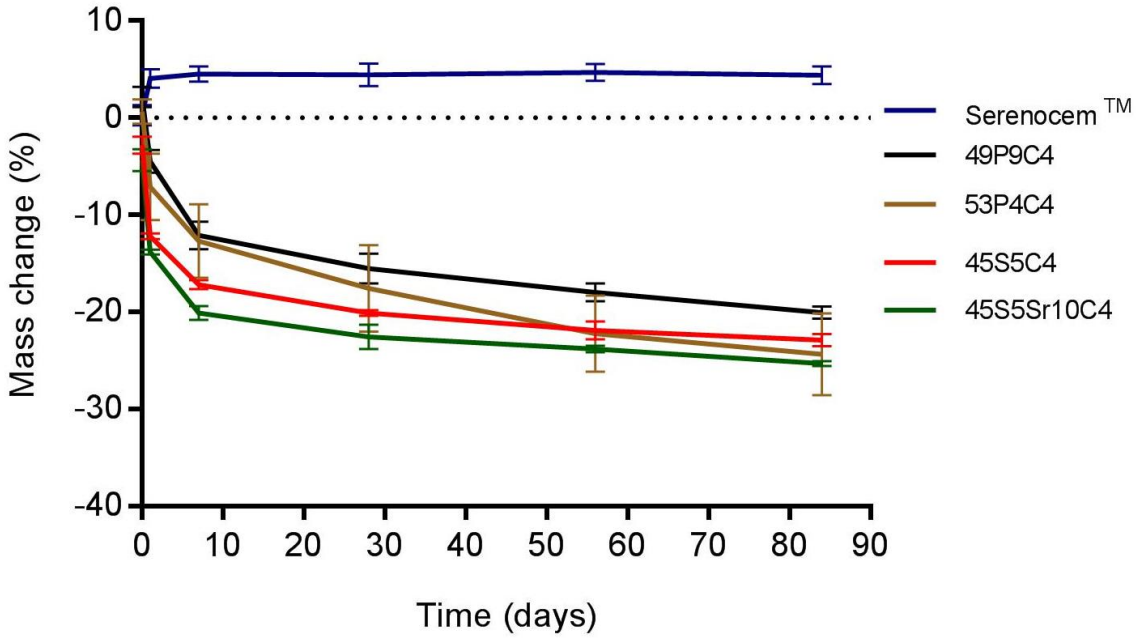

Figure 5-9 Mass change of cement discs (9 x 2 mm) set for one day at 37ºC. The formulations corresponding to 45S5C4, 45S5Sr10C4, 49P9C4, 53P4C4 and Serenocem™ are shown after one hour, one day, one week, one month, two months and three months after immersion in distilled water. Error bars= ± SD; n=4.

A two-way repeated measures ANOVA with Greenhouse-Geiser correction showed that the mean mass change % differed significantly between at least two time points ($p<0.001$). Therefore, a one-way ANOVA was performed per time point to determine the specific pair differences. Table 5-9 shows the p values for each time point and the comparisons between pairs of cements.

For all the time points, normality test were carried out on the residuals, which were approximately normally distributed, with one outlier value repeating through all the time points (except for one-day time point) corresponding to sample #4 of the 53P4C4 group. This was attributed to a higher mass reduction for this sample, since it fractured in four pieces between one hour and one-day time point, this being a cause for the high variability in this group.

For one-hour time point, there was a significant difference between all the groups except between the 45S5C4 and 45S5Sr10C4 cements. The cements prepared with higher SiO_2 content (49P9C4 and 53P4C4) and Serenocem™ showed average differences varying 3.1% (45S5C4 vs. Serenocem™) and 6.5% (45S5Sr10C4 vs. 49P9C4).

After one-hour, all the pair comparisons carried out with the 53P4C4 cement did not show significant differences. As previously mentioned, sample # 4 broke after one hour, which caused a high variability. For the rest of the time points, the post hoc test showed that there were significant differences between the mass change percent for all the cements. However, as shown in Table 5-9, the 45S5C4 and 45S5Sr10C4 group showed significant difference for two time points only: one day and one week.

Table 5-9 Post hoc test p values for mass change of the cements. Pairs with significant differences are marked with an asterisk. Levene's P value is shown under each time point. For p<0.05, a Games-Howell post hoc test is used; otherwise a Tukey's test was used.

Time point (Levene's test)	Cement	45S5C4	45S5Sr10C4	49P9C4	53P4C4	Serenocem™
One hour p=0.986	45S5C4	X	0.301	<0.001*	0.003*	0.008*
	45S5Sr10C4	0.301	X	<0.001*	<0.001*	<0.001*
	49P9C4	<0.001*	<0.001*	X	0.325*	0.152
	53P4C4	0.003*	<0.001*	0.325	X	0.987
	Serenocem™	0.008*	<0.001*	0.152	0.987	X
One day p=0.017	45S5C4	X	0.001*	0.002*	0.208	<0.001*
	45S5Sr10C4	0.001*	X	0.001*	0.110	<0.001*
	49P9C4	0.002*	0.001*	X	0.648	<0.001*
	53P4C4	0.208	0.110	0.648	X	0.022*
	Serenocem™	<0.001*	<0.001*	<0.001*	0.022*	X
One week p=0.040	45S5C4	X	0.004*	0.016*	0.331	<0.001*
	45S5Sr10C4	0.004*	X	0.002*	0.109	<0.001*
	49P9C4	0.016*	0.002*	X	0.998	<0.001*
	53P4C4	0.331	0.109	0.998	X	0.009*
	Serenocem™	<0.001*	<0.001*	<0.001*	0.009*	X
One month p=0.030	45S5C4	X	0.102	0.035*	0.775	<0.001
	45S5Sr10C4	0.102	X	0.003*	0.354	<0.001*
	49P9C4	0.035*	0.003*	X	0.902	<0.001*
	53P4C4	0.775	0.354	0.902	X	0.006*
	Serenocem™	<0.001*	<0.001*	<0.001*	0.006*	X
Two Months p<0.001	45S5C4	X	0.081*	0.006*	1.000	<0.001*
	45S5Sr10C4	0.081	X	0.002*	0.913	<0.001*
	49P9C4	0.006*	0.002*	X	0.382	<0.001*
	53P4C4	1.000	0.913	0.382	X	0.002*
	Serenocem™	<0.001*	<0.001*	<0.001*	0.002*	X
Three Months p=0.015	45S5C4	X	0.10	0.005*	0.943	<0.001*
	45S5Sr10C4	0.10	X	0.001*	0.989	<0.001*
	49P9C4	0.005*	0.001*	X	0.418	<0.001
	53P4C4	0.943	0.989	0.418	X	0.002*
	Serenocem™	<0.001*	<0.001*	<0.001*	0.002*	X

5.4.5 Inductively coupled plasma spectrometry

Ion release concentration of silica (Si), calcium (Ca), sodium (Na), phosphorus (P) and strontium (Sr), was analysed, with Al release also reported due to its relevance for this study. In addition, ICP analysis showed the presence of magnesium (Mg) and sulphur (S). Mg concentration was less than 0.2 mg/L, and S concentration was ≤ 1.1 mg/L for up to one day, after which their concentration decreased to ≤ 0.1 mg/L. For all the time points, the storage distilled water was checked for loose particles, with no residues detected by visual inspection, except for one sample corresponding to the 53P4C4 discs that fractured after one hour.

Figure 5-10 shows the release of Si ions between one hour and two months for all the cements, after immersion in water. The Si concentration in the distilled water used as control was less than 1.5 mg/L. This figure illustrates the difference between the cements prepared with lower and higher SiO_2 content. The 45S5C4 and 45S5Sr10C4 cements, showed a rapid Si release, reaching a peak after one day, while the 49P9C4 and 53P4C4 reached their maximum Si release after one week. After these time points, all the cements showed a decline in Si release. The commercial cement Serenocem™, showed a lower Si release when compared with the experimental cements, and seemed to increase linearly to a maximum of 5.13 mg/L at one month.

A one-way ANOVA was conducted for each time point. Normality and Levene's tests were carried out. The normality test showed that standardised residuals were normally distributed ($p > 0.05$), while Levene's homogeneity of variance could not be assumed ($p < 0.05$) except for the one-week time point ($p=0.067$).

Overall, all the cements had significant differences with respect to the Serenocem™ Si release, except at one hour, when there was a significant difference only between this cement and the 45S5Sr10C4 and 49P9C4 groups. The statistical analysis showed that there were no significant differences between the 45S5C4 and 45S5Sr10C4 cements (lower Si content) through the experiment. Similarly, there was no significant difference between the 49P9C4 and 53P4C4 cements (higher Si content). Within these two groups, no definite trend was observed: in addition to the previously described similarities, at one week no difference was observed between the 53P4C4 cement and the lower Si content cements, while at one month, there were no differences between any of the experimental cements. This slightly changed after two months when there was only a difference between the 45S5C4 and 49P9C4 cement.

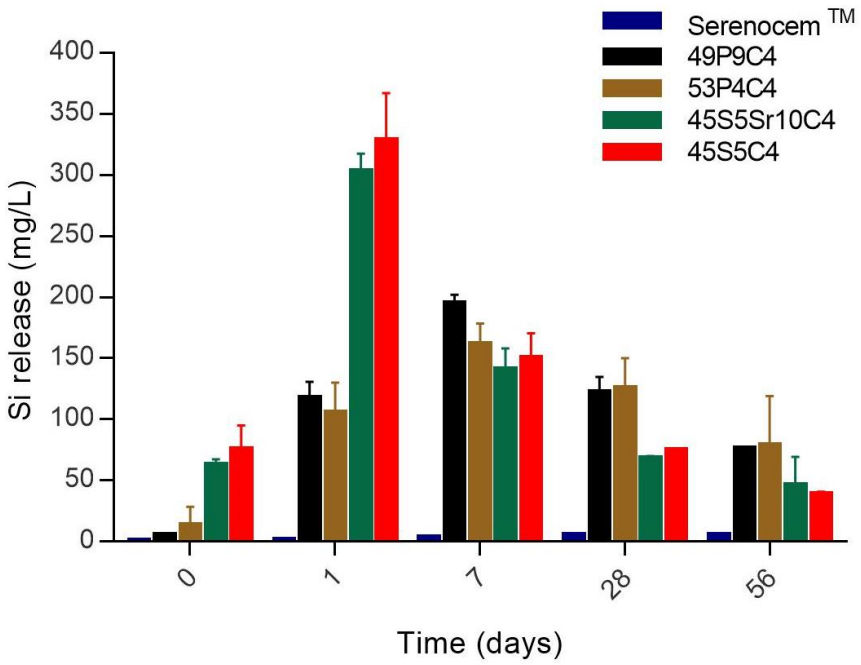

Figure 5-10 Si ion release (mg/L) for cement discs (9 x 2 mm) set for one day at 37ºC, at one hour, one day, one week, one month and two months after immersion in distilled water. Values reported as negligible or not detected were assumed to be 0.0005. Error bars= ± SD; n=3.

Figure 5-11 shows the release of Ca ions for all the cements, between one hour and two months after immersion in water. The Ca concentration in the distilled water used as control was less than 0.01 mg/L.

During the first week, Ca release was low and did not show significant changes. The maximum Ca concentration was reached after twenty-eight days for the 45S5C4, 45S5Sr10C4, and 53P4C4 cements, while the 49P9C4 showed a maximum at fifty-six days. The 49P9C4 samples had the lowest calcium release from the experimental samples along with Serenocem ™. The commercial cement Serenocem™, showed a negligible Ca release that seemed to increase linearly to a maximum of 0.45 mg/L at one month.

A one-way ANOVA was conducted for each time point. Normality and Levene's tests were carried out. The normality test showed that standardised residuals were normally distributed ($p > 0.05$), except for the one-week time point. Levene's homogeneity of variance could not be assumed ($p < 0.05$) except for one day ($p=0.230$) and one week ($p=0.051$).

The pair differences varied along the experiment: at one hour, there was significant difference between Serenocem™ and the 45S5Sr10C4 and 49P9C4 cements. After one

day no significant differences were observed between the experimental cements, but only with the Serenocem™ group, due to its low Ca release. After one week, there was no significant difference between the 53P4C4 group and the rest of the cements (except Serenocem™). Regarding the rest of the cements, there were no significant differences between them, except for the Sr containing cement that showed a higher Ca release. At one month, no significant differences were observed between the lower SiO_2 content cements, and the 53P4C4 group. Finally, after two months, no significant differences were obtained within any of the cements.

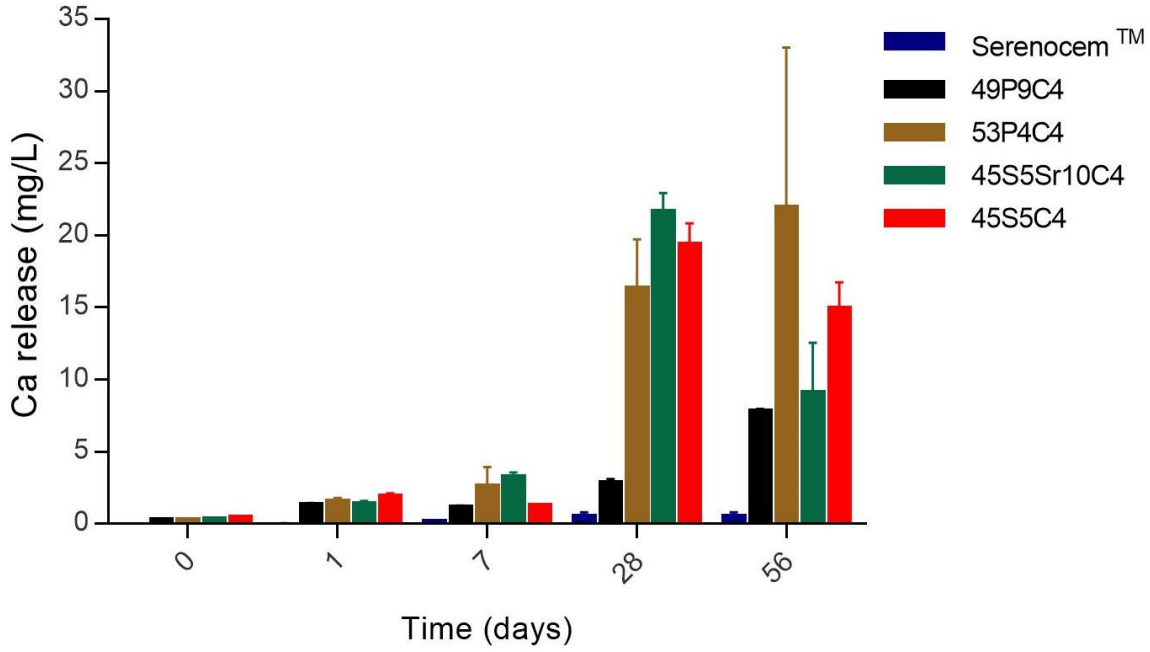

Figure 5-11. Ca ion release (mg/L) for cement discs (9 x 2 mm) set for one day at 37°C, at one hour, one day, one week, one month and two months after immersion in distilled water. Values reported as negligible or not detected were assumed to be 0.0005. Error bars= ± SD; n=3.

Figure 5-12 shows the release of Sr ions between one hour and two months after immersion in water for the 45S5Sr10C4 cement. The rest of the groups are not shown due to negligible quantities of Sr being released from these samples (≤ 0.02 mg/L). The Sr concentration in the distilled water used as control was less than 0.0001 mg/L.

For earlier time points, small amounts of Sr (0.36 ± 0.07 mg/L) were detected for up to one day, reaching a peak at 28 days (13.70 ± 0.36 mg/L), to then decrease to approximately half of this concentration by the end of the experiment.

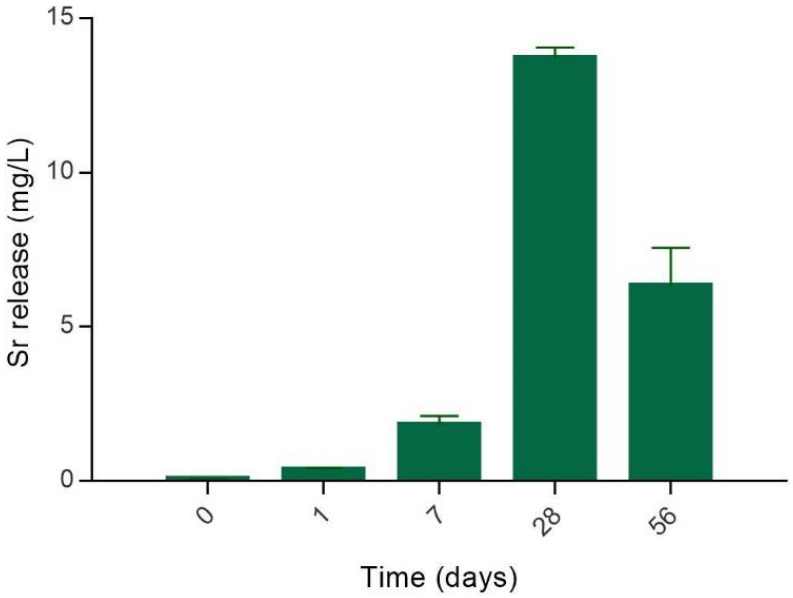

Figure 5-12 Sr ion release (mg/L) for cement discs (9 x 2 mm) set for one day at 37ºC, at one hour, one day, one week, one month and two months after immersion in distilled water. Values reported as negligible or not detected were assumed to be 0.0005. Error bars= ± SD; n=3.

Figure 5-13 shows the release of Na ions between one hour and two months after immersion in water for all the cements. The Na concentration in the distilled water used as control was less than 0.01 mg/L.

All the cements reached a maximum of Na release after one day, with 45S5C4 and 45S5Sr10C4, having the highest concentration, with values ranging between 300 and 400 mg/L, while for the 49P9C4 and 53P4C4 samples, the concentration after one day varied between 150 and 200 mg/L. After reaching this peak, Na release continuously decreased to concentrations under 3 mg/L, with the exception of the 53P4C4 cement. On the other hand, Serenocem™ exhibited low Na release, with concentrations maintained under 3 mg/L over time.

A one-way ANOVA was conducted for each time point. Normality and Levene's tests were carried out. The normality test showed that standardised residuals were normally distributed ($p>0.05$), except for the two months' time point ($p=0.001$). This was attributed to two outliers corresponding to sample #2 and #4 of the 53P4C4 group. As previously observed in the mass change study, this group showed high variability, which was also reflected in the ion release values. The normality test was repeated without the 53P4C4 samples, resulting in a normal distribution ($p=0.393$), confirming that this result was due to this group of samples. Levene's homogeneity of variance could not be assumed ($p< 0.05$) except for the one-hour time point ($p=0.095$).

Overall, all the cements had significant differences with respect to Serenocem™ Na release. At one-hour time point, no significant difference was detected between the lower Si content cements (45S5C4 and 45S5Sr10C4) or within the higher Si content cements (49P9C4 and 53P4C4), however there was no significant difference between the 45S5Sr10C4 cement and the higher Si content cements. There was a similar result for the one-day time point; however, the 45S5Sr10C4 cement did show significant differences with the higher Si content cements. After one week no significant differences were observed between any of the experimental cements. This result was comparable until the end of the experiment, with an exception for the 45S5Sr10 cement having significant differences again with the higher Si content cements at one-month time point.

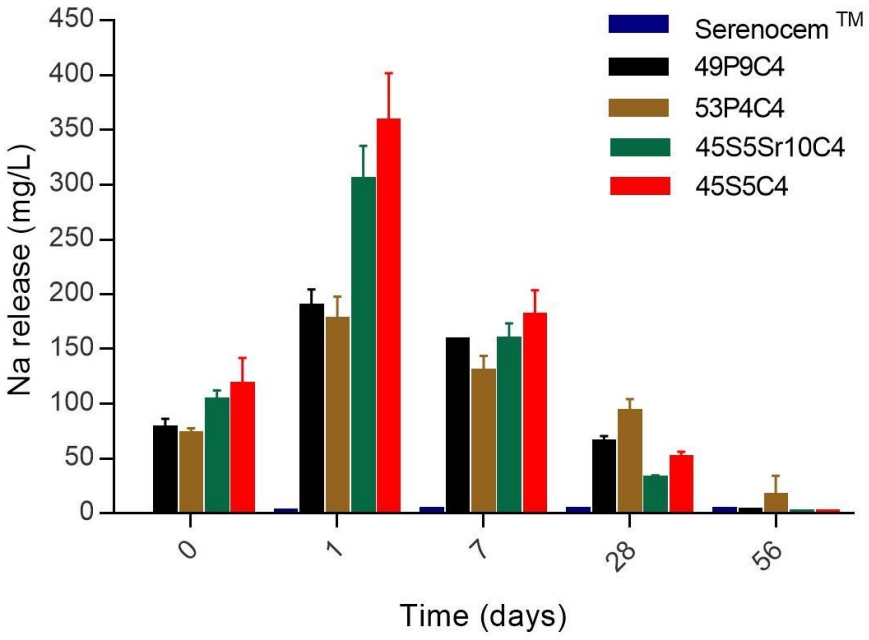

Figure 5-13 Na ion release (mg/L) for cement discs (9 x 2 mm) set for one day at 37°C, at one hour, one day, one week, one month and two months after immersion in distilled water. Values reported as negligible or not detected were assumed to be 0.0005. Error bars= ± SD; n=3.

Figure 5-14 shows the release of PO_4^{3-} ions between one hour and two months after immersion in water for all the cements. The PO_4^{3-} concentration in the distilled water used as control was less than 0.01 mg/L.

All the groups reached a maximum of phosphate release after one day, with the lowest concentration corresponding to 45S5Sr10C4 cement and the highest to 49P9C4 cement, with values of 14.63 ± 0.95 and 47.97 ± 5.50 mg/L respectively. The cement that exhibited the highest P release was in agreement with the glass with the highest P_2O_5

content. As previously observed for the rest of the profiles, Serenocem™ showed negligible P release, with values under 0.15 mg/L throughout the experiment.

A one-way ANOVA was conducted for each time point. Normality and Levene's tests were carried out. The normality test showed that standardised residuals were normally distributed ($p > 0.05$); except for the two months' time point. Levene's homogeneity of variance could not be assumed ($p < 0.05$) except for the one-day time point ($p=0.097$)

At one day, there was a significant difference between the 49P9C4 group, the lower SiO_2 content cements and with Serenocem™. The lower phosphate content in the 53P4 glass did not show to be relevant for the results observed at one hour. After one day the cements with the lower SiO_2 content, showed significant differences with the rest of the cements. After one week, the group with the highest release was still the 49P9C4, with no significant differences observed for the rest of the cements. Nonetheless the PO_4^{3-} release from the Sr containing cement was slightly higher respect to Serenocem™. For the last two time points, there were no significant differences between groups except after one month, when the 49P9C4 cement showed a slightly higher release respect to the other cements.

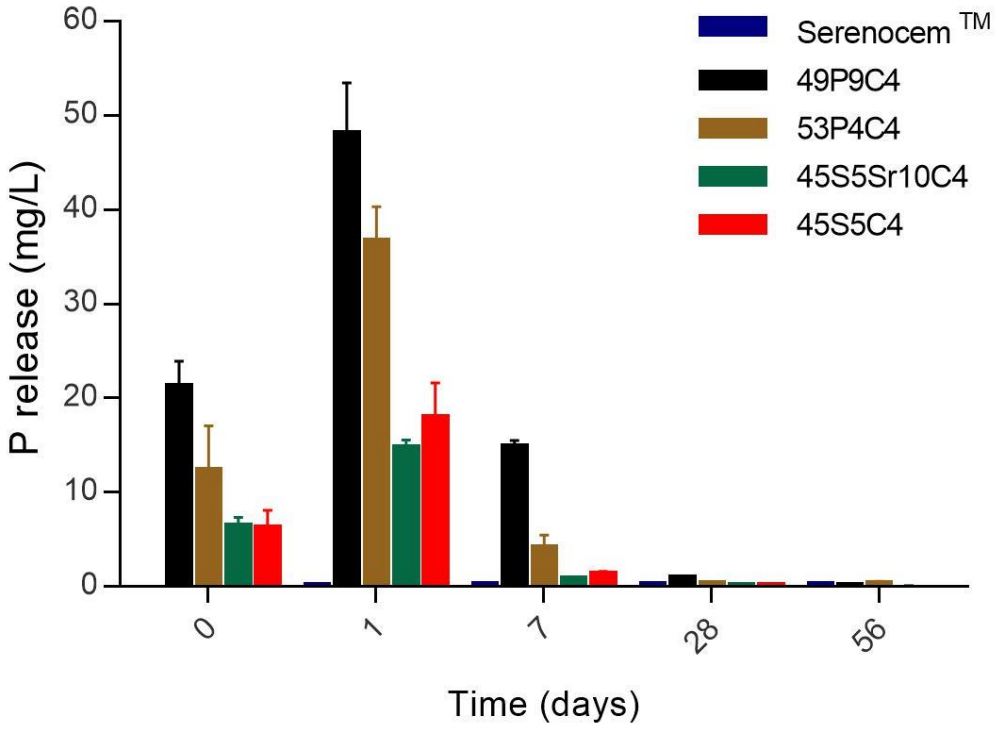

Figure 5-14 P ion release (mg/L) for cement discs (9 x 2 mm) set for one day at 37ºC, at one hour, one day, one week, one month and two months after immersion in distilled water. Values reported as negligible or not detected were assumed to be 0.0005. Error bars= ± SD; n=3.

Figure 5-15 shows the release of Al ions for all the cements, between one hour and one month after immersion in water. The Al concentration in the distilled water used as control was less than 0.001mg/L.

Surprisingly, all the cements released small amounts of Al even though strict measures were taken in order to avoid Al contamination in the parent glasses. However, the highest detected concentration was 0.12 ± 0.01 mg/L for the 49P9C4 cement, which decreased to a concentration of less than 0.002 mg/L at the end of the experiment.

The maximum Al release for the cements prepared with the lower SiO_2 content glasses (45S5, 45S5Sr10) was reached at one day, while the cements prepared with the higher SiO_2 content glasses (49P9, 53P4) had a peak at seven days. Interestingly, Serenocem™ samples showed a steady increase on Al release up to one month, in contrast with the pattern obtained for the experimental cements.

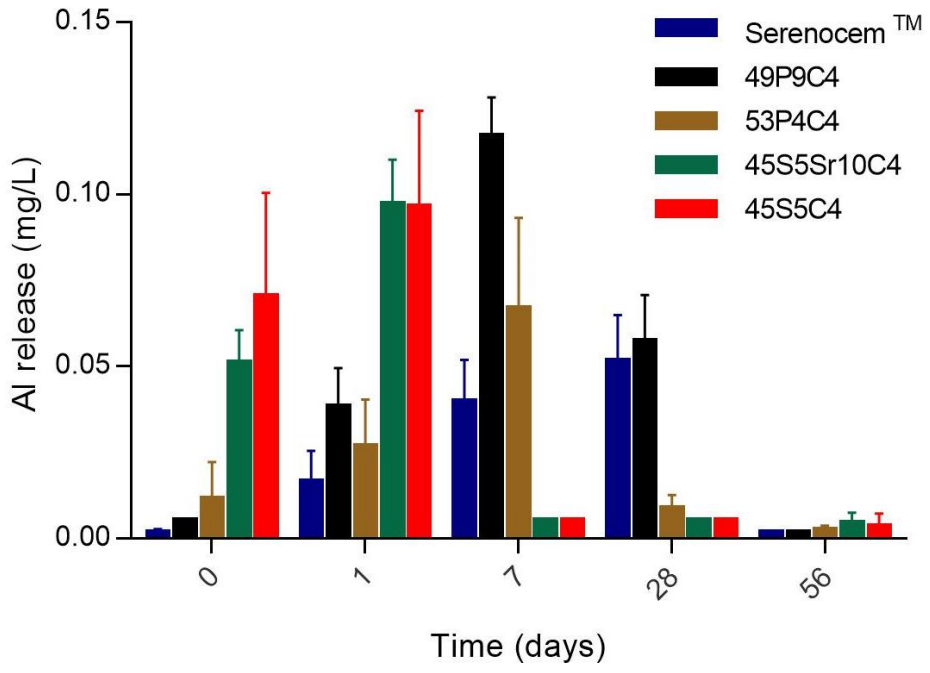

Figure 5-15 Al ion release (mg/L) for cement discs (9 x 2 mm) set for one day at 37ºC, at one hour, one day, one week, and one month after immersion in distilled water. Values reported as negligible or not detected were assumed to be 0.0005. Error bars= ± SD; n=3.

5.5 Dissolution testing: pH and conductivity

Figure 5-16 shows the pH variation of the storage water at one hour, one day, one week, one month, and two months. The pH of the distilled water used as control was alkaline (pH=9).

For earlier time points (up to one week) the 45S5C4 and 45S5Sr10C4 samples showed alkaline pH with values within 10.3 and 11.6, while the 49P9C4 and 53P4C4, varied within 9.5 and 10.6. Serenocem™ showed the lowest pH, with variations within 7.4 and 8.5, this being similar to those obtained for the distilled water used as control. The pH after two months for all the experimental cements were within a value of 10, with Serenocem™ showing no significant variations respect to previous time points.

A one-way ANOVA was conducted to compare the pH of the water leachate of the cements at each time point. Normality and Levene's tests were carried out. The normality test showed that standardised residuals were normally distributed ($p > 0.05$), while Levene's homogeneity of variance could not be assumed ($p < 0.05$), except for the time point corresponding to one hour ($p=0.119$). Post hoc comparisons using the Games-Howell test were carried out for $p < 0.05$ and Tukey for $p > 0.05$. As previously described, for earlier time points (up to one week), there were significant differences between the lower SiO_2 content cements (45S5C4-45S5Sr10C4), and the higher SiO_2 content cements (49P9C4-53P4C4). However, the 45S5Sr10C4 cement did not show significant difference with the 53P4C4 cement from one week, with the 45S5C4 cement exhibiting this behaviour from one month. All the samples showed a significant difference with the commercial cement Serenocem™ for earlier time points.

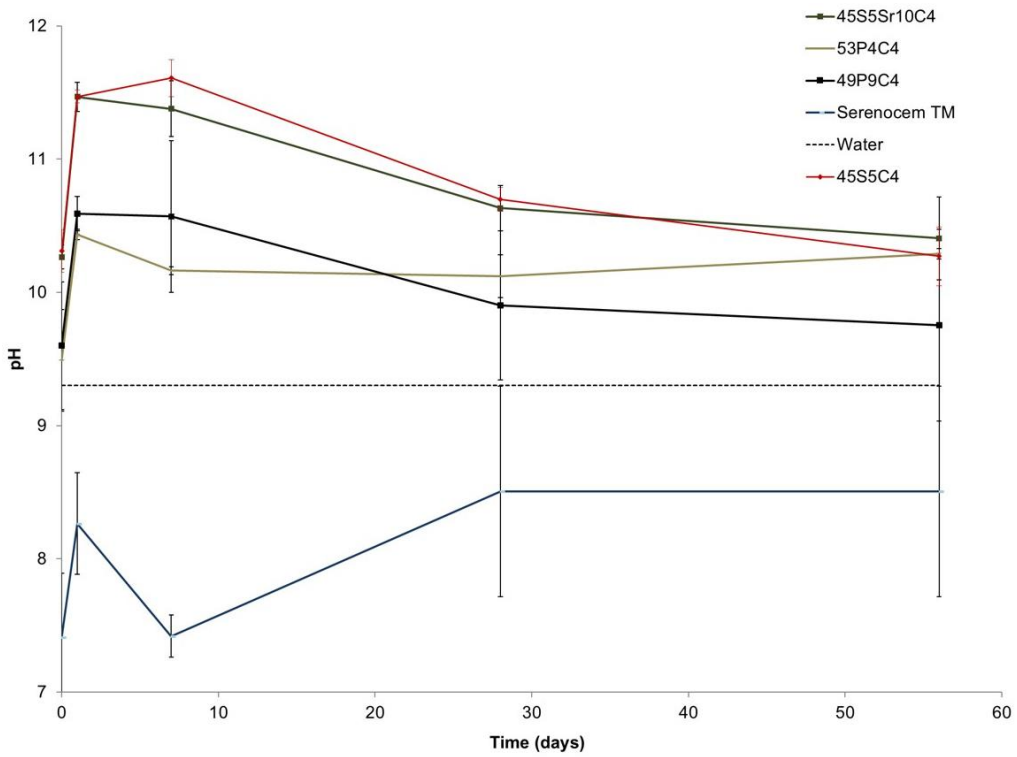

Figure 5-16 pH variation for cement discs (9 x 2 mm) set for one day at 37ºC for the 45S5C4, 45S5Sr10C4, 49P9C4, 53P4C4 and Serenocem™ cements, at one hour, one day, one week, one month and two months after immersion in distilled water. Error bars= ± SD; n=4.

Figure 5-17 shows the conductivity variation (µs/cm) of the distilled water at one hour, one day, one week, one month, and two months. The conductivity of the distilled water used as control was less than 6 µs/cm.

In a similar trend to the one observed for the mass change, the conductivity had a peak at one day after cements were immersed in water. At this time point, two trends were observed: the conductivity of the 45S5C4 and 45S5Sr10C4 cements were the highest, with values over 1000 µs/cm, while the values for the 49P9C4 and 53P4C4 samples had an average of 491 µs/cm and 729 µs/cm, respectively. At the end of the experiment all the values were below 500 µs/cm, with the lowest corresponding to the Serenocem™ samples (< 20 µs/cm).

A one-way ANOVA was conducted to compare the conductivity of the storage water at each time point. Normality and Levene's tests were carried out. The normality test showed that standardised residuals were normally distributed ($p > 0.05$), while Levene's homogeneity of variance could not be assumed ($p < 0.05$), except for the time point corresponding to one month ($p=0.088$). Post hoc comparisons using the Games-Howell test were carried out for $p < 0.05$ and Tukey for $p > 0.05$.

The comparisons at one hour did not show significant differences between the experimental cements. As previously described, for one day and one week, two trends were observed and confirmed by statistical analysis: between the 45S5C4-45S5Sr10C4 and the 49P9C4-53P4C4 cements, with the first group having the highest conductivity averages. However, as can be seen from the figure below, after one month, the 49P9C4 cement did not show significant difference with the lower SiO_2 content cements. By the end of the study, there were significant differences only between the 49P9C4 and 53P4C4 cements. For all the time points, the low values detected for the Serenocem™ samples, indicated that there were significant differences throughout, except with the 45S5Sr10 cement at two months.

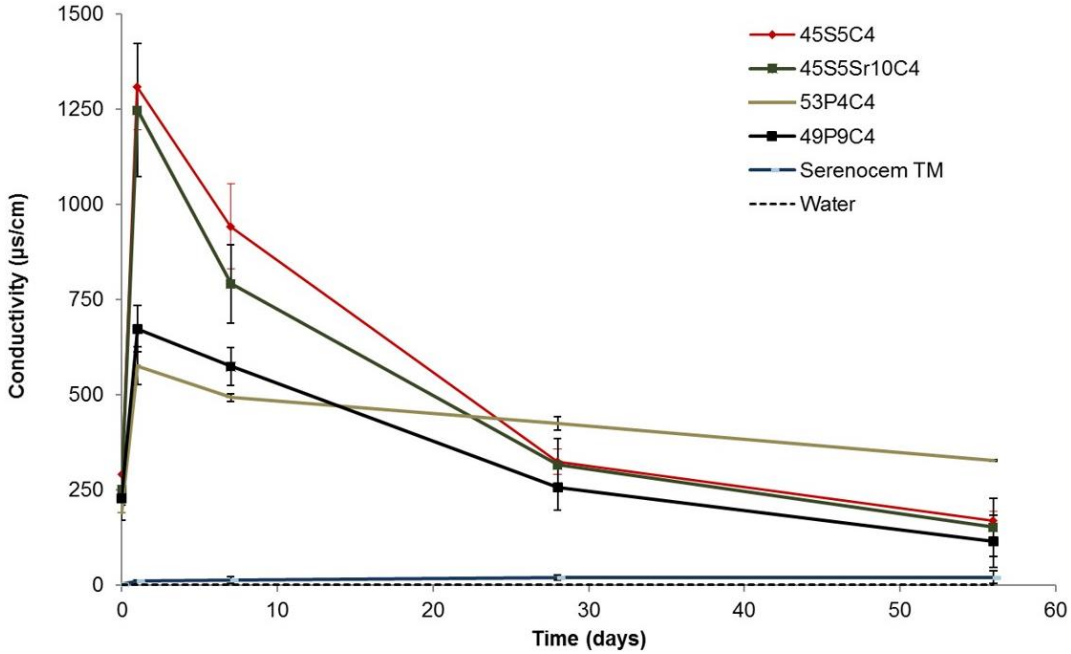

Figure 5-17 Conductivity (µs/cm) variation for cement discs (9 x 2 mm) set for one day at 37ºC for the 45S5C4, 45S5Sr10C4, 49P9C4, 53P4C4 and Serenocem™ cements, at one hour, one day, one week, one month and two months after immersion in distilled water. Error bars= ± SD; n=4.

Overall, these results, indicated a clear difference in the conductivity and pH of the storage solution, between the lower SiO_2 content cements (45S5C4 and 45S5Sr10C4) and the higher SiO_2 content cements (49P9C4 and 53P4C4), predominantly during the first week of the experiment. This difference showed that the storage solutions of the cements prepared with the 45S5 glass and its Sr variation, had a higher ionic concentration that resulted in an increase of the alkalinity of the solution, which was in agreement with the higher concentration of ions such as Na and Si, previously described in section 5.4.5. Furthermore, the low ion concentration detected by ICP for the

commercial cement Serenocem™, was in agreement with the pH and conductivity results, that in average was lower when compared with the distilled water used as control, and significantly lower when compared with the experimental cements.

5.6 Cement setting by Fourier transformed infrared spectroscopy with attenuated total reflectance

This study was carried out to evaluate and compare the changes occurring in the glass structure after mixing with an acid containing solution. As previously described in the literature review, this technique was used in traditional GICs and aluminium free cements to characterise their setting chemistry. These FTIR-ATR results correspond to the cements prepared with the C4 formulation and the glasses that were previously characterised for mass change, ICP, pH, and conductivity.

45S5C4 cement

Figure 5-18 shows the FTIR-ATR spectra for the 45S5C4 cement during setting. The analysis started immediately after mixing at 70 s until 60 min. From these spectra, four main areas are distinguished: a broad band centred at approximately 3280 cm^{-1}, a series of six peaks between 1650 and 1320 cm^{-1} (represented as A), an intense peak at 1060 cm^{-1} (represented as B), and a broad peak at approximately 525 cm^{-1}.

The band at 3280 $cm^{-1,}$ decreased with time, and coincided with a peak positioned at the same wavenumber for the $H_3PO_{4\ (sol)}$ spectrum. The series of six peaks (denoted as A) are further illustrated in Figure 5-19, whilst the peak at approximately 1060 cm^{-1} is further illustrated in Figure 5-20. The peak at 525 cm^{-1}, did not show a pattern change with time; however, it appeared to become more defined for the later time points.

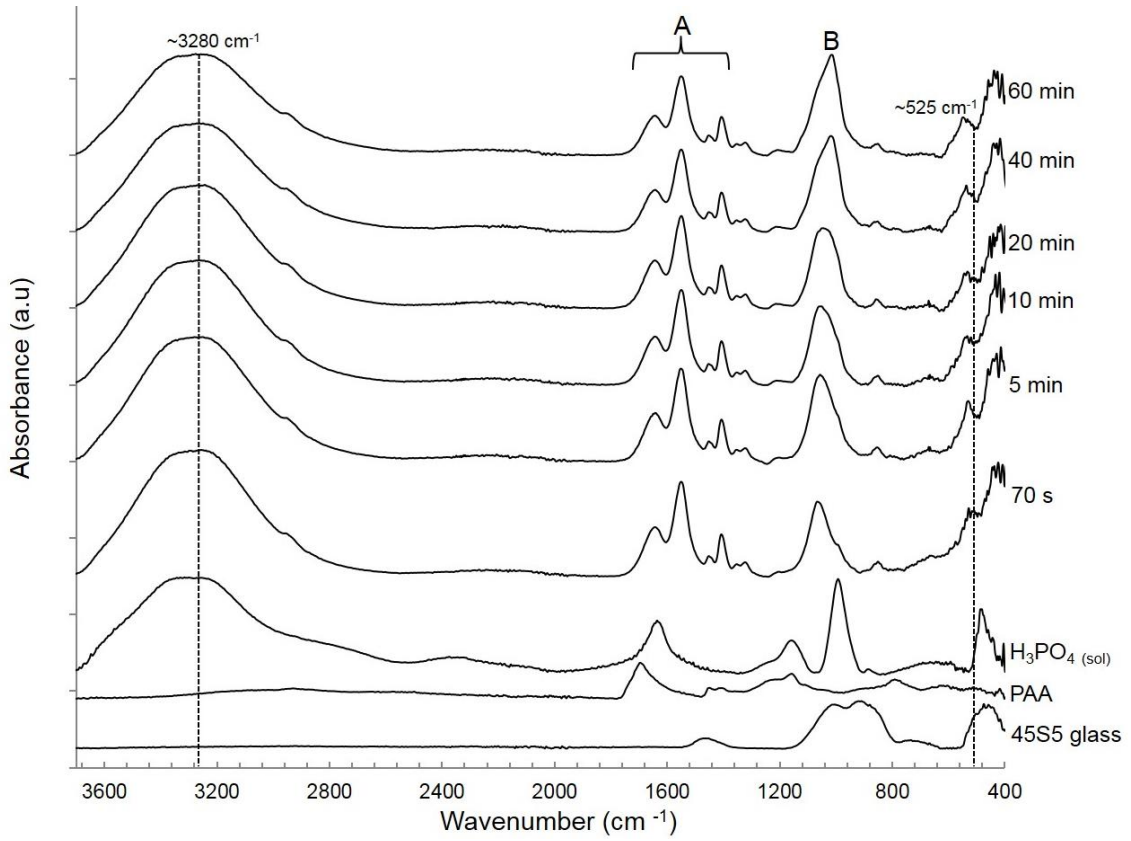

Figure 5-18 FTIR-ATR spectra of 45S5C4 cement, showing the setting from the start of mixing to 60 min. The spectra of the parent glass, PAA and $H_3PO_{4\ (sol)}$ are included for reference

Figure 5-19, shows the "A" area with six peaks positioned at approximately 1650, 1550, 1450, 1400, 1350 and 1320 cm^{-1}. For this range, no significant shifts were observed, however the peaks at 1650, 1550 and 1400 cm^{-1} slightly decreased over time, especially at the later time points of 40 and 60 min.

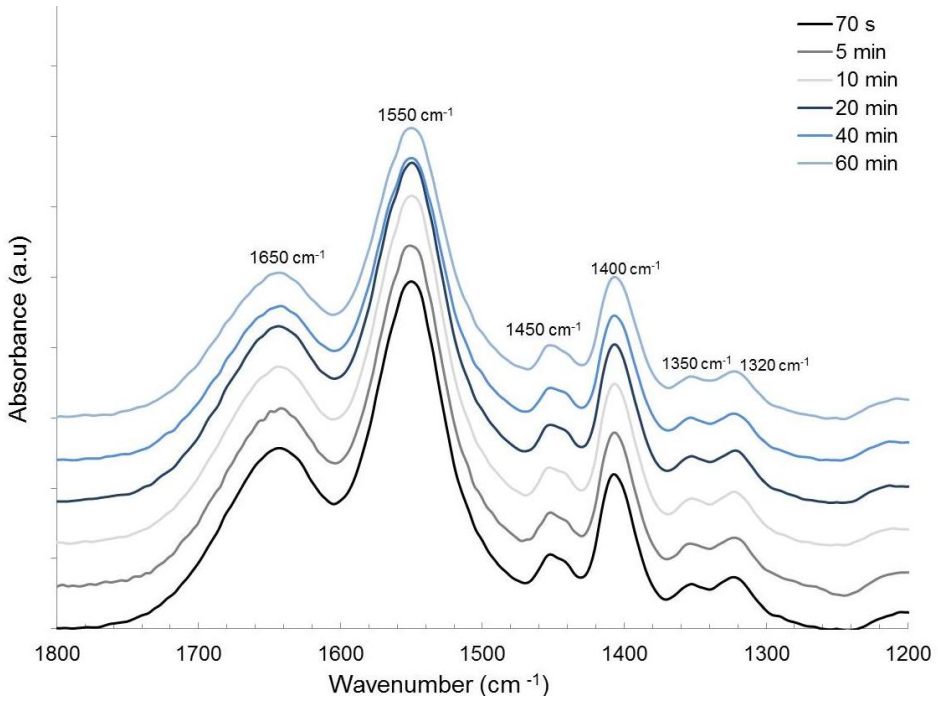

Figure 5-19 FTIR-ATR spectra of 45S5C4 cement corresponding to region A shown in Figure 5-18, with the main peaks observed for this area. Graphs are stacked for comparison purposes

Figure 5-20 presents the "B" area, showing that the band initially centred at approximately 1060 cm^{-1} shifted to lower wavenumbers over time with a final position at 1010 cm^{-1}. It also can be seen that the intensity varied over time, with no defined pattern up to 20 min, to then slightly increase between 40 and 60 min. A small band at approximately 850 cm^{-1} was identified, and did not show significant changes or pattern throughout the experiment.

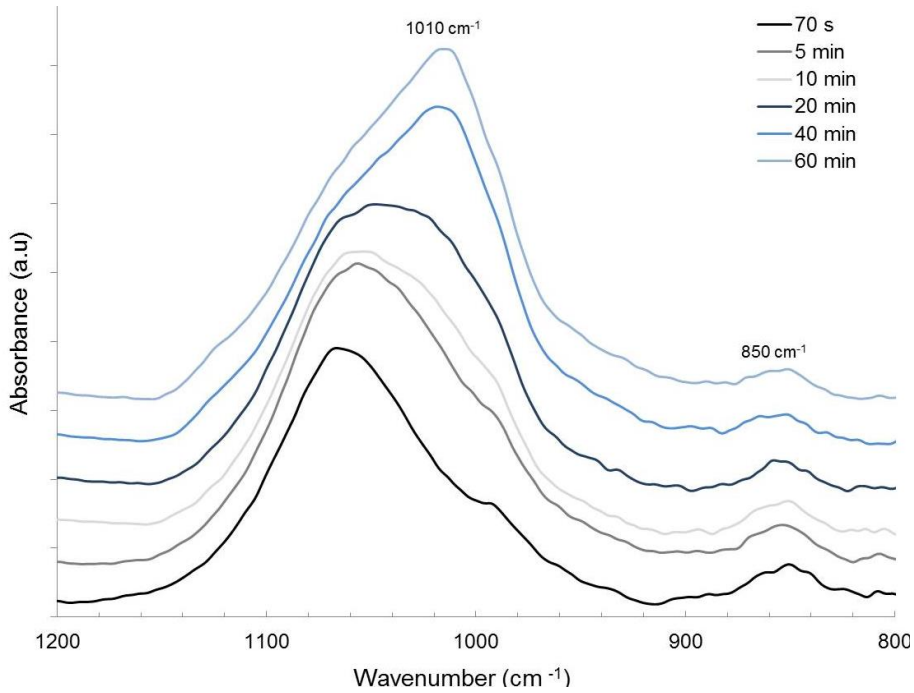

Figure 5-20 FTIR-ATR spectra of 45S5C4 cement corresponding region B shown in Figure 5-18, with the main peaks observed for this area. Graphs are stacked for comparison purposes

45S5Sr10C4 cement

Figure 5-21 shows the FTIR-ATR spectra for the 45S5Sr10C4 cement during setting. The analysis started immediately after mixing at 76 s until 60 min. From these spectra, four main areas are distinguished: a broad band centred at approximately 3280 cm^{-1}, a series of six peaks between 1645 and 1320 cm^{-1} (represented as A), an intense peak at 1060 cm^{-1} (represented as B), and a broad peak at approximately 520 cm^{-1}.

The band at 3280 $cm^{-1,}$ decreased with time and coincided with a peak positioned at the same wavenumber for the $H_3PO_{4\ (sol)}$ spectrum. The series of six peaks (denoted as A) are further illustrated in Figure 5-22, whilst the peak at 1060 cm^{-1} is further illustrated in Figure 5-23. The peak at 520 cm^{-1}, did not show a pattern change; however, it appeared to increase over time.

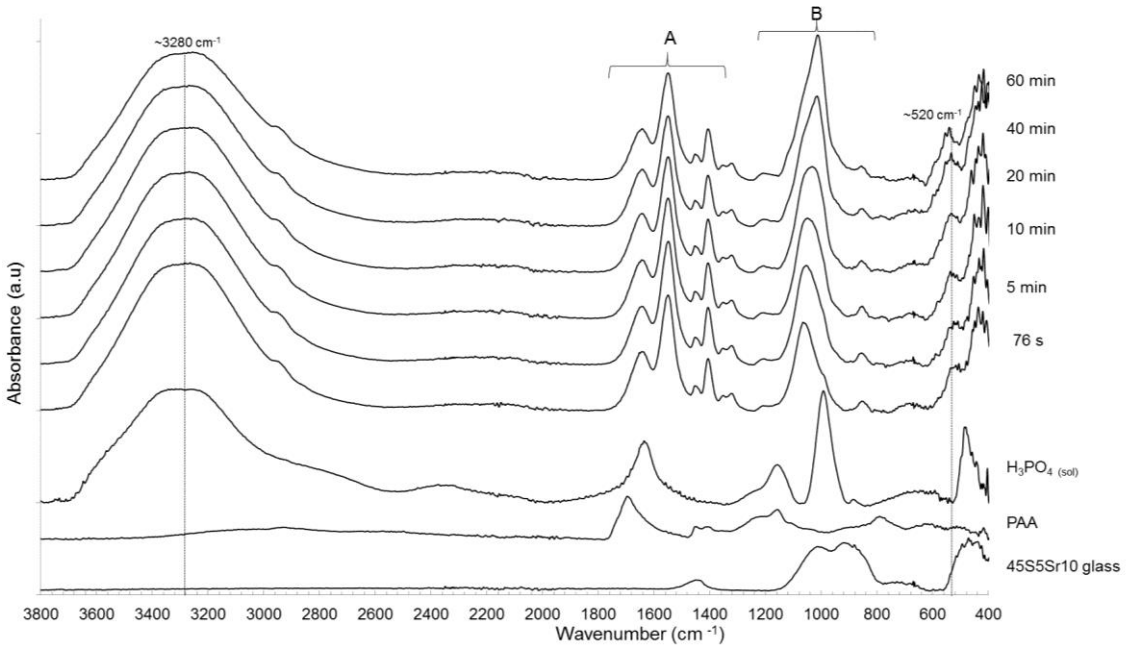

Figure 5-21 FTIR-ATR spectra of 45S5Sr10C4 cement, showing the setting from the start of mixing to 60 min. The spectra of the parent glass, PAA and $H_3PO_{4(sol)}$ are included for reference

Figure 5-22 shows the "A" area, with peaks similarly positioned to those described for the 45S5C4 cement, at 1645, 1545, 1450, 1400, 1350 and 1320 cm^{-1}. For this cement, the bands at 1545 and 1400 cm^{-1} decreased over time, with the rest of the peaks not changing significantly through the experiment.

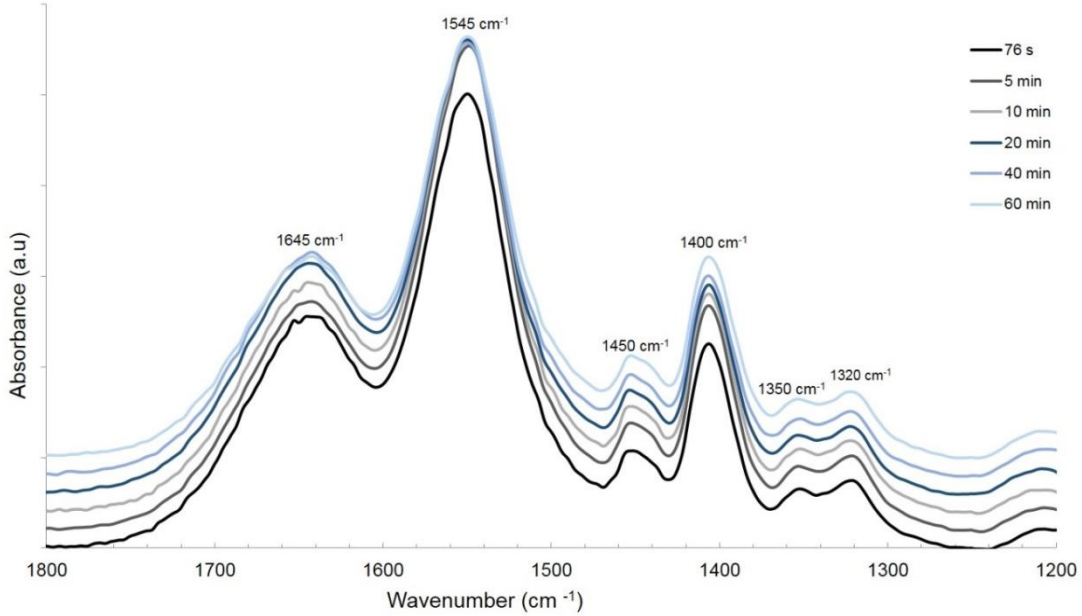

Figure 5-22 FTIR-ATR spectra of 45S5Sr10C4 cement corresponding region A shown in Figure 5-21, with the main peaks observed for this area. Graphs are stacked for comparison purposes

Figure 5-23 presents the "B" area, showing a similar pattern to that observed for the 45S5SC4 cement, shifting from its initial position at 1060 cm^{-1} and progressively shifting to 1010 cm^{-1}. In these spectra, a small shoulder positioned at approximately 990 cm^{-1}, appeared to increase with time and merge with the peak at 1060 cm^{-1}. Similarly, the intensity of this band, increased over time and the peak became more defined at its final position. Finally, a small band at approximately 855 cm^{-1} did not have significant changes.

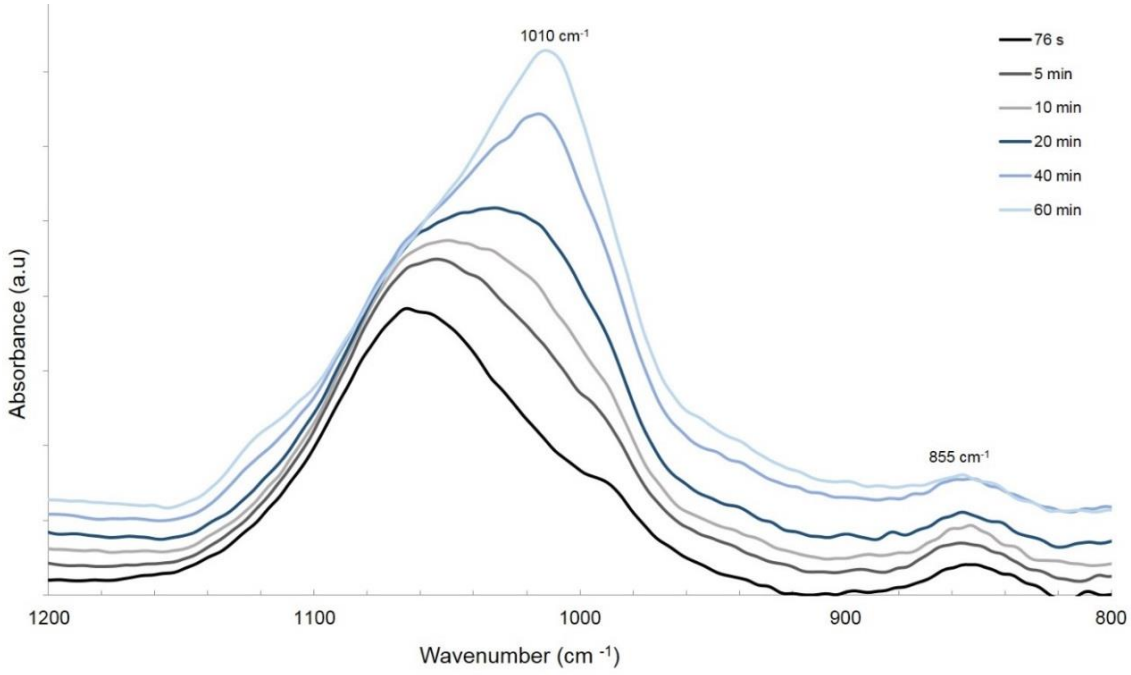

Figure 5-23 FTIR-ATR spectra of 45S5Sr10C4 cement corresponding region B shown in Figure 5-21, with the main peaks observed for this area. Graphs are stacked for comparison purposes

49P9C4 cement

Figure 5-24 shows the FTIR-ATR spectra for the 49P9C4 cement during setting. The analysis started immediately after mixing at 80 s until 60 min. From these spectra, also four main areas are distinguished: a broad band centred at approximately 3280 cm^{-1}, a series of six peaks between 1645 and 1320 cm^{-1} (represented as A), an intense peak at 1060 cm^{-1} (represented as B), and a broad peak at approximately 520 cm^{-1}. An important difference between this cement and the rest of the samples was noted for the peak at 3280 cm^{-1}, which significantly decreased its intensity over time. Similarly, the intensity of the peak at 1640 cm^{-1} appeared to decrease faster when compared with other cement formulations.

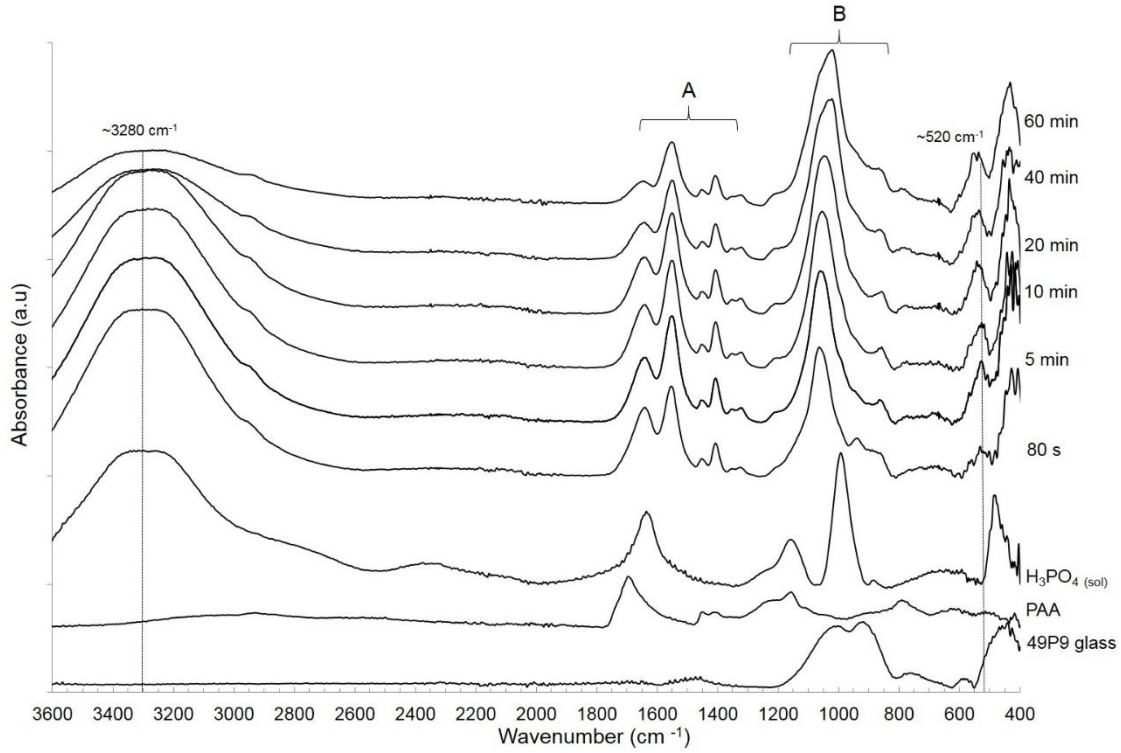

Figure 5-24 FTIR-ATR graph showing the setting of the 49P9C4 cement the start of mixing to 60 min. The spectra of the parent glass, PAA and $H_3PO_{4(sol)}$ are included for reference

Figure 5-25, shows the "A" area with six peaks positioned at 1640, 1545, 1450, 1400, 1340 and 1320 cm^{-1}. In these spectra, the peaks at 1640 and 1545 cm^{-1} did not seem to change with a specific pattern, however overall, the intensity decreased over time.

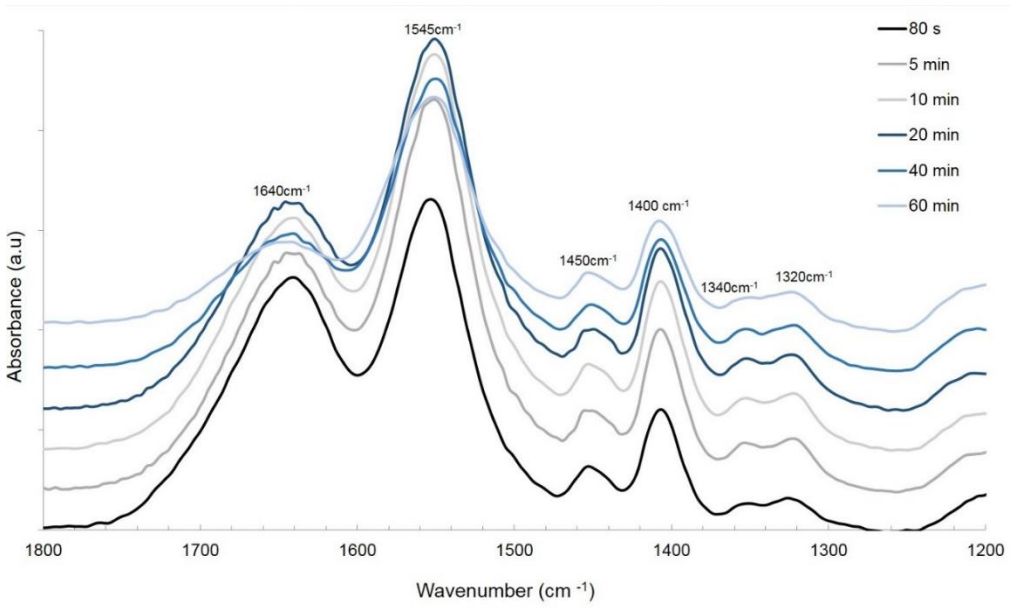

Figure 5-25 FTIR-ATR spectra of 49P9C4 cement corresponding region A shown in Figure 5-24, with the main peaks observed for this area. Graphs are stacked for comparison purposes

Figure 5-26 presents the "B" area, showing that the band initially centred at approximately 1060 cm^{-1}; increased its intensity and shifted to lower wavenumbers over time with a final position at 1025cm^{-1}. A small band at approximately 860 cm^{-1} was identified, and did not change over time, however, at 40 min, it appeared to be less defined and become part of the 1025 cm^{-1} band as a small shoulder, which was very clear on the software view of the experiment

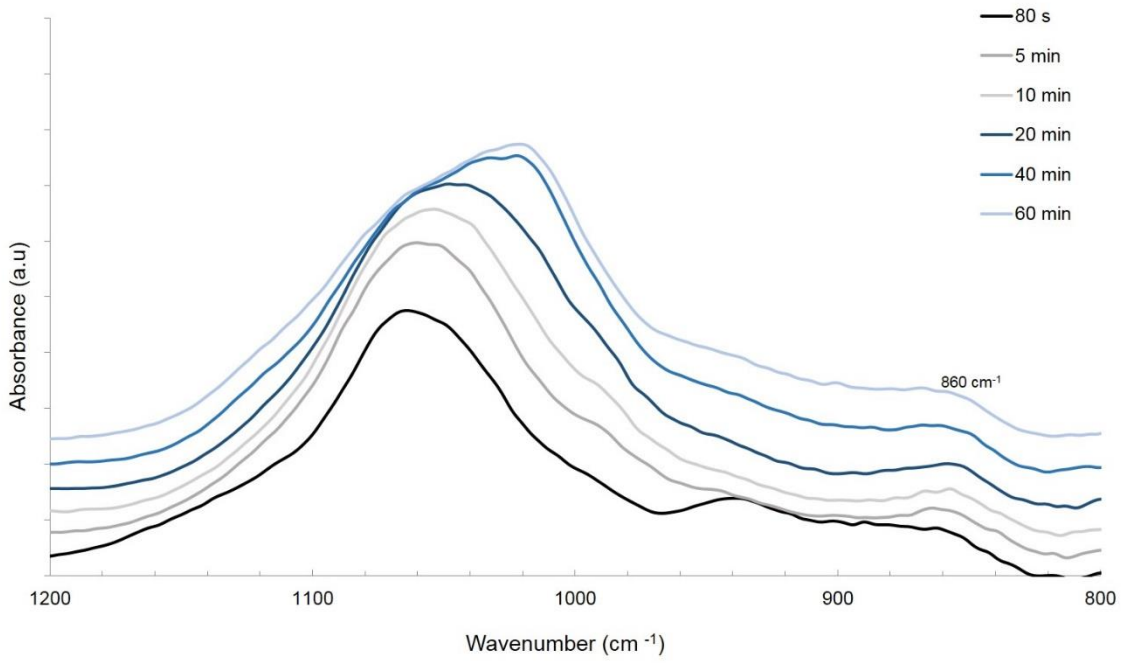

Figure 5-26 FTIR-ATR spectra of 49P9C4 cement corresponding region B shown in Figure 5-24, with the main peaks observed for this area. Graphs are stacked for comparison purposes

53P4C4 cement

Figure 5-27 shows the FTIR-ATR spectra for the 53P4C4 cement during setting. The analysis started immediately after mixing at 66 s until 60 min. Similarly, to previous spectra, four main areas are distinguished: a broad band centred at approximately 3280 cm^{-1}, a series of six peaks between 1645 and 1320 cm^{-1} (represented as A), an intense peak at 1060 cm^{-1} (represented as B), and a broad peak at approximately 510 cm^{-1}. The band at 3280 $cm^{-1,}$ decreased with time, and the peak at 510 cm^{-1}, did not appear to change.

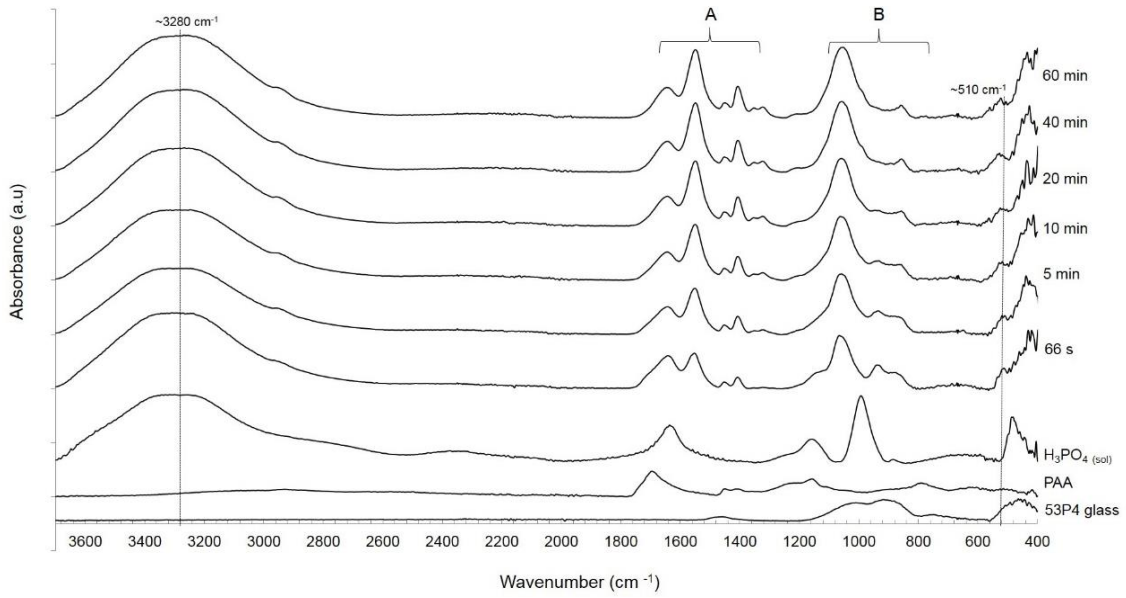

Figure 5-27 FTIR-ATR spectra of 53P4C4 cement, showing the setting from the start of mixing to 60 min. The spectra of the parent glass, PAA and $H_3PO_{4(sol)}$ are included for reference

Figure 5-28, shows the "A" area with six peaks positioned at 1640, 1550, 1450, 1405, 1350 and 1325 cm^{-1}. All the peaks except for band positioned at 1640 cm^{-1}, increased over time, particularly for the peaks at 1550 and 1405 cm^{-1}, with no significant shifts on their position.

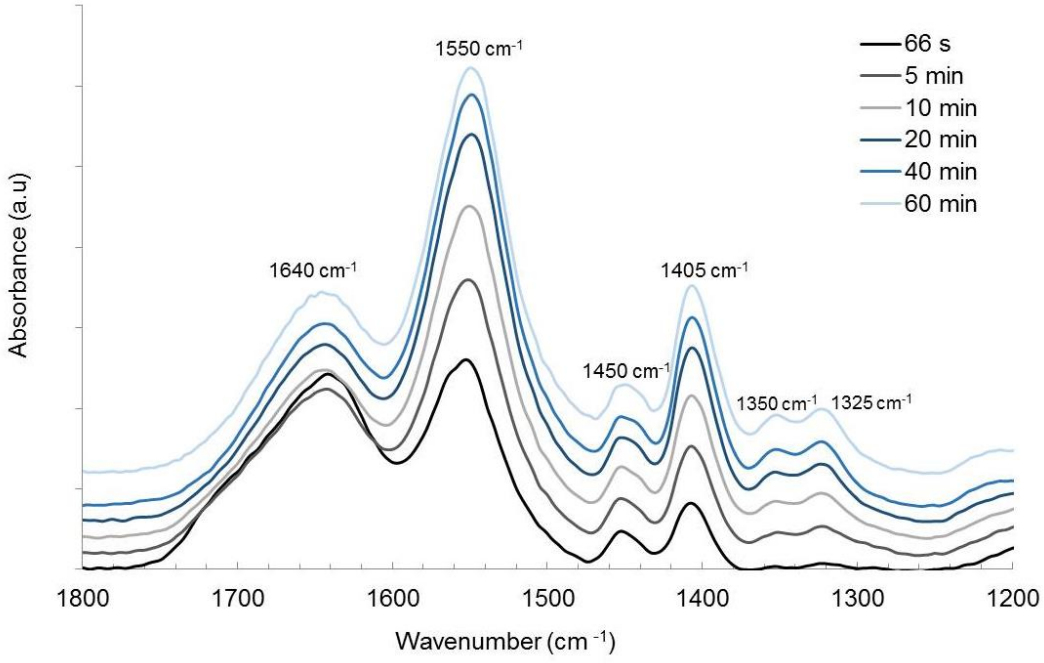

Figure 5-28 FTIR-ATR spectra of 53P4C4 cement corresponding to region A shown in Figure 5-27, with the main peaks observed for this area. Graphs are stacked for comparison purposes

Figure 5-29 presents the "B" area, showing a band centred at approximately 1055 cm^{-1}. This peak increased over time with no significant shifts in its wavenumber, which could be an indication of a setting mechanism difference in comparison with the previously described setting reactions.

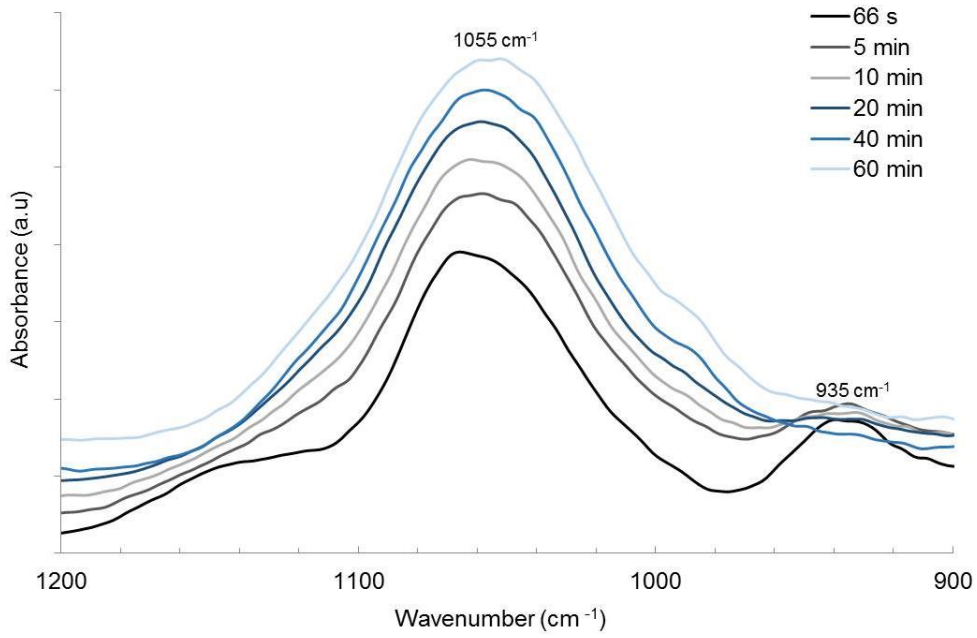

Figure 5-29 FTIR-ATR spectra of 53P4C4 cement corresponding to region B shown in Figure 5-27, with the main peaks observed for this area. Graphs are stacked for comparison purposes

5.7 Short term *in vitro* direct contact test

5.7.1 Washing protocol study: measurement of pH and conductivity

In general, the pH variation in the storage water was not as evident as expected. The initial pH values of the leachate varied from 10.15 ± 0.07 and 10.24 ± 0.05 for 20 and 50 ml of storage solution respectively to 9.89 ± 0.08 and 9.81 ± 0.04 after 19 solution washes spread through 75 h. The decrease in pH was observed just during consecutive washes, since it increased again to the initial value when the solutions were left overnight. Overall, no significant pH variation was observed between the two volumes of water used. Figure 5-30 shows the variation on the pH value of the storage solutions in which cement discs (9 x 2 mm) were stored: the minimum and maximum varied between eight and nine as defined with by the dotted lines.

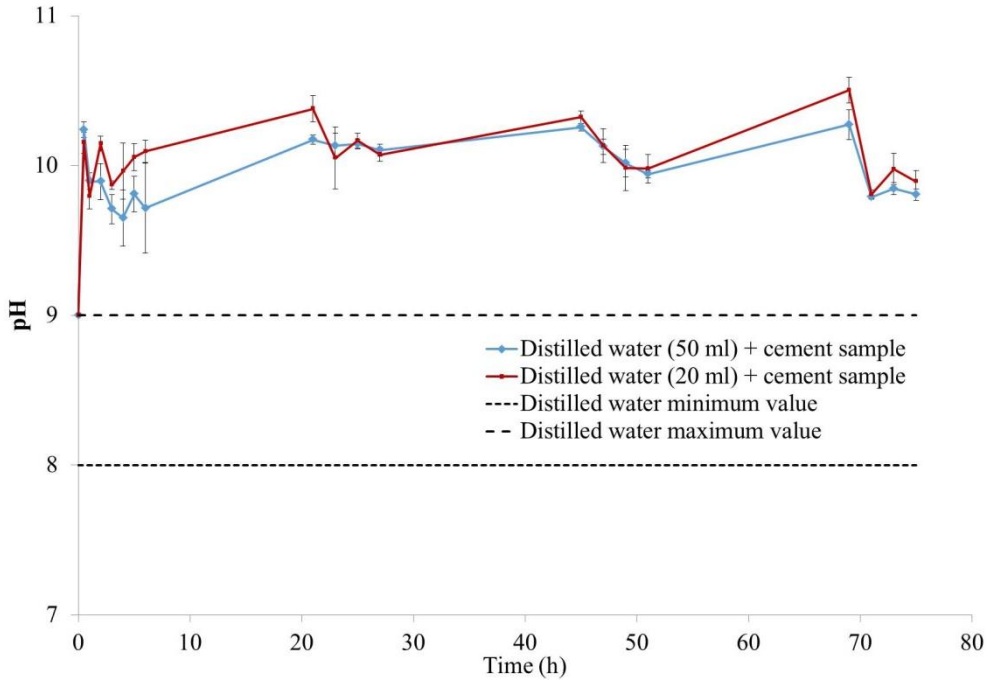

Figure 5-30 Variation of pH values for 45S5C4 discs (9 x 2 mm) pre-treated in 20 ml and 50 ml of distilled water. Error bars= ± SD; n=3.

The conductivity values obtained for both storage volumes fluctuated broadly and significant differences were obtained for both conditions. Conductivity decreased from 574.33 ± 118.15 to 81.30 ± 8.03 µs/cm, for a 20 ml washing volume; and from 214.17 ± 27.27 to 34.47 ± 5.00 µs/cm, for a 50 ml washing volume. Figure 5-31 shows these results, with maximum readings observed at the same time points to the maximum pH values previously shown. The volume chosen for the *in vitro* sample preparation corresponded to the 20 ml washing protocol, since no significant differences were observed between the two volumes. In addition, using 20 ml implied the use of less water and smaller containers that were easier to handle for the pH and conductivity measurements.

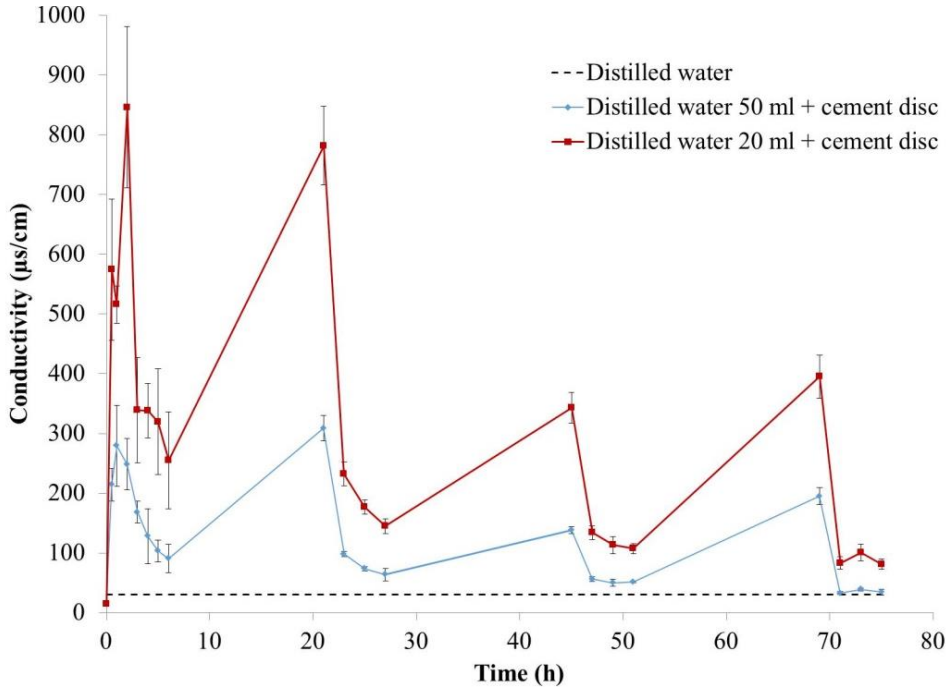

Figure 5-31 Variation of conductivity values (µs/cm) for 45S5C4 cement discs (9 x 2 mm) pre-treated in 20 ml and 50 ml of distilled water. Error bars= ± SD; n=3.

A preliminary *in vitro* test with Presto Blue® (results not shown) with discs of the same size used for the pH and conductivity tests (9 x 2 mm) resulted in cell cytotoxicity and no apparent difference between pre-treated (washed) and untreated (not-washed) samples, which was interpreted as the discs being too big in relation with the well volume. Therefore, the sample size was reduced to 4 x 1 mm discs in order to have a free area, where it was possible to observe if cells were migrating to and/or from to the disc. Figure 5-32 shows the conductivity values for these smaller sized discs when washed in 20 ml of distilled water: the pattern in the conductivity variation was similar to the 9 x 2 mm discs. The smaller discs had lower conductivity values, with a maximum of 200.65 ± 34.15 in comparison with 781.67 ± 65.58 µs/cm. Pre-treatment or washing of smaller discs required nine changes of distilled water to decrease the conductivity (20 µs/cm.). This reference value was chosen for two motives: the conductivity of distilled water varied between 20 and 30 µs/cm, which signified that this value was a limitation to decrease further the conductivity. In addition, for the *in vitro* preliminary test (Figure 5-33) cell viability was considerably improved with respect to the non-washed samples when cements were pre-treated in this manner.

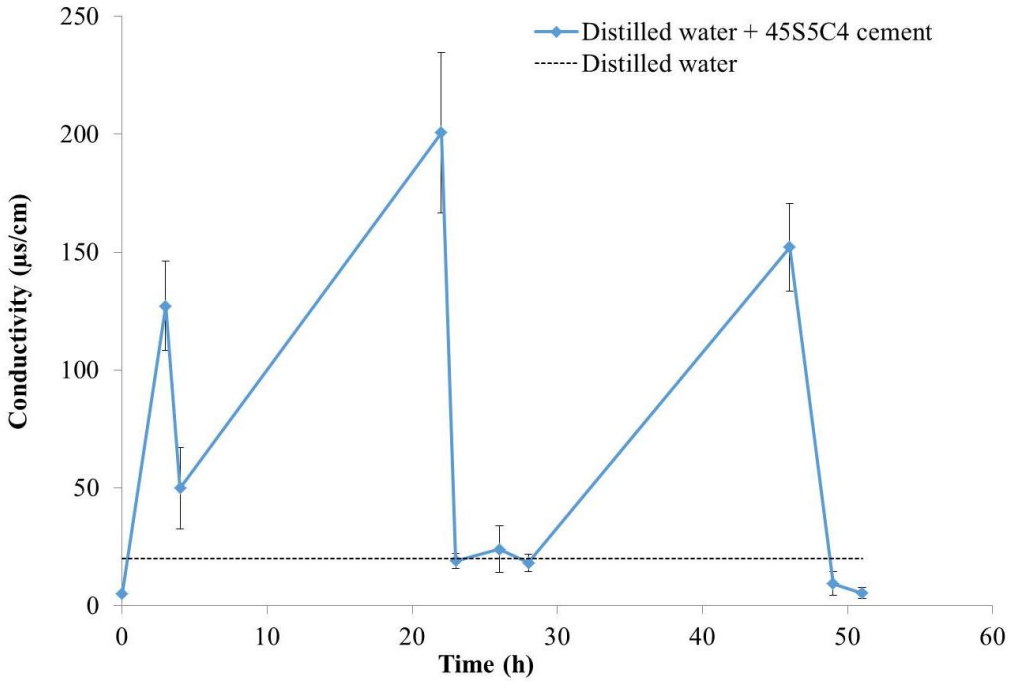

Figure 5-32 Variation of conductivity values for 45S5C4 discs (4 x 1 mm) for the preliminary washing protocol carried out for the *in vitro* testing. The maximum conductivity registered for the distilled water was 20 µs/cm. Error bars= ± SD; n=4.

Figure 5-33 and Figure 5-34 shows the comparison between the pre-treated and non-treated samples after 24 h from cell seeding. The non-treated samples showed no cell survival with absence of cell spreading and a gel like appearance of the media. An indication of this result was visually confirmed by the rapid colour media change from light pink to fluorescent pink after samples were placed in the wells, suggesting a fast pH change. The media colour of the wells containing pre-treated samples had a slight change, which did not differ considerably with respect to the control wells. The 45S5C4 cement showed to have induced a good cell coverage away from the sample and medium coverage near the edges of the disc. Although some rounded cells were noted, the general morphology was similar to that of the control wells (TCP).

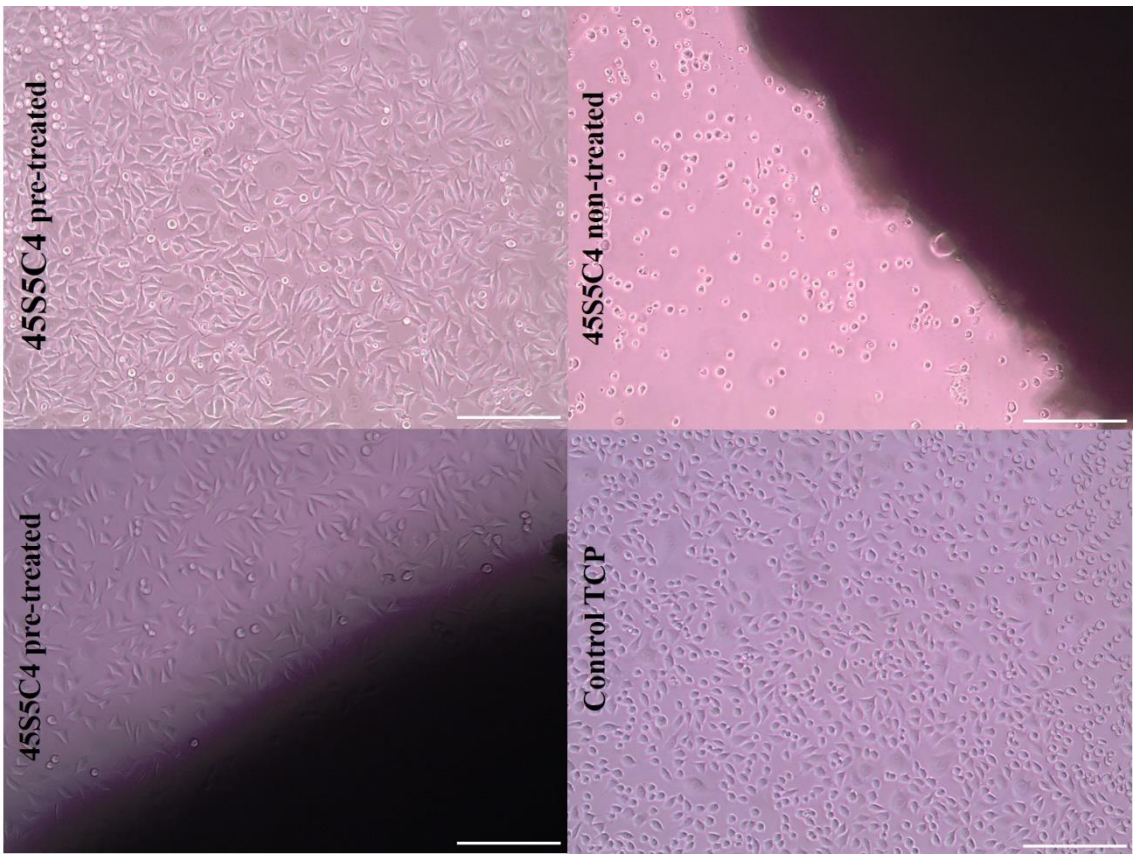

Figure 5-33 Light microscopy images showing the wells with the 45S5C4 pre-treated and non-treated cement discs, and comparison with the tissue culture plastic (TCP) used as control. L929 mouse fibroblasts cells were seeded at 50,000 cells/well. Scale bar is 100 µm

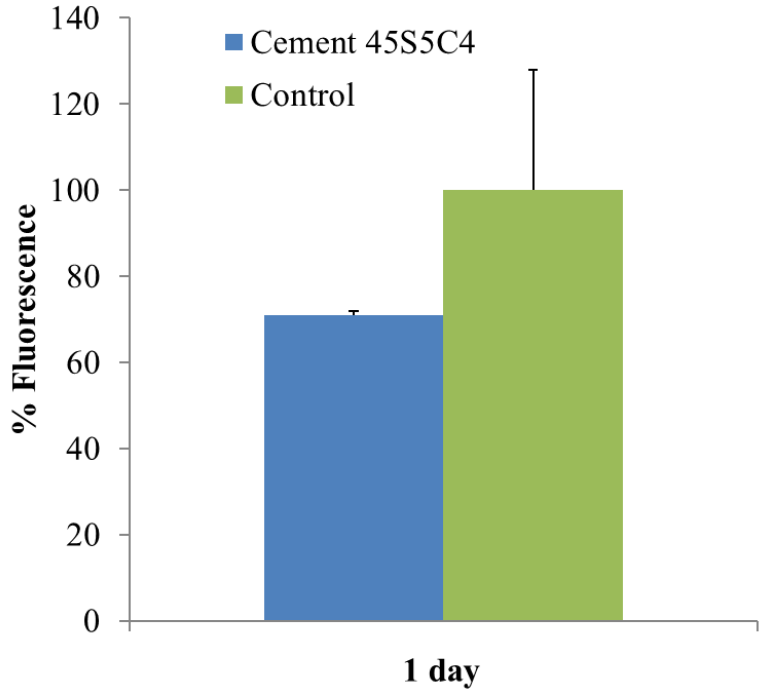

Figure 5-34. Preliminary Presto Blue® results showing the % Fluorescence for the 45S5C4 pre-treated cements and the tissue culture plastic (TCP) used as control ($p < 0.05$). L929 mouse fibroblasts cells were seeded at 50,000 cells/well. Error bars= ± SD; n=4.

Figure 5-35 shows SEM images of a representative area of a pre-treated 45S5C4 cement discs (previously presented on Figure 5 33) nine days from cell seeding, presenting a well-covered area of the disc surface and details of the L929 cells showing a characteristic elongated morphology with filopodia clearly adhered on the surface. These results showed that the washing protocol was appropriate to decrease the conductivity levels to more stable values. Initially, the main objective was to decrease the pH value of the leachate, which was not possible to lower to neutral pH values. However, decreasing the leachate conductivity values to less 20 µs/cm proved sufficient to minimise the abrupt ion release from the cements to the media and therefore a negative effect on cell viability.

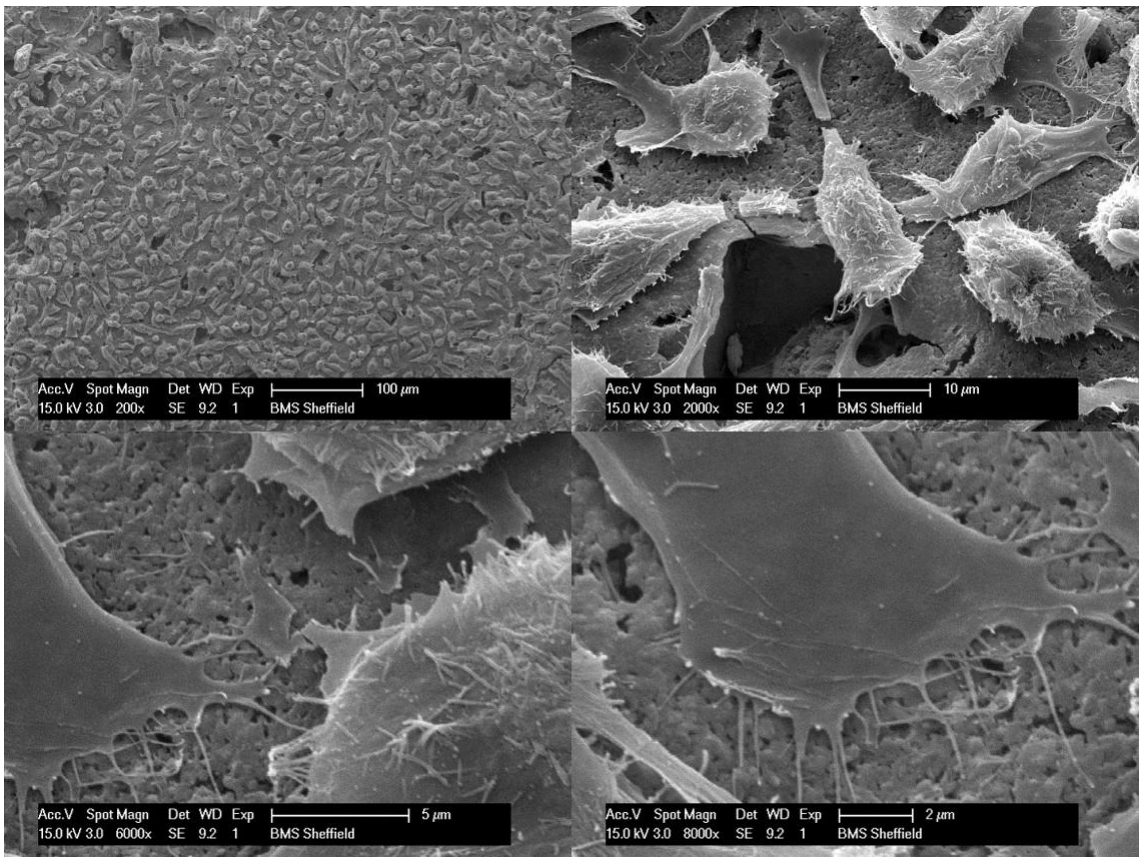

Figure 5-35 SEM images showing 45S5C4 pre-treated cements (from Figure 5 33) after nine days from cell seeding. The SEM images show one area of the disc surface with good cell coverage and attachment. L929 mouse fibroblasts cells were seeded at 50,000 cells/well

For the final cell viability test, cell type was changed to MG63 cells due to issues with the fluorescence values obtained with the L929 cells. During the Presto Blue® test, there was evidence of cell growth on the well plates (by light microscopy evaluation), however, no difference between the fluorescence of experimental samples and the control TCP were obtained. The incubation time was extended for up to three hours

with no changes on the fluorescence levels. It was then decided to change the cell type to MG63 cells due to their osteoblastic nature and due to the reliable results obtained with the cells in previous experiments.

5.7.2 *In vitro* short term direct contact test: 45S5C4 cement and Serenocem™

Figure 5-36 shows the Presto Blue® test % fluorescence values for the 45S5C4 cement, Serenocem™, and control (TCP). For day one, the cell viability for the 45S5C4 cement was 53.37 ± 19.16 %, and for Serenocem™, 87.09 ± 18.48 %, respect to the control TCP. For the second day, cell viability for the 45S5C4 cement was 69.66 ± 21.82 %, and for Serenocem™ cement was 77.28 ± 10.15 %, respect to the control TCP

A one-way ANOVA was conducted to compare cell viability between the 45S5C4 cement, Serenocem™, and control (TCP). The normality test showed that standardised residuals were normally distributed ($p > 0.05$), while Levene's homogeneity of variance could not be assumed for the two days' time point ($p = 0.002$). Therefore, post-hoc comparisons using the Tukey test were used for one day, and Games-Howell for two days.

As seen in the figure below, for day one, there were significant differences between the 45S5C4 cement and the other two groups, with the cell viability being 46.67% in average lower respect to the control. However, for day two, the 45S5C4 cement did not show a significant difference with the commercial cement Serenocem™, but only with the control group.

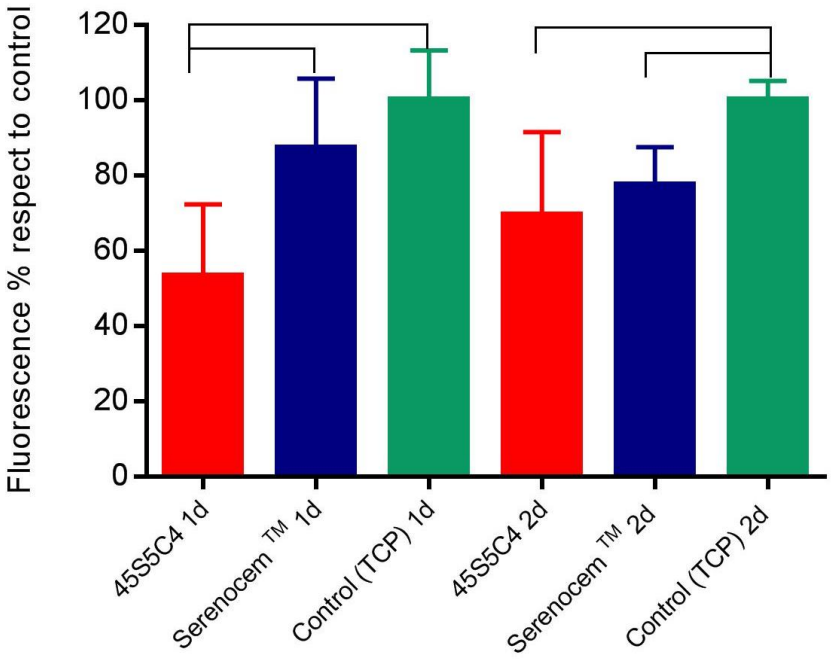

Figure 5-36 Fluorescence % results for the Presto Blue® cell viability test between 45S5C4 and Serenocem™ after one and two days . Discs (4 x 1 mm) were pre-set in dry conditions for one day at 37 °C and washed according to protocol described in section 4.4.1. Error bars= ± SD; n=9.

Figure 5-37 and Figure 5-38 show optical microscopy images corresponding to 45S5C4, Serenocem™, and control samples for one and two days of the *in vitro* direct contact test. For day one, the cells seeded on the 45S5C4 discs, were spread on the bottom of the well plate, although from a qualitative consideration, the cell concentration was less evident in comparison with the Serenocem™ samples, which was also reflected on the cell viability assay. Around the cement, there was a reduced amount of cells with the presence of a few with rounded morphology. For the first day, cells were not generally positioned near the disc, while for Serenocem™ it was possible to observe them positioned around the samples. The control group (TCP) showed the behaviour that is expected for this material, with well covered areas and some others with slightly less coverage of the TCP surface. The samples observed after two days from seeding, seemed to have a more homogeneous distribution on the TCP. The samples corresponding to the 45S5C4 cement showed a full coverage on the areas further away from the sample, while closer to the discs; the cells were not as densely distributed. However, various samples were examined, and while some had fewer cells on the border on the sample, others resembled more to the cell distribution observed for the Serenocem™ group.

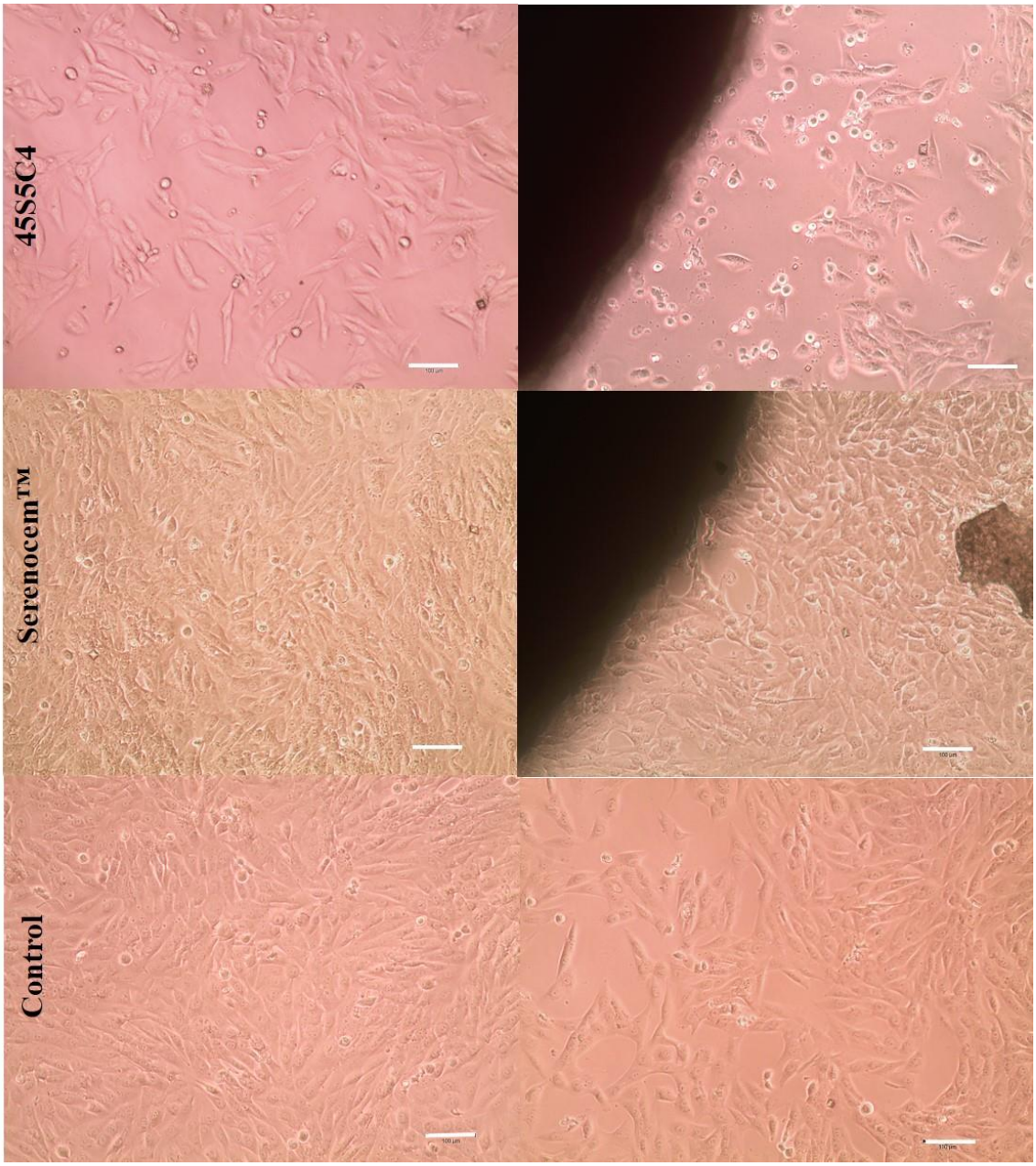

Figure 5-37 Light microscopy images after one day from cell seeding, showing the L929 cell distribution on the well plate (left row) and near the cement disc (right row); scale bar = 100 µm.

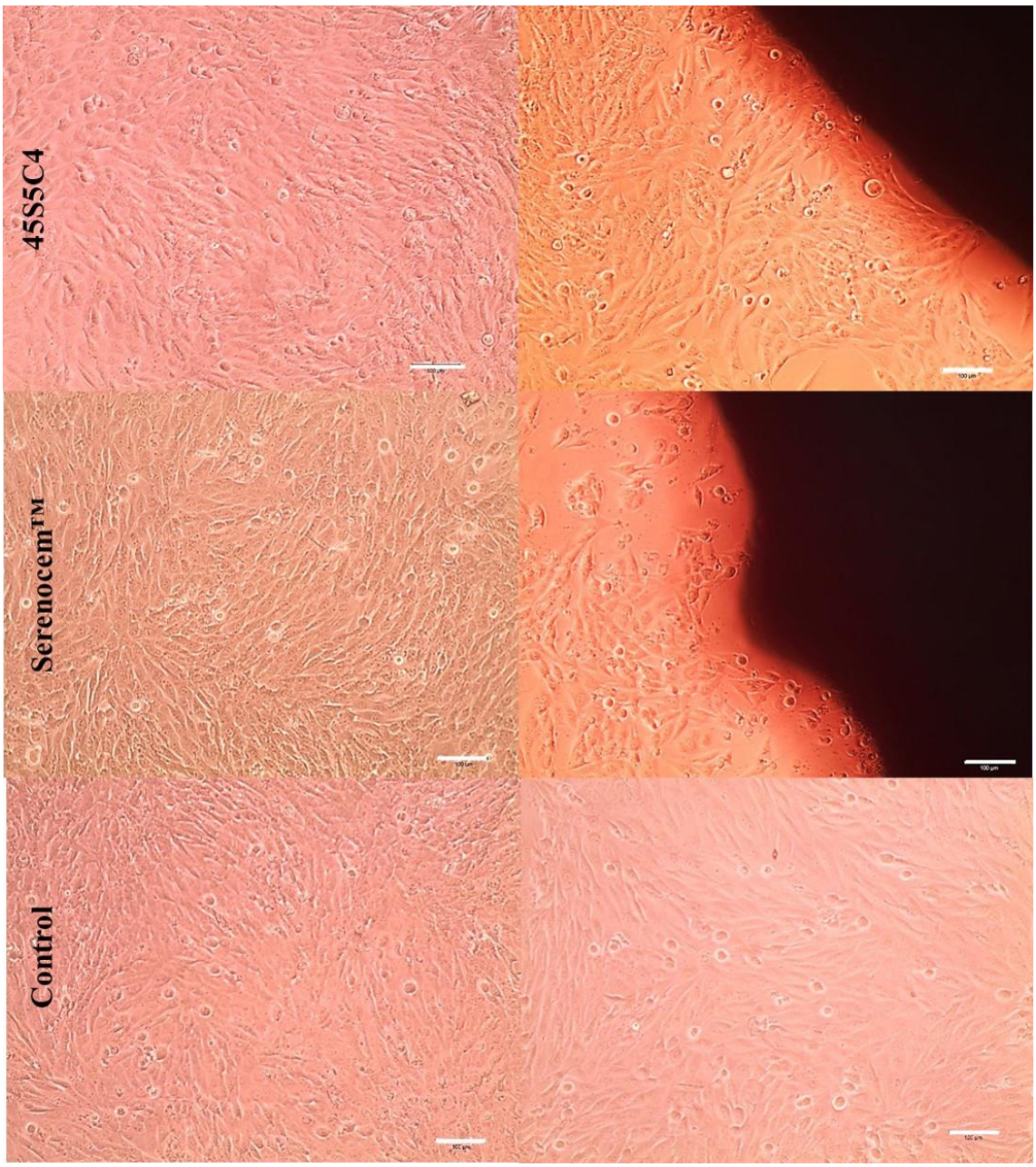

Figure 5-38 Light microscopy images after two days from cell seeding showing the L929 cell distribution on the well plate (left row) and near the cement disc (right row). Scale bar = 100 µm

6 Discussion

The aim of the present research was to use aluminium free glasses to prepare and characterise a series of cements for their use as setting pastes, and compare their properties with a commercially available aluminium containing cement Serenocem™. Therefore, six main objectives were identified and enclosed in the following procedures: glass melting and characterisation, description of a range of cement forming parameters (H_3PO_4 concentration and powder/liquid ratio), definition of suitable cements formulations for further characterisation, and *in vitro* testing of a cement formulation.

6.1 Glass preparation

As previously explained, glasses were produced by a melt-quench route, with two issues encountered during melting of the 35P6 and 45S5 compositions with the presence of white opaque particles, mainly attributed to a lack of melt homogeneity. This issue led to increasing the SiO_2 content of the 35P6 glass composition from 35 wt. % SiO_2 to 42 wt. % SiO_2. This increase was 2 wt. % higher than the minimum SiO_2 content defined by Hench in the SiO_2-Na_2O-CaO-SrO-P_2O_5 system for bone bonding compositions. In addition, the crucible volume was increased in order to allow for the entire batch to be melted in one step.

The issue encountered with the 35P6 glass, was consistent with the non-glass forming area described by Hench in the SiO_2-Na_2O-CaO-P_2O_5, for glasses with SiO_2 content of less than 40 wt. % (Hench, 2006). This result was attributed to the low proportion of SiO_2 as a glass network former since the melting parameters were considered within the reported values for bioactive glasses (Table 2-4). The presence of white opaque particles in the preliminary melting for the 45S5 composition was associated with crystallisation of the glass. Rawson described that devitrification can occur on the surface due to non-uniform heating and thermal shock when the crucible is taken out of the furnace (Rawson, 1991), which occurred each time the crucible needed to be taken out for re-batching. An additional explanation was associated to a lack of batch homogeneity, as in the preliminary tests there was no pre-mixing method in practice. This was in agreement with previous research, and attributed to the clustering of large silica particles due to incomplete batch mixing, and particle agglomeration generated by the bubbles movement through low viscosity areas in the melt (Schweiger *et al.*, 2010). Therefore, an additional step was included previously to melting, by mixing the glass batch in a rotatory mixer to improve the homogeneous distribution of raw materials.

6.2 X-ray powder diffraction

Characterisation of the glasses by XRD confirmed that all the powders were amorphous. The broad halo located between 26 and $37^{0}2\Theta$ corresponds to the characteristic amorphous pattern of vitreous silica (Warren and Biscce, 1938) and this 2Θ range is consistent with previous studies in melt-derived bioactive glasses (Chen *et al.*, 2006;Mneimne *et al.*, 2011); (Groh *et al.*, 2014). This result suggested that the designed melt-quench route was effective to avoid crystallisation and would imply that the appropriate melt viscosity and quench rate was achieved to prevent the formation of crystals. Nevertheless, it was not possible to discard the possibility of localised crystallisation, since testing the whole batch is unfeasible.

For cement preparation, this technique was important to evaluate if the starting glasses maintained their amorphous nature, since partial crystallisation would retard ion leaching and therefore make the glass less degradable, which could delay setting. This was previously reported in Fe containing aluminium free GICs, where partial glass crystallisation increased the cement setting time (Hurrell-Gillingham *et al.*, 2006). In addition, crystallisation was associated with an inhibition of its bioactive properties, due to a decreased ion exchange (Wallace *et al.*, 1999).

6.3 Wavelength dispersive X-ray fluorescence

XRF confirmed that the glasses were appropriate for cement preparation. Nonetheless, some compositional variations were obtained that could have been influenced by various factors such as: number of tested samples, purity of raw materials, melting process and loss in ignition.

Firstly, one sample was tested for each glass composition, since for the purpose of this research; XRF was used as a tool to evaluate if the differences between theoretical and post-melt values were in agreement. Additionally, the nature of the melt quench route and milling process signified that there were local compositional variations independently of the number of samples tested. Another factor that was associated to the difference of the post-melt composition was the melting itself. For example, previous research reported an additional step involving re-melting of the frit to improve glass homogeneity. However, bioactive glasses had also been successfully produced by casting the melt directly into a frit or block (Peitl *et al.*, 2001). Volatilisation of elements was also described during glass melting, with authors previously reporting phosphorus deficiency in the post-melt composition (Hill, 1996;Shelby, 2005) .

The purity of raw materials could have influenced the compositional variations, considering that the tendency (higher or lower oxide content) was maintained through all the glasses: each raw material had an associated content of impurities, however this factor was not considered in the literature when calculating the theoretical glass batch at a laboratory scale. Finally, the loss in ignition, which is defined as the change in mass of a material when heated under specific conditions (ASTM, 2013), could be an additional source for the composition variations of the glasses, since this factor was not included when calculating the initial batch, and therefore the required mass would be higher than the calculated one. For instance, the loss in ignition for SiO_2 was 0.1% and for $CaHPO_4$ was 7.4%, which could explain the decrease of SiO_2 and CaO detected by XRF in the post-melt composition. For the rest of the raw materials, this value was not specified; therefore, it would be not possible to include the associated mass loss into the glass batch calculations.

In spite of these factors, post melt compositions variations, were found to be within the range reported in the literature: a study on a melt derived 45S5 glass powder described variations in mol % of SiO_2 (1.8), CaO (1.0), Na_2O (1.5) and P_2O_5 (0.2) (Bruckner *et al.*, 2016). For another study, 45S5 glass bars were analysed by XRF, showing variations slightly over 2 wt. %, even though the initial frit was re-melted to improve homogeneity (Plewinski et al., 2013).

The elemental impurities in melt-derived glasses were not extensively described in the literature, but a study reported this value to be less than 0.43 wt. % in a vitreous silica glass (Serra *et al.*, 2003), and to vary between 0.2 wt. % and 0.5 wt. % in 45S5 glass nanoparticles (El-Kady *et al.*, 2012), with both considered comparable to the experimental results. Furthermore, the presence of impurities is also inherent to the raw materials, with the $CaCO_3$ chemical analysis reporting the presence of Cl, Fe, Pb, Cu, Mg, K, Na, Zn, S, P, and Si, in agreement with several of the oxides detected by XRF.

In relation to the traces of alumina (Al_2O_3) in the melt-derived glasses, it was unclear if its source was due to the raw materials or the glass preparation. Furthermore, precaution steps were considered during glass melting to avoid aluminium contamination such as the use of reagent grade SiO_2 instead of sand, zirconia for ball milling, and equipment only intended for preparation of these glasses and cements. In addition, no previous research on aluminium free cements was found to report the Al content either on the glass or the ion release data, and consequently it was not possible to present

comparisons with this research. The presence of aluminium, was considered to be low enough to not interfere on the setting process, with a study in GICs by Wilson *et al.*, reporting that Si/Al ratios higher than two generated very slow cements or no cement formation at all (Wilson *et al.*, 1980).

6.4 Differential thermal analysis

DTA is a standard technique used to determine the glass transition temperature (T_g) and crystallisation temperatures ($T_{p1,}$ T_{p2}) of glasses. T_g showed a gradual increase with the network connectivity (NC), implying an increase in the energetic requirement to reach the glass transition range. A more rigidly cross-linked glass network increases the activation energy barrier associated with the glass transition temperature and viscous flow of the glass (Fredholm *et al.*, 2010), therefore the lower the crosslink of the glass, the lower the glass transition temperature (Hill, 1996). Nonetheless, no clear trend was observed with variations in P_2O_5 content, where its increase caused a decrease in T_g (when comparing 49P3 with the 49P6 glass), and an increase in T_g (when comparing 49P3-49P6 with the 49P9 glass). As previously described in the literature review, an increase in the phosphate content, depolymerises the glass by removing Ca and Na ions from the main silicate network (Tilocca and Cormack, 2007), which in consequence would increase the T_g. However, for the experimental glasses, this was not the case between the 49P3 and 49P6 compositions, which could be attributed to the slight decrease of SiO_2 content for the 49P6 glass.

The T_g for the 45S5 glass was 529 °C, with data from several studies reporting the following values: 520 °C (Groh *et al.*, 2014), 525 °C (Santocildes-Romero *et al.*, 2015), 538 °C (O'Donnell and Hill, 2010), and 560°C (Chatzistavrou *et al.*, 2004;Boccaccini *et al.*, 2007). Furthermore, O'Donnell *et al.* reported a theoretical value of 532 °C based on a linear equation that correlates the molar compositions with parameters obtained from fitting a series of values reported in the literature (O'Donnell, 2011). The T_g for the 45S5Sr10 was 521 °C, in agreement with a T_g of 525 °C reported in the literature (O'Donnell *et al.*, 2010;Santocildes-Romero *et al.*, 2015). When compared with the 45S5 glass T_g, this result was consistent with previous research, that described a decrease in T_g with Sr substitution (O'Donnell and Hill, 2010;Santocildes-Romero *et al.*, 2015), with this effect being associated with a slightly larger atomic size in comparison with Ca, that expands the glass network and decreases the energy barrier to achieve the glass transition range (O'Donnell and Hill, 2010). Due to the similarity between T_g of these two glasses, it was possible to assume that both structures were

comparable, in agreement with their NC number. Contrary to the expected result, the 53P4 showed a T_g of 527 °C, which was comparable to the lower SiO_2 content glasses. This temperature was also lower to that reported by Massera *et al.* of 561 °C (Massera *et al.*, 2012a). Similarly, the T_g obtained for the 58P6 glass was the lowest for all the glass compositions, which was unexpected due to this glass having the highest NC value; however, this glass had the lowest Ca/Na ratio which could be related to an increase in the proportion of Na in the glass, and the softening of the network. The decrease of T_g with increase of Na_2O content is well documented in bioactive glasses, and was described to be a linearly dependant (Andersson, 1992;Wallace *et al.*, 1999); with Na_2O having a more disruptive effect on the glass network than CaO (Kusumoto *et al.*, 2016). Additionally, the lower content of CaO could have had a predominant influence in comparison with the higher SiO_2 content, since in soda-lime silicate glasses, the Ca^{2+} has been attributed to block the displacement of the Na^+ ions (Braunger *et al.*, 2012), which would suggest the presence of a less rigid glass network, that contributed to a drop in the T_g.

For the 42P6, 45S5, and 45S5Sr10 glasses, one crystallisation temperature was observed, varying between 594 °C and 687 °C. Other authors also reported one T_p for the 45S5 composition at 682 °C (Santocildes-Romero *et al.*, 2015), 720 °C (Chatzistavrou *et al.*, 2004) and 736 °C (O'Donnell and Hill, 2010). Nonetheless, due to the phase separation mechanisms in this system, other authors reported the possibility of two crystallisation peaks: one corresponding to $Na_2Ca_2Si_3O_9$ (Clupper and Hench, 2003;Bretcanu *et al.*, 2009;O'Donnell *et al.*, 2010), and the second corresponding to $Na_2Ca_4(PO_4)_2SiO_4$ (Bretcanu *et al.*, 2009). A possible explanation for the presence of one peak, could be associated to the duration of the experiment, since Arstila *et al.* reported the presence of this second phase after 6 h at 1000 °C by SEM (Arstila *et al.*, 2008) which was previously attributed to phosphorus ions staying in solid solution (Peitl *et al.*, 2001).

The presence of these two phases could be evidenced by the two well defined, although shallow, endotherms for the three compositions (42P6, 45S5 and 45S5Sr10) corresponding to the melting points of two phases that ranged between 1169 °C and 1232 °C. These results were consistent with those obtained by Boccaccini *et al.* and O'Donnell *et al.*, that reported this range to vary between 1070 °C-1278 °C (Boccaccini

et al., 2007), and 1190 °C-1264 °C (O'Donnell and Hill, 2010) for the 45S5 glass, and between 1145 °C-1259 °C for the 45S5Sr10 glass (O'Donnell and Hill, 2010).

For the 53P4 glass, the crystallization range was in accordance with the values reported in the literature, with temperatures varying between 748 °C and 796 °C (Massera *et al.*, 2012a;Massera *et al.*, 2012b), with the main detected phase reported to be $Na_2Ca_2Si_3O_9$ (Massera *et al.*, 2012a).

In terms of the glass series with 49 wt. % SiO_2 and variation of P_2O_5, there was not a clear trend of T_g. Nonetheless, there was a drop in T_g between the 49P3 and 49P6 glass, which was in accordance with the study by O'Donnell *et al*. for a glass series in which increasing the P_2O_5 content caused a decrease in T_g (O'Donnell *et al.*, 2008). For this glass series, there was not a diverse source of references to compare with in the literature, however, a study by O'Donnell, evaluated the thermal properties of a glass that was comparable with the 49P3 glass (ICIE1), with a reported T_g of 513 °C. This value was lower in comparison with the 49P3 composition (539 °C), but was considered a good reference point due to the ICIE1 composition having lower content of SiO_2 and higher content of Na_2O. These two factors were previously referred in this section to influence a decrease in T_g by lowering the NC of the glass.

The 49P3, 49P6, and 49P9 glasses, showed two crystallisation peaks, which was in agreement with the study by O'Donnell *et al.*, where the influence of P_2O_5 content with a fixed Ca/Na ratio was studied. These peaks are associated with the presence of a clustered phosphate phase in addition to a silicate phase, due to a phase separation mechanism (O'Donnell *et al.*, 2008).

With regards to the T_m, the endothermic peaks were weak and broad for the three glasses; with 49P3 and 49P9 glasses showing one T_m, in contrast with two T_m for the 49P6 glass. The presence of one endotherm for these compositions was in disagreement with the presence of the two crystallisation peaks in the DTA curve. This result could be explained by a postulation from O'Donnell, that described the formation of a single phase in two separated regions or that crystallise by two different mechanisms (O'Donnell *et al.*, 2008) which could melt at the same temperature or within a narrow temperature range that did not allow the presence of two defined peaks in the DTA curve. In summary, the patterns observed in the DTA results, were similar to those in the literature, and whilst there were variations for various of the parameters, these are

likely the result of compositional variations, heating rate (Bretcanu *et al.*, 2009), particle size (Massera *et al.*, 2012a) and rate of glass cooling (Paul, 1990).

6.5 Scanning electron microscopy

SEM characterisation of the sieved glass powder showed that two groups were predominantly found: small particles (about 2-10 μm) and larger particles (about 37-64 μm). The particle size range was in accordance with the methodology used for sieving (≤ 45 μm); however, some particles were larger than this upper limit. This could be due to their irregular geometry, for which the size measured across the particle was less than 45 μm and larger in the transverse direction. Additionally, this could also be attributed to the position of the particles on the sample holder, which does not allow for an exact measurement to be carried out. For this reason, SEM was used as a guideline and not as a definite method to study the particle size, since the influence of specific particle size ranges on cement formation, was not within the aims of this research.

When comparing with previous studies, it was found that the powder morphology was in agreement with previous studies on melt-derived bioactive glasses, in which a mixture of agglomerates and irregular-angular particles were observed (Sepulveda *et al.*, 2001;Santocildes-Romero *et al.*, 2015). Similarly, the angular particles observed for the larger size range, were comparable to the 45S5 commercial product, Novabone® that is used as a bone graft substitute. Regarding the presence of agglomerates, Sepulveda *et al*., previously attributed this to the presence of van der Waals forces; while the combination of agglomerates with angular particles was characteristic of the milling. Sepulveda *et al*., also reported that fine particles (~5-20 μm) exhibited a higher surface area, which could enhance the glass dissolution and increase the deposition of Ca-P later *in vitro* (Sepulveda *et al.*, 2001). Similarly, Cerruti *et al.*, reported that small particles (~2 μm) would react faster, thus aiding glass dissolution (Cerruti *et al.*, 2005). Therefore, the presence of fines in the experimental glasses could be beneficial during cement setting through a faster release of Ca, Na and Sr.

6.6 Fourier transformed infrared spectroscopy with attenuated total reflectance

FTIR-ATR was used to characterise the main peaks of the experimental glasses that are associated with the silica network and presence of network modifiers such as Ca, Na and Sr. As previously presented in section 0, the identified peaks were associated with characteristic C-O, Si-O-Si, Si-O-NBO and Si-O-2NBO groups. Firstly, the peak at 1500 cm^{-1} was identified for all the glasses, with slight intensity variations. This band

was attributed in the literature to the presence of small quantities of carbonates, formed by a reaction between atmospheric CO_2 and available Ca/Sr surface ions (Cerruti *et al.*, 2005;Fredholm *et al.*, 2010;Massera *et al.*, 2012b).

Secondly, the two peaks positioned in the region between 1200 cm^{-1} and 800 cm^{-1} were associated with the Si-O and P-O groups (Sepulveda *et al.*, 2002;Young *et al.*, 2004;Cerruti *et al.*, 2005). The shift towards higher wavenumbers (at 1000 cm^{-1}) as the NC increased was attributed to the increase of SiO_4 groups. These changes were described by Serra *et al*. to be associated to an increase in silica content and a decrease in network modifiers (Serra *et al.*, 2003). The presence of network modifiers in the glasses was confirmed with a broad band at approximately 910 cm^{-1}, and was assigned to the Si-O-NBO bond. This band was associated to the presence of Na_2O, CaO and SrO (Serra *et al.*, 2003;Cerruti *et al.*, 2005;Massera *et al.*, 2012b), and corresponds to Q^3 units in the glass structure (Fredholm *et al.*, 2010). The small peak at approximately 840 cm^{-1}, appeared to become more defined when silica content decreased, and was associated to the presence of a Si-O-2NBO (Q^2) structure and linked to the increase of network modifiers at the expense of silica (Serra *et al.*, 2003;Fredholm *et al.*, 2010). These differences showed that the increase in the NC of the glasses, had an structural effect with a decrease of the Si-O-2NBO bonds, suggesting the conversion of a number of Q^2 for Q^3 units, which occurs with the decrease of Na_2O/CaO content (Fredholm *et al.*, 2010).

Thirdly, the region between 800 cm^{-1} and 700 cm^{-1} showed a peak definition change with glass compositional variations. This peak was described in the literature with Si-O-Si bonds (Jones *et al.*, 2001;Sepulveda *et al.*, 2002;Cerruti *et al.*, 2005), and to the presence of glass network modifiers (Ca, Na) when the Si-O-Si rings are highly distorted. Finally, the region between 500 cm^{-1} and 400 cm^{-1} was associated in the literature with the P-O bending mode (Sepulveda *et al.*, 2001;Sepulveda *et al.*, 2002) and Si-O-Si vibration (Sepulveda *et al.*, 2001;Sepulveda *et al.*, 2002;Cerruti *et al.*, 2005). The broadness of this signal was linked with the amorphous nature of the experimental glasses.

Returning to the aims, this research has shown that it was possible to successfully melt a series of glasses based on a SiO_2-Na_2O-CaO-SrO-P_2O_5 system, with SiO_2 ranging between 43.1 and 60.0 mol%; and P_2O_5 ranging between 1.3 and 5.1 mol%. The melt quench route was suitable to obtain a clear and amorphous glass frit, with the post melt

compositions having a close match with the theoretical compositions, and with characteristic DTA, FTIR-ATR and SEM patterns comparable to those reported in the literature.

6.7 Preliminary study on cement preparation

The results from the preliminary study of the cements showed that the pastes prepared with the bioactive glasses set to a hard material. Nonetheless, this was not feasible for cements prepared with the 58P6 glass. A possible explanation for this was the high silica content and a low CaO content that was associated with a polymerised glass and a low availability of Ca ions for crosslinking, with previous research reporting the importance of CaO on the setting of Al-free GICs (Dickey *et al.*, 2013).

In the same way to what occurs in traditional GICs (Crisp *et al*., 1980) it was found that variations on PAA and use of a setting modifier (phosphoric acid) changed the mixing properties of the cement and the stability outcome. However, as previously described, small modifications in the cement formulations, changed the outcome in the paste mixing and stability in water, suggesting that the setting of aluminium free cements had irregular patterns, in contrast with the sharp setting reactions that characterise GICs. This inconsistent setting behaviour of Si based Al-free GICs, was described by Dickey *et al.* with setting times being as fast as one minute and other pastes that did not set (Dickey *et al.*, 2013). Additionally, working with small variations meant that deviations related to the user or instruments could have influenced the results. Consequently, the concept of the second stage for cement assessment was developed to have comparable cement combinations within glass compositions, and ensure that the increments between them were significant to evaluate possible trends.

As previously described in section 5.3, the mixing properties were influenced by the P/L ratio, volume of phosphoric acid and PAA. From the qualitative point of view, increasing the P/L ratio, required faster mixing, however, when this value was three it was not possible to form a paste, except when using the 53P4 glass or for smaller discs. This was attributed to a lack of water to completely hydrate the powder to produce a malleable paste, which was associated to a decrease in water acting as a plasticiser in the setting reaction (Alan and Wilson, 1993).

This effect was more noticeable when the phosphoric acid concentration increased, which was similarly associated with a decrease in water content. The fact that a paste

prepared with the 53P4 glass, was possible to mix at a higher P/L ratio (only at 20% concentration of phosphoric acid) was attributed to the lower P_2O_5 content. This compositional difference, could have delayed the precipitation of phosphate containing salts that were thought to intervene in the setting, which in response increased the time available to properly mix the paste, even with low content of water in the mix. However, this result could also be attributed to the higher network connectivity of the glass that resulted in lower glass degradation, as previously observed in the FTIR-ATR study, which translated into a longer time for the cement to set.

When phosphoric acid was added as a setting modifier, an increase in its concentration would make the paste less liquid-like and promote setting. This was specially noted at 35% concentration, since the samples tended to deform at the end of the mixing. This was related to the lower pKa constant of H_3PO_4, in comparison with PAA (Crisp, 1974), thus aiding glass degradation. In addition, increasing phosphoric acid concentration decreased the water content. As previously described, water is associated with the medium for ionic transport, which could have reduced the mobility of the carboxylate ions from the PAA, that confers the plastic/malleability character to the pastes.

Regarding the stability outcome, the addition of phosphoric acid was essential to prevent gelation and dissolution of the cements in water. This behaviour was previously explained by Milne *et al*. to be linked to the stabilisation of calcium by phosphoric acid through the formation of an insoluble calcium phosphate (Milne *et al.*, 1997). Moreover, previous research described the importance of adding a copolymer of PAA and/or a setting modifier to achieve stability in water in traditional GICs (Alan and Wilson, 1993), this being attributed to the availability of a higher number of carboxylic acid groups and acid strength (Smith, 1998;Fuchs *et al.*, 2015). Indeed, previous research in Al-free GICs by Brauer *et al*. and Fuchs *et al*. reported the low stability in water of aluminium free cements when PAA alone was used as the acid component (Brauer *et al.*, 2011a;Fuchs *et al.*, 2015), and the lower reactivity of bioactive glasses with PAA, in comparison with traditional GICs (Yli-Urpo *et al.*, 2005). Otherwise, cements prepared without a copolymer or solely with PAA, required longer aging times (> 7 days) or high Mw PAA (80,000) to be stable in water (Towler *et al.*, 2002). However, increasing the setting time would be a drawback for clinically relevant applications, while adding high PAA molecular weights do not facilitate mixing due to the increase in the paste viscosity, limiting their use to low concentrations, which can produce a weak cement (Wilson *et al.*, 1977).

The preparation of these range of cement formulations was valuable to define the variables affecting the qualitative characteristics of the cement pastes in terms of malleability, hardening and stability in water, and as previously defined in the aims of this research, it allowed having an overview to subsequently identify a comparative system in which all the cements were stable in water to be able to further characterise the samples.

6.8 Handling characterisation of cement pastes

For the studied cement combination (C4), the only considered variable was the glass composition, since the P/L ratio, PAA, and phosphoric acid concentration were kept constant. However, external factors were noted to affect results with the Gillmore needle method: sample size, temperature, surface quality of the sample, section of the sample (centre-edge), and sample thickness. Regarding ambient conditions, cement setting is accelerated with increase in temperature, as reported by Deb and Nicholson when comparing the setting of a series of cements at 21 ºC and 37 ºC (Deb and Nicholson, 1999). However, from a practical consideration some surgeons would check the cement *in situ*, for which it would be necessary to develop a formulation with a sufficiently stable setting profile to allow its use in various ambient conditions.

In terms of the mixing time, there was no significant difference between cements, except between the 42P6C4 samples and those prepared with the 49 % wt. SiO_2 glass. This result was associated to its network connectivity, resulting in a highly degradable glass, and liquid-like paste. Nevertheless, it is important to note that this result was mainly attributed to the mixing technique and qualitative consistency of the pastes, rather than dissolution mechanism of the glasses, since the mixing speed was altered to be able to obtain a paste that could be moulded into disc-shaped samples. Similarly, in previous work on aluminium free cements (Wren *et al.*, 2010;Wren *et al.*, 2013;Dickey *et al.*, 2016), the authors did not report specific values, but a maximum time in which mixing was completed, suggesting that this measure was not as relevant to characterise.

The experimental cements with longer initial setting times were 42P6C4 and 45S5Sr10C4, which was expected due to the liquid-like texture of the pastes. Nonetheless, as discussed above, a lower network connectivity is equivalent to a less polymerised glass that should translate into a faster setting (Fuchs *et al.*, 2015), which was not the case for these two cements. Consequently, this result suggested that for a cement prepared with a bioactive glass based on the SiO_2-Na_2O- SrO-CaO-P_2O_5 system,

the degradability of the glass was not proportional to the setting time of the cement, and that relevant phases for the hardening of the cement, such as polyacrylates and phosphate salts, require longer times to develop the necessary strength for the cement to set when compared Serenocem™, which in spite of exhibiting an initial setting time slightly over 10 min, had the shortest net setting time within the examined cements.

Another point to consider was the difference between the initial setting time for the 45S5C4 and 45S5Sr10C4 cements, with the latter having a longer initial setting time. The numerical equivalence of the NC parameter implied an equivalent glass network within these two glasses, with the slight expansion caused by a larger atomic size of Sr, however, it was not certain how a 10% mol substitution on Ca affected the cement setting. This outcome was contrary to previous research describing that Sr substitution on Ca, increased ion release (O'Donnell and Hill, 2010), glass dissolution (Santocildes-Romero *et al.*, 2015) and glass basicity (Boyd *et al.*, 2008b), which consequently, would decrease the setting time in aluminium free GICs (Boyd *et al.*, 2008b;Fuchs *et al.*, 2015). A possible explanation for this might be that these studies were based on higher Sr/Ca substitutions and cements based on silicate glasses with other network modifiers such as Zn (Boyd *et al.*, 2008a) and Mg (Fuchs *et al.*, 2015), for which the interaction between Sr and other components could have influenced the release and phase formation in a manner that aided setting. This could also imply that formation of Ca based salts are more significant in the early setting of the cement (< 15 min) than Sr based salts, at least for low Sr/Ca substitutions, since the net setting time between these cements did not show significant differences.

One unanticipated finding was that the cements prepared with two of the highest NC' values (49P6 and 49P9) had the lowest initial and net setting times. As previously mentioned, an increase in the NC' value and therefore in the glass network connectivity has a delaying effect on ion release and their availability for crosslinking during setting (Wren *et al.*, 2012;Chen *et al.*, 2014). Under this premise, the lower NC glasses such as 42P6, 45S5, and 45S5Sr10 were expected to set faster, due to a faster degradation in aqueous-acidic media. This result suggested that the degradation of the 49P6 and 49P9 glasses was sufficient for ion crosslinking and with a faster setting in comparison with a glass that is more degradable. In addition, a higher silica content, could be assumed to aid formation of the silica gel phase, and the inorganic matrix of the cement (Hatton and Brook, 1992;Nicholson, 1998a), that was previously reported to be essential in GIC setting. This might be explained by the significant decrease of the 3280 cm^{-1} band

corresponding to the OH^- signal seen by FTIR-ATR for the 49P9C4 cement; and where more importantly a silica containing phase, could have more strength when compared with the polyacrylate salts or phosphate based compounds. This was previously described by D'Onofrio (2016), and attributed to the principle of the Gillmore needle test, that is based on the strength of the cement; hence a weaker cement would be more likely to have a longer setting time, since more time is required for specific phases to form in order to resist the indentation. Another possible explanation for this result was associated to a mixed effect between the NC and phosphate increase in the glass, since in bioactive compositions, the dissolution of the silicate and the orthophosphate phases occur as independent processes, with phosphate content directly influencing PO_4^{3-} release (Hill and Brauer, 2011). Consequently, for the 49P9 glass, an increase in PO_4^{3-} release could have improved crosslinking and precipitation of salts involved in the cement setting.

Regarding the 53P4C4 cement, there was a high variability on the initial and net setting time results, which indicated the glass degradation was not uniform for each sample, which could be related to local variations throughout the glass batch. Another possible explanation might be due to the presence of larger particle sizes in the glass powder, which was noted while mixing the cement. The presence of larger particles, could decrease the contact points and increase the presence of voids that made this cement more prone to breakage, which was previously reported to generate a less cohesive paste (Prentice *et al.*, 2005). In addition, the presence of larger particles have less surface area available for dissolution (Sepulveda *et al.*, 2001) in contact with the acidic solution, hence reducing ion release and crosslinking during setting.

The setting times obtained for the experimental cements, were longer than the values required for clinical applications, which range between ten and twenty minutes. An implication of the results could be the need of adding an acid washing step and/or annealing treatment to the preparation of the most reactive glasses (49P6 and 49P9), in combination with a change in the PAA molecular weight and setting modifier concentration. These changes, would allow time for complete mixing and reducing the net setting time. Alternatively, for the less reactive glasses (45S5 and 45S5Sr10), applications such as pre-set granules for bone grafting could be considered, since such a drastic decrease in their setting time might be achieved through compositional variations in the glass rather than in the cement formulation parameters.

These results were comparable with the inconsistency of setting in other aluminium free GICs: Zn based cements with modifications including Ti and Ge exhibited setting times that vary between two minutes (Boyd *et al.*, 2008a), seven minutes (Wren *et al.*, 2010;Wren *et al.*, 2013) and forty minutes (Valliant *et al.*, 2016). Therefore, the characterisation of the setting times for the experimental cements, showed that the degradability of the glasses, associated with their NC, was not the only factor influencing the setting of the cements, with specific quantities of each oxide acting as network modifiers and/or network formers having complex interactions during setting.

6.9 Degradation in water of the cements: mass change

A mass change study in water has not been extensively reported for aluminium-free GICs, for which reference points for this analysis was limited. It was considered that such evaluation is important since visual inspection of the samples and the leachate solutions showed that this was not sufficient to corroborate if the cements were actively dissolving. Moreover, this could be backed up with the ion release of the leachate solution which corroborates the release of important species from the glass and a variation on the release profile during the experiments.

The variations on ion release profiles for all the cements suggested that chemical reactions were sustained for the duration of the experiments, and it is comparable to the early reports by Kuhn and Wilson, which reported that ion release and conductivity studies confirmed long term continued reactions (Kuhn and Wilson, 1985)

The more significant mass loss observed for the earlier time points for the 45S5C4 and 45S5Sr10C4 samples, in comparison with the 49P9C4 and 53P4C4 samples, was attributed to the less polymerised glass structure, and their lower NC, which translated into a more pronounced dissolution of glass particles.

For the cements having a mass decrease, this behaviour was first described for ASPA cements (Crisp *et al.*, 1980) and is comparable with zinc phosphates and zinc polycarboxylate cements (Nicholson and Amiri, 1998). This was related to dissolution mechanisms previously described in the literature: “wash off” of debris and loose surface particles and by the formation of water soluble salts with the matrix forming ions (Crisp *et al.*, 1980) and soluble sodium phosphates (Kuhn and Wilson, 1985). Another cause for the cement mass change was associated with the dissolution of glass particles. As previously described, a GIC is formed by unreacted glass particles in a salt

based matrix (Alan and Wilson, 1993). In traditional GICs, the unreacted glass particles do not considerably dissolve due to the higher polymerisation of the aluminium containing glasses and the more covalent nature of the Si-Al-Si bonds. In contrast, bioactive based glasses are less polymerised, which further supported the idea that the glass particles that did not completely react with the PAA and phosphoric acid, were continuously dissolving after the cements were stored in water.

The commercial cement Serenocem™, exhibited a sustained increase in mass that did not considerably vary through the experiment (< 5 %). This behaviour was related to the swelling up of the silica gel phase, characteristic of traditional GICs (Nicholson and Amiri, 1998), and to the formation of Al hydrates (Crisp *et al.*, 1980). These results were consistent with a previous study on a ASPA III cement, where mass gain occurred as well during the first 24h (Crisp *et al.*, 1980); and similarly to a study on commercial GIC Vitremer™, that showed a mass gain of 3% when stored in a NaCl solution (Nicholson *et al.*, 1999). Furthermore, the reported NC (3.3) for the glass used in this cement was considerably higher than the bioactive glasses, and its formulation does not have sodium oxide, which further supports the cause for the low degradation of this aluminium containing cement, as discussed above. In addition to this cement, the 49P9C4 and 53P4C4 samples also showed an increase in mass for earlier time points that was associated with the higher Si content. For these time points, it was probable that the dissolution of the cement was lower than the hydration of the silica gel in the unreacted particles.

The study of the mass change showed that the cements prepared with bioactive glasses had long term stability in distilled water for up to three months, and suggested that these cements have potential as scaffolds for bone grafting without the possibility of rapid dissolution after implantation. Furthermore, it was shown that at least for earlier time points, there was a link between the NC of the glasses used to prepare the cements and their degradation in water. Nonetheless, further research should be carried out to study the influence of other variables such as cement ageing, sample volume, and storage media.

6.10 Inductively coupled plasma spectrometry

The advantage of bioactive glasses with respect to less degradable glasses, is related to their open silicate structure that promotes the release of ions such as Si, Ca, Sr and P when in contact with aqueous solutions (Fuchs *et al.*, 2015), with these ions being of

importance due to their role in the formation of an amorphous silica rich layer and crystallisation of the $CaO\text{-}P_2O_5$ rich phase (Pantano *et al.*, 1974;Hench, 2006), linked to the bioactive fixation of a material with the biological tissue (Cao and Hench, 1996).

As previously described in section 5.4.5, it was shown through ICP analysis that these ions were released into distilled water by the bioactive glass based cements. Furthermore, these results indicated that the cements were the main ion source, in comparison with other cement and glass degradation studies (Boyd and Towler, 2005;Shi *et al.*, 2006;Brauer *et al.*, 2010) that used SBF, which already contains Ca^{2+} and HPO_4^{2-} (Yoshihara *et al.*, 1994).

Silica ($Si(OH)_4$) release

The release of soluble silica was related to the surface reactions occurring in a bioactive glass surface when exposed to an aqueous media, as described in section 2.2.1. The contact between the melt-derived glasses and the acids generated the hydrolysis of Si-O-Si groups and formation of soluble $Si(OH)_4$ (Pantano *et al.*, 1974;Hench, 2006). In aluminium free cements, these Si-O-Si bonds were thought to be loosely bound on the surface of the glass particles and dissolve when immersed in water, with Si^{4+} easily entering the aqueous media (Alhalawani *et al.*, 2013). The faster release of silica for the 45S5C4 and the 45S5Sr10C4 cements was attributed to the lower NC, which allowed for a faster release of calcium and sodium ions, leaving an ion depleted silica layer on the surface of glass particles. Moreover, the decrease in silica release after one day, was previously linked to the accumulation of a Ca-P rich surface layer, that takes place within the silica structure, causing the stabilisation of the surface and delaying ion leaching (Andersson and Kangasniemi, 1991). The formation of an apatite-like compound was detected by FTIR-ATR during the early setting stage; however, confirmation of this apatite layer would require further investigation, by analysis of these samples with techniques such as SEM and XRD.

Calcium (Ca^{2+}) release

The reduced Ca^{2+} release during the first seven days with a peak observed at twenty-eight days, was associated with the formation of hydrolytically stable calcium acrylate salts, observed by FTIR-ATR (section 2.7) which caused Ca to become part of the matrix in the set cement (Czarnecka *et al.*, 2002), thus impeding Ca^{2+} release into solution as it occurs in bioactive glass powders. Matsuya *et al.* also suggested that in the set cement, PAA is preferentially combined with Ca, which would have delayed the

Ca^{2+} release in distilled water (Matsuya *et al.*, 1999). As previously described there were no significant differences between the cements with exception of the 49P9C4 samples, which exhibited a lower release: as Ca was expected to be also bonded to phosphate groups (PO_4^{3-} and HPO_4^{2-}) coming from the ionisation of the phosphoric acid, which were expected to become part of the cement matrix, preventing its release when exposed to water.

Later increase on the profile release at one month might be related to the slow dissolution of these phases. An additional explanation for this was related to a longer time between measurements (change of distilled water between one week and one month), that allowed more time for Ca^{2+} release into solution, when compared with earlier time points. Similarly to the 49P9C4 group, the Serenocem™ samples showed a very low Ca^{2+} release. This result was in agreement with a study in GICs by Crisp *et al.*, where Ca was not found in acid or basic conditions (Crisp *et al.*, 1980). An implication of this is the possibility that this cement could be less bioactive by slowing down apatite formation (Matsuya *et al.*, 1999).

Strontium (Sr^{2+}) release

Negligible values of Sr^{2+} release occurred as expected from the Sr free glasses. For the 45S5Sr10C4 cement, low levels were observed during the first week. This result could imply the formation of insoluble strontium polyacrylates salts, which was previously reported by Deb and Nicholson (Deb and Nicholson, 1999). A subsequent increase was identified by ICP at twenty-eight days, and was attributed to the longer exposure of the samples to the distilled water after seven days. In addition, the maximum SrO concentration (~15 mg/L), was found to be within values previously reported to have an antibacterial effect in a PAA based cement formulation (Brauer *et al.*, 2012), and to induce a significant decrease in osteoclast differentiation, with this effect previously reported to start at 0.1 mM (~9 mg/L) (Bonnelye *et al.*, 2008).

Sodium (Na^{+}) release

Na release was high for all the cement compositions. This result was associated with two possible explanations: firstly, due to dissolution of sodium based salts, and secondly to leaching from unreacted glass particles. As previously described, sodium forms soluble salts such as phosphate and acrylate salts (Kuhn and Wilson, 1985) and due to the ionic nature of its bond with Si in the glass structure, it would be preferentially released when in contact with an aqueous media.

Phosphorus (PO_4^{3-}) release

The increase in phosphate ion release up to one day, was associated with the dissolution of salts, probably sodium based, which also coincided with the peak observed for sodium ions release (Kuhn and Wilson, 1985). The negligible concentration of PO_4^{3-} after seven days for the 45S5C4 cement could be attributed to the possible precipitation of phosphate as apatite on the cement surface, which is a mechanism extensively reported for bioactive glasses and described in section 2.2.1. However, the phosphate precipitation would have occurred between one and seven days, when the ion release was not measured and therefore, no change in the distilled water was carried out. An additional implication of the lower phosphate release for the 45S5C4 and 45S5Sr10 cements could be due to the formation of a higher proportion of hydrolytically stable calcium and strontium acrylate salts, over sodium based salts.

Aluminium (Al^{3+}) release

The ICP results showed that Al was released by all the cements, and was associated with impurities not reported in the raw materials used to prepare the glasses, as described in section 5.1.2. Nonetheless, it is important to remark that the Al release from the experimental cements was very low, and decreased with time to negligible concentrations (< 0.005 mg/L). The accumulated Al was ~ 0.20 mg/L, which is significantly lower than the 14 mg/L concentration linked to neurologic deficits (Becaria *et al.*, 2002).

Interestingly, the Serenocem™ samples released similar quantities of Al (accumulated ~ 0.10 mg/L) but this ion release increased with time, suggesting that a longer term experiment should be carried out to study possible implications for *in vivo* conditions, since chronic aluminium exposure and accumulation in brain was linked to neurodegeneration (Becaria *et al.*, 2002). Equivalent studies with this commercial cement were not found; however Crisp and Wilson reported a similar behaviour in GICs, where Al release increased with time when exposed to water (Crisp and Wilson, 1974), with comparable results observed in neutral and acid solutions (Crisp *et al.*, 1980). At the current stage, it would be difficult to identify if the Al had a role in cement setting, however the small quantities detected by XRF in the parent glasses would imply otherwise. In addition, it was not possible to detect by FTIR-ATR the peaks that are associated with aluminium polyacrylate salts, suggesting that Al did not have an important role during crosslinking. Nonetheless, due to the issues associated

with its release, it would be necessary to further evaluate the biocompatibility of the cement *in vitro* and *in vivo*.

In summary, these results showed that the bioactive glass based cements were able to release Si, Ca, P and Na ions. The release of these ions was associated in the literature to the ability of glasses of stimulating osteoblast lines at a genetic level (Xynos *et al.*, 2000;Hench, 2009), and to the rapid nucleation and crystallisation of an amorphous calcium-phosphate layer that provides binding sites for the recruitment of specialised proteins associated with bone matrix deposition (Hench *et al.*, 2004). Conversely, the low concentrations of these ions detected for the Serenocem™ samples, could be linked to the reports of bone reabsorption due to the inhibition of hydroxyapatite formation and growth (Malluche, 2002), which is also supported by the inert nature reported for Al_2O_3 surfaces (Cao and Hench, 1996).In summary, these results showed that the conductivity of the distilled water increased when exposed to the cements, with a peak observed after one day of exposure, coinciding with the increase in pH. The conductivity and pH increase was mainly associated with the Na peak detected by ICP at one day, which was consistent with preliminary studies on bioactive glasses (Cerruti *et al.*, 2005) and GICs (Crisp and Wilson, 1973). Similarly, Wilson described the increase of pH in GICs to occur due to ion release from the glass (Na^+, Ca^{2+}, PO_4^{3-}) and their accumulation into the solution (Wilson, 1978). The later decrease in conductivity over time was associated with the gradual depletion of Na^+ ions, in agreement with the Na^+ concentration detected by ICP. In the case of the pH, these results were associated in the literature to the release of Ca^{2+} and Na^+ in the glass and H_3O^+ protons in the distilled water (Sepulveda *et al.*, 2001).

6.11 Dissolution testing: pH and conductivity

The difference in conductivity and pH observed for earlier time points between the lower SiO_2 containing cements (45S5 and 45S5Sr10) and higher SiO_2 containing cements (49P4C4 and 49P9C4) was attributed to their NC: as the glass polymerisation increases, the glass becomes less degradable, which caused the conductivity and pH to rise less, due to a lower release of basic ions into solution (O'Donnell and Hill, 2010). In this way, the glass particles with lower NC might have a higher concentration of Na^+ and Ca^{+2} near their surface, which can go into solution in exchange for H^+ ions, causing these pH variations (Brauer *et al.*, 2010).

The change in pH was not as marked as the conductivity. This result may be explained by the fact that the pH of the distilled water ranged between eight and nine, which further increased due to the basic nature of the glass. The high pH for deionised water was attributed to the environmental CO_2 which was previously reported by Nicholson *et al*. to produce an increase on the water pH according to the following equilibrium reaction (Nicholson and Amiri, 1998):

$$H_2O + CO_2 \rightleftharpoons H^+ + HCO_3^-$$

These results were similar to a study by Czarnecka *et al*., where the pH did not vary significantly, even though there was evident variation on ion release through the experiment (Czarnecka *et al.*, 2002). Regarding the Serenocem™ samples, the low conductivity registered was associated with the dissolution behaviour of the cement in water, and was in agreement with the Na^+ and Ca^{2+} concentrations detected by ICP. As indicated previously, this cement does not contain sodium, and its parent glass has a high NC, translating into a low ion release and conductivity fluctuations.

The evaluation of pH and conductivity in bioactive glass based cements, indicated that future studies of similar cements systems could require stabilisation of the pH according to a specific application: for example, low pH if the aim is to model the oral environment when exposed to acid conditions, or a neutral pH if the aim is to model the bone environment. In addition, these findings implied that the experimental cements did not act as a buffer, by regulating the pH of the distilled water, as previously reported for GICs. Nonetheless, alkaline environments are not entirely detrimental for the performance of biomaterials. Even though, Na^+ rapid release is a drawback for *in vitro* evaluation due to the limited buffering capacity of cell culture media, it was reported that for a 45S5 glass, at higher pH, the precipitation of calcium phosphate occurred faster when compared with pH values of less than seven (Cerruti *et al.*, 2005). In addition, this finding could have an implication for the development of bioactive glass based cements with antibacterial properties, since it was reported that a S53P4 based glass showed a strong bactericidal activity due to the local pH increase (~ 9), elicited by the high dissolution of the glass (Zhang *et al.*, 2010).

6.12 Cement setting by Fourier transformed infrared spectroscopy with attenuated total reflectance

The setting of the cements was studied by FTIR-ATR to determine the changes occurring in the main peaks of the glass spectra when mixed with PAA and the phosphoric acid solution.

The acid neutralisation mechanisms observed in the FTIR-ATR results were compared to that of traditional GICs as described in the literature (Crisp and Wilson, 1973;Young *et al.*, 2004): initial acid ionisation and attack, glass rearrangement, ion exchange or leaching, and salt precipitation.

All the cements spectra showed two peaks at 3280 and 1636 cm^{-1}, corresponding with a O-H stretch from water previously reported at 3300 cm^{-1} (Young, 2002), 1635 cm^{-1} (Young *et al.*, 2004) and 1640 cm^{-1} (Crisp *et al.*, 1974). These two peaks continuously decreased with time, confirming that water was involved in the setting reaction. As previously described, water, which was also present in the phosphoric acid solution, functions as a medium where ionic species interact (Alan and Wilson, 1993;Young *et al.*, 2004) and in PAA neutralisation (Young *et al.*, 2004). Nonetheless, this method allows analysing a few microns of the sample in contact with the diamond tip, and due to the setting of the experiment, the surface might be losing water due to desiccation, which could not be discarded to partly be a cause for the decrease of these bands.

The acid ionisation stage was referred to the PAA powder spectra, which showed that the band at approximately 1695 cm^{-1} does not appear in the cement setting spectrum, although it could be overlapped by the 1640 cm^{-1} O-H band. Bands positioned in this area, were reported to correspond to a C=O stretch at 1700 cm^{-1} (Crisp *et al.*, 1974;Young *et al.*, 2004) and 1720 cm^{-1} (Matsuya *et al.*, 1999) (Young *et al.*, 2004). This result was described by Crisp *et al.* and Young *et al.* to be associated with the complete reaction of the PAA (Crisp *et al.*, 1974;Young *et al.*, 2004), and by Gomes *et al.* to a shifting of the C=O stretch peak to a symmetric and asymmetric stretching between 1640 and 1550 cm^{-1} (Gomes *et al.*, 2013). Nonetheless, for GICs it is possible to calculate the degree of crosslinking by measuring the ratio between the 1720 and 1640 cm^{-1} peaks, while the COOH peak gradually disappears (Matsuya *et al.*, 1996). For the experimental cements, this change appeared to occur during mixing time and prior to the first measurement, since the COOH peak at 1695 cm^{-1} is no longer

distinguishable at the first time point, probably due to the high reactivity of these glasses in comparison with the traditional aluminosilicate based glasses used in GICs.

The acid neutralisation and salt precipitation stages, corresponding with the early maturation stage of the cement, were attributed to the bands positioned between 1550 and 1320 cm^{-1}, which in traditional GICs occurs due to the ion exchange between the glass and the PAA, with this rate being determined mainly by the glass composition and the molecular weight of the acid (Young *et al.*, 2004). As previously described in the results section, there was not a significant variation regarding the position of the peaks, when comparing between the four cements, with bands approximately positioned at: 1550, 1450, 1400, 1350, and 1320 cm^{-1}. The 1550 and 1400 cm^{-1} peaks were identified as the strong asymmetric C-O stretch and the medium symmetric C-O stretch of the Ca salts respectively (Crisp *et al.*, 1976). However the band a 1550 cm^{-1} was previously attributed to a partially covalent Sr polyacrylate salt (Deb and Nicholson, 1999). Crisp *et al.*, also reported a Na-PAA asymmetric stretching at 1540 cm^{-1} and a Na-PAA symmetric stretch at 1406 cm^{-1}, while the weak peak at 1350 cm^{-1} corresponds to PAA (Aljabo *et al.*, 2015). These salts were reported to be of an ionic nature, and located in the vicinity of the polyanionic chain by electrostatic attraction (Crisp *et al.*, 1976). The formation of these peaks were previously reported as an evidence of the setting of the cements through crosslinking of the COO^- groups by Ca^{2+}, which is comparable with the traditional GIC setting mechanism (Matsuya *et al.*, 1999).

The glass rearrangement stage was associated with the band centred at approximately 1060 cm^{-1} that shifted with time to 1010 cm^{-1}, and attributed to the Si-O-Si stretching vibration arising from the unreacted glass and silica gel (Si-OH), previously reported at 1020 cm^{-1} (Matsuya *et al.*, 1999) and 1050 cm^{-1} (Crisp *et al.*, 1974). It seems possible that these results were due to an overlapping of the Si-O-Si and Si-OH bands with the phosphate stretching frequencies from the glass. In addition, the formation of a P-O vibration in the salt matrix was also described at 930 cm^{-1} (Matsuya *et al.*, 1999), 950 cm^{-1} (Matsuya *et al.*, 1996) and 1050 cm^{-1} (Fuchs *et al.*, 2015). This result was consistent with previous FTIR studies, describing a considerable overlap in the region of 1066 cm^{-1}, where the phosphate stretching frequencies and the silicate network bands arise (Deb and Nicholson, 1999). Similarly, Cerruti *et al*. (2005) pointed out the difficulties to distinguish the Si and P containing groups, within the 1040 to 940 cm^{-1} region, suggesting that an increase in the 1040 cm^{-1} band was related to the formation of new P containing species. Moreover, the broad band at ~520 cm^{-1}, was previously

assigned to an apatite phase at 576 cm^{-1}(Wu *et al.*, 2011) and 560 cm^{-1} (Fredholm *et al.*, 2012;Sriranganathan *et al.*, 2015); and in combination with the phosphate band (positioned at ~1010 cm^{-1}), it was described to support the presence of an apatite like phase (Sriranganathan *et al.*, 2015). These reported studies were performed in SBF and Tris-Buffer; suggesting that the experimental cements potentially developed a readily present apatite-like chemistry without the need of being immersed in these test solutions.

As a summary, the characterisation of the cements based on the C4 formulation, showed that the setting times achieved for the experimental cements were significantly longer than the required values for clinical purposes (~ 10 min), which was also observed for the commercial cement Serenocem™. However, further characterisation carried out by mass change, ICP, pH, conductivity and FTIR-ATR was valuable to correlate the dissolution behaviour of the cements in water with the degradability of the glasses, previously defined by their network connectivity. Furthermore, these results were useful to compare the ion release between the experimental cements and the Serenocem™ samples, and suggested that the higher network connectivity of the glass used to prepare this commercial cement was related to the low ion release observed for the cement.

6.13 Short term *in vitro* direct contact test

As previously described in section 5.7, the short term *in vitro* test, showed that the washing protocol was important for cell survival. Nonetheless, this result was attributed to the rapid release of alkaline ions that significantly changed the environment of the cells, where a neutral pH of seven is regarded as optimum for their maintenance. Even though this washing protocol was carried out in distilled water, Bioglass® pre-treatment in other conditions such as culture medium was previously reported as a method to minimise pH related cell damage (Xynos *et al.*, 2000). The effect observed in the *in vitro* test, was also described on a Zn based aluminium free cement, and attributed to a high rate of zinc release which the authors partially attributed to the closed system characteristic of *in vitro* testing techniques (Towler *et al.*, 2002). In addition, the pH and conductivity results showed that even though it was possible to reduce the ion release by implementing a washing protocol, the frequency of the water change was also an important factor to consider, as longer exposure times of the samples water (overnight), resulted in a significant increase of ion release, when compared to shorter time intervals. These variations in ion release per sample and time point, could then explain the high

variability observed for the Presto Blue® results, since changes in the pH environment would directly influence cell viability.

Regarding the results observed for the commercial cement Serenocem™, at one day, these samples showed better cell viability in comparison with the 45S5C4 group. This result, contradicts those by Towler and Hurrell-Gillingham (Towler *et al.*, 2002;Hurrell-Gillingham *et al.*, 2006), that described a decreased cell survival in Serenocem™, due to Al release. This difference could be explained by the low ion release detected by ICP for the Serenocem™ samples, and in agreement with the low conductivity values previously described. This confirmed the low degradation of these cements when immersed in distilled water (section 5.4.5), and in the cell culture media used for the *in vitro* testing. These quantitative results were visually confirmed by the slight colour change in the cell culture media, which is also a buffer, before and after immersing the Serenocem™ discs. In contrast, the rapid colour change in the experimental cement containing media showed that the samples still released ions after the washing protocol. As described before, the close *in vitro* environment and the rapid ion release, translated in the reduced cell viability of the 45S5C4 group when compared with the commercial cement.

After two days from cell seeding, there was no significant difference between the 45S5C4 cement and Serenocem™. However, there was significant difference with the control group. This suggested that after the detrimental effect of the release of alkaline ions during the first day of the experiment, this effect was not as important for the second day, suggesting that the released ions were not cytotoxic. This improvement in cell viability with time was previously reported by Xinos *et al.*, for Bioglass® discs when cultured with osteoblasts, describing that an increase in cell density on the glass surface was not apparent until the 12^{th} day of culture, with the previous time points, showing higher cell densities for cells cultured on a culture grade polystyrene (Xynos *et al.*, 2000). Even though the quantitative data was lower when compared to the controls, in terms of morphology, it was noted that the cells were elongated and with good coverage of the well plate, particularly after two days. The reduced cell number seen around the cement discs was linked to the continuous release of alkaline ions, causing unfavourable conditions for the cells to migrate to this area. Nonetheless, for a longer term SEM evaluation, it was shown that the experimental cements promoted cell migration and adhesion onto the samples, with images showing good cell coverage on the surface of the scaffolds, and fibre-like processes that are characteristic of cell

activation (Hench *et al.*, 2004). Consequently, further work is required for a longer term study, as well as quantification of osteoblastic differentiation markers such as ALP, and osteocalcin (Xynos *et al.*, 2000).

These results showed that the 45S5C4 cement cell viability was lower than the control sample. Nonetheless, cell viability was comparable to Serenocem™ after two days, suggesting that the bioactive glass based cement is a viable alternative as an aluminium free material. Furthermore, as previously mentioned, the Serenocem™ granules, were withdrawn from the market due to bone reabsorption issues in the middle ear, which is an application where setting time is not relevant as the cement is pre-set, making the studied cements a potential alternative to explore as bone grafts for ENT applications.

7 Conclusions

Cements based on GIC chemistry have potential for use in bone tissue repair, but the aluminium in their formulation is associated with biocompatibility issues including neurotoxicity and inhibition of bone mineralisation. The aim of this research was therefore to fabricate and characterise a series of aluminium-free GICs to overcome this limitation, with the following conclusions drawn from the data in Chapter 5.

A series of eight glasses were successfully fabricated and characterised, with compositions defined within the bone bonding area described by Hench for the SiO_2-Na_2O-CaO-SrO-P_2O_5 glass system. The glass with 35.8 mol% SiO_2 was not produced due to homogenisation issues during its melting, confirming the non-glass forming area also described by Hench. The study showed that using a crucible with sufficient volume to melt the glass batches in one stage was effective to obtain a clear and amorphous glass frit, with satisfactory post-melt compositions and powder morphology as shown by XRD, XRF and SEM. The DTA analysis showed no clear trends between the network connectivity and T_g, especially when P_2O_5 content was varied. Nonetheless, FTIR-ATR analysis did show slight shifts to higher wavenumbers of the Si-O-Si peak, in accordance with the increase of the network connectivity of the glasses.

The cement forming properties of the experimental glasses were investigated, showing that it was possible to prepare pastes with all the glasses that set within two hours except with the 58P6 composition, which required at least twenty-four hours to set. This glass had the lowest CaO content, confirming the relevance of Ca^{2+} ions in the crosslinking and setting of aluminium free cements. Furthermore, these experiments showed that using the phosphoric acid as a setting modifier was essential to obtain a stable sample after immersion in water, and that using PAA only led to the gelation and subsequent dissolution of the cements.

A range of stable cements in water for all the glasses was identified. These formulations, named as C4 and C10 had a P/L ratio of two and a phosphoric acid concentration of 25 and 35% respectively, and both were prepared for further characterisation. However, further characterisation required an increase in the sample size, which was not feasible to carry out for the C10 formulation due to its fast hardening. This showed that for these series of glasses and liquid components, the

powder/liquid ratios and the concentration of phosphoric acid should be adjusted if the sample size is changed.

The handling properties of the experimental cements and the commercial cement Serenocem™ were evaluated by measurement of their initial and net setting time. The initial setting times of the experimental cements ranged between three and thirteen minutes for the 49P6 and the 45S5Sr10 cements respectively, while for Serenocem ™ it was ten minutes, showing that the initial ion release for the experimental cements was at least comparable and even faster than the commercial cement. Nonetheless, the net setting times of the experimental cements were over the required times for clinical applications, and ranged between thirty-four minutes and two hours for the 49P6 and 42P6 cements respectively. However, the setting time for Serenocem ™ was twenty-two minutes, which was also considerably longer than the setting of ten minutes reported by the manufacturer.

This research also showed that the 49P6C4 and 49P9C4 cements had the shortest setting times, indicating their potential to be used as injectable cements. However, this rapid hardening translated into pastes that were difficult to mix, which represents a limitation in a laboratory and clinical environment, suggesting that further research is required to increase the malleability of the pastes. Nevertheless, alternative applications such as pre-set granules for bone grafting were thought to be relevant for cements with longer setting times.

The present study identified four cement formulations for further characterisation by mass change, ICP, pH, conductivity and FTIR-ATR. The cement formulation corresponded to the C4 combination with the following glasses: 45S5, 53P4 and 45S5Sr10, due to their commercial availability, and the 49P9C4 cement since it combined one of the lowest setting times with a good paste malleability. The slight mass increase showed by the commercial cement Serenocem™, confirmed the traditional swelling behaviour reported for GICs, and the low degradation of this cement was associated with a reduced bioactive nature in comparison with the experimental cements.

The ICP characterisation of the distilled water used to store the cements confirmed the release of the ions required for apatite formation such as silica, calcium and phosphate, since no additives were used with the distilled water, showing that the ion source came entirely from the samples Conversely, the commercial cement Serenocem™, showed a

very low release of these ions, suggesting that this cement is less likely to develop a bioactive surface after implantation. Therefore, the present study proposed that the reported drawbacks associated with aluminium containing cements could be associated to their low degradability and release of ions of interest for cell function, which in turn induces bone reabsorption due to the presence of a biomaterial-tissue interface of an inert nature. The increase in pH and conductivity values for the storage solutions containing the cements was associated with the release of sodium. However, the washing protocol showed to be effective to reduce ion release over time.

An overview of the setting reaction was achieved by FTIR-ATR characterisation, and it was found to be comparable to a dental zinc phosphate cement system due to the use of phosphoric acid, and to a GIC due to the use of poly (acrylic acid). The study showed the immediate change of the Si-O-Si and Si-O bands from the glass after mixing with the PAA and $H_3PO_{4\ (sol)}$, and the presence of bands assigned to sodium, calcium, and strontium polyacrylates. In addition, the presence of a silica gel peak was suggested to overlap the P-O band, and therefore it was not possible to categorically assign these peaks. Nevertheless, this peak was shown to coincide with an apatite band reported in the literature that forms when bioactive glasses are exposed to simulated body fluid and Tris-Buffer. Whilst this study did not confirm the presence of an apatite like phase, it suggested that the experimental cements promoted the formation of a similar phosphate containing specie without the need of exposing the cements to these solutions.

The 45S5 glass based cement was chosen to study the *in vitro* cell response, showing that the samples maintained cell viability by day one, and by day two there was no significant difference with the commercial cement Serenocem™. The qualitative characterisation by light microscopy showed fewer cells positioned in the areas adjacent to the cements in comparison with the areas further away from the samples, suggesting that the release of alkaline ions affected cell proliferation. However, a longer term SEM study showed that cells were able to migrate on to the surface of the samples with a clear presence of attachment sites on the surface of the cements.

To summarise, stable cements were successfully produced and characterised with a series of aluminium-free glasses generally based on existing bioactive compositions. The best performing cements showed good stability in water, with mass loss associated with the dissolution of sodium salts and partially reacted glass particles. On this matter, the presence of these particles released beneficial ions for cell function such as Si, Ca, P

and Sr. Conversely, the pH of the storage solutions was high due to sodium release, which was detrimental for cell viability during *in vitro* testing. A significant advantage of these bioactive glasses for cement applications is the flexibility in which their composition can be adjusted and studied through variation of the glass network connectivity, to aid their degradation and specific ion release during and after setting. In contrast, this was not evident for the commercially available cement Serenocem™, due to its low degradation in aqueous media after setting. Therefore, the present study provides evidence of a novel application of a series of bioactive glass compositions, with a comparative characterisation of the commercial cement Serenocem™. This study showed the advantages of the experimental cements when compared with the commercial product, and presented a promising alternative for the recently withdrawn Serenocem™ granules previously used in ENT applications.

8 Future work

The data presented in this research, showed that the SiO_2-Na_2O-CaO-SrO-P_2O_5 based cement formulations are a valuable alternative route for preparation of aluminium-free cements for applications in ENT (Ear, Nose, and Throat) as injectable pastes and/or pre-set grafts. Nonetheless, further development is required for these materials to be used at a clinical level. Therefore, the following future work is recommended:

- With the aim of these pastes to be used as injectable cements, the mixing process window should increase, and the setting times need to be within 10 and 20 minutes. Therefore, fundamental changes are required to achieve these values: decreasing the reactivity of the glasses, and its associated increase in mixing times could be obtained either by acid washing or by annealing; while a decrease in the setting time could also be achieved by studying the influence of a higher molecular weight PAA and $H_3PO_{4\ (sol)}$ concentration.

- It is recommended that the setting times are determined under controlled temperature at 37 °C and a humidity level close to that of its application; this however was outside the remit of this study and the results are believed to represent the trend associated with the material variations.

- Regarding the glass compositions, a future study investigating a bioactive glass with higher CaO and lower Na_2O content (e.g., 13-93 composition), could have a beneficial effect on the setting time, by maximising Ca^{2+} availability for crosslinking, and by reducing the release of alkaline ions (Na^{2+}) into the solution, which was shown to be detrimental for cell viability *in vitro*.

- Further research is required to evaluate ion release in other aqueous media such as simulated body fluid and Tris-Buffer, to assess how these pH and ionic concentrations affect the cement dissolution.

- Further research could be conducted to study the presence and evolution of compounds during the cement setting. It would be interesting to compare the functional groups observed by FTIR-ATR with SEM-EDX and XRD, to establish whether the initial compounds change over time (in dry and in aqueous media), to evaluate the nature of the phosphate based compounds detected by

FTIR-ATR, and to define if there is a pattern associated with their distribution on the cement matrix.

- A further study could assess the longer-term effect of the cements on cell viability, with quantification of osteoblastic differentiation markers such as alkaline phosphatase (ALP) and osteocalcin.

- A natural progression of this work is to study the mechanical properties of the optimised cements by compression testing and hardness, and compare their behaviour in dry and an aqueous media, with emphasis on associating these properties with changes on their chemical structure over time.

References

Alan, D. W. & Wilson, A. D. 1993. *Acid-base cements : their biomedical and industrial applications*, Cambridge, Cambridge : Cambridge University Press, 1993.

Alberts, B. 2008. *Molecular biology of the cell,* New York, Garland Science.

Aldrich, S. 2015. *Calcium phosphate Dibasic Product 21177* [Online]. Available: http://www.sigmaaldrich.com/catalog/product/sial/21177?lang=en&region=GB [Accessed Sept 16 2015].

Alhalawani, A., Curran, D., Pingguan-Murphy, B., Boyd, D. & Towler, M. 2013. A Novel Glass Polyalkenoate Cement for Fixation and Stabilisation of the Ribcage, Post Sternotomy Surgery: An ex-Vivo Study. *Journal of Functional Biomaterials,* 4**,** 329.

Aljabo, A., Xia, W., Liaqat, S., Khan, M. A., Knowles, J. C., Ashley, P. & Young, A. M. 2015. Conversion, shrinkage, water sorption, flexural strength and modulus of re-mineralizing dental composites. *Dental Materials,* 31**,** 1279-1289.

Andersson, Ö. H. 1992. Glass transition temperature of glasses in the SiO_2-Na_2O-CaO-P_2O5-Al_2O_3-B_2O_3 system. *Journal of Materials Science: Materials in Medicine,* 3**,** 326-328.

Andersson, Ö. H. & Kangasniemi, I. 1991. Calcium phosphate formation at the surface of bioactive glass in vitro. *Journal of Biomedical Materials Research,* 25**,** 1019-1030.

Andersson, Ö. H. & Karlsson, K. H. 1991. On the bioactivity of silicate glass. *Journal of Non-Crystalline Solids,* 129**,** 145-151.

Andersson, Ö. H., Liu, G., Karlsson, K. H., Niemi, L., Miettinen, J. & Juhanoja, J. 1990. In vivo behaviour of glasses in the SiO_2-Na_2O-CaO-P_2O_5-Al_2O_3-B_2O_3 system. *Journal of Materials Science: Materials in Medicine,* 1**,** 219-227.

Anstice, H. M. & Nicholson, J. W. 1992. Studies on the structure of light-cured Glass-ionomer cements. *Journal of Materials Science: Materials in Medicine,* 3**,** 447-451.

Arcos, D., Greenspan, D. C. & Vallet-Regí, M. 2003. A new quantitative method to evaluate the in vitro bioactivity of melt and sol-gel-derived silicate glasses. *Journal of Biomedical Materials Research Part A,* 65A**,** 344-351.

Arstila, H., Hupa, L., Karlsson, K. H. & Hupa, M. 2008. Influence of heat treatment on crystallization of bioactive glasses. *Journal of Non-Crystalline Solids,* 354**,** 722-728.

Astm 2013. ASTM D7348 - 13 Standard Test Methods for Loss on Ignition (LOI) of Solid Combustion Residues.

Astm 2015. Terminology of Glass and Glass Products ASTM C162 - 05. ASTM International.

Avramov, I., Zanotto, E. D. & Prado, M. O. 2003. Glass-forming ability versus stability of silicate glasses. II. Theoretical demonstration. *Journal of Non-Crystalline Solids,* 320**,** 9-20.

Bakry, A. S., Takahashi, H., Otsuki, M. & Tagami, J. 2013. The durability of phosphoric acid promoted bioglass–dentin interaction layer. *Dental Materials,* 29**,** 357-364.

Bayode, A. & Grumbridge, M. 2016. *Medical Device Alert SerenoCem Granules- risk of bone reabsorption around granules implanted in the middle ear* [Online]. UK: Medicines & Healthcare products Regulatory Agency. Available: https://www.gov.uk/drug-device-alerts/serenocem-granules-risk-of-bone-reabsorbtion-around-granules [Accessed 2016].

Becaria, A., Campbell, A. & Bondy, S. 2002. Aluminum as a toxicant. *Toxicology and Industrial Health,* 18**,** 309-320.

Bentz, D. P., Garboczi, E. J., Haecker, C. J. & Jensen, O. M. 1999. Effects of cement particle size distribution on performance properties of Portland cement-based materials. *Cement and Concrete Research,* 29**,** 1663-1671.

Bertolini, M. J., Zaghete, M. A., Gimenes, R., Padovani, G. C. & Cruz, C. a. S. 2009. Preparation and evaluation of an experimental luting glass ionomer cement to be used in dentistry. *Journal of Materials Science: Materials in Medicine,* 20**,** 1781-1785.

Boccaccini, A. R., Chen, Q., Lefebvre, L., Gremillard, L. & Chevalier, J. 2007. Sintering, crystallisation and biodegradation behaviour of Bioglass (R)-derived glass-ceramics. *Faraday Discussions,* 136**,** 27-44.

Bohner, M. 2000. Calcium orthophosphates in medicine: from ceramics to calcium phosphate cements. *Injury,* 31, Supplement 4**,** D37-D47.

Bohner, M. 2010. Resorbable biomaterials as bone graft substitutes. *Materials Today,* 13**,** 24-30.

Bonalive®. 2017. *BonAlive® product line The new era of bone regeneration* [Online]. Available: http://www.bonalive.com/products/ [Accessed 14-03-17 2017].

Bonassar, L. J. & Vacanti, C. A. 1998. Tissue engineering: The first decade and beyond. *Journal of Cellular Biochemistry,* 72**,** 297-303.

Bonnelye, E., Chabadel, A., Saltel, F. & Jurdic, P. 2008. Dual effect of strontium ranelate: Stimulation of osteoblast differentiation and inhibition of osteoclast formation and resorption in vitro. *Bone,* 42**,** 129-138.

Boyd, D., Clarkin, O. M., Wren, A. W. & Towler, M. R. 2008a. Zinc-based glass polyalkenoate cements with improved setting times and mechanical properties. *Acta Biomaterialia,* 4**,** 425-431.

Boyd, D., Towler, M., Watts, S., Hill, R., Wren, A. & Clarkin, O. 2008b. The role of Sr^{2+} on the structure and reactivity of SrO–CaO–ZnO–SiO_2 ionomer glasses. *Journal of Materials Science: Materials in Medicine,* 19**,** 953-957.

Boyd, D. & Towler, M. R. 2005. The processing, mechanical properties and bioactivity of zinc based glass ionomer cements. *J Mater Sci Mater Med,* 16**,** 843-50.

Boyd, D., Towler, M. R., Law, R. V. & Hill, R. G. 2006. An investigation into the structure and reactivity of calcium-zinc-silicate ionomer glasses using MAS-NMR spectroscopy. *Journal of Materials Science: Materials in Medicine,* 17**,** 397-402.

Bramall, N. Email correspondence. Sept 17, 2015. *RE: Sample Methodology.*

Brauer, D. S., Gentleman, E., Farrar, D. F., Stevens, M. M. & Hill, R. G. 2011a. Benefits and drawbacks of zinc in glass ionomer bone cements. *Biomedical Materials,* 6.

Brauer, D. S., Karpukhina, N., Kedia, G., Bhat, A., Law, R. V., Radecka, I. & Hill, R. G. 2012. Bactericidal strontium-releasing injectable bone cements based on bioactive glasses. *Journal of The Royal Society Interface*.

Brauer, D. S., Karpukhina, N., O'donnell, M. D., Law, R. V. & Hill, R. G. 2010. Fluoride-containing bioactive glasses: Effect of glass design and structure on degradation, pH and apatite formation in simulated body fluid. *Acta Biomaterialia,* 6**,** 3275-3282.

Brauer, D. S., Mneimne, M. & Hill, R. G. 2011b. Fluoride-containing bioactive glasses: Fluoride loss during melting and ion release in tris buffer solution. *Journal of Non-Crystalline Solids,* 357**,** 3328-3333.

Braunger, M. L., Escanhoela Jr, C. A., Fier, I., Walmsley, L. & Ziemath, E. C. 2012. Electrical conductivity of silicate glasses with tetravalent cations substituting Si. *Journal of Non-Crystalline Solids,* 358**,** 2855-2861.

Bretcanu, O., Chatzistavrou, X., Paraskevopoulos, K., Conradt, R., Thompson, I. & Boccaccini, A. R. 2009. Sintering and crystallisation of 45S5 Bioglass® powder. *Journal of the European Ceramic Society,* 29**,** 3299-3306.

Brie, J., Chartier, T., Chaput, C., Delage, C., Pradeau, B., Caire, F., Boncoeur, M.-P. & Moreau, J.-J. 2013. A new custom made bioceramic implant for the repair of large and complex craniofacial bone defects. *Journal of Cranio-Maxillofacial Surgery,* 41**,** 403-407.

Brook, I. M. & Hatton, P. V. 1998. Glass-ionomers: bioactive implant materials. *Biomaterials,* 19**,** 565-571.

Brown, W. E. & Chow, L. C. 1986. Combinations of sparingly soluble calcium phosphates in slurries and pastes as mineralizers and cements. Google Patents.

Bruckner, R., Tylkowski, M., Hupa, L. & Brauer, D. S. 2016. Controlling the ion release from mixed alkali bioactive glasses by varying modifier ionic radii and molar volume. *Journal of Materials Chemistry B,* 4**,** 3121-3134.

Buric, N., Jovanovic, G., Krasic, D. & Kesic, L. 2003. Investigation of the bone tissue response to glass-ionomer microimplants in the canine maxillary alveolar ridge. *J Oral Sci,* 45**,** 207-12.

Cao, W. & Hench, L. L. 1996. Bioactive materials. *Ceramics International,* 22**,** 493-507.

Carter, D. H., Sloan, P., Brook, I. M. & Hatton, P. V. 1997. Role of exchanged ions in the integration of ionomeric (glass polyalkenoate) bone substitutes. *Biomaterials,* 18**,** 459-466.

Cerruti, M., Greenspan, D. & Powers, K. 2005. Effect of pH and ionic strength on the reactivity of Bioglass 45S5. *Biomaterials,* 26**,** 1665-74.

Charnley, J. 1960. Anchorage of the femoral head prosthesis. *Journal of Bone and Joint Surgery,* 42B**,** 28-30.

Chatzistavrou, X., Zorba, T., Kontonasaki, E., Chrissafis, K., Koidis, P. & Paraskevopoulos, K. M. 2004. Following bioactive glass behavior beyond melting temperature by thermal and optical methods. *physica status solidi (a),* 201**,** 944-951.

Chen, Q. Z., Thompson, I. D. & Boccaccini, A. R. 2006. 45S5 Bioglass®-derived glass–ceramic scaffolds for bone tissue engineering. *Biomaterials,* 27**,** 2414-2425.

Chen, X., Brauer, D. S., Karpukhina, N., Waite, R. D., Barry, M., Mckay, I. J. & Hill, R. G. 2014. 'Smart' acid-degradable zinc-releasing silicate glasses. *Materials Letters,* 126**,** 278-280.

Clark, M. P. & Bottrill, I. 2007. SerenoCem -glass ionomeric granules: a 3-year follow-up assessment of their effectiveness in mastoid obliteration. *Clin Otolaryngol,* 32**,** 287-90.

Clupper, D. C. & Hench, L. L. 2003. Crystallization kinetics of tape cast bioactive glass 45S5. *Journal of Non-Crystalline Solids,* 318**,** 43-48.

Crisp, S., Lewis, B. G. & Wilson, A. D. 1980. Characterization of glass-ionomer cements. *Journal of Dentistry,* 8**,** 68-74.

Crisp, S., Pringuer, M. A., Wardleworth, D. & Wilson, A. D. 1974. Reactions in Glass Ionomer Cements: II. An Infrared Spectroscopic Study. *Journal of Dental Research,* 53**,** 1414-1419.

Crisp, S., Prosser, H. J. & Wilson, A. D. 1976. An infra-red spectroscopic study of cement formation between metal oxides and aqueous solutions of poly(acrylic acid). *Journal of Materials Science,* 11**,** 36-48.

Crisp, S. & Wilson, A. D. 1973. Formation of a glass-ionomer cement based on an ion-leachable glass and polyacrylic acid. *Journal of Applied Chemistry and Biotechnology,* 23**,** 811-815.

Crisp, S. & Wilson, A. D. 1974. Reactions in glass ionomer cements: I. Decomposition of the powder. *J Dent Res,* 53**,** 1408-13.

Czarnecka, B., Limanowska-Shaw, H. & Nicholson, J. W. 2002. Buffering and ion-release by a glass-ionomer cement under near-neutral and acidic conditions. *Biomaterials,* 23**,** 2783-2788.

D'onofrio, A., Kent, N. W., Shahdad, S. A. & Hill, R. G. 2016. Development of novel strontium containing bioactive glass based calcium phosphate cement. *Dent Mater,* 32**,** 703-12.

Davidson, C. L. 2006. Advances in glass-ionomer cements. *Journal of applied oral science : revista FOB,* 14 Suppl**,** 3-9.

Deb, S. & Nicholson, J. W. 1999. The effect of strontium oxide in glass–ionomer cements. *Journal of Materials Science: Materials in Medicine,* 10**,** 471-474.

Debenedetti, P. G. & Stillinger, F. H. 2001. Supercooled liquids and the glass transition. *Nature,* 410**,** 259-267.

Diba, M., Tapia, F., Boccaccini, A. R. & Strobel, L. A. 2012. Magnesium-Containing Bioactive Glasses for Biomedical Applications. *International Journal of Applied Glass Science,* 3**,** 221-253.

Dickey, B., Price, R. & Boyd, D. 2016. Evidence of a complex species controlling the setting reaction of glass ionomer cements. *Dental Materials,* 32**,** 596-605.

Dickey, B. T., Kehoe, S. & Boyd, D. 2013. Novel adaptations to zinc–silicate glass polyalkenoate cements: The unexpected influences of germanium based glasses on handling characteristics and mechanical properties. *Journal of the Mechanical Behavior of Biomedical Materials,* 23**,** 8-21.

El-Kady, A. M., Ali, A. F., Rizk, R. A. & Ahmed, M. M. 2012. Synthesis, characterization and microbiological response of silver doped bioactive glass nanoparticles. *Ceramics International,* 38**,** 177-188.

Elgayar, I., Aliev, A. E., Boccaccini, A. R. & Hill, R. G. 2005. Structural analysis of bioactive glasses. *Journal of Non-Crystalline Solids,* 351**,** 173-183.

Elmer, P. 2005. Technical note: FT-IR Spectroscopy Attenuated Total Reflectance (ATR). Available: http://www.utsc.utoronto.ca/~traceslab/ATR_FTIR.pdf [Accessed Sept 15 2015].

Engelbrecht, E., Von Foerster, G. & Delling, G. 2000. Ionogran in revision arthroplasty. *The Journal of bone and joint surgery. British volume,* 82**,** 192-199.

Fredholm, Y. C. 2011. *Development and characterisation of strontium-containing bioactive glasses and aluminium-free glass polyalkenoate cements.* Doctor of Philosophy, Imperial College London.

Fredholm, Y. C., Karpukhina, N., Brauer, D. S., Jones, J. R., Law, R. V. & Hill, R. G. 2012. Influence of strontium for calcium substitution in bioactive glasses on degradation, ion release and apatite formation. *Journal of the Royal Society Interface,* 9**,** 880-889.

Fredholm, Y. C., Karpukhina, N., Law, R. V. & Hill, R. G. 2010. Strontium containing bioactive glasses: Glass structure and physical properties. *Journal of Non-Crystalline Solids,* 356**,** 2546-2551.

Freeman, M., Bradley, G. & Revell, P. 1982. Observations upon the interface between bone and polymethylmethacrylate cement. *Journal of Bone & Joint Surgery, British Volume,* 64-B**,** 489-493.

Freshney, I. 1994. *Culture of animal cells A Manual of Basic Technique* [Online]. Wiley Subscription Services, Inc., A Wiley Company. Available: http://dx.doi.org/10.1002/mrd.1080390221 [Accessed 2 39].

Fuchs, M., Gentleman, E., Shahid, S., Hill, R. G. & Brauer, D. S. 2015. Therapeutic ion-releasing bioactive glass ionomer cements with improved mechanical strength and radiopacity. *Frontiers in Materials,* 2.

Ghasemi, A. & Zahediasl, S. 2012. *Normality Tests for Statistical Analysis: A Guide for Non-Statisticians*.

Ginebra, M. P., Espanol, M., Montufar, E. B., Perez, R. A. & Mestres, G. 2010. New processing approaches in calcium phosphate cements and their applications in regenerative medicine. *Acta Biomaterialia,* 6**,** 2863-2873.

Goehner, R. & Nichols, R. 1986. Metals Handbook. *ASM Metals Handbook.* Ninth Edition ed.

Gomes, F. O., Pires, R. A. & Reis, R. L. 2013. Aluminum-free glass-ionomer bone cements with enhanced bioactivity and biodegradability. *Materials Science and Engineering: C,* 33**,** 1361-1370.

Griffin, S. & Hill, R. 1998. Influence of poly(acrylic acid) molar mass on the fracture properties of glass polyalkenoate cements. *Journal of Materials Science,* 33**,** 5383-5396.

Griffin, S. G. & Hill, R. G. 1999. Influence of glass composition on the properties of glass polyalkenoate cements. Part I: influence of aluminium to silicon ratio. *Biomaterials,* 20**,** 1579-1586.

Groh, D., Döhler, F. & Brauer, D. S. 2014. Bioactive glasses with improved processing. Part 1. Thermal properties, ion release and apatite formation. *Acta Biomaterialia,* 10**,** 4465-4473.

Guggenberger, R., May, R. & Stefan, K. P. 1998. New trends in glass-ionomer chemistry. *Biomaterials,* 19**,** 479-83.

Guida, A., Hill, R. G., Towler, M. R. & Eramo, S. 2002. Fluoride release from model glass ionomer cements. *Journal of Materials Science: Materials in Medicine,* 13**,** 645-649.

Harmand, M. 1997. Cytotoxicity. *In:* BRAYBROOK, J. (ed.) *Biocompatibility and assessment of medical devices and materials.* Wiley.

Harrison, L., Kumar, S., Bull, M., Hatton, P. V., Bottrill, I. & Aldren, C. 2017. Clinical case series describes a contraindication for SerenoCem Granules™ in mastoid obliteration: Our experience in sixty-four patients. *Clinical Otolaryngology***,** n/a-n/a.

Hatton, P. V. & Brook, I. M. 1992. Characterisation of the ultrastructure of glass-ionomer (poly-alkenoate) cement. *Br Dent J,* 173**,** 275-277.

Hench, L. L. 1991. Bioceramics - from Concept to Clinic. *Journal of the American Ceramic Society,* 74**,** 1487-1510.

Hench, L. L. 2005. 1 - Introduction. *Biomaterials, Artificial Organs and Tissue Engineering.* Woodhead Publishing.

Hench, L. L. 2006. The story of Bioglass (R). *Journal of Materials Science-Materials in Medicine,* 17**,** 967-978.

Hench, L. L. 2009. Genetic design of bioactive glass. *Journal of the European Ceramic Society,* 29**,** 1257-1265.

Hench, L. L. 2013. Chronology of bioactive glass development and clinical applications.

Hench, L. L. & Jones, J. R. (eds.) 2005. *Biomaterials, artificial organs and tissue engineering*: Woodhead Publishing in Materials.

Hench, L. L., Splinter, R. J., Allen, W. C. & Greenlee, T. K. 1971. Bonding mechanisms at the interface of ceramic prosthetic materials. *Journal of Biomedical Materials Research,* 5**,** 117-141.

Hench, L. L., Xynos, I. D. & Polak, J. M. 2004. Bioactive glasses for in situ tissue regeneration. *Journal of Biomaterials Science, Polymer Edition,* 15**,** 543-562.

Hill, R. 1996. An alternative view of the degradation of bioglass. *Journal of Materials Science Letters,* 15**,** 1122-1125.

Hill, R., Rawlinson, S., Davis, G., Nehete, S. & Shahdad, S. 2014. A clinical case study: Using a strontium substituted bioactive glass-- StronBone®-- to fill alveolar sockets. *Eur Cells Mater,* 28**,** 51.

Hill, R. G. & Brauer, D. S. 2011. Predicting the bioactivity of glasses using the network connectivity or split network models. *Journal of Non-Crystalline Solids,* 357**,** 3884-3887.

Hill, R. G. & Labok, S. A. 1991. The influence of polyacrylic acid molecular weight on the fracture of zinc polycarboxylate cements. *Journal of Materials Science,* 26**,** 67-74.

Hill, R. G. & Stevens, M. M. 2009. Bioactive Glass. Google Patents.

Hofmann, M. P., Young, A. M., Gbureck, U., Nazhat, S. N. & Barralet, J. E. 2006. FTIR-monitoring of a fast setting brushite bone cement: effect of intermediate phases. *Journal of Materials Chemistry,* 16**,** 3199-3206.

Hurrell-Gillingham, Reaney, I. M., Brook, I. M. & Hatton, P. V. 2005. Novel Fe_2O_3-Containing Glass Ionomer Cements: Glass Characterisation. *Key Engineering Materials,* 284-286**,** 799-802.

Hurrell-Gillingham, K., Reaney, I. M., Brook, I. & Hatton, P. V. 2006. *In vitro* biocompatibility of a novel Fe_2O_3 based glass ionomer cement. *Journal of Dentistry,* 34**,** 533-538.

Hurrell-Gillingham, K., Reaney, I. M., Miller, C. A., Crawford, A. & Hatton, P. V. 2003. Devitrification of ionomer glass and its effect on the in vitro biocompatibility of glass-ionomer cements. *Biomaterials,* 24**,** 3153-3160.

Iso 2007. Dentistry Water Based Cements Part 1: Powder/liquid acid based cements ISO 9917-1. *ISO 9917-1*.

Jones, J. R., Brauer, D. S., Hupa, L. & Greenspan, D. C. 2016. Bioglass and Bioactive Glasses and Their Impact on Healthcare. *International Journal of Applied Glass Science,* 7**,** 423-434.

Jones, J. R. & Clare, A. 2012. *Bio-Glasses An Introduction*, Wiley.

Jones, J. R. & Hench, L. L. 2001. Biomedical materials for new millennium: perspective on the future. *Materials Science and Technology,* 17**,** 891-900.

Jones, J. R., Sepulveda, P. & Hench, L. L. 2001. Dose-dependent behavior of bioactive glass dissolution. *Journal of Biomedical Materials Research*, 58**,** 720-726.

Joon Bu, P. & Park, J. B. 2007. *Biomaterials : an introduction*, New York, N.Y., New York, N.Y. : Springer, c2007.

Kenny, S. M. & Buggy, M. 2003. Bone cements and fillers: A review. *Journal of Materials Science: Materials in Medicine,* 14**,** 923-938.

Kerner, R. & Phillips, J. C. 2000. Quantitative principles of silicate glass chemistry. *Solid State Communications,* 117**,** 47-51.

Khashaba, R. M., Moussa, M. M., Mettenburg, D. J., Rueggeberg, F. A., Chutkan, N. B. & Borke, J. L. 2010. Polymeric-Calcium Phosphate Cement Composites-Material Properties: In Vitro and In Vivo Investigations. *International Journal of Biomaterials,* 2010.

Kim, I., Ohtsuki, C., Coughlan, A., Placek, L., Wren, A. & Towler, M. 2013. Characteristics of glass ionomer cements composed of glass powders in CaO–SrO–ZnO–SiO_2 system prepared by two different synthetic routes. *Journal of Materials Science: Materials in Medicine,* 24**,** 2677-2682.

Kim, S. B., Kim, Y. J., Yoon, T. L., Park, S. A., Cho, I. H., Kim, E. J., Kim, I. A. & Shin, J.-W. 2004. The characteristics of a hydroxyapatite–chitosan–PMMA bone cement. *Biomaterials,* 25**,** 5715-5723.

Kuhn, A. T. & Wilson, A. D. 1985. The dissolution mechanisms of silicate and glass-ionomer dental cements. *Biomaterials,* 6**,** 378-382.

Kupperman, D. & Tange, R. A. 2001. Ionomeric Cement in the Human Middle Ear Cavity: Long-Term Results of 23 Cases. *The Laryngoscope,* 111**,** 306-309.

Kusumoto, H., Abolghasemi, S., Woodfine, B., Hill, R. G., Karpukhina, N. & Law, R. V. 2016. The effect of phosphate, fluorine, and soda content of the glass on the mechanical properties of the glass ionomer (polyalkenoate) cements. *Journal of Non-Crystalline Solids,* 449**,** 94-99.

Lakhkar, N. J., Lee, I.-H., Kim, H.-W., Salih, V., Wall, I. B. & Knowles, J. C. 2013. Bone formation controlled by biologically relevant inorganic ions: Role and controlled delivery from phosphate-based glasses. *Advanced Drug Delivery Reviews,* 65**,** 405-420.

Leung, D., Spratt, D. A., Pratten, J., Gulabivala, K., Mordan, N. J. & Young, A. M. 2005. Chlorhexidine-releasing methacrylate dental composite materials. *Biomaterials,* 26**,** 7145-7153.

Li, C. D., Mason, J. & Yakimicki, D. 2004. Thermal characterization of PMMA-based bone cement curing. *Journal of Materials Science-Materials in Medicine,* 15**,** 85-89.

Malluche, H. H. 2002. Aluminium and bone disease in chronic renal failure. *Nephrology Dialysis Transplantation,* 17**,** 21-24.

Martin, E. & Hine, R. 2008. Oxford Dictionary of Biology. *In:* HINE, R. (ed.) *Oxford Dictionary of Biology.* Sixth ed. Oxford, London: OXFORD University Press.

Martin, R. B. 2007. Aluminium Speciation in Biology. *Ciba Foundation Symposium 169 - Aluminium in Biology and Medicine.* John Wiley & Sons, Ltd.

Massera, J., Fagerlund, S., Hupa, L. & Hupa, M. 2012a. Crystallization Mechanism of the Bioactive Glasses, 45S5 and S53P4. *Journal of the American Ceramic Society,* 95**,** 607-613.

Massera, J. & Hupa, L. 2013. Influence of SrO substitution for CaO on the properties of bioactive glass S53P4. *Journal of Materials Science: Materials in Medicine,* 25**,** 657-668.

Massera, J., Hupa, L. & Hupa, M. 2012b. Influence of the partial substitution of CaO with MgO on the thermal properties and in vitro reactivity of the bioactive glass S53P4. *Journal of Non-Crystalline Solids,* 358**,** 2701-2707.

Matsuya, S., Maeda, T. & Ohta, M. 1996. IR and NMR Analyses of Hardening and Maturation of Glass-ionomer Cement. *Journal of Dental Research,* 75**,** 1920-1927.

Matsuya, S., Matsuya, Y. & Ohta, M. 1999. Structure of Bioactive Glass and its Application to Glass Ionomer Cement. *Dental Materials Journal,* 18**,** 155-166.

Mehdawi, I., Neel, E. a. A., Valappil, S. P., Palmer, G., Salih, V., Pratten, J., Spratt, D. A. & Young, A. M. 2009. Development of remineralizing, antibacterial dental materials. *Acta Biomaterialia,* 5**,** 2525-2539.

Milne , K. A., Calos , N. J., O'donnell , J. H., Kennard , C. H. L., Vega , S. & Marks , D. 1997. Glass-ionomer dental restorative: Part I: a structural study. *Journal of Materials Science: Materials in Medicine,* 8**,** 349-356.

Miller, C., Hatton, P. V. & Mirvakily, F. 2014. A novel glass-ionomer cement. United Kingdom patent application PCT/GB2013/053386.

Mirvakily, F. 2009. *Development of regenerative therapies for periodontal bone loss.* PhD in Dentistry, The University of Sheffield.

Mirvakily, F. 2010. Fabrication of novel bioglass cement: Modification of setting characteristics. *Internal Report.* Sheffield: The University of Sheffield.

Mneimne, M., Hill, R. G., Bushby, A. J. & Brauer, D. S. 2011. High phosphate content significantly increases apatite formation of fluoride-containing bioactive glasses. *Acta Biomaterialia,* 7**,** 1827-1834.

Mulari, M. T. K., Qu, Q., Härkönen, P. L. & Väänänen, H. K. 2004. Osteoblast-like Cells Complete Osteoclastic Bone Resorption and Form New Mineralized Bone Matrix In Vitro. *Calcified Tissue International,* 75**,** 253-261.

Murphy, S., Boyd, D., Moane, S. & Bennett, M. 2009. The effect of composition on ion release from Ca–Sr–Na–Zn–Si glass bone grafts. *Journal of Materials Science: Materials in Medicine,* 20**,** 2207.

Nicholson, J. W. 1998a. Chemistry of glass-ionomer cements: a review. *Biomaterials,* 19**,** 485-494.

Nicholson, J. W. 1998b. Glass-ionomers in medicine and dentistry. *Proceedings Of The InstitutionOF Mechanical Engineers Part H-Journal Of Engineering In Medicine,* 212**,** 121-126.

Nicholson, J. W. & Amiri, M. A. 1998. The interaction of dental cements with aqueous solutions of varying pH. *Journal of Materials Science: Materials in Medicine,* 9**,** 549-554.

Nicholson, J. W., Braybrook, J. H. & Wasson, E. A. 1991. The biocompatibility of glass-poly(alkenoate) (Glass-Ionomer) cements: A review. *Journal of Biomaterials Science, Polymer Edition,* 2**,** 277-285.

Nicholson, J. W., Czarnecka, B. & Limanowska-Shaw, H. 1999. The long-term interaction of dental cements with lactic acid solutions. *Journal of Materials Science: Materials in Medicine,* 10**,** 449-452.

Nih. 2014. *Strontium Carbonate: PubChem Compound Database; CID=15407* [Online]. NIH. Available: https://pubchem.ncbi.nlm.nih.gov/compound/15407 [Accessed Sept. 16, 2015 2015].

O'brien, J., Wilson, I., Orton, T. & Pognan, F. 2000. Investigation of the Alamar Blue (resazurin) fluorescent dye for the assessment of mammalian cell cytotoxicity. *Eur J Biochem,* 267**,** 5421-6.

O'donnell, M. D. 2012. Melt-Derived Bioactive Glass. *Bio-Glasses.* John Wiley & Sons, Ltd.

O'donnell, M. D., Candarlioglu, P. L., Miller, C. A., Gentleman, E. & Stevens, M. M. 2010. Materials characterisation and cytotoxic assessment of strontium-substituted bioactive glasses for bone regeneration. *Journal of Materials Chemistry,* 20**,** 8934-8941.

O'donnell, M. D., Watts, S. J., Hill, R. G. & Law, R. V. 2009. The effect of phosphate content on the bioactivity of soda-lime-phosphosilicate glasses. *Journal of Materials Science-Materials in Medicine,* 20**,** 1611-1618.

O'donnell, M. D. 2011. Predicting bioactive glass properties from the molecular chemical composition: Glass transition temperature. *Acta Biomaterialia,* 7**,** 2264-2269.

O'donnell, M. D. & Hill, R. G. 2010. Influence of strontium and the importance of glass chemistry and structure when designing bioactive glasses for bone regeneration. *Acta Biomaterialia,* 6**,** 2382-2385.

O'donnell, M. D., Watts, S. J., Law, R. V. & Hill, R. G. 2008. Effect of P2O5 content in two series of soda lime phosphosilicate glasses on structure and properties – Part I: NMR. *Journal of Non-Crystalline Solids,* 354**,** 3554-3560.

Oonishi, H., Hench, L., Wilson, J., Sugihara, F., Tsuji, E., Matsuura, M., Kin, S., Yamamoto, T. & Mizokawa, S. 2000. Quantitative comparison of bone growth behavior in granules of Bioglass, A-W glass-ceramic, and hydroxyapatite. *Journal of biomedical materials research,* 51**,** 37-46.

Pantano, C. G., Clark, A. E. & Hench, L. L. 1974. Multilayer Corrosion Films on Bioglass Surfaces. *Journal of the American Ceramic Society,* 57**,** 412-413.

Paul, A. 1990. *Chemistry of glasses,* London, London : Chapman and Hall, 1990.

Peitl, O., Dutra Zanotto, E. & Hench, L. L. 2001. Highly bioactive P_2O_5–Na_2O–CaO–SiO_2 glass-ceramics. *Journal of Non-Crystalline Solids,* 292**,** 115-126.

Peltola, M., Aitasalo, K., Suonpaa, J., Varpula, M. & Yli-Urpo, A. 2006. Bioactive glass S53P4 in frontal sinus obliteration: A long-term clinical experience. *Head and Neck-Journal for the Sciences and Specialties of the Head and Neck,* 28**,** 834-841.

Philips. 2011. *X-Ray Fluoresce Spectroscopy (XRF) Fast and precise inorganic solid analysis* [Online]. Available: http://www.innovationservices.philips.com/sites/default/files/materials-analysis-xrf.pdf

Plewinski, M., Schickle, K., Lindner, M., Kirsten, A., Weber, M. & Fischer, H. 2013. The effect of crystallization of bioactive bioglass 45S5 on apatite formation and degradation. *Dental Materials,* 29**,** 1256-1264.

Prentice, L. H., Tyas, M. J. & Burrow, M. F. 2005. The effect of particle size distribution on an experimental glass-ionomer cement. *Dental Materials,* 21**,** 505-510.

Ratner, B., Hoffman, F., Schoen, F. & Lemons, J. 2004. *Biomaterials Science: An Introduction to Materials in Medicine*.

Ratner, B. 1993. Chapter 8 Characterization of Biomaterial Surfaces. Cardiovascular Pathology, 2, 87S-100S.

Rawson, H. 1991. *Glasses and their applications,* London, The Institute of Metals.

Revell, P. A., Braden, M. & Freeman, M. a. R. 1998. Review of the biological response to a novel bone cement containing poly(ethyl methacrylate) and n-butyl methacrylate. *Biomaterials,* 19**,** 1579-1586.

Righini-Grunder, F., Häusler, R., Chongvisal, S. & Caversaccio, M. 2015. Glass ionomer cement in otological microsurgery: experience over 16 years. *European Archives of Oto-Rhino-Laryngology,* 272**,** 2749-2754.

Rohanová, D., Boccaccini, A. R., Yunos, D. M., Horkavcová, D., Březovská, I. & Helebrant, A. 2011. TRIS buffer in simulated body fluid distorts the assessment of glass–ceramic scaffold bioactivity. *Acta Biomaterialia,* 7**,** 2623-2630.

Salih, V. & Thomas, D. 2013. 1 - Fundamentals of cell and matrix biology for tissue engineering. *Standardisation in Cell and Tissue Engineering.* Woodhead Publishing.

Salonen, J., Argasmaa, M., Tuominen, U., Behbehani, M. & Zaatar, E. 2009. Bioactive glass in dentistry. *J. Minim Inter Dent,* 2**,** 209-219.

Santocildes-Romero, M. E., Crawford, A., Hatton, P. V., Goodchild, R. L., Reaney, I. M. & Miller, C. A. 2015. The osteogenic response of mesenchymal stromal cells to strontium-substituted bioactive glasses. *Journal of Tissue Engineering and Regenerative Medicine,* 9**,** 619-631.

Schweiger, M. J., Hrma, P., Humrickhouse, C. J., Marcial, J., Riley, B. J. & Tegrotenhuis, N. E. 2010. Cluster formation of silica particles in glass batches during melting. *Journal of Non-Crystalline Solids,* 356**,** 1359-1367.

Sepulveda, P., Jones, J. R. & Hench, L. L. 2001. Characterization of melt-derived 45S5 and sol-gel–derived 58S bioactive glasses. *Journal of Biomedical Materials Research,* 58**,** 734-740.

Sepulveda, P., Jones, J. R. & Hench, L. L. 2002. In vitro dissolution of melt-derived 45S5 and sol-gel derived 58S bioactive glasses. *Journal of Biomedical Materials Research,* 61**,** 301-311.

Serotec, A. 2014. *What is alamarBlue* [Online]. Available: http://www.abdserotec.com/alamarblue-cell-viability-assay-resazurin.html [Accessed 31-10-14].

Serra, J., González, P., Liste, S., Chiussi, S., León, B., Pérez-Amor, M., Ylänen, H. O. & Hupa, M. 2002. Influence of the non-bridging oxygen groups on the bioactivity of silicate glasses. *Journal of Materials Science: Materials in Medicine,* 13**,** 1221-1225.

Serra, J., González, P., Liste, S., Serra, C., Chiussi, S., León, B., Pérez-Amor, M., Ylänen, H. O. & Hupa, M. 2003. FTIR and XPS studies of bioactive silica based glasses. *Journal of Non-Crystalline Solids,* 332**,** 20-27.

Shelby, J. E. 1997. *Introduction to glass science and technology*, Cambridge, Cambridge : Royal Society of Chemistry, 1997.

Shelby, J. E. 2005. *Introduction to glass science and technology*, Cambridge, Cambridge : Royal Society of Chemistry, c2005.

Shen, L., Coughlan, A., Towler, M. & Hall, M. 2014. Degradable borate glass polyalkenoate cements. *Journal of Materials Science: Materials in Medicine,* 25**,** 965-973.

Shi, Q. H., Wang, J. F., Zhang, J. P., Fan, J. & Stucky, G. D. 2006. Rapid-Setting, Mesoporous, Bioactive Glass Cements that Induce Accelerated *In Vitro* Apatite Formation. *Advanced Materials,* 18**,** 1038-1042.

Smith, D. C. 1998. Development of glass-ionomer cement systems. *Biomaterials,* 19**,** 467-478.

Sriranganathan, D., Kanwal, N., Hing, K. A. & Hill, R. G. 2015. Strontium substituted bioactive glasses for tissue engineered scaffolds: the importance of octacalcium phosphate. *Journal of Materials Science: Materials in Medicine,* 27**,** 39.

Stanley, H. R., Hench, L., Going, R., Bennett, C., Chellemi, S. J., King, C., Ingersoll, N., Ethridge, E. & Kreutziger, K. 1976. The implantation of natural tooth form bioglasses in baboons. *Oral Surgery, Oral Medicine, Oral Pathology,* 42**,** 339-356.

Temenoff, J. S. & Mikos, A. G. 2008. *Biomaterials : the intersection of biology and materials science,* Upper Saddle River, N.J. ; London, Pearson Prentice Hall.

Tilocca, A. 2010. Models of structure, dynamics and reactivity of bioglasses: a review. *Journal of Materials Chemistry,* 20**,** 6848-6858.

Tilocca, A. & Cormack, A. N. 2007. Structural Effects of Phosphorus Inclusion in Bioactive Silicate Glasses. *The Journal of Physical Chemistry B,* 111**,** 14256-14264.

Tortora, G. J. & Derrickson, B. 2010. *Essentials of anatomy and physiology,* Hoboken, N.J., Wiley.

Towler, M. R., Crowley, C. M., Murphy, D. & O'callaghan, A. M. C. 2002. A preliminary study of an aluminum-free glass polyalkenoate cement. *Journal of Materials Science Letters,* 21**,** 1123-1126.

Tysome, J. R. & Harcourt, J. 2005. How we do it: ionomeric cement to attach the stapes prosthesis to the long process of the incus. *Clinical Otolaryngology,* 30**,** 458-460.

Uhlmann, D. R. 1972. A kinetic treatment of glass formation. *Journal of Non-Crystalline Solids,* 7**,** 337-348.

Valliant, E. M., Dickey, B. T., Price, R., Boyd, D. & Filiaggi, M. J. 2016. Fourier transform infrared spectroscopy as a tool to study the setting reaction in glass-ionomer cements. *Materials Letters,* 185**,** 256-259.

Van Der Stok, J., Weinans, H., Kops, N., Siebelt, M., Patka, P. & Van Lieshout, E. M. M. 2013. Properties of commonly used calcium phosphate cements in trauma and orthopaedic surgery. *Injury,* 44**,** 1368-1374.

Van Noort, R. 2013. *Introduction to dental materials,* Edinburgh ; New York, Edinburgh ; New York : Mosby Elsevier, 2013.

Varshneya, A. K. 2006. *Fundamentals of inorganic glasses,* Sheffield, Sheffield : Society of Glass Technology, 2006.

Varshneya, A. K. September, 4th 2016 2016. *RE: Unique Short Course in Glass Technology.*

Wallace, K. E., Hill, R. G., Pembroke, J. T., Brown, C. J. & Hatton, P. V. 1999. Influence of sodium oxide content on bioactive glass properties. *Journal of Materials Science: Materials in Medicine,* 10**,** 697-701.

Wang, J. S. & Dunne, N. 2008. 10 - Bone cement fixation: acrylic cements. *In:* REVELL, P. A. (ed.) *Joint Replacement Technology.* Woodhead Publishing.

Warren, B. E. & Biscce, J. 1938. The structure of silica glass by X-Ray difraction studies. *Journal of the American Ceramic Society,* 21**,** 49-54.

Wasson, E. A. & Nicholson, J. W. 1991. Studies on the setting chemistry of glass-ionomer cements. *Clinical Materials,* 7**,** 289-293.

Wasson, E. A. & Nicholson, J. W. 1993. New Aspects of the Setting of Glass-ionomer Cements. *Journal of Dental Research,* 72**,** 481-483.

West, A. R. 1996. *Basic Solid State Chemistry*, John Wiley and Sons, Ltd.

West, A. R. 2014. *Solid state chemistry and its applications [electronic resource]*, Chichester, West Sussex : John Wiley & Sons, Inc., 2014.

Williams, D. F. 2009. On the nature of biomaterials. *Biomaterials,* 30**,** 5897-5909.

Williams, R. J. P. 2007. Aluminium in Biology: An Introduction. *Ciba Foundation Symposium 169 - Aluminium in Biology and Medicine.* John Wiley & Sons, Ltd.

Wilson, A. & Mclean, J. 1988. *Glass ionomer cement*, Quintessence Publishing Co.

Wilson, A. D. 1978. The chemistry of dental cements. *Chemical Society Reviews,* 7**,** 265-296.

Wilson, A. D. 1996. A Hard Decade's Work: Steps in the Invention of the Glass-ionomer Cement. *Journal of Dental Research,* 75**,** 1723-1727.

Wilson, A. D., Crisp, S. & Abel, G. 1977. Characterization of glass-ionomer cements 4. Effect of molecular weight on physical properties. *Journal of Dentistry,* 5**,** 117-120.

Wilson, A. D., Crisp, S., Prosser, H. J., Lewis, B. G. & Merson, S. A. 1980. Aluminosilicate Glasses for Polyelectrolyte Cements. *Industrial & Engineering Chemistry Product Research and Development,* 19**,** 263-270.

Wilson, A. D., Kent, B. E., Clinton, D. & Miller, R. P. 1972. The formation and microstructure of dental silicate cements. *Journal of Materials Science,* 7**,** 220-238.

Wren, A. W., Coughlan, A., Placek, L. & Towler, M. R. 2012. Gallium containing glass polyalkenoate anti-cancerous bone cements: glass characterization and physical properties. *Journal of Materials Science: Materials in Medicine,* 23**,** 1823-1833.

Wren, A. W., Hansen, J. P., Hayakawa, S. & Towler, M. R. 2013. Aluminium-free glass polyalkenoate cements: ion release and in vitro antibacterial efficacy. *Journal of Materials Science-Materials in Medicine,* 24**,** 1167-1178.

Wren, A. W., Kidari, A., Cummins, N. M. & Towler, M. R. 2010. A spectroscopic investigation into the setting and mechanical properties of titanium containing glass polyalkenoate cements. *Journal of Materials Science: Materials in Medicine,* 21**,** 2355-2364.

Wright, A. C., Connell, G. a. N. & Allen, J. W. 1980. Amorphography and the modelling of amorphous solid structures by geometric transformations. *Journal of Non-Crystalline Solids,* 42**,** 69-86.

Wu, Z. Y., Hill, R. G., Yue, S., Nightingale, D., Lee, P. D. & Jones, J. R. 2011. Melt-derived bioactive glass scaffolds produced by a gel-cast foaming technique. *Acta Biomaterialia,* 7**,** 1807-1816.

Xynos, I. D., Hukkanen, M. V. J., Batten, J. J., Buttery, L. D., Hench, L. L. & Polak, J. M. 2000. Bioglass ®45S5 Stimulates Osteoblast Turnover and Enhances Bone Formation In Vitro: Implications and Applications for Bone Tissue Engineering. *Calcified Tissue International,* 67**,** 321-329.

Yli-Urpo, H., Lassila, L. V. J., Närhi, T. & Vallittu, P. K. 2005. Compressive strength and surface characterization of glass ionomer cements modified by particles of bioactive glass. *Dental Materials,* 21**,** 201-209.

Yoshihara, S., Kokubo, T., Nishimura, N., Yamamuro, T. & Nakamura, T. 1994. Effects of glass composition on compressive strength of bioactive cement based on CaO-SiO_2-P_2O_5 glass powders. *Journal of Materials Science: Materials in Medicine,* 5**,** 123-129.

Young, A. M. 2002. FTIR investigation of polymerisation and polyacid neutralisation kinetics in resin-modified glass-ionomer dental cements. *Biomaterials,* 23**,** 3289-3295.

Young, A. M. & Ho, S. M. 2008. Drug release from injectable biodegradable polymeric adhesives for bone repair. *Journal of Controlled Release,* 127**,** 162-172.

Young, A. M., Ng, P. Y. J., Gbureck, U., Nazhat, S. N., Barralet, J. E. & Hofmann, M. P. 2008. Characterization of chlorhexidine-releasing, fast-setting, brushite bone cements. *Acta Biomaterialia,* 4**,** 1081-1088.

Young, A. M., Rafeeka, S. A. & Howlett, J. A. 2004. FTIR investigation of monomer polymerisation and polyacid neutralisation kinetics and mechanisms in various aesthetic dental restorative materials. *Biomaterials,* 25**,** 823-33.

Zachariasen, W. H. 1932. The Atomic Arrangement in Glass. *Journal of American Chemical Society,* 54**,** 3481-3851.

Zarzycki, J. 1991. *Glasses and the vitreous state,* Cambridge, Cambridge : Cambridge University Press, 1991.

Zhang, D., Leppäranta, O., Munukka, E., Ylänen, H., Viljanen, M. K., Eerola, E., Hupa, M. & Hupa, L. 2010. Antibacterial effects and dissolution behavior of six bioactive glasses. *Journal of Biomedical Materials Research Part A,* 93A**,** 475-483.

9 Appendix

Batch calculations

The batch calculations were based on the chemical reactions shown in Table 2-3, and the required CaO for each composition was calculated from two sources: $CaHPO_4$ and $CaCO_3$. Quantities are expressed in grams (g) required to obtain a theoretical batch of 100 g of glass

Glass composition	SiO_2	Na_2CO_3	$CaCO_3$	$CaHPO_4$	$SrCO_3$	Total batch weight	CaO from $CaHPO_4$	CaO from $CaCO_3$
35P6	35.0	51.3	43.3	11.5	0.0	141.1	4.7	24.3
42P6	42.0	46.2	36.2	11.5	0.0	135.8	4.7	20.3
45S5	45.0	41.9	35.3	11.5	0.0	133.7	4.7	19.8
45S5Sr10	44.0	41.2	30.2	11.3	6.3	133.0	4.7	16.9
49P3	50.7	38.6	37.7	5.9	0.0	133.0	2.4	21.2
49P6	49.0	37.6	32.6	11.5	0.0	130.7	4.7	18.3
49P9	46.4	35.4	22.6	21.7	0.0	126.1	8.9	12.7
53P4	53.0	39.3	30.1	7.7	0.0	130.1	3.2	16.8
58P6	58.0	41.0	13.0	11.5	0.0	123.5	4.7	7.3

Conference Proceeding

Injectable bone graft substitutes & cements based on bioactive glass ionomer chemistry. Hatton P, Brook I, **Contreras A**, Mirvakily F, Moorehead R, Ryabenkova Y, Rawlinson A, Crawford A, Freeman C & Miller C (2014). Journal of Tissue Engineering and Regenerative Medicine, 8, 26-27.

Presentations

Poster presentation Society of Glass Technology Centenary Conference. Sheffield, UK. 2016.

Oral presentation UK Society of Biomaterials (UKSB). Belfast, UK. 2015.

Poster presentation Regener8 Annual Conference. Leeds, UK. 2014.

Poster presentation International Association for Dental Research Conference (IADR). Dubrovnik, Croatia. 2014.

Poster presentation European Society for Biomaterials Conference (ESB). Liverpool, UK.2014.

Injectable Bone Graft Substitutes & Cements Based on Bioactive Glass-Ionomer Chemistry

Paul V. Hatton*, Ian Brook, Altair Contreras, Felora Mirvakily, Robert Moorehead, Yulia Ryabenkova, Andrew Rawlinson, Aileen Crawford, Christine Freeman, Ian M. Reaney, and Cheryl Miller
*Corresponding author: paul.hatton@sheffield.ac.uk
Bioengineering & Health Technologies Research Group, School of Clinical Dentistry, University of Sheffield, UK

Introduction

Glass-ionomer cements (GICs) have been in dentistry for over 40 years, and they were later adopted for use as bone cements and graft substitutes where they have been employed successfully in ENT surgery. They have though been restricted to use in a narrow range of procedures due to the release of aluminium ions that interfere with the mineralisation of new bone tissue[1]. There have therefore been reports of replacement of alumina in the parent glasses with other metal oxides including iron, zinc and magnesium to form cements that could be used in a wider range of clinical applications. The aim of this research was to review progress in the field of glass-ionomer bone cement development, focussing in particular on novel cements formed using bioactive glass compositions.

Materials and Methods

Bioactive glass compositions were prepared by the melt route to obtain final compositions that included 45S5 and 53P4. The amorphous nature of the glasses was demonstrated using X-ray diffraction (XRD), with post-melt compositions analysed using X-ray fluorescence (XRF). Experimental glasses were milled and sieved to obtain particles with a maximum size of 45 μm. Cements were prepared by mixing with poly (acrylic acid) (PAA) and distilled water or aqueous solutions of phosphoric acid (50/50 v/v). Two PAAs were used to form cements, one with a mean molecular weight of 45,000 (First Scientific GmbH) or another with a mean molecular weight of 52,000 (Advanced Healthcare Ltd.). Working and setting times were determined by Gillmore needle and rheometer. Aqueous stability was investigated using cement discs (5 mm x 1 mm) stored in distilled water at 37 °C. Preliminary studies of cement setting chemistry were undertaken using Fourier transform infrared spectroscopy (FT-IT). *In vitro* biocompatibility of specific cements was investigated using cultured bone cells, while in vivo bone response was evaluated using a healing defect (1 mm) in the midshaft of the rat femur. The glass compositions and cements reported here formed the basis of a new patent application[2].

Results

Bioactive glasses were produced with no crystalline phases detected by XRD. Bioactive glass powders were capable of forming a stable cement with poly (acrylic acid) from the two suppliers, and the use of a phosphoric acid solution accelerated the setting reaction and improved the stability of the cement in water. All cements reported here were stable in distilled water at 37 °C for at least six months. Cell culture studies showed a reduction in the metabolic activity of bone cells cultured in the presence of cements formed using 45S5 bioactive glass when compared to a Thermanox® control material, but cells remained viable for up to 21 days in the presence of cement. *In vivo* investigation demonstrated the formation of a direct bone-implant interface after only 4 weeks (Figure 1), showing that osseointegration had occurred with no mineral defect reported previously for conventional glass-ionomer bone cements[1].

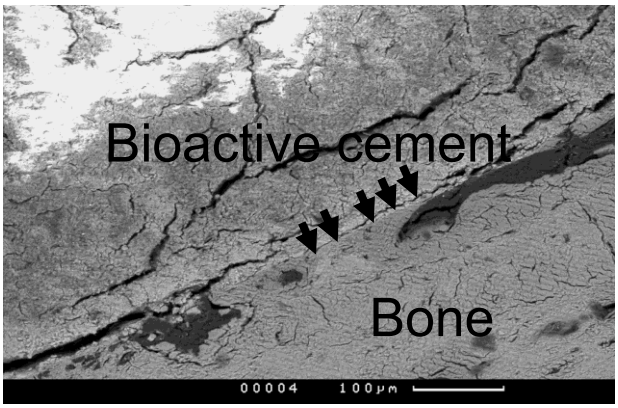

Figure 1. Scanning electron photomicrograph of the bone-cement interface (arrowed) formed after 4 weeks implantation of a bioactive glass-ionomer cement rod (2 x 1 mm) prepared with 45S5 bioactive glass and poly (acrylic acid), mean molecular weight of 52,000.

Discussion and Conclusions

It was concluded that new glass-ionomer cements could be prepared using classical bioactive glass compositions in combination with poly (acrylic acid). This cement formation was greatly improved by the addition of phosphoric acid solution. The mechanism for the setting reaction of these new bioactive glass ionomers is undoubtedly more complex than for conventional GICs. Analysis including FT-IR implied formation of a number of phases including apatite, suggesting that when phosphoric acid was present a calcium phosphate cement-like setting reaction (in addition to silicate cement features) accompanied salt bridge generation. New cements based on bioactive glass compositions are potentially biocompatible *in vitro* and *in vivo*. This new class of biomaterial has significant potential for use as bone cements or a pre-set graft substitute.

REFERENCES

1. Carter, D.H. *et al.*, 1997. *Biomaterials* 18: 459-466
2. International Patent Application PCT/GB2013/053386

ACKNOWLEDGMENTS

The authors acknowledge Dr Robert Burton (Hallam University) for XRF. Hatton, Crawford & Miller are members of MeDe Innovation, the EPSRC Centre for Innovative Manufacturing in Medical Devices. We are grateful to the EPSRC for funding through our local KTA account and the Regener8 IKC programme (POC020) managed by the University of Leeds.

Degradable bioactive glasses for development of aluminium free bone cements

Altair Contreras Jaimes*, Paul V. Hatton, Ian M. Brook & Cheryl A. Miller

Bioengineering & Health Technologies Research Group, School of Clinical Dentistry, University of Sheffield, UK

POSTER presentation

Abstract

Glass ionomer cements (GICs) have been traditionally used in dentistry as luting and restorative materials. Their low exothermic setting reaction and ability to bond to bone have extended their applications to other areas such as middle ear surgery. However, the aluminium contained in the glass had been classified as a neurotoxin and linked to Alzheimer's disease when the material was exposed to the nervous system. Moreover, aluminium had been reported to induce bone mineralisation defects.

Recent research has been targeted towards the substitution of the Al_2O_3 component in the parent glass, since Al salt complexes are linked to the cement setting and its stability in aqueous media. Ions such as Zn, Mg, Ge and Fe have resulted in different drawbacks such as reduced hydrolytic stability of the cements, poor *in vitro* performance and glass crystallisation during melting. However, compositions such as Bioglass®, with known osteoinductive and osteoconductive properties had been overlooked as a potential degradable glass for cement formation. Therefore, in this research a series of glasses based on the Bioglass® composition were produced with compositions ranging within the bone bonding area described by Hench for the SiO_2-Na_2O-CaO-P_2O_5 glass system (Hench, 2006).

The glasses were produced by a melt quench route and the frit was ball milled to obtain particles sizes < 45μm. The glass powders were characterised by X-ray diffraction (XRD), X-ray fluorescence (XRF) and Attenuated Total Reflectance Fourier Transform Infrared (ATR-FTIR) spectroscopy. Cements with varying powder liquid (P/L) ratios, setting modifier content (H_3PO_4 $_{sol}$) and 10.7 % of poly (acrylic acid) were evaluated. Mass change after immersion in deionised water was measured in order to establish possible correlations between the glass compositions and the stability of the cements in water. Setting cements were successfully produced; showing the potential of these Bioglass® based cement formulations to be used in bone related applications.

Acknowledgements
This work was supported by the Medical Technologies Innovation and Knowledge Centre, funded by the EPSRC, BBSRC and the Technology Strategy Board under grant number EP/G032483/1.

References

Hench, L. L. 2006. The story of Bioglass (R). Journal of Materials Science-Materials in Medicine, 17**,** 967-978.

Characterization of a bioactive glass-based cement for bone graft applications

Altair Contreras[1]*, Yulia Ryabenkova[2], Paul Hatton[1], Ian Brook[1], Cheryl Miller [1]
[1]Bioengineering and Health Technologies Research Group, School of Clinical Dentistry, University of Sheffield
[2]Department of Materials Science and Engineering, University of Sheffield
*Corresponding author: a.contreras@sheffield.ac.uk – PhD student (2nd year)

Introduction

Glass ionomer cements (GICs) have been used in dentistry as luting and restorative materials for many years. They have good biocompatibility, a low setting endotherm, and reduced shrinkage, encouraging their adoption for use as bone cements in middle ear surgery. However, the glass component, traditionally aluminium containing, has prevented their extended use in applications requiring contact with the nervous system due to its toxicity and negative effects on bone formation. Therefore, the aim of this research was to investigate the preparation of novel compositions based on aluminium-free bioactive glass compositions.

Materials and Methods

Bioactive glass based on the 45S5 composition was produced using a conventional melt route or purchased from GTS Ltd. (Chapeltown, South Yorkshire). Cements were prepared by mixing the glass powder (< 45 µm), poly (acrylic acid) (PAA $_{Mw}$=45.5k) and a 25% phosphoric acid solution at a powder/liquid ratio of 2:1. Glass characterization was performed using X-ray diffraction (XRD), Differential thermal analysis (DTA) and X-ray fluorescence (XRF). Cement stability in aqueous media was evaluated by immersing set discs (9 x 1 mm) in 20 ml of distilled water and weight changes recorded at 1 hour, 1 day and 1 week. Setting chemistry at 5 minutes and 4 hours was investigated by attenuated total reflectance Fourier transform infrared spectroscopy (ATR-FTIR). For *in vitro* studies, L929 fibroblasts were cultured on washed pre-set cement discs (4 x 1 mm) for up to 9 days to evaluate cell adhesion on the cement surface.

Results and Discussion

Chemical analysis obtained by XRF showed good correlation with theoretical composition and no evidence of crystallization was observed by XRD. Glass transition temperature (Boyd *et al.*) was 543 ºC and crystallization temperature Tc $_{(max)}$ was 687 ºC. Samples appeared to be stable in water, however, after 1 week the weight was reduced to 82.8 ± 0.5 % compared to the original weight. Using ATR-FTIR, the 45S5 commercial glass showed Si-O interactions between 1000 and 900 cm^{-1} (O'Donnell *et al.*, 2009). PAA's carbon and oxygen interactions signals are shown in Fig. 1. Set cement spectra did not show a PAA related peak at 1695 cm^{-1}, assigned to a C=O bond (Wren *et al.*, 2010),which has been reported as an indication of the neutralization process. The peak at approximately 1555 cm^{-1} has been associated with Ca-PAA salts and vibration at approximately 1015 cm^{-1} has been attributed to a $(PO_4)^{3-}$ group (Matsuya *et al.*, 1999), which could be associated with calcium ions resulted from the glass dissociation. Preliminary SEM showed good cell coverage of the disc surface with healthy cell morphology (Fig 2).

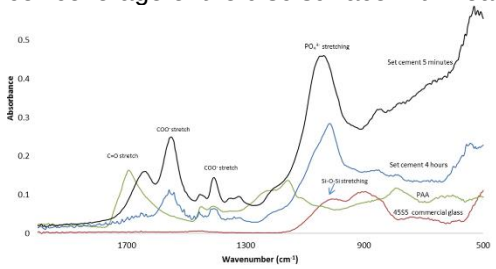

Fig.1 FTIR for set cement and starting materials

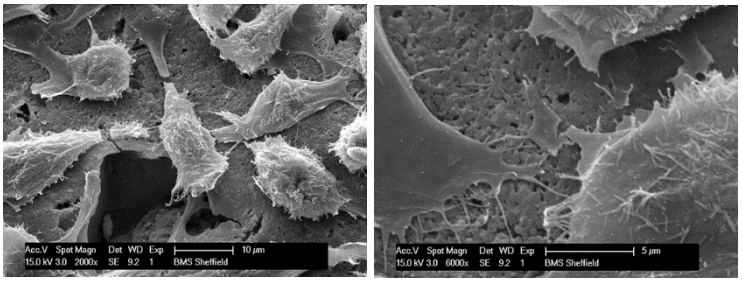

Fig.2 SEM images showing L929 fibroblasts grown onto the cement surface

Conclusions

PAA was combined with 45S5 glass and dilute phosphoric acid to form a setting cement. Samples were stable in water although some mass loss was detected over 1 week. Preliminary FTIR-ATR studies suggested that the cement could have been formed in a similar manner to a combination of a silicate cement with a calcium phosphate cement, but further work is needed. Cell activity on the pre-set discs showed a homogenous cell growth on the material's surface. Therefore, the pre-set cement has potential to be used as bone graft substitute in geometries such as blocks and granules.

Acknowledgements

This work was supported by the Medical Technologies Innovation and Knowledge Centre, funded by the EPSRC, BBSRC and the Technology Strategy Board under grant number EP/G032483/1.

Fabrication of aluminium free pre-set granules to be used as bone graft substitutes

A. CONTRERAS JAIMES, C.A. MILLER, I. BROOK, P.V. HATTON
School of Clinical Dentistry, University of Sheffield

Abstract

Conventional glass-ionomer cements are used as injectable cements and as pre-set porous scaffolds in middle ear surgery. Their aluminium content has, however, restricted their clinical use to a small range of specific interventions. A new formulation based on glass compositions that include 45S5 bioactive glass has been patented by The University of Sheffield. The aim of this Regener8 co-sponsored project was to investigate the adaptation of this cement composition to form a porous bone graft substitute. 45S5 glass powder (<45 μm) produced by a melt-quench route was prepared and mixed with poly (acrylic acid) and an aqueous solution of phosphoric acid. Calcium carbonate powder (5 % w/w) was used to create porosity. The cement paste was allowed to set for one week before grinding and sieving to obtain particle sizes from 0.5 to 1.0 mm. The glass retained a 45S5 composition after melting and its amorphous nature was confirmed using X-ray diffraction (XRD). Scanning electron microscopy (SEM) and m*icro-computed tomography* (μCT) were used to characterise individual particles. It was concluded that a pre-set, porous and potentially bioactive granule could be obtained using the new cement. Further work is ongoing to determine the osteoconductive or inductive potential of this new class of biomaterial.

Preparation and characterization of bone cements based on bioactive glass compositions

A. CONTRERAS JAIMES[1], P.V. HATTON[1], I.M. BROOK[1], Y. RYABENKOVA[1], R. MOOREHEAD[1], C. MILLER[1]
Bioengineering & Health Technologies Research Group, School of Clinical Dentistry, University of Sheffield, UK

Introduction: Bioactive glasses such as the 45S5 composition are reported to be osteoinductive and osteoconductive via CaP layer formation on the surface [1]. Bioactive glasses have been used as bone graft substitutes, and reportedly as additives to conventional glass ionomer cements (GICs) [2]. However, there are no scientific papers describing the complete substitution of the fluoroaluminosilicate ionomer glass with a bioactive glass, and it is not known if this would allow the formation of stable cement. Objective: The aim of this research was therefore to investigate the preparation of cements based entirely on 45S5 and 53P4 bioactive glass compositions. Method: Glasses were produced using a conventional melt-quench route. Cements were then prepared by mixing glass powder (< 45 μm), poly (acrylic acid) (Mw 45k) and a 50% (w/v) phosphoric acid solution. X-ray fluorescence (XRF) was used to determine the composition of the glasses. Cement stability in aqueous media was evaluated by immersing discs (5 x 1 mm) in distilled water. Assessment of the viscosity was studied using rheology, and setting chemistry was investigated using FTIR and XRD. Results: XRF showed good correlation between the theoretical and pre-melt glass compositions, while rheology determined that the storage modulus (G') for the bioactive glass cements increased rapidly but reached a plateau approximately 10 min after mixing (in contrast with conventional dental GICs). FTIR and XRD suggested that the setting process was very complex, probably combining aspects of conventional GIC, silicate cement, and calcium phosphate cement chemistry. Conclusion: Bioactive glass compositions may be used to produce GIC-like cements, and the behaviour and stability of these novel materials was improved by addition of dilute phosphoric acid to the formulation. [1] Jones, J. et al. Bio-Glasses An Introduction. 2012, [2] Yli Urpo, H et al. *J Biomater Appl* 2004.19:5. This work is funded by EPSRC through the Regener8 IKC programme Grant number 135623

Fabrication of a Bone Graft Substitute based on a Pre-set Bioactive Glass-Ionomer Cement

Altair Contreras[1], Paul V. Hatton[1], Ian Brook[1], Abigail Pinnock[1] and Cheryl A. Miller [1]

[1]Bioengineering & Health Technologies Research Group, School of Clinical Dentistry, University of Sheffield, UK

INTRODUCTION

Bioactive glasses based on 45S5 have been used as bone graft substitutes with some success[1]. However, calcium phosphates, dominate the medical market due to their excellent biocompatibility, but they have a complex setting chemistry and are difficult to handle clinically. On the other hand, glass ionomer cement systems are widely known, and a recent patent describes the fabrication of glass ionomer cements (GICs) where the glass component is based on Hench's 45S5 bioactive glass[2]. Therefore, the aim of this research was to fabricate and characterise a granule prototype prepared from the aforementioned bioactive glass ionomer cement (BGIC). If successful, the resulting medical device could potentially combine the excellent biocompatibility of set GICs with the advantages of bioactive glasses, addressing current clinical needs.

EXPERIMENTAL METHODS

Glass based on 45S5 composition was prepared by a melt-quench route. X-ray diffraction (XRD) was used to assess glass formation, and post-melt composition was investigated using X-ray fluorescence (XRF). Scanning Electron Microscopy (SEM.) was used to characterise the granules morphology and presence of a porous structure by *Micro Computed Tomography* (μCT). Glass frit was processed to obtain particles of < 45 μm. Cement granules were prepared by mixing glass, calcium carbonate powder (5% weight), 45k Mw poly(acrylic) acid (Advanced Healthcare Ltd) and an aqueous solution of phosphoric acid (50% w/v). The resultant material was left to age at 37°C. Granules were obtained by grinding and sieving to achieve particle sizes ranging from 0.5 to 1.0 mm, which is commonly used in commercial bone grafting products. The *in vitro* response of MG63 cells cultured on the granules (50 mg and 100 mg) and Tissue Culture Polystyrene was investigated using Presto blue assay.

RESULTS AND DISCUSSION

The amorphous nature of the glasses was confirmed by XRD. It was possible to produce stable granules in media at 37°C under the conditions described above.

XRF showed good correlation between the theoretical and experimental composition values. SEM showed that the obtained granules have irregular shapes and surfaces while μCT indicated the presence of a porous internal structure. *In vitro* studies showed a reduction in the metabolic activity of cultured cells in the presence of the granules compared to Tissue Culture Polystyrene, possibly due to the rapid release of alkaline ions from the glass.

.

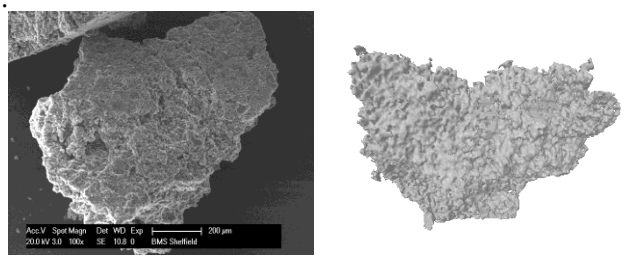

Figure 1. (a) SEM micrograph and (b) μCT image of the prototype granules produced from the pre-set BGIC.

CONCLUSION

It was concluded that it was possible to prepare novel bone graft substitutes based on bioactive glass-ionomer cement technology i.e using only 45S5 based glass composition in combination with poly (acrylic acid) and a phosphoric acid solution. Future work includes testing with other bioactive glass compositions and application of alternatives fabrication methods to improve granule morphology.

REFERENCES

1. Hench, L.L. 2006. *J Mater Sci: Mater Med* **17**:967-978
2. International Patent Application PCT/GB2013/053386

ACKNOWLEDGMENTS

The authors are grateful to Robert Burton at Hallam University for XRF, Advanced Healthcare for providing the PAA. Hatton and Miller are members of MeDe Innovation. We acknowledge the EPSRC for funding through the Regener8 IKC program.